Feasibility study on the application of fiber-reinforced polymers in large lock gates

By

A. Zorgdrager

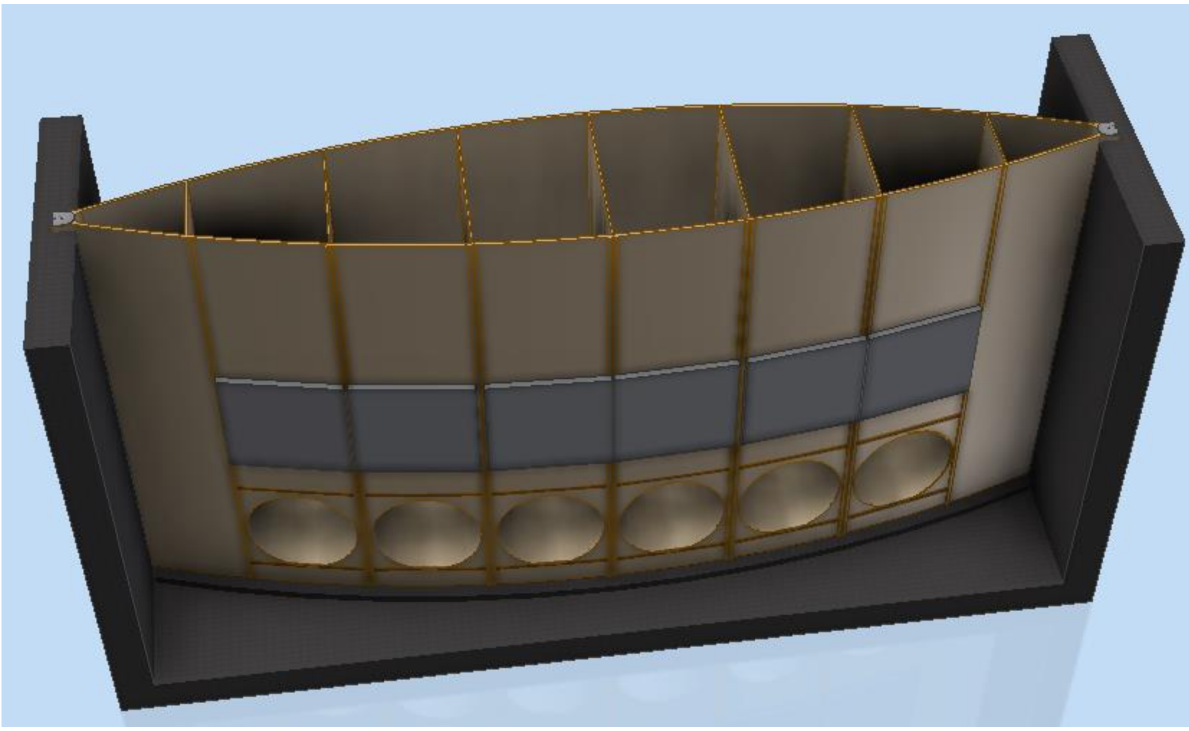

In partial fulfillment of the requirements for the degree of

MASTER OF SCIENCE

Submitted to

Delft University of Technology

December 2014

Feasibility study on the application of fiber-reinforced polymers in large lock gates

By

A. Zorgdrager

In partial fulfillment of the requirements for the degree of

MASTER OF SCIENCE

Submitted to

Delft University of Technology

December 2014

Thesis committee:

Prof. dr. ir. S.N. Jonkman	TU Delft, Department of Hydraulic Engineering
Ir. W.F. Molenaar	TU Delft, Department of Hydraulic Engineering
Dr. M.H. Kolstein	TU Delft, Department of Design and Construction
Ir. P.J.C. van Lierop	Iv-Infra

Preface

This thesis marks the finalization of my Master of Science at Delft University of Technology, faculty of Civil Engineering. The five years I have spent at the university have passed quickly due to the pleasant working environment, the great projects in which I was involved and the interesting people I have met during my study.

It is not a surprise that my subject of graduation is related to lock gates: these structures always had my special attention. This is not in the last place because of the combination of hydraulic- and structural engineering which has to be combined during the design, both disciplines I truly enjoy.

I would like to thank Iv-Infra Amsterdam for providing me with a pleasant working environment. Special thanks go out to Pieter van Lierop for his guidance during my thesis. Our discussions were always very helpful.

I would like to extend my gratitude to my supervisors at Delft University of Technology, which are Prof. Dr. Ir. S.N. Jonkman, Ir. W.F. Molenaar and Dr. Ir. M.H. Kolstein. Not only did you provide me with some practical notes on the documentation, you were also helpful with recommendations on literature.

Finally, I would like to thank FiberCore Europe, and Jan Peeters in particular, for providing me with practical answers to questions which were raised during the study. The enthusiasm with which Jan talks about fiber-reinforced polymers is unprecedented, and so is his knowledge on the material.

Arjen

Abstract

Currently, steel is the most frequently applied material in large lock gates. However, corrosion of the material results in frequent maintenance works to the gates. The strict environmental requirements make these activities quite costly. Besides, maintenance to the lock gates leads to downtime of the lock chamber and thus decreases the availability for vessels. The demand arises to apply different materials in lock gates which are more resistant to the harsh environment to which they are exposed. One of the materials which may be able to fulfill the requirements and to satisfy this demand for durability for application in large lock gates are fiber-reinforced polymers (FRP).This study focusses on an assessment of the feasibility of FRP in large lock gates in comparison to application of steel. The feasibility is based on the structural performance, life-cycle costs and specific risks which are accompanied.

Firstly, a literature study has been performed to gather information on the material composition, specific material properties, available design codes and possible production methods of FRP. The literature study has given insight into the strengths and weaknesses of application of the material. The largest advantages of the material are its high specific strength, the possibility to fully optimize the structure due to the large number of design variables and an expected better durability, although studies on the long term performance of the material are still required. The largest disadvantages of the material are its low interlaminar shear strength, making FRP structures vulnerable to delaminations. Besides, the lack of ductility in the material is at the expense of the robustness of the designs because no redistribution of forces can take place. Finally, the low strain at which fiber rupture occurs results in a poor impact resistance.

The design of the lock gates of the third Beatrixlock (spanning a length of 25 meters) served as a case study to investigate the feasibility of FRP in large lock gates. Based on the material knowledge gathered during the literature study, lifting gates appear to be the most suitable gate type for application of FRP because of a combination of good inspectability and large advantages of the lower weight for the supporting structure and driving equipment.

Consequently, a study to different gate alternatives has been performed to find the optimal structural shape for the gate. The five considered alternatives are the vierendeel gate, Warren truss gate, curved gate, lens-shaped gate and stiffened gate (see Figure 1).

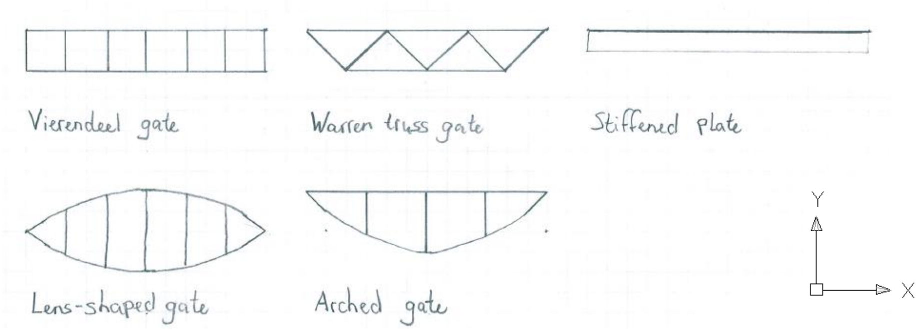

Figure 1: Considered geometries during the study to gate alternatives (top view)

Each gate alternative has been globally designed on strength (maximum strain criterion) and stability of individual members based on a 2D-schematization, after which each concept has been optimized on weight. A multi-criteria analysis indicated the lens-shaped gate as the most promising solution, based on the combination of good inspectability, good producability and an efficient use of materials compared to the other gate alternatives.

Consequently, the 2D-schematization of the lens-shaped gate has been translated to a 3D-model. The gate has also been equiped with openings required for filling and emptying of the lock chamber and with vertical blocks at the connection to the lock walls to improve the watertightness (see Figure 2).

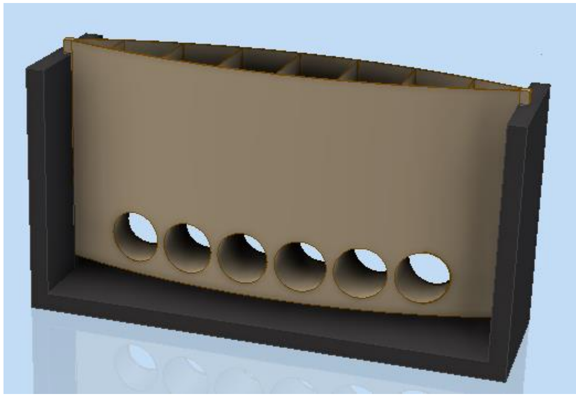

Figure 2: Conceptual design of the lens-shaped gate in 3D

The structural performance of the gate has been investigated with help of finite element software Ansys to study the effects of the adjustments to the design on local stress concentrations. The complexity of the finite element model has been increased stepwise and the outcomes have been validated after each step to keep track of the correctness of the model. The calculations showed that the stress concentrations around the openings result in local exceedance of the shear strength and allowabe normal strains. A total of 8 possible structural adjustments have been described qualitatively to increase the strength.

In order to assess the relative feasibility of FRP, a design of the gate has been elaborated in steel quality S235 as well.The same structural shape has been selected for both designs, so that only the material properties become decisive for the feasibility. The steel gate has been designed on strength (Von-Mises criterion) and plate stability.

The feasibility of FRP compared to steel is examined by a combination of mass (which is a measure for the forces on the supporting structure), life-cycle costs and specific risks related to the designs. Firstly, the mass of the gate constructed from FRP appeared to be considerably less than the design in steel (120 tons versus 202 tons). Secondly, the life-cylce costs for both designs turned out to be very compareable. These costs consist of initial costs related to the production and construction of the gates and annual costs related to maintenance, inspection, operation and repair. A discount rate of 4% has been assumed. The net present value of the costs for both designs are estimated on 1,2 million euros over the considered lifetime of 50 years (see Figure 3).

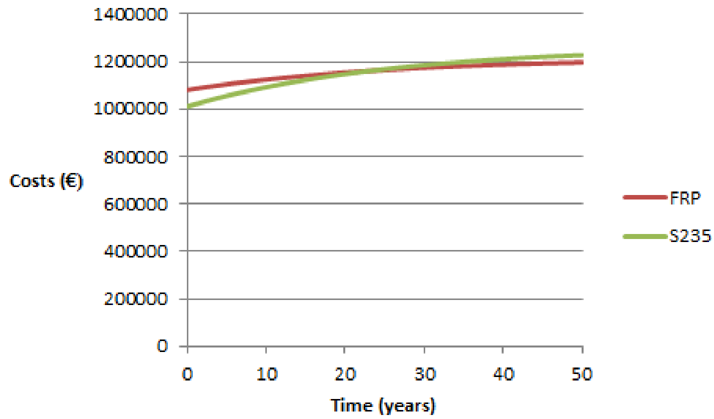

Figure 3: Overview of the net present value over the considered lifetime of the gate

Thirdly, the design in FRP has a considerably higher risk profile than the gate in steel. The largest risks which were identified ,based on the available literature and consultancy of FRP-experts, were a lack of knowledge on the (long term) strength of connections, failure of the gate due to ship collision and a lack of knowledge on the fatigue performance of the material, especially at the connections between members. A similar risk analysis has been performed for the design in steel, which pointed out that ship collisions form the largest risk for the gate in steel as well.

Since ship collisions turned out to be the largest risk for both designs, the structural response of the gates due to such an impact has been investigated in the final part of this report. The underlying assumption is that the watertightness of the gate needs to be preserved during the governing impact. The kinetic energy related to the design impact which has to be resisted has been derived from a probabilistic study on the risks of a ship collision by Deltares. A full dynamic approach has been applied to study the structural response to the governing impact. The design in steel showed plastic deformations, but the strains at which fracture occurs were never reached. The gate constructed from FRP on the other hand was not able to resist the impact without a loss of the water retaining function. Furthermore, the ultimate limit states of the FRP gate were exceeded by such a large margin that adjustments to the gate itself do not seem to be feasible to improve the resistance to collisions. Therefore, external devices to resist such an impact are recommended.

This study has proved the potential of FRP for application in large lock gates, although the absence of ductility in the material, the relatively low material stiffness, low interlaminar shear strength and the lack of (publicly avaiable) knowledge on the detailing and long term performance of FRP structures seem to be large challenges which have to be conquered first before application is possible in projects where the consequences of failure are large.

Table of contents

List of symbols

Roman symbols

D	Miner's sum	[-]
E_{11}	Young's modulus in principal direction	[N/mm^2]
E_{22}	Young's modulus perpendicular to principal direction	[N/mm^2]
E_{12}	Young's modulus	[N/mm^2]
G_{12}	Shear modulus	[N/mm^2]
E_F	Young's modulus of the fibers	[N/mm^2]
E_R	Young's modulus of the resin	[N/mm^2]
G_F	Shear modulus of the fibers	[N/mm^2]
G_R	Shear modulus of the resin	[N/mm^2]
k	Slope of the S-N curve	[-]
R	Resistance	[-]
S	Load	[-]
V_F	Fiber volume fraction	[-]

Greek symbols

ε_1	Strain in the main direction of loading	[-]
ε_2	Strain perpendicular to the main direction of loading	[-]
v_{12}	Poisson ratio related to strains in principal direction	[-]
v_{21}	Poisson ratio related to strains perpendicular to principal direction	[-]
γ_f	Load factor	[-]
γ_m	Material factor	[-]
γ_c	Safety factor related to manufacturing process	[-]
γ_{ct}	Safety factor related to temperature effects	[-]
γ_{cv}	Safety factor related to moisture effects	[-]
γ_{ck}	Safety factor related to creep effects	[-]

γ_{cf}	Safety factor related to fatigue effects	[-]
ε_{max}	Maximum strain	[-]
σ_x	Normal stress in the x-direction	[N/mm^2]
σ_y	Normal stress in the y-direction	[N/mm^2]
σ_z	Normal stress in the z-direction	[N/mm^2]
σ_{Rd}	Strength of the material in the main direction of loading	[N/mm^2]
τ_{xy}	Shear stress	[N/mm^2]
ρ	Density	[kg/m^3]

General introduction

Currently, steel is the most frequently applied material in large lock gates. A large downside of steel is its vulnerability to corrosion, resulting in frequent maintenance works to the gates. The strict environmental requirements related to maintenance and repair make these activities quite costly. Besides, maintenance to the lock gates leads to downtime of the lock chamber and thus decreases the availability for vessels. The demand arises to apply different materials in lock gates which are more resistant to the harsh environment to which they are exposed.

The demand for durability has given rise to the introduction of fiber-reinforced polymers (FRP), not only in lock gates, but actually in the entire civil engineering branch. FRP's are already being used as reinforcement of concrete, bridge decks, laminates, wraps, beams and girders [1]. Not only is FRP more resistant to environmental conditions than the traditional building materials, it also has a superior strength-to-weight ratio. Besides, the production process and composition of FRP allows a large freedom in shape. This makes it possible to fully tailor the structures and design them according to the principle "form follows force", resulting in a great effectiveness of material use.

Recent applications of FRP in the lock gates of the Spieringsluis [2] and in a gate of the Kreekraksluizen [3] have proved the applicability of the material in small[1] lock gates. The question is raised whether the material would also be feasible for application in large lock gates, so that the light weight and expected durability of the material can be optimally utilized.

With five large lock upgrades planned for the near future in The Netherlands (located near Limmel (2018), Eefde (2018-2020), Nieuwegein (2017-2020), IJmuiden (2019) and Terneuzen (2017-2021)), the outcome of this study will be relevant for the lock gate design of the future.

Objective

The objective of this thesis is to study the feasibility of fiber-reinforced polymers in large lock gates compared to application of steel. The feasibility will be based on a combination of the total mass (as a measure for the forces on the surrounding structures), life-cycle costs and risks accompanied. The design of the lock gates of the Beatrixlock 3, both in steel and FRP, will function as a case study.

Structure of the report

The main research question to be answered is: "Do fiber-reinforced polymers form a feasible alternative for steel for application in large lock gates?". In order to answer this question, the main research question has been subdivided into 19 subquestion which are answered throughout the report. These subquestions and the chapters in which they are treated are presented in Table 1.

[1] A gate is considered to be small if the length of the span is shorter than 10 meters. Large means that the span exceeds 20 meters.

Table 1: Research questions to be answered throughout the report

Chapter	Title	Research questions to be answered
1	Introduction to fiber-reinforced polymers	1.) What are the specific properties of FRP? 2.) How are composite structures designed? 3.) What fiber- and resin type will be most suitable for application in lock gates?
2	Introduction to locks	4.) What gate type will be the most suitable for application of FRP? 5.) What specific properties are required for lock gates?
3	Introduction to case study: Beatrixlock 3	6.) What are the site-specific functional requirements and boundary conditionsfor the case study? 7.) What will be the physical boundaries for the design?
4	Study to gate alternatives constructed from FRP	8.) What is the optimal shape for a large lock gate constructed from FRP?
5	Conceptual design of the lens-shaped gate	9.) What adjustments are required to turn the 2D model into a 3D-design? 10.) What is the optimal shape for the openings required for filling and emtpying of the lock chamber?
6	Structural design of the lens-shaped gate	11.) What will be the results of the conversion from 2D to 3D regarding peak stresses?
7	Detailed design	12.) What will be the best way to connect the different elements to each other?
8	Comparison of the FRP gate to a gate constructed from steel	13.) What will be the total structural weight compared to application of steel? 14.) What specific risks are related to application of FRP compared to application of steel?
9	Elaboration of the effects of ship impact	15.) What collision energy needs to be considered for the design? 16.) What damage will occur to the FRP gate during collision of the design vessel compared to the damage for the steel gate?
10	Conclusion	17.) Is FRP feasible for application in large lock gates?
11	Recommendations	18.) What future research is required?

Chapter 1 serves as an introduction on fiber reinforced polymers. Firstly, application of the material in different branches is reviewed. The second paragraph touches upon the composition of the material and explains the different types of FRP. Hereafter the different production processes are described. The fourth paragraph explains the mechanical properties and failure mechanisms for composite structures. Hereafter, subjects such as joint geometry, durability and costs are treated. Chapter 1 is concluded with a summary of the design decisions concerning the material selection and production methods for the case study.

In the second chapter, a general introduction is given on locks. This chapter starts with a description of the functions and role of the locks compared to the total water defence system. The second paragraphs serves as an overview of the most important elements of navigation locks, after which the third paragraph zooms in on one of the most important parts of the locks, which are the gates. The different types of gates are investigated to see which type would be most suitable for application of FRP in the new Beatrixlock. Hereafter, different types of filling and emptying systems are reviewed. The first chapter is concluded with an overview of the materials which can be applied in lock gates.

The case study "Beatrixlock 3" is introduced in chapter 3. This chapter touches upon an environmental analysis and current lay-out of the lock, the functional requirements and the boundary conditions for the lock gates. A study to the most promising shape for application of FRP has been executed in chapter 4. A total of 5 options are investigated by schematization of the gates to 2D frameworks. Each structural shape is translated to a static scheme after which each variant is designed on strength and optimized based on hand calculations. The most promising gate alternative is selected at the end of the chapter by means of a multi-criteria analysis.

Chapter 5 touches upon the conceptual design of the lens-shaped gate. The design of the openings, the connection to the lock head and the production process are treated in this chapter. This conceptual design has been designed on strength and stiffness in chapter 6. For this purpose, finite element software Ansys have been used. The complexity of the model has gradually been increased to be able to track of the correctness of the model. The chapter is concluded with an investigation of the fatigue- and creep effects during the lifetime of the structure.Chapter 7 covers the detailed design of the gate. This chapter discusses the design of the connections between the plates, the culvert design, the attachment of the lifting equipment and the valve design.

In chapter 8, a reference design in steel has been elaborated based on the same structural shape as for the gate in FRP. Both designs are consequently compared on mass, life-cycle costs and specific risks related to application of both materials. Ship collision was indicated as one of the largest risks for application of FRP. The probability of such an event, together with an elaboration of the structural response based on a dynamic analysis is to be found in chapter 9 for both the design in steel and FRP. In chapter 10, a conclusion is drawn on the feasibility of FRP in large lock gates based on the final mass, life-cycle costs and specific risks in comparison to steel. This report is concluded with recommendations on further research required to test the feasibiltiy of FRP in large lock gates in chapter 11.

1. Introduction to fiber-reinforced polymers

This chapter serves as an introduction to fiber-reinforced polymers and is especially useful for the reader who is not yet familiar with the material. The second objective of this chapter is to investigate the specific properties of the material so that the advantages of FRP can be optimally used during the design of the lock gate. The third and final objective of this chapter is to investigate the material composition which is most favourable for the civil industry as a whole, and with special focus on application in lock gates.

The applications of the material in other branches are discussed In the first paragraph of this chapter. Hereafter, the decomposition of the material is elaborated together with the specific properties of the individual ingredients. This is followed by a discussion on the existing design documents of FRP structures. Hereafter, the different production processes, joint configurations and the durability of the material are described. This chapter is concluded with estimations on the costs and design decisions made for the case study.

More basic information on fiber-reinforced polymers can be found in the literature study related to this thesis [4], lecture notes of the course CT5128 [5], and the (Dutch) book “Composieten: Basiskennis” [6].

1.1. Current applications of FRP

Fiber-reinforced polymers are only applied in civil structures for a few decades, while the aerospace, maritime and mechanical sectors use the material already for a longer time. This paragraph touches upon the different applications of FRP in the different sectors in order to gain knowledge on the design decisions to be made for the case study.

1.1.1. Application of FRP in aerospace industry

In the aerospace industry, fiber-reinforced polymers are often applied because of their excellent strength to weight ratio. Shortly after introduction, application of composites was limited to small parts because of the high initial costs of the material. The main and tail rotor blades of a helicopter were one of the first strucutral parts constructed with composites at the end of the 1960s [7] In the early 1980s, the first FAA (Federal Aviation Administration) certificated (small) airplane was built. The fuselage of this airplane was made of a sandwich consisting of graphite/epoxy skins and a Nomex® core. It was co-cured in large pieces that were bonded together. The critical connections were also fastened [7].

As the fuel prices kept rising, composites were becoming more and more important due to their excellent strength to weight ratio. Approximately 50% of the mass of modern airplanes consist of composites, as Figure 4 shows.

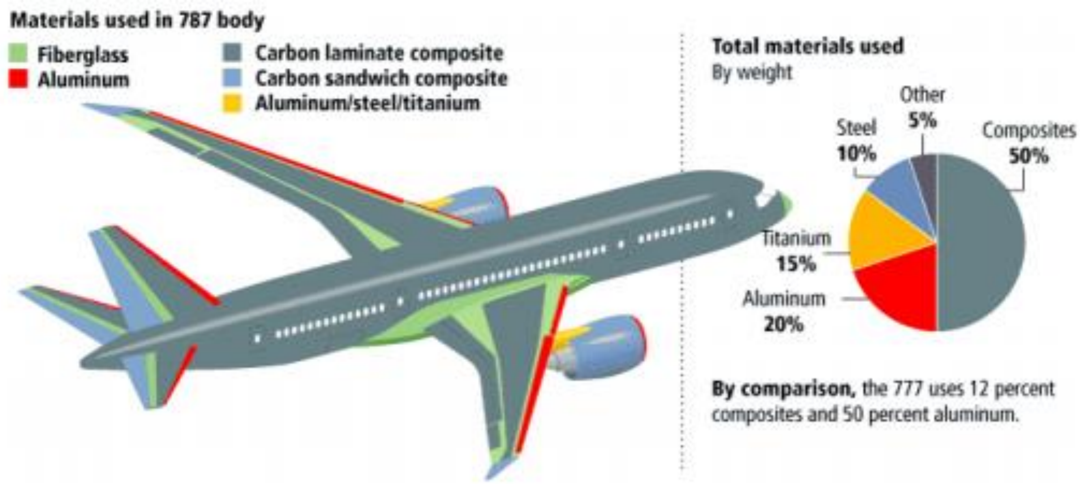

Figure 4: Materials used for construction of the boeing 787 [8]

Most frequently applied materials are glare (a combination of glassfibers and alumnium) and carbon. The evolution of the share of composites compared to the total weight of a plane in both commercial and military aircrafts is illustrated in Figure 5.

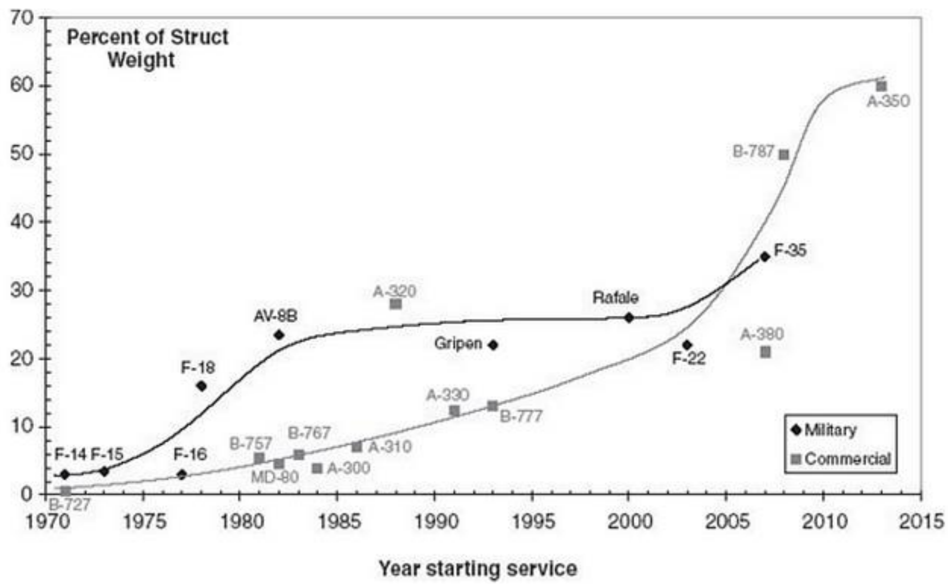

Figure 5: Share of composites in military and civilian aircraft structures [9]

Although these materials show excellent mechanical properties, they are considered to be too expensive for application in the civil construction industry where minimization of weight is not as important as in the aviation industry.

An important point of application of composites in aviation is monitoring the performance of composites and to detect voids and anomalies inside the laminates. Especially during impacts (e.g. bird strike, luggage impact, lightning strike) the subsurface of the laminate can be damaged while the surface is still intact. This makes it impossible to detect damages by eye. Ultrasonic equipment is available to detect subsurface damage, although this technique is time- and money consuming [9].

1.1.2. Application of FRP in the martime industry

Just like in the aerospace industry, composites are already used in the maritime sector for decades. Since the environment for both the vessels and lock gates are comparable (temperature, humidity, hydrostatic forces etc.), experience on the sustainability and maintenace of the material can be extracted from the maritime sector.

Figure 6: Example of a composite yaught [10]

Basically, three materials can be used for the construction of vessels: wood, steel and composites. Composites are the most frequently used material for relatively small vessels as an alternative for wood. Over 80% of the small craft are costructed from FRP [10].

For economical reasons, a combination of E-glass & polyester is the most frequently used combination of materials. The hull of the vessels are either constructed from solid plates with stiffeners or sandwich structures with foam as core material.Larger vessels are still mostly constructed from steel, mainly due to conservatism of the maritime industry.

The hulls of composite vessels can either be manufactured by hand lay-up or vacuum injection (see chapter 1.3 for an explanation of these terms). Hand lay-up is time consuming and generally speaking the quality of the product can not be guaranteed. Hand lay-up however does not require expensive equipment and allows for the construction of more complex shapes. Vacuum injection is less labour intensive but requires more equipment. For vacuum injection, the design and positioning of the infusion points and vacuum pumps is a key factor. If the flowpath of the resin is too long, the resin may cure before it has covered the entire surface. The resin is usually injected in a main channel which diverges into smaller subchannels. An example of an infusion strategy is given in Figure 7.

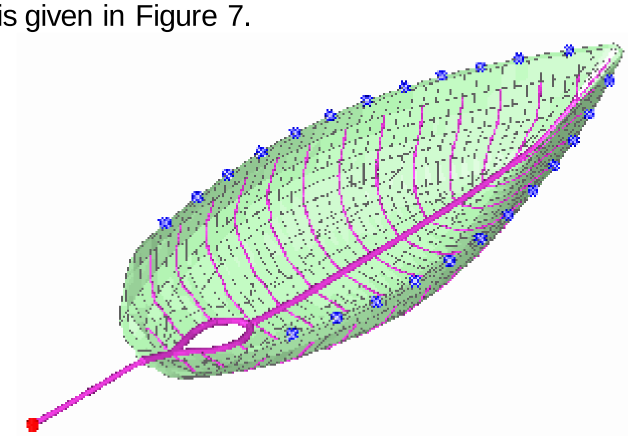

Figure 7: Infusion strategy for a hull of a vessel [11]

Although the short term mechanical properties of composites are good, several degradation mechanisms lead to great deterioration of the material in time. The following degradation mechanisms are identified for vessels made from a combination of E-glass and polyester:

- Blistering due to either trapped air or water absorbtion;
- Fading of the colour and a loss of sheen by UV-radiation;
- Stress rupture.

1.1.3. Application of FRP in the construction industry

Fiber-reinforced polymers are still relatively new in civil engineering, but its market share is increasing rapidly. Fiber-reinforced polymers serve for a great variety of applications. The most important structural applications are the following [1]:

- Cables and tendons
- Beams and girders
- Trusses
- Laminates and wraps
- Bridge deck systems
- All-composite FRP bridge deck structures
- Hybrid new bridge structures
- Columns and poles
- Gratings and handrails
- (small) Lock gates
-

Composites are often applied in cables and tendons. For example in bridge cables (Stork Bridge, Switzerland), as reinforcement of concrete (Crowchild Trail Bridge, Canada) or for prestressing of concrete (Beddinton Trail Bridge, Canada), the material becomes an increasingly accepted alternative for application of steel.

Figure 8: Example of FRP in bridge cables (Storchenbrücke Bridge, Switzerland) [12]

Another application of composites is in the form of repair material. Wraps or laminates can be placed at damaged areas of existing structures to increase load bearing capacity and prevent structural deterioration. For example, composite wraps are often used to prevent moisture entering damaged concrete structures [1].

Except for the previous two applications, where composites have been used in combination with other construction materials, numerous examples exist of structures entirely made of fiber-reinforced polymers. The material has for example been used in pultruded beams, girders, truss structures, bridge decks and small lock gates.

The following two specific projects in The Netherlands are described below and serve as reference projects for the design of the new Beatrixlock gates:

- Pedestrian bridge Rijkerswoerd
- Drawbridge Andel

The next subsection summarizes these projects, which are in more detail described in the article "Projects in The Netherlands" by M.H. Kolstein, written for the course CT5128 [5].

Pedestrian bridge Rijkerswoerd'

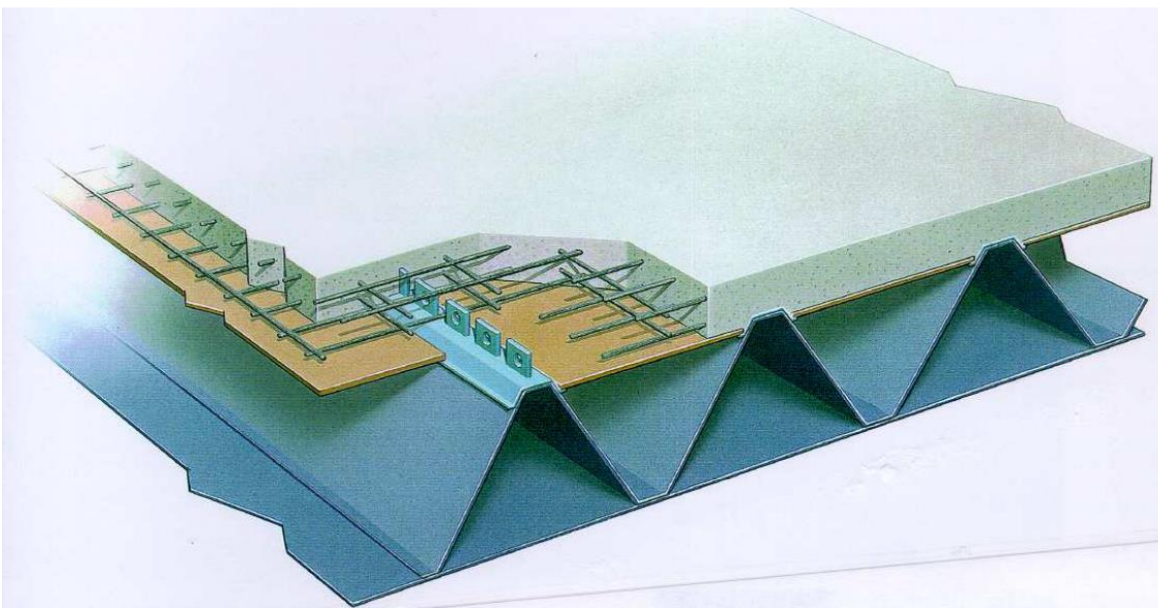

Figure 9: Artist impression of the pedestrian bridge Rijkerswoerd [5]

The pedestrian bridge in Rijkerswoerd is constructed in 1999 and has a span of 10 meters. Besides cyclists and pedestrians, the bridge is also designed for a 4 tons ice truck. It was decided to apply two (horizontal) plates which are connected by troughs. The upper plate is mainly loaded in compression while the lower plate is loaded in tension. The need to resist impact loadings and concentrated loads resulted in application of concrete in the bridge deck instead of FRP. The other parts are constructed using a combination of Twaron aramyde fibers and a polyester resin.

The choice for aramyde fibers is for a large part driven by innovation: this was the first time that this material was applied in a bridge. The fiber volume was 40% according to the design, but eventually turned out to be 36% after manufacturing. Sufficient safety factors were incorporated in the design to account for this difference.

The lower plate consists of 12 layers of 0° stitched mats, 3 layers of 90° stitched mats, combined with 2 layers of $\pm 45°$ woven fabrics. The total thickness of the plate is 7mm.`
The troughs are equiped with a $\pm 45°$ laminate: 8 layers of a $\pm 45°$ woven fabric are combined with 2 layers of $0/90°$ stitched mats. The thickness of the troughs are approximately 5mm.

The troughs are connected to the lower plate by adhesive bonding with epoxy as a glue. Adhesive bonding is chosen to prevent local peak forces which can induce fatigue failure. The contact surface is made as large as possible. The connection is presented in Figure 10.

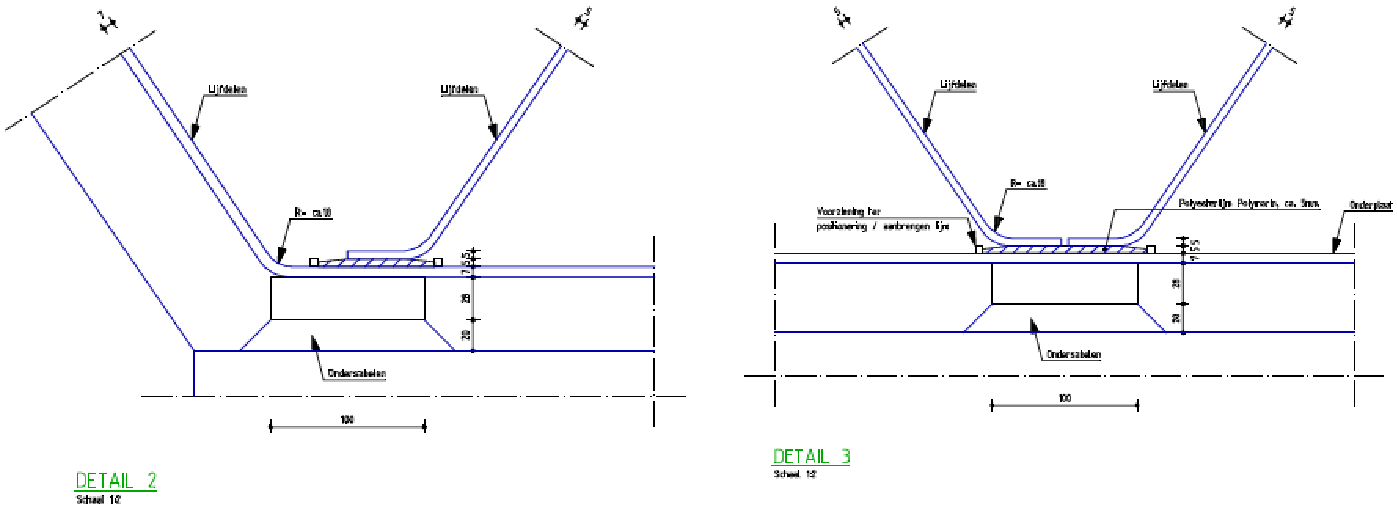

Figure 10: Connection between trough and lower plate for the pedestrian bridge in Rijkerswoerd [5]

The connection between the concrete deck and the throughs are executed by means of steel top-hat profiles. The concrete is casted directly on top of the steel, leading to a stiff connection. This principle is presented in Figure 11.

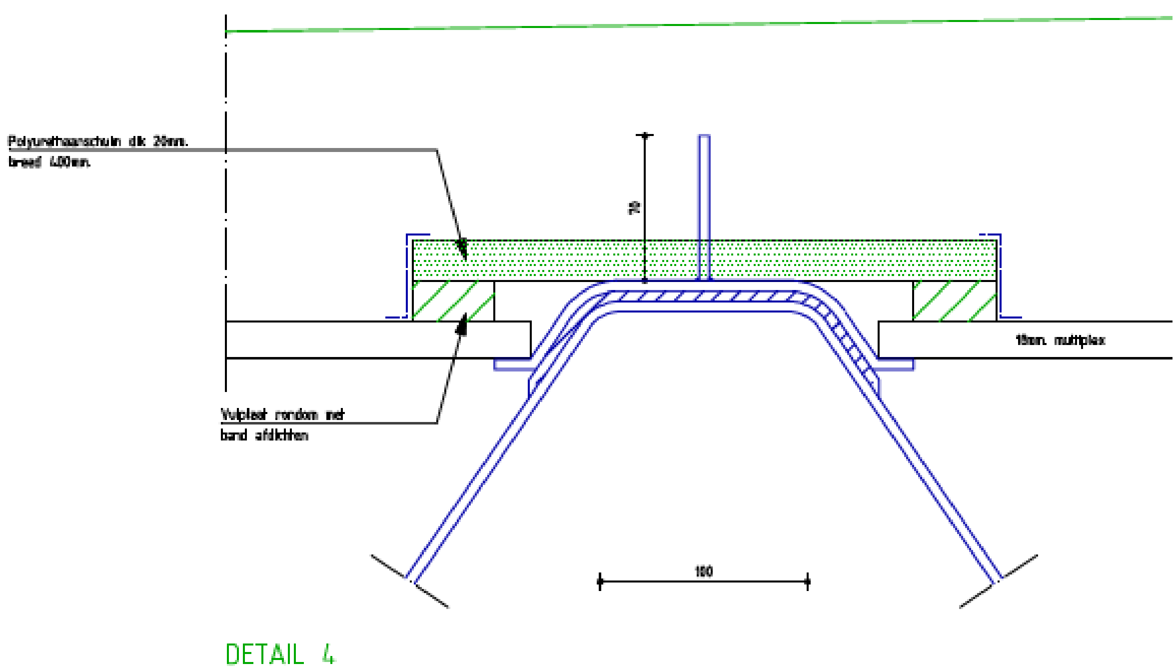

Figure 11: Connection between the trough and deck for the pedestrian bridge Rijkerswoerd [5]

This project has shown that the connection of FRP to other materials gives a lot of troubles, especially due to differences in thermal expansion and variation of stiffness between the connected members. At the time this bridge was built (1999), the costs of the composite bridge (which were approximately €1400,-/m^2) were not competitive with a bridge constructed from steel or wood. This can be explained by the following: there was still little experience with the material back than, selection of E-glass would have resulted in a cheaper solution and only the initial costs are considered, while the maintenance costs are expected to be beneficial for composite bridges.

Drawbridge Andel

This drawbridge is located above the southern lock head of the Wilhelminasluis in Andel. A study to the feasilibity of composites has been executed by Rijkswaterstaat in 1998. The bridge has been designed for traffic class 600 according to the VOSB 1995, which is the heaviest class. The lifetime of the bridge needed to be at least 50 years. To prevent height differences in the bridge deck, the maximum deflection has been limited to 1/1000 of the length of the span. The geometry is presented in Figure 12.

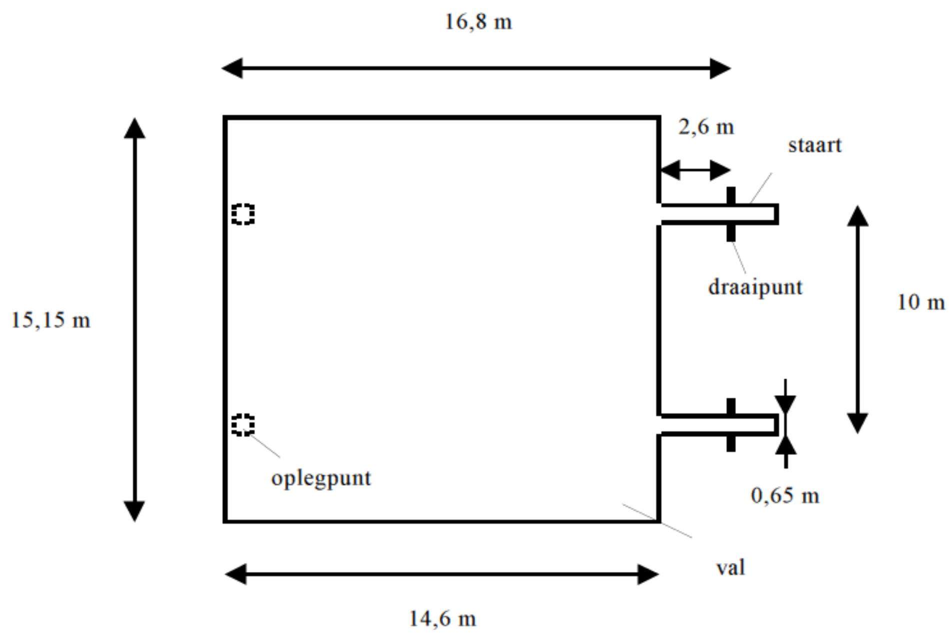

Figure 12: Dimensions of the drawbridge Aandel [5]

Four concepts are considered which are all based on a stiffened deck plate. The stiffeners range from troughs, Z-profiles, longitudinal profiles and crossing longitudinal and transvese profiles. The Z-profiles turned out to be the most beneficial.

The stiffness requirements forced the use of (expensive) carbon fibers for the Z-profiles. Epoxy was selected as resin. The Z-profiles are both on the bottom and top connected to carbon plates. The connections are realized by a combination of bolts and adhesive bonding. The profiles have a height of 1380mm, width of 505mm, web thickness of 13mm and flenge thickness of 17mm. The webs of the profiles are stiffened by top-hat profiles every 950mm to prevent buckling. The profiles are manufactured by hand-lamination, for which a fiber volume of 35% is assumed to be reasonable.To account for fatigue, all the four main directions are equiped with at least 20% of the fibers.

The deck itsself is constructed as hollow profiles which are connected to each other by two top layers. For the deck, a combination of E-glass and polyester is used. Again, hand lay-up is used as production method with a fiber volume fraction of 35%. The geometry is presented in Figure 13.

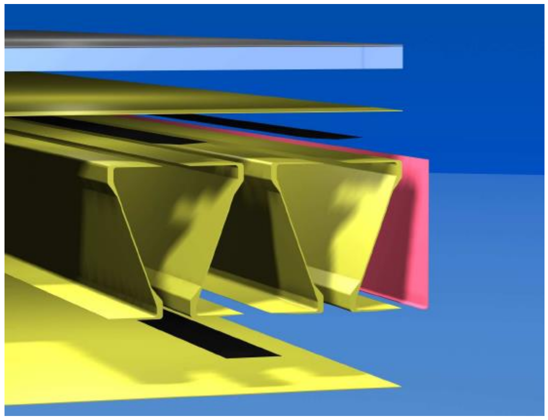

Figure 13: Impression of the lay-up of drawbridge Andel [5]

The costs of the composite bridge are compared to a variant in steel. The following results were obtained[2]:

Table 2: Cost comparision between steel and composites for the drawbridge Andel [5]

Cost factor	Composite bridge	Steel bridge
Realization	f 6.357.000,-	f 2.233.000,-
Maintenance	f 176.250,- /10 years	f 330.250,- /10 years
Removal	f 38.600,-	f 13.100,-

The Maintenance costs are subdivided into different categories:

Table 3: Break-down of the maintenance costs [5]

Maintenance costs	Composite bridge	Steel bridge
Wear layer	f 36.500,-/10 years	f 36.500,-/10 years
Conservation	f 72.000/5 years	f 352.500,-/12,5 years
Inspection	f 5.875/5 years	f 5.875,-/5 years
Monitoring	f 8.000,-/year	f 0,-
Total	f 176.250/10 years	f 330.250/10 years

The expected lifecycle costs turned out to be higher for composites than for steel. This is mainly caused by the labour-intensive production technique, the application of carbon fibers and the little experience with the material back in 1998.

Application of FRP would have resulted in a mass of 86 tons compared to 108 tons for the variant in steel. In the end, Rijkswaterstaat decided to construct the bridge from steel for economical reasons.

---

[2] Costs are in Dutch florin (f 2,20 ≈ €1,-), and are based on the price level of 1998.

1.1.4. Application of FRP in water retaining gates

The application of FRP in water retaining gates is still limited in The Netherlands to two cases: the Kreekraksluizen & the Spieringsluis. Besides, the new gates of the Wilhelminalock are now also being designed as composite mitre gates. Outside the Netherlands, composite lock gates have only also applied in Lorient, France [13]

Next to these actual constructed gates, several studies are performed at the Delft University of Technology on the feasibility of FRP in water retaining gates by Kok [14], Tuin [15], Veraart [16] and Van Straten [17], of which the studies performed by Kok and Van Straaten are the most relevant. All four students concluded that application of FRP was feasible, although all these conclusions are only based on a very global design. Detailing of composite structures was left out of scopes. The next subsections discuss the two Dutch projects and the two most relevant feasibility studies related to application of FRP in water retaining gates.

Spieringsluis [2]

Figure 14: Mitre gates of the Spieringsluis [2]

The Spieringsluis is located in the Biesbosch and is mainly used for locking of small pleasure vessels. The lock chamber has a length of 40 meters and is 6 meters wide. The water is retained by mitre gates, which have to be able to withstand a maximum head difference of 1,3 meters. Rijkswaterstaat decided in 2000 to replace the wooden lockgates by gates made out of FRP. The arguments to use composites instead of wood or steel are the expected lower maintenance costs and the relatively low mass of the gates. This lower mass leads to smaller forces on the hinges and the operation mechanism [2].

A single gate has dimensions of 3,6x6,4 meters (width x height), and weights approximately 2550 kg. It is decided to apply E-glassfibers in combination with with a polyester resin. This decision is mainly based on the low costs compared to other FRP-materials. The fibers are for a large part oriented in one direction: 55% of the fibers are in the main direction while the other directions (-45°,+45°,+90°) are each equipped with 15% of the total amount of fibers. The fibers are processed into chopped strand mats with a mass of 800g/m^2 before being placed. The total fiber volume was 32%, a relatively low value which is caused by the decision to produce the gates by hand lay-up. The gate is designed with an overall safety factor of 2,05 for stiffness calculations and a safety factor of 4,35 for strength calculations.

The gate is designed as a corrugated plate stiffened at the edges by respectively the top- and bottom girder and heel- and mitre post. The total thickness of the gate equals 325mm. The global dimensions are illustrated in Figure 15.

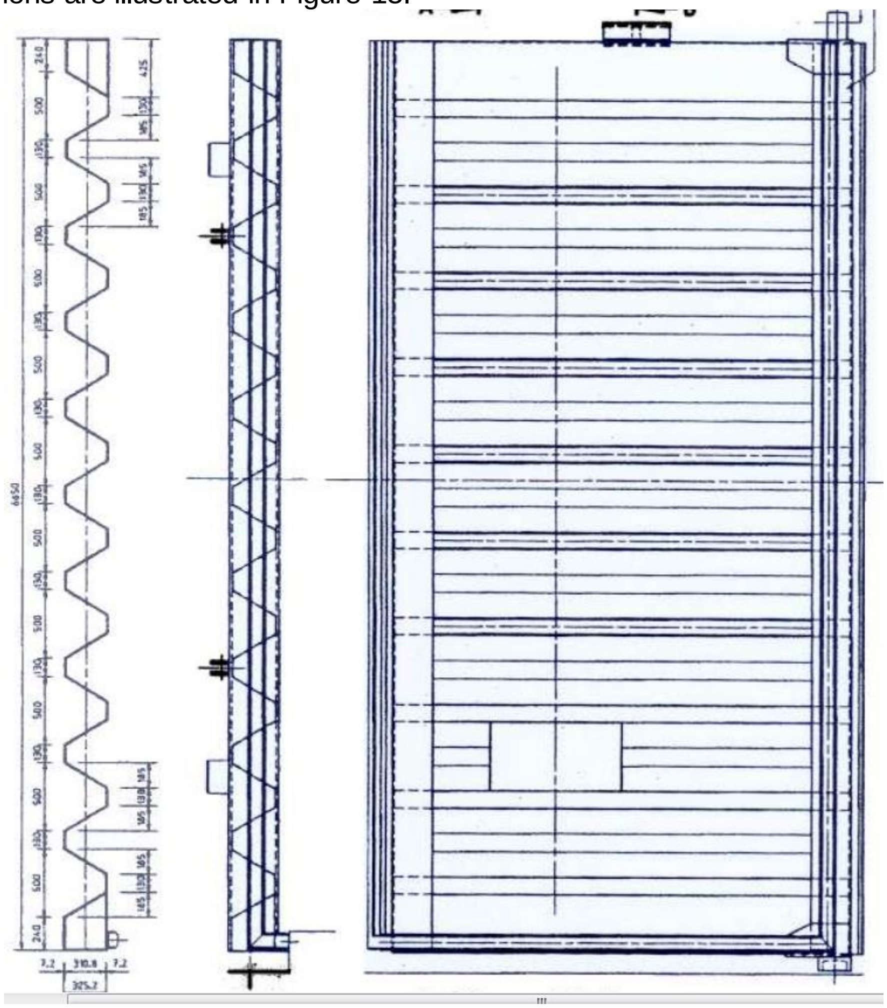

Figure 15: Global dimensions of the gate of the Spieringsluis [5]

The spots where local stress peaks occur, such as the connection to the driving mechanism, pivot, socket and shoe for the pivot are executed in stainless steel (quality A4 class 316L). The joints between the FRP and steel are performed as a combination of glueing and bolting. The glue takes care of a solid contact area to connect the parts by friction bolts.

The total costs of the gates came down to 435.000,- Dutch gulders (approximately €200.000,-), of which 12% were a result of costs for the mould. This leads to a price of €15,-/kg for the gates. The new gates are interchangeable with the old wooden gates, which are stored and are currently being used as spare parts.

Kreekraksluizen [3]

The second Dutch project involving composites in water retaining structures is a valve in the Kreekraksluizen. The Kreekraksluizen used to form a barrier between the fresh- and salt water in the Oosterschelde, consisting of 256 gates. In the first instance, all the gates were made from steel. This required a lot of maintenance because the corrosion rate was up to as much as 1 millimeter per year.

Figure 16: gate of kreekraksluis [3]

As a pilot project, the barrier was equipped with one gate of FRP, which has functioned for about 4 years until the seperation between fresh- and salt water was declared redundant. The gate has resisted about 20.000 load cycles and has a total slideway of approximately 20 kilometres without showing any signs of damage. Since the removal of the gate, TNO kept the gate in fresh water and still monitors it for research purposes. The gate was constructed from a combination of E-glass and vinylester. Production of the take took place by vacuum injection. The water retaining plate was equiped with stiffeners on all four edged which were filled with polymer concrete. The dimensions of the gate are approximately 1,80x0,80 metres, with a maximum head difference of 3,2 meters. The weight of the door was 200 kg and the costs are estimated on €1815,- [3].

Kok (2013) [14]

Kok studied the feasilibilty of application of FRP in large movable barriers for his Master thesis in 2013. Kok made a design for the small gate of the Hartel Canal Barrier in FRP. The barrier has a span of 49,3m, height of 9,3m and is subjected to a maximum head difference of 5,5m. A multi-criteria analysis has led to the lens as global structural shape. Figure 17 shows the global design of the gate.

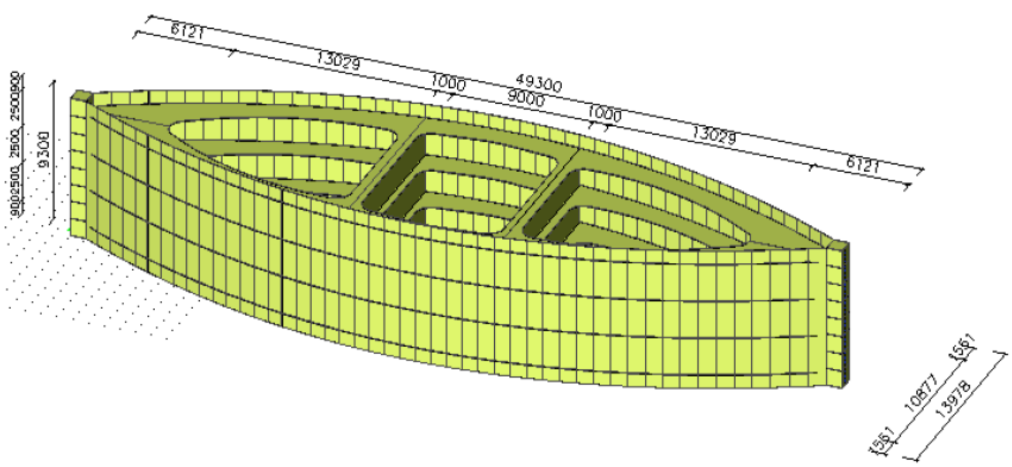

Figure 17: Design of the hartel canal barrier by Kok (2013) [14]

It was concluded that the weight reduction would be 22% if the gate was constructed from FRP instead of steel (210 tons instead of 270 tons). The weight reduction is quite small (compared to the weight reduction found for the case study in this report) for the following reasons:

- The design of Kok is not fully optimized;
- The original steel gate originally functions as a storm surge barrier, and therefore does not receive the same amount of load cycles as Kok designed the gate for.

Kok concluded that the life-cycle costs of the gate made of FRP are comparable to those of the current steel gate. Although the study is performed quite carefully, some important parts are overlooked which makes this conclusion not necessarrily correct:

- The life cycle costs contain a lot of uncertainties;
- Detailing of the composite design is kept out of the scope of the project;
- Dynamic behaviour (vibrations) is excluded from the research, which is especially for storm surge barriers important due to the low weight in combination with high flow velocities underneath the gate when partially opened;
- Effects of a ship collision are based on indicative static forces where an energy approach would have given much more reliable results.

Van Straten (2013) [17]

Van Straten performed a research on the feasibility of FRP for the gates of the Eastern Scheldt Storm Surge Barrier. The governing gate spans a length of 41,5 meters and has a height of 22 meters. The maximum positive head difference is 6,2 meters while also a negative head difference of 3,4 meters can occur. Together with wave impact, the loads are schematized as a distributed load of 99 kN/m^2 over the full height of the gate. Van Straten designed the gate as a straight box girder consisting of 2 plates connected to each other by 8 horizontal plates.

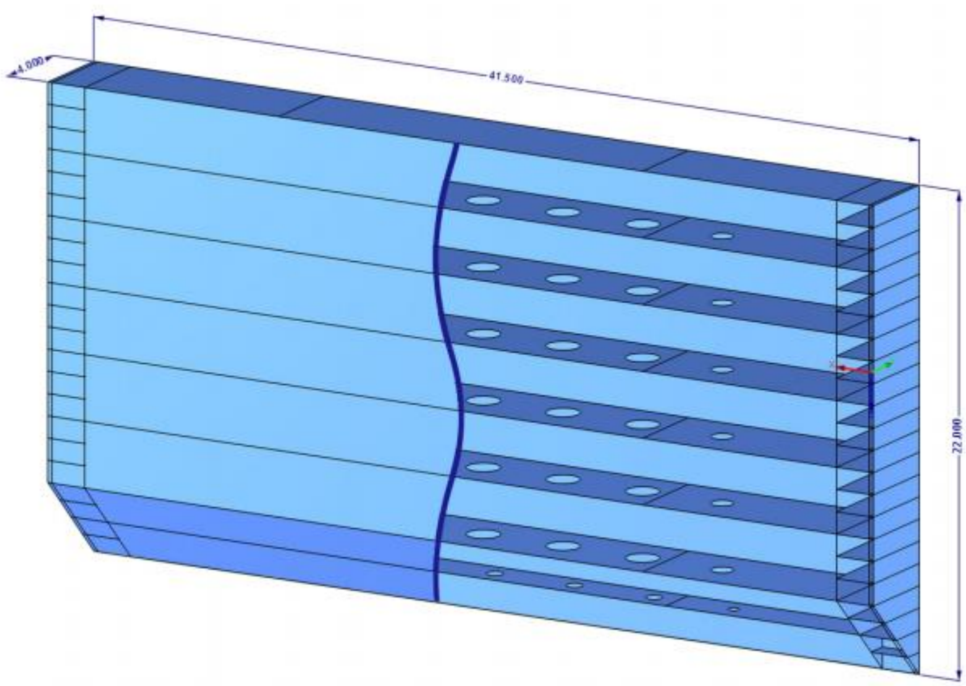

Figure 18: Final design by Van Straten [17]

The two vertical plates are constructed as sandwich elements; each plate consists of two skins with a thickness of 34 mm and a core of 50 mm in between, so that the total thickness of a vertical plate is 118 mm. The totale gate thickness is equal to 4 meters. The laminates are stacked according to the $55\%/15\%/15\%/15\%$ configuration, where 55 percent of the fibers are placed in the 0° (horizontal) direction. Because of the relatively large thickness of the plies (the thickness of the largest ply is 18,7 mm), the danger of microcracking exist. The horizontal plates which are placed to connect the vertical plates are equiped with holes to save on material. The total mass of a single gate is approximately 180 tons. The gate needs to be filled with water in order to be closed because the mass of the displaced water is higher than the self-weight of the gate.

The failure criterion which is used for the gates is an overall maximum strain of 0,52%, based on a maximum strain in the serviceability limit state (SLS) of 1,2%, a material factor γ_m of 1,62 and a a safety factor related to environmental influences γ_c of 1,43.

The bottom of the gate is constructed under a vertical angle in order to fix the separation point of the flow underneath the gate during closing. This is done to prevent vibrations of the gate by oscilations of the separation point. Details like the support, attachment of the cilinders, and connection to the sill are not elaborated in this thesis.

Van Straten has showed that the combination of E-glass and polyester is the most attractive material combination for application in lock gates. Besides, from this report it was concluded that vacuum assisted resin injection would be the most suitable production technique for application of FRP.

1.2. Composition of FRP

After discussing the different applications and feasibility studies on fiber-reinforced polymers, this section touches upon the composition and functions of the different components of fiber-reinforced polymers.

1.2.1. Functions of different components

Fiber-reinforced polymers are an anisotropic, imhomogeneous material. This means that the mechanical properties vary both in space and direction. The material consists of fibers which are embedded in a matrix formed by a resin. The fibers are merely responsible for the stiffness and strength of the material while resin has the following five main functions [18]:

- Binding the fibers together;
- Protecting the fibers from abrasion and environmental degradation;
- Seperating and dispersing the fibers within the matrix;
- Transferring force between the individual fibers;
- Providing shape to the FRP component

The material is typically applied in laminates consisting of a large amount (order of magnitude 30) of stacked plies. In each individual ply, the fibers can be placed in a certain desired direction. This leads to a structure which can be completely tailored to the desired properties. Although this is a positive feature, optimization of the stacking sequence does require a lot of skill and knowledge about the material. Fiber reinforced polymers are often applied in sandwich structures to increase the strength and stiffness, where the core consists of a cheap and lightweight material. The aviation industry recommends the following points regarding the stacking of plies [19]:

- Apply a symmetric lay-up;
- Apply a balanced lay-up;
- Prevent coupling between bending & twisting;
- Place at least 10% of all the fibers in each of the 4 main directions (0°/45°/-45°/90°);
- Place the 0° plies as far from the neutral axis as possible if stiffness is governing;
- Place the (45°/-45°) plies as far from the neutral axis as possible if the laminate is susceptible to buckling, crippling, or impact.

1.2.2. Resins

The following three resin types are most frequently applied:

- Polyesters
- Vinylesters
- Epoxies

Polyesters can be cured at room temperature which makes the material particularly suitable to be applied for large components since no large oven is needed. Polyesters are the cheapest resins available at this moment.
Vinylesters have a reduced moisture absorption and shrinkage compared to polyesters. Besides, the material is also more resistant to strong acids and alkalis. The largest disadvantage of vinylester are the costs, which are nearly twice as high as the costs of polyesters.
Epoxies offer the best properties for application in FRP. Vinylesters however have two big disadvantages: the first one is the high initial costs, which can be up to five times the costs of polyesters. The second disadvantage is the fact that the resin only cures above $40°C$, which is especially a problem for production of large components.The specific properties of the three resin types are summarized in Table 4.

Table 4: Properties of three types of resins [6]

Property	Polyester	Vinylester	Epoxy
Young's modulus (GPa)	2,4-4,6	3-3,5	3,5
Stress at rupture (MPa)	40-85	50-80	60-80
Strain at rupture (%)	1,2-4,5	5	3-5
Density (kg/m^3)	1150-1250	1150-1250	1150-1200
Shrinkage during curing (%)	6-8	5-7	<2

1.2.3. Fibers

For structural purposes, the following three fiber types are most frequently applied:

- E-glass
- Polyaramid
- Carbon

E-glass is by far the cheapest option. For the construction industry, where the costs are at least as important as the weight, E-glass dominates the market. Compared to the other fiber options, E-glass has the worst mechanical properties. Other types of glass fibers, which are less applied for construction, are C-glass (which is chemical resistant), D-glass (which has a low dielectric constant, used for radar domes) and S-glass (high strength glass, mainly used for aerospace applications).

Polyamarid, also know by its brand names Kevlar and Twaron, has excellent wear resistance and a good heat resistance. Besides, the material is compared to the other fiber types relatively ductile which makes it for example suitable for application in bullet-proof vests.

Carbon has the best mechanical properties of the three considered fiber types.This results in application of carbon for example in the fuselage of an airplane, where weight reduction is a very important factor for saving of fuel. used The high material costs are the cause that it is only applied if weight reduction is the main objective rather than cost reduction.

The most relevant properties of the three different types of fibers are summarized in Table 5.

Table 5: Mechanical properties of the three fiber types [6]

Property	E-glass	Polyaramid	Carbon
Tensile modulus (GPa)	70-80	60-180	160-440
Stress at rupture (Mpa)	2400	2000-5300	3100-3600
Strain at rupture (%)	2,6	1-1,5	1,7
Density (kg/m^3)	2500-2600	1540	1800-2000
Relative costs (-)	1	20	35

1.2.4. Forms of reinforcement

The fibers can be placed in different configurations. Reinforcements can be processed to the following forms:

- Strands
- Mats
- Unidirectional rovings
- Woven fabrics

Strands are the easiest form, although their application is limited to specific processes such as filament winding and pultrusion (see section 1.3 for an explaination of these terms) [1]. Strands are for example used as reinforcement of concrete or in cables of bridges. Because of the limited area of application for strands, they are usually concerted into various fabrics.

One possibility is to process the strands into mats. A combination of short- and long strands are more or less randomly glued to form a mat. This results in a fabric with uniform properties in the XY-plane. This type suffers from high creep deformations and has a poor fatigue strength.

The strands can also be processed into unidirectional rovings. The strands are stitched together to form a very strong reinforcement in one direction, while the other direction is weak. In many cases it is required to have multi-axial stiffness. This can be achieved by placing the individual plies under different angles or by combination of UD-rovings and woven fabrics.

The third possibility is to process the strands into woven fabrics. The crimp of the fabric is determined by the pattern with which warp en weft are alternating, which is a function of the weave type. Available types are the plain weave, basket weave, twill weave and satin weave [6]. Figure 19 shows to which extent the stifnesses of the different fabrics are direction-dependent.

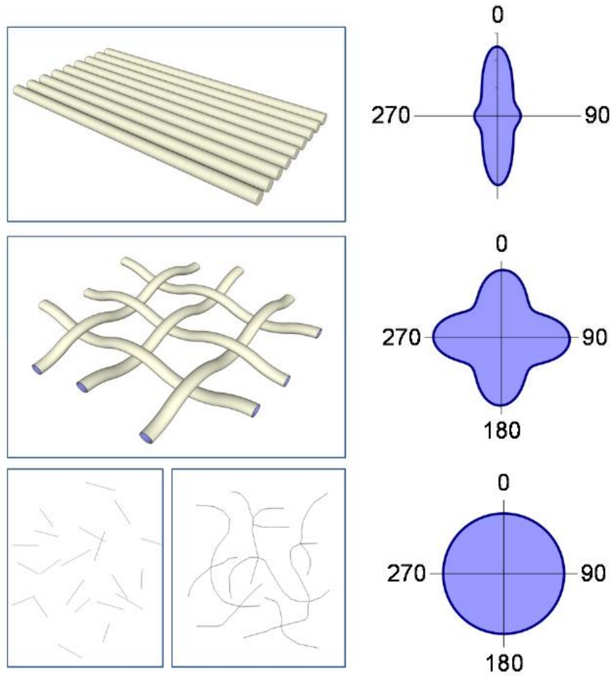

Figure 19: Polar stiffness diagram for different types of fabrics (from top to bottom: UD-roving, woven fabric, chopped strand mat) [6]

1.2.5. Comparison of FRP to steel

The specific material properties of FRP have been compared to those of steel in Table 6 and Table 7.

Table 6: Specific properties of GFRP compared to steel

Property	E-glass/polyester (50% fibers)	Steel (S235)
E-modulus	25,8 GPa	200 GPa
Maximum charasteristic strain	1,2%	20%
Maximum charasteristic stress	310 MPa	210 MPa
Safety factor	2,4-4,3	1
Maximum design stress	70-129 MPa	210 MPa
Density	1950 kg/m^3	7850 kg/m^3
Estimation of initial costs	€7,-/kg	€4,-/kg
Relative stiffness (E/ρ)	13,2*10^6 kgN/m^5	26,6*10^6 kgN/m^5
Relative strength ($\sigma_{R;d}/\rho$)	51,3*10^3 kgN/m^5	26,7*10^3 kgN/m^5

Table 7: Overview of important differences between GFRP and steel

FRP	Steel
Linear elastic up until rupture	Ductile behaviour before material failure
Many failure criteria exist due to the different failure modes and complexity of the material	Von mises criterion performs reasonibly well for failure predictions
Designs are mostly based on stiffness criteria	Sometimes strength based, sometimes stiffness based
Structural stiffness is reached by either construction of stiffeners or sandwiches	Structural stiffness is reached by construction of stiffeners

1.3. Overview of production processes for FRP

Basically, three different types of production processes for composite structures can be distinguished: open mould processes, closed mould processes and continuous processes. Within these three main types, several ways of production are possible. The selection of the most suitable manufacturing process depends on many factors, such as the required geometry, fiber-orientation, repetition factor, required fiber fraction and element size.

Each production process consists of five different steps [1]:

1.) Mixing resin and activator
2.) Dispensing resin into the mould
3.) Curing
4.) Positioning reinforcement
5.) Impregnating reinforcement with resin

The following paragraphs present additional information on the different manufacturing processes. These processes are more extensively elaborated in [1], [4] and [6]. The manufacturing process is one of the key factors for the design of composite structures. A distinction has to be made between open mould processes, closed mould processes and continuous processes.

1.3.1. Open mould processes

By application of open mould techniques the components are only on one side covered by the moulds. The following open mould processes exist [1]:

- Hand laminating: The fibers are placed in the mould. Hereafter, the resin is added by manual rolling.
- Saturation: The resin is automatically mixed and sprayed on to the mould. The other stages of the production are identical to hand laminating.
- Spray-up: Both fibers and resin are mixed before being sprayed into the mould, resulting in a random fiber orientation. The spray gun is operated by hand.
- Auto spray-up: Same technique as spray up, except that the spray gun is now automatically operated.
- Filament winding: The fibers pass a resin bath before being wrapped around a rotating former. Only a limited number of geometries and fiber directions can be achieved.
- Spray winding: A combination of auto spray-up and filament winding.
- Centrifugal casting: Resin and fibers are placed inside a cylindrical mould which is rotated at high speed.

1.3.2. Closed mould processes

During closed mould processes the components are on both sides isolated from the atmosphere. The following closed mould processes can be distinguished [1]:

- Vacuum bag moulding: Resin and fibers are placed by hand lay-up. Subsequently, a film and rubber bag is laid over the laminate and sucked to a vacuum to improve the quality.
- Pressure bag moulding: The same process as vacuum bag moulding, except that instead of a vacuum, now an overpressure is used to improve the quality of the laminate.

- Auoclave moulding: Combination of vacuum bag- and pressure bag moulding. Basically, the preparated mould is sucked to a vacuum inside a pressurized vessel.
- Leaky moulding: Reinforcement is placed in a female mould together with the resin. The male part is placed on top and the whole is squeezed by clamps.
- Cold press moulding: The same as leaky moulding, except now a hydraulic press is used to compress the moulds.
- Hot press moulding: Same as cold press moulding, except now the temperature is raised to increase the production rate.
- Resin injection: The fibers are placed between male and female mould. Resin is injected through a small gap in the mould.
- Vacuum assisted resin injection: Reinforcement is placed covered with a seal which is hereafter sucked to a vacuum. The resin is injected through the seal.
- Injection moulding: The resin and fibers are mixed before being injected between male- and female mould.

1.3.3. Continuous processes

When large quantities, high repetition and simple geometries are required, it might be useful to use a contiuous manufacturing process. The following continuous processes exist [1]:

- Continuous laminating: Resin and fibers are combined and contained between two layers of release film which act as a conveyer belt. The mix is transported through a curing oven whereafter the films are removed and the components are cut to the right length.
- Pultrusion: Reinforcement is impregnated with resin and pulled through a heated die.

1.3.4. Summary of different manufacturing processes

The different manufacturing processes and their specific properties are presented in Table 8, Table 9 and Table 10. The properties of these specific production processes are based on the the lecture notes by Kolstein [1] and the thesis by Kok [14].

Table 8: Overview of the continuous production processes

Process	Fiber volume [%]	Size range [m^2]	Specific fiber direction	Relative production costs	Relative equipment costs	Limitation part geometry	Special remarks
			Continuous processes				
Continuous laminating	10-25	<2m width	Not possible	Very low	High	Flat sheets or profiles	Only for large amounts
Pultrusion	30-65	<1m width	Not possible	Low	High	Constant sections	Results in good quality
Continuous filament winding	55-70	<2m tubes	Several directions possible	Low	High	Circular tubes only	Excellent quality

Table 9: Overview of the open moulded production processes

Process	Fiber volume [%]	Size range [m^2]	Specific fiber direction	Relative production costs	Relative equipment costs	Limitation part geometry	Special remarks
Hand laminating	13-50	0.25-2000	Possible	High	Very low	Almost no limitations	Low prodution rates
Saturation	13-50	0.25-2000	Possible	High	Low	Almost no limitations	Low quality control
Spray-up	13-21	2-100	Not possible	Low	Moderate	No fine details	Low quality control
Auto spray-up	13-21	2-100	Not possible	Low	Moderate	No fine details	Only for simple geometry
Filament winding	55-70	0.1-100	Determined by winding direction	Low	Moderate to high	Only hollow profiles	Applied in high pressure applications
Spray winding	40-60	0.1-100	Mainly determined by winding direction	Low	High	Only hollow profiles	Not suitable for high pressure applications
Centrifugal casting	20-60	0.5-100	Possible	Low	Moderate to high	Only hollow profiles	Good quality control

Table 10: Overview of the closed mould production processes

Process	Fiber volume [%]	Size range [m^2]	Specific fiber direction	Relative production costs	Relative equipment costs	Limitation part geometry	Special remarks
Closed mould processes							
Vacuum bag	15-60	0.5-200	Possible	High	Low	Complex detail difficult	Fairer finish than hand laminating
Pressure bag	15-60	0.5-200	Possible	High	Moderate	Almost no limitations	Robust mould required
Autoclave	35-70	0.25-5	Possible	High	High	Best with shallow shapes	No large forces on mould
Leaky mould	15-35	0.25-5	Possible	Low	Moderate	Best with shallow shapes	Results in a good quality
Cold press	15-25	0.25-5	Possible	Low	Moderate	Best with shallow shapes	Accurate components
Hot press	12-40	0.1-2.5	Possible	Low	Very high	Thin skin parts	High production rates
Resin injection	10-15	0.25-5	Possible	Moderate	Moderate	Almost no limitations	Low fiber content
Vacuum-assisted resin injection	15-35	1-30	Possible	Moderate	Low	Best for large, simple plates	Relatively large shapes possible
Injection moulding	5-10	0.01-1	Not possible	Very low	Very high	Almost no limitations	Only for small shapes

1.4. Structural design of composite structures

Due to the nature of fiber-reinforced polymers, the determination of mechanical properties, design rules an failure mechanisms are different than for steel. This section explains these differences and serves as a global guideline on how to design composite structures.

1.4.1. Determination of mechanical properties of laminates

To determine the material stiffness of the individual plies consisting of a combination of fibers and resin in different directions, the semi-empirical formulations of Halpin-Tsai can be used. These formulations are further explained in Appendix B).

The classical laminate theory can be used in order to determine the properties of the laminates which consist of a stacking of many different plies. The classical laminate theory is further explained in Appendix C). In order to avoid large hand calculations, software programs such as Kolibri are (freely) available to determine the laminate properties.

Generally, the strain at rupture for a fiber is smaller than for the matrix. The failure criteria are mostly based on a maximum strain, for which the fibers are governing. This maximum allowable stress can be found by mulitplication of the maximum strain by the Young's modulus of the combination of fibers and matrix.

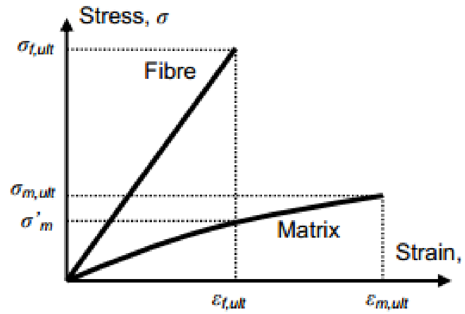

Figure 20: Stress-strain relation for fibers and matrix [18]

The schematized stress-strain diagrams for both steel and FRP are presented in Figure 21. A woven fabric composed of E-glass and polyester with a fiber fraction volume of 50% is considered to be representative.

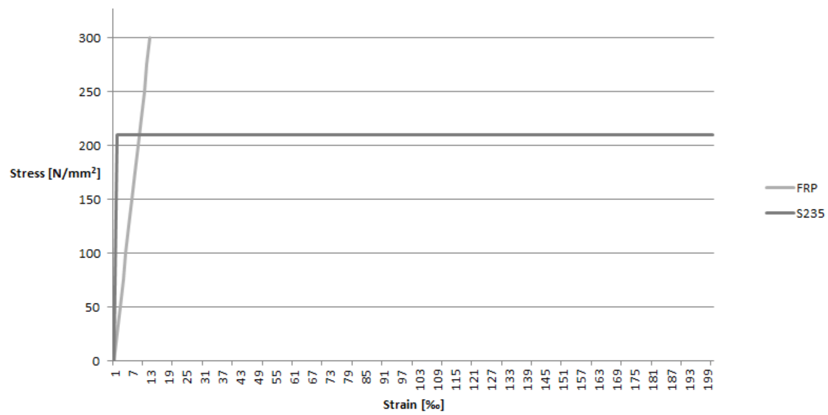

Figure 21: Stress-strain relations for both steel and an avarage FRP member

The stiffness and strain at rupture of FRP are significantly smaller than for steel. In order to increase the stiffness and strength of composite structures, a sandwich is often applied. The core consists of a low weight and cheap material such as balsawood, foam or honeycomb materials. This increases the internal lever arm and results in a larger moment of intertia and section modulus for the same amount of FRP.

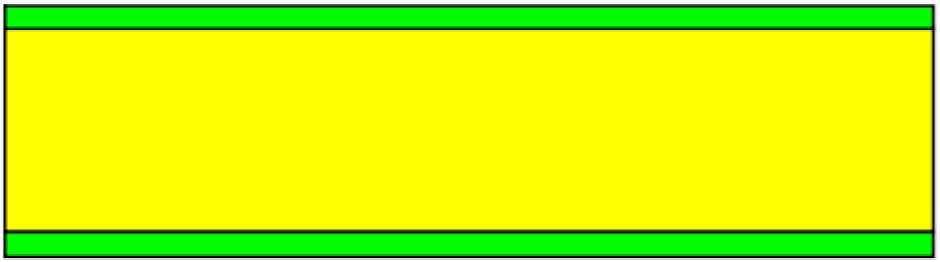

Figure 22: Classical sandwich structure [20]

A weak spot in regular sandwiches is the connection between core and skin of the sandwich. Especially during impacts, delamination between these two components is a great risk. The resistance to delaminations between core and skin can be prevented by applying the InfraCore Inside technology®. The fibers are placed in a Z-shape around the blocks of core material. This concept is visualized in Figure 23.

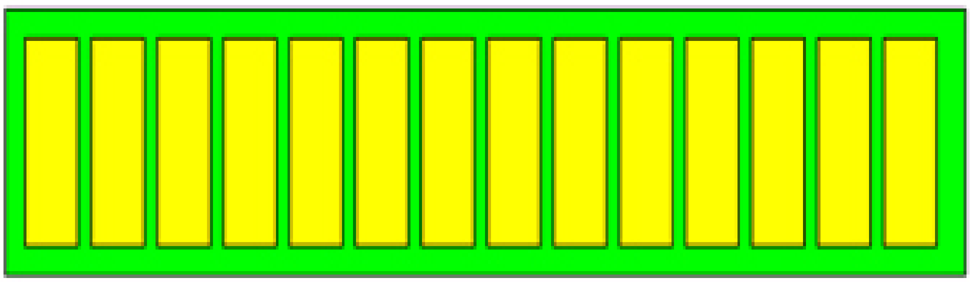

Figure 23: Sandwich equiped with InfraCore Inside technology to prevent delamination [29]

Overlap of the individual fibers results in a solid structure. This technique is applied in nearly all the bridges and lock gates constructed from FRP in The Netherlands by FiberCore [20].

1.4.2. Failure mechanisms

The laminates can fail in many different ways, on three different levels. These levels are micro failure, meso failure and macro failure. Macro failure is related to failure of large components, meso failure is related to failures on laminate level while micro failure is a result of failure within a single ply.The failure tree for fiber-reinforced polymers is presented in Figure 24. In general, every failure mode will result in failure of the entire structure, unless redistribution of loads is possible because of alternative loading paths in the FRP structure.

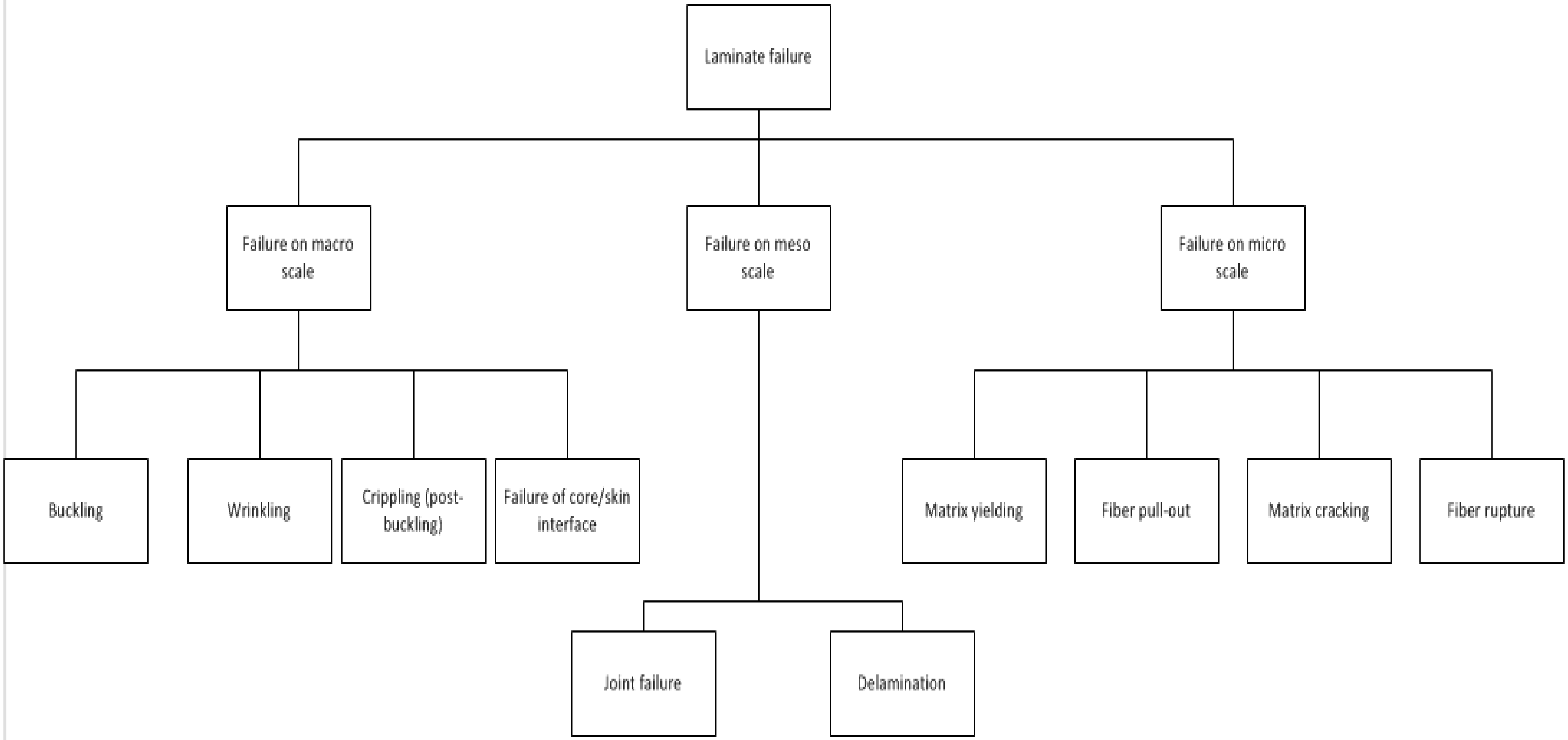

Figure 24: Failure tree for FRP structures

Macro failure consists of loss of stability of large elements which can either be caused by buckling, core crimping, skin wrinkling or skin dimpling. These different failure modes are illustrated in Figure 25.

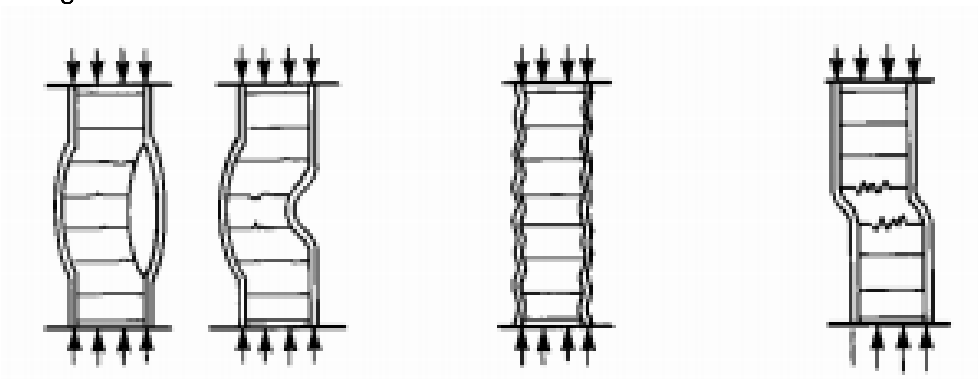

Figure 25: Failure modes for sandwich structures on macro-level. From left to right: skin wrinkling (2x), skin dimpling and core crimpling [1]

Meso failure can either be caused by delamination or joint failure. Delamination is defined as splitting, physical separation or loss of bond along the plane of layers. It can occur between the plies or between skin and core of a sandwich structure. Delaminations leads to large cracks in the structure which are not always visible because the delamination are mostly located beneath the surface. Joint failure is further discussed in section 1.4.

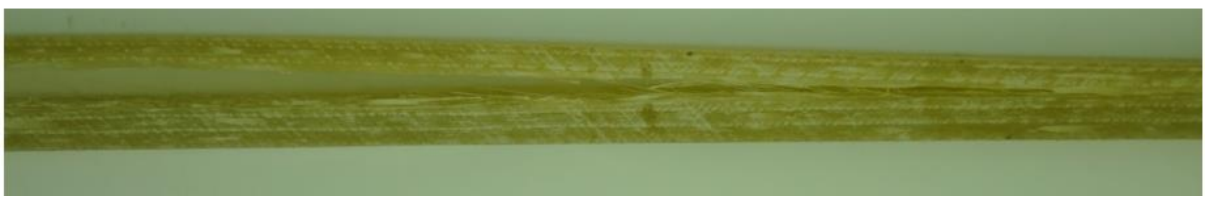

Figure 26: Delamination between plies [6]

The third level is micro failure, which is induced by failure within a single ply. This failure can be induced by matrix yielding, matrix cracking, fiber pull-out or fiber rupture. Usually, fiber rupture is governing for the design because the strains at which fibers fail is relative low (see Table 5).

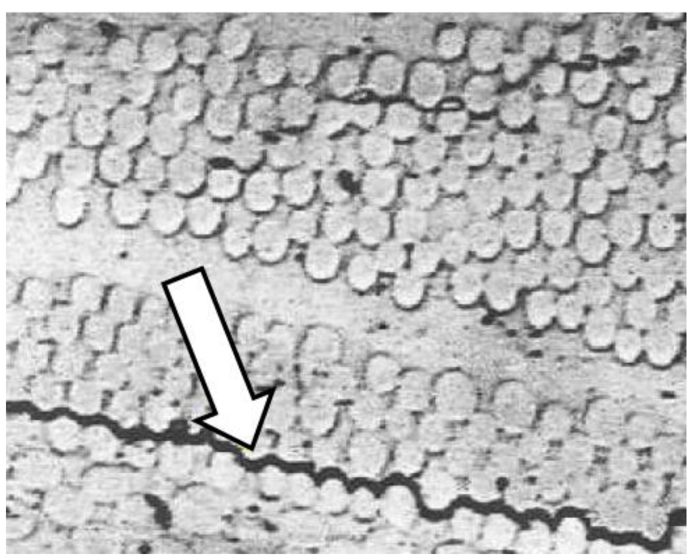

Figure 27: Example of matrix cracking [21]

As shown in Figure 21, fiber reinforced polymers show almost fully linear-elastic behaviour up until rupture. This has major implications for the material properties:

- Failure of the material happens abruptly;
- Redistribution of forces is limited to matrix yielding and damage zones;
- The von Mises failure criterion is not valid.

Instead of the Von Mises criterion, many other failure criteria are proposed to account for multi-axial stress states, all based on different (combinations) of) failure modes. The most well-known criterion is the Tsai-Hill criterion to account for micro failure within a ply. This formula is presented below:

$$\frac{\sigma_x^2}{X^2} - \frac{\sigma_x \sigma_y}{X^2} + \frac{\sigma_y^2}{Y^2} + \frac{\tau_{xy}^2}{S^2} = 1$$

Where:

σ_x = Active stress in x-direction

σ_y = Active stress in y-direction

τ_{xy} = Active shear stress

X = Maximum stress in x-direction

Y = Maximum stress in y-direction

S = Maximum shear stress

The limit strains for the different fabric types are presented in Table 11.

Table 11: Limit strains for the fibers in different directions [22]

Fabric type	ε_{1tR}	ε_{1cR}	ε_{2tR}	ε_{2cR}	ε_{12R}
UD-ply	2,4%	1,6%	0,34%	1,1%	0,58%
Woven fabric	1,7%	1,5%	1,7%	1,5%	1,4%
Mat	1,6%	1,9%	1,6%	1,9%	1,5%

In which:

$\varepsilon_{1cR} =$ Maximum compression in the main direction

$\varepsilon_{1tR} =$ Maximum tension in the main direction

$\varepsilon_{2cR} =$ Maximum compression in the secondairy direction

$\varepsilon_{2tR} =$ Maximum tension in the secondairy direction

$\varepsilon_{12} =$ Maximum shear strain

Two theories exist to describe failure of a laminate: first ply-failure and last ply-failure. First ply failure assumes that a structure fails as soon as the maximum strain in one single ply in a single direction is exceeded. This theory is very conservative since in most cases the forces are transferred to the other plies (which have their main strength in a different direction) if a single ply fails. Last ply-failure assumes that a structure only fails if all the plies fail.

1.4.3. Fatigue

Fatigue is a process which takes place after repeated (dynamic) load cycles during the lifetime of a structure. Once small cracks are formed, the cross section constantly decreases after repetition of cyclic loads. Eventually, the remaining cross section can be reduced to such an extent that it is no more able to resist the static loads.The following factors determine the resistance against fatigue for a structure [23]:

- Stress concentrations
- Amplitude of stress cycle
- Number of stress cycles
- Material
- Environment

A structure can be designed for fatigue according to two different philosophies: the safe load principle and the fail safe principle. The safe load principle is mainly used for major structures and overestimates the lifetime of the structure to minimize the risk of fatigue failure. The fail safe principle however assumes regular inspection which is able to detect and repair cracks before they become vital for the structural safety.

Just like steel, FRP is also susceptible to fatigue. The degradation process is however different for both materials. In steel structures, after a considerable amount of load cycles a small crack is formed. This small crack grows gradually after continuation of load cycles until a critical crack length has been reached and the structure collapses. Fatigue design for steel structures is very well described in the Eurocode NEN-EN 1993-1-9.

In FRP structures, fatigue is induced by many very small fatigue cracks happening at the same time. These cracks grow under repeated load cycles in different directions under different angles until the many small cracks are evolved into large cracks and delaminations [6]. Although this process seems worse than for steel, in fact it is not. Generally speaking, the S-N curve for FRP is flatter than for steel, which means that a reduction of the stress-amplitude leads to a larger gain in number of load cycles to failure. Where the tangent of the S-N curve is in the order 3 to 5 for steel on double logarithmic scale [24]. It is approximately 9 for FRP [6] [25].

The fatigue process can be characterized by three different stages. In the first stage, the stiffness of the structure is reduced by 10-20%. This stage is followed by a period where very limited reduction of stiffness occurs. As soon as the structure reaches the third and final stage, the stiffness is reduced very rapidly. The three different stages are visualized in Figure 28.

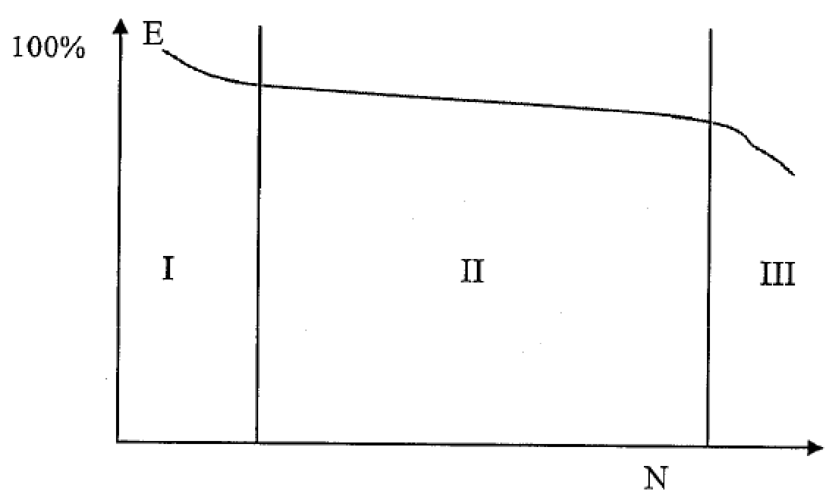

Figure 28: Three stages of stiffness reduction induced by fatigue [22]

Fatigue of FRP structures can be analyzed by three different types of models:

- Empirical models (S-N curves)
- Phenomenological models
- Micro-mechanical models

The empirical- and phenomenological models describe the time to failure and sometimes macroscopic stiffness and strength degradation, but do not provide information on damage progression within the material. This subject can be covered by micro-mechanical models.

Fatigue testing of FRP structures is an ongoing topic of research. Among others, Nijssen (2006) and Qian (2010) studied the performance of GFRP structures under cyclic loading during their promotion at Delft University of Technology.

Cheng Qian [26] designed a micro-mechanical model in order to predict fatigue failure of wind turbines. The model is valid for unidirectional GFRP laminates loaded by axial tension-tension cycles. The only input which is required for his model are the material properties of fibers and matrix. Fatigue behaviour is simulated by considering sequential fiber breakages as the dominant mechanism on micro-scale. The results on micro-scale are geometrically scaled up to analyze the fatigue behaviour of entire structures.

Nijssen [27] studied the performance of S-N curves to describe fatigue behaviour of different GFRP laminates. The two models which were investigated are the Miner's sum method and the strength-based life prediction. In the Miner's sum, the results of a counting method and constant amplitude fatigue behaviour description are converted into a damage parameter. This parameter only indicates wheter or not failure has occured, but the damage is not quantifiable. In the strength-based model, the effect of each load cycle on the residual strength is calculated. Failure occurs when the loads exceed the residual strength. Nijssen concluded that the strength-based life prediction results in more conservative results than the Miner's sum method. The better performance of the Miner's sum method is however deminshed by the larger computational effort required. Therefore, Nijssen recommends further research in improvement of the description of the constant life diagram.

The selection of the type of fabric is important for the fatigue resistance of fiber-reinforced polymer structures. UD-rovings show the best fatigue resistance, followed by woven fabrics. Mats show the worst fatigue properties of the possible forms of reinforcement.

1.4.4. CUR 96

Because the material is still relatively new in the civil industry, no globally acknowledged design codes are yet available. In the Netherlands, a group is currently working on such a code. The first step towards this code is available in the form of CUR report 96. This report describes among other things the safety factors which should be applied, possible stacking methods and some material properties. This document will be considered as the leading document for this feasibility study. More information on the CUR 96 can be found in Appendix A).

Instead of the multi-axial strain states, the CUR 96 recommends an overall maximum strain to predict charasteristic values for micro-failure. This maximum strain is equal to 1,2% for regular structures while the maximum strain for structures where any leakage is unacceptable is limited to 0,27%. This overall-strain method is valid for fiber volume fractions of at least 20%, and the four main directions each need to be equiped with at least 15% of the total amound of fibers [25].

Delaminations are covered by comparing the interlaminar shear stresses and peel stresses with the design values of the strength of the resins. The charasteristic values of these strengths are presented in Table 13. These values only need to be devided by material factors $\gamma_{m,1}$ and $\gamma_{m,2}$ to obtain the design values of the strength.

Table 12: Charasteristic values of the strength between the plies [25]

Resin type	Interlaminar shear strength	Interlaminar peel strength
Polyester	20 MPa	10 MPa
Vinylester	25 MPa	12,5 MPa
Epoxy	30 MPa	15 MPa

The charasteristic values of the strength of the fibers need to be divided by a material factor and a conversion factor in order to obtain the design values. For the resin dominated failure states, division of the interlaminar shear- and peel stress just by material factors γ_{m1} and γ_{m2} is sufficient. Table 13 shows the safety factors which need to be applied for different limit states. More information on the individual terms of the safety factors can be found in Appendix A).

Table 13: Safety factors which have to be applied for different limit states [25]

	Ultimate limit state			Servicability limit state		
	Strength	Stiffness	Fatigue	Deformation	Vibrations	Cracking
$\boldsymbol{\gamma_{m,1}}$	X	X	X	X	X	X
$\boldsymbol{\gamma_{m,2}}$	X	X	X	X	X	X
$\boldsymbol{\gamma_{ct}}$	X	X	X	X	X	X
$\boldsymbol{\gamma_{cv}}$	X	X	X	X	X	X
$\boldsymbol{\gamma_{ck}}$	X	X	-	X	-	X
$\boldsymbol{\gamma_{cf}}$	-	X	-	X	X	X

In which:
$\boldsymbol{\gamma_{m,1}}$ = Material factor related to the uncertainties in material properties
$\boldsymbol{\gamma_{m,2}}$ = Material factor related to the production process
$\boldsymbol{\gamma_{ct}}$ = Conversion factor related to temperature effects
$\boldsymbol{\gamma_{cv}}$ = Conversion factor related to moisture effects
$\boldsymbol{\gamma_{ck}}$ = Conversion factor related to creep effects
$\boldsymbol{\gamma_{cf}}$ = Conversion factor related to fatigue effects

Stability of components need to be tested according to the classical mechanics formula. The Young's moduli of the material need to be reduced by material factors which are also discussed in Appendix A).

The CUR 96 makes use of a strength-based life prediction for fatigue failure. Both the average stresses in the material and the amplitude of the stress-cycles need to be incorporated in the model. The model is only valid for uni-axial load situations. For multi-axial load situations, CUR 96 recommends to perform the fatigue-analysis on the two main-directions of the laminate.
If the mean stress in the material is equal to zero, the following formula can be used to determine the number of load cycles until failure:

$$N_f = \left(\frac{\sigma_{amp} * \gamma_m * \gamma_c}{\sigma_{Rk}}\right)^k$$

$N_f =$	Number of load cycles up until failure of the structure
$\sigma_{amp} =$	Amplitude of the load cycle
$\gamma_m =$	Material factor
$\gamma_c =$	Conversion factor
$\sigma_{Rk} =$	Charasteristic value of the maximum strain
$k =$	Slope of the S-N curve; equal to 10 for glass/epoxy and 9 for glass/polyester

For a mean stress unequal to zero, the following formulae can be used:

$$N_f = \left(\frac{\sigma_{amp}}{\sigma_{Rd}[1 - \frac{\sigma_{mean}}{\sigma_{Rd}}]}\right)^k$$

$$\sigma_{Rd} = \frac{\sigma_{Rk}}{\gamma_m * \gamma_c}$$

$\sigma_{mean} =$	Mean stress in the material

The damage caused by variable loading amplitudes need to be based on the linear damage rule of Miner:

$$D = \sum_{i=1}^{M} \frac{n_i}{N_i}$$

$n_i =$	Number of load cycles with a certain amplitude
$N_1 =$	Number of load cycles until failure for load cycles with a certain amlitude
$D =$	Damage number, the structure fails if $D = 1$

The number of load cycles N until failure as a function of the stress amplitude divided by the design strength $\sigma_{amp} / \sigma_{Rd}$ (which has been given the name v) is presented in Figure 29.

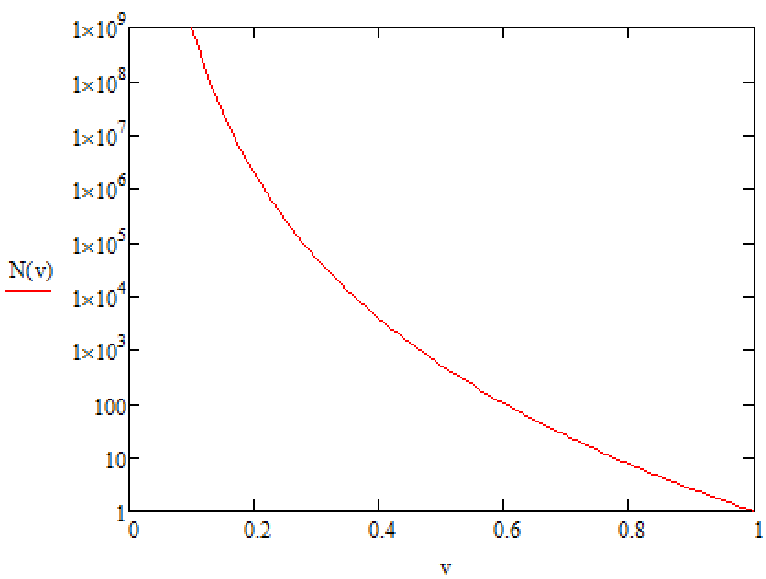

Figure 29: Number of loads until failure as a function of the stress amplitude divided by the design strength

Where for steel, the resistance against fatigue is mainly determined by the load concentration factors induced by the details rather than material quality, for FRP structures the opposite is recommended by the CUR96. This document recommends to relate the fatigue resistance to the static strength of the material and the average stress level [22]. This guideline does not provide any information on fatigue strength of joints neither does it provide any information about the actual effects of fatigue failure. It can be concluded that this method can only be used to check if fatigue failure can be ruled out on beforehand. If the unity check appears to be close to 1, further research is required in the form of physical tests.

1.5. Joints

Joints form almost exclusively weak spots in composite structures [1] [6]. Therefore it is important to keep the number of connections to a minimum. If connections in composites are inevitable, they can be realised in two ways: by mechanical fastening or by adhesive bonding. The selection of the joint type depends among other things on whether the joint needs to be dismountable, the importance of weight and the environmental conditions of the structure.

1.5.1. Mechanichally fastened joints

Bolts are mostly applied if the connected members need to be replaceable. Another advantage of application of bolts is that, unlike adhesively bonded joints, it is a proven technology. Besides, bolted connections are less sensitive to peel stresses. The disadvantage of bolts are the stress concentrations around the bolts which can be up to 7 times the average stress as a result of the non-ductile behaviour of FRP. Besides, application of bolts result in an added mass of the structure, which is especially an issue if the joints are applied in highly dynamic objects (e.g. airplanes, wind turbines). Figure 30 shows the different failure modes which need to be considered during the design of mechanically fastened connections.

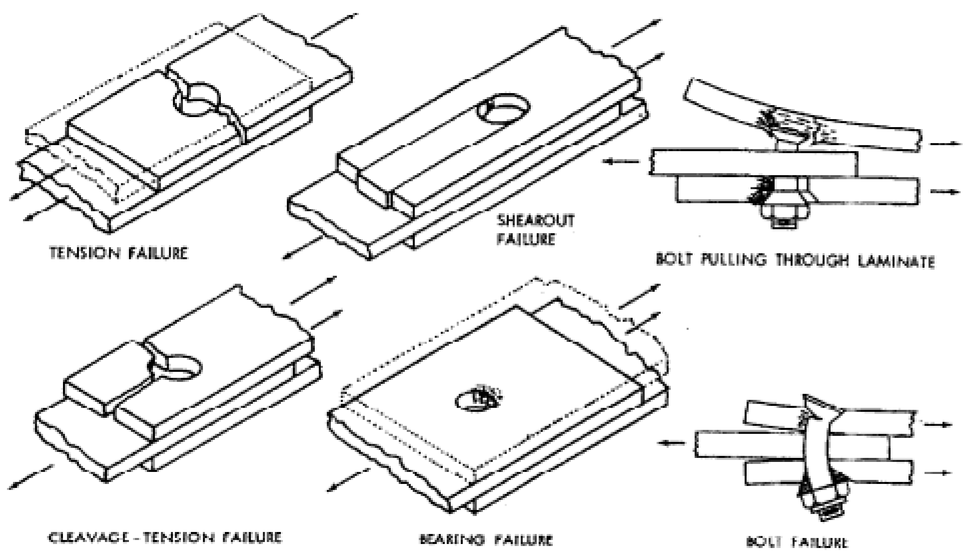

Figure 30: Failure modes for mechanically fastened joints [28]

Peak stresses induced by mechanically fastened joints can be reduced by integration of inserts within the laminate during production. These inserts take care of a better introduction of forces, a feature which is especially useful for sandwich structures. Another way to reduce the stress concentrations is by combining bolting and adhesive bonding.

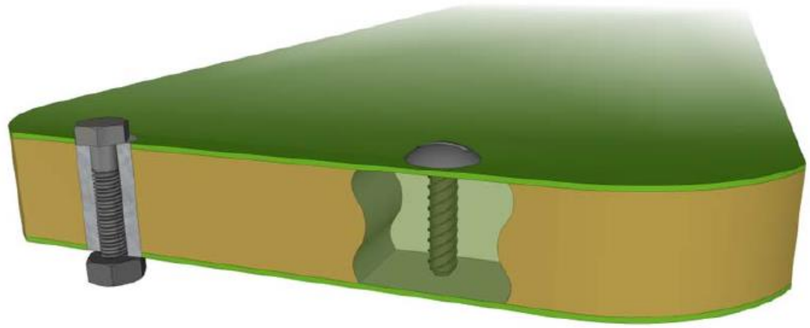

Figure 31: Insert placed inside a sandwich panel [6]

1.5.2. Adhesively bonded joints

Adhesively bonded joints are cheaper to apply than bolted connections. Besides, the forces are distributed over a larger surface which results in lower peak stresses. Disadvantages of adhesively bonded joints are the fact that the surface needs to be prepared before assembly and that uncertainties related to application of these joints in combination with harsh environments.

Figure 32 shows the different failure modes which need to be considered during the design.

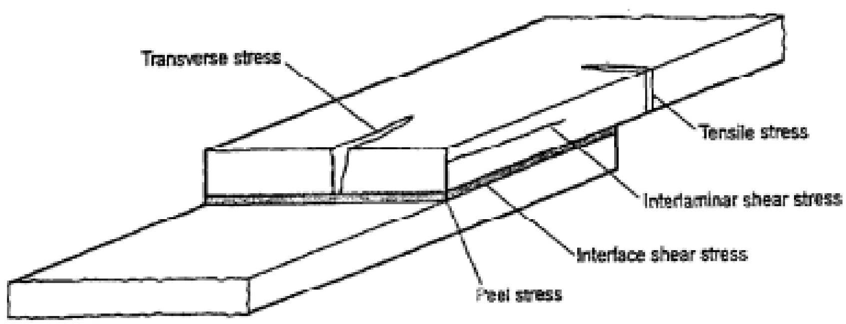

Figure 32: Failure modes for adhesively bonded joints [29]

High peel stresses (stresses perpedicular to the layer of glue) should be prevented by selection of a decent joint configuration. It is better to design an adhesively bonded connection on pure shear. Some examples of good- and bad joint configurations are presented in Figure 33.

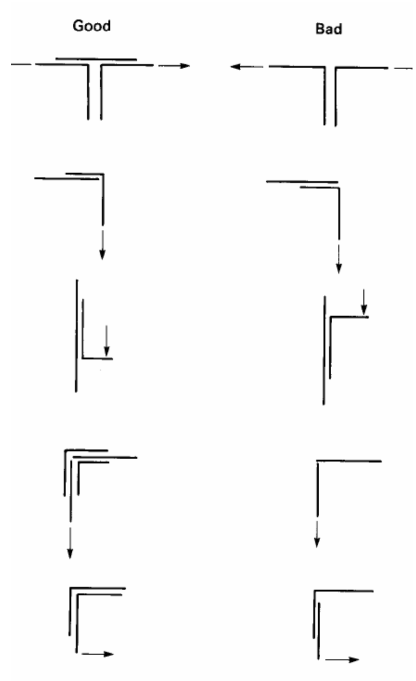

Figure 33: Examples of good- and bad joint configurations for adhesive bonding [1]

Several geometries are possible for the overlap area between connected members in adhesively bonded joints. As a general rule, one can say that the simplest configurations are also the weakest ones. The most common types are compared based on relative strength in Figure 34.

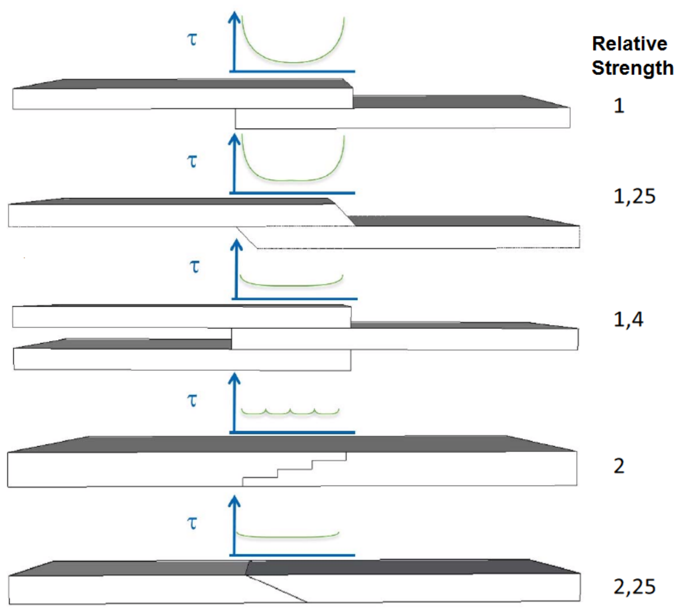

Figure 34: Relative strength of the connection for several overlap areas of adhesively bonded joints [6]

Increasing the thickness of the layer of glue results in a higher strength of the joint because redistribution of shear stresses can happen more easily. However, the stiffness of the joint is decreased resulting in larger deformations of the structure.

1.6. Sustainability of FRP

The sustainability and environmental Impact of fiber-reinforced polymers are examined twice. During both assessments, bridge decks have been designed in different materials after which the environmental impact has been determined based on available databases which relate the masses and volumes to the environmental impact. During the first study, only experts from the FRP-branche were involved with the design assessment. This resulted in a lot of critics from the steel and concrete branches. In 2013, BECO decided to re-examine the sustainability, but now with a team which also consisted of members from the steel, timber and concrete branche (which were Bouwen met Staal, BFBN and VVNH). The results of both assessments were completely different. The following section describes the two assessments after which a conclusion is drawn on the sustainability of FRP compared to steel, concrete and timber.

1.6.1. BECO (2009) [30]

The first study on the sustainability of fiber-reinforced polymers has been performed by BECO in 2009. BECO composed a team with members from two companies specialized in fiber-reinforced polymers (which were FiberCore and DSM Resins) together with the FRP branche organizations VKCN and SenterNovem.

As a case study, a bridge deck has been designed and optimized in glassfiber-reinforced polymers (GFRP) and carbonfiber-reinforced polymers (CFRP). These designs have been compared to designs from steel and concrete on Energy-consumption, CO2 footprint and an ECO-indicator over the lifetime of the structure. The designs from steel and concrete are not fully elaborated but are solely based on source data and reference projects. The considered bridge had to be able to resist traffic class 60, had a length (between the sheetpiles) of 11,85 meters and a freeboard of 1,3 meters was required above the high water of 1,0 m+NAP. The considered lifetime for the bridge was equal to 100 years, in which the two FRP bridges only had to be moved once while the steel- and concrete bridges had to be fully replaced after 50 years. The following stages are taken into account: construction, maintenance & repair, relocation and end of life. The software program which have been used to examine the sustainability is SimaPro 7.1.8, while the input data has been received from the database EcoInvent 2.0.. The results of the study are presented in Table 14.

Table 14: Results of the study to sustainability of different materials (2009)

Material	Energy-consumption (GJ)	Carbon foot print (ton CO2 eq)	Eco-Indicator (Points)
GFRP	652	75	3950
CFRP	2156	103	11398
Concrete	1978	145	12858
Steel	3380	178	12736

According to this study, GFRP is by far more sustainable than the three other materials on all three considered criteria. This conclusion does not have to be entirely true however, because the study has three main drawbacks. Firstly, only experts from the FRP branches were involved, which makes the study partisan. Secondly, the level of detail of the four designs is unequal: while the tweo FRP bridges are fully optimized, the bridges from steel and concrete are only based on reference projects. Thirdly, the bridges from FRP are considered to be completely free of maintenance and are considered to have a technical lifetime of 100 years, while this has not been sufficiently proved.

1.6.2. BECO (2013) [31]

Due to the criticism from the steel and concrete sectors, BECO decided to re-examine the sustainability of the different materials in 2013, but now with experts from all material sectors involved in order to obtain more reliable results. The sustainability of concrete, steel, timber and GFRP are examined during this study. In order to do so, both a cycle bridge and a heavy traffic bridge are examined. Each sector involved was responsible for the design of the bridges in their field of expertise. The starting points for the design are presented in Table 15. The full list of functional requirements can be found in the original report by BECO [31].

Table 15: Starting points for the case study studies selected to examine the sustainability

	Cycle bridge	Heavy traffic bridge
Free span	14 m	24 m
Width	3 m	12 m
Loads	5 kN/m^2+ emergency vehicle	Traffic class 2
Technical lifetime	50 years	100 years

The following stages are identified for the elaboration of the sustainability of the different materials: production of materials, transport, construction, maintenance and end of lifetime. The enviromental costs indicator (MKI in Dutch) is considered to be governing for the sustainability. Data on this subject has been extracted from DuboCalc and the Dutch National Environmental Database. The results of this study are presented in Figure 35 and Figure 36.

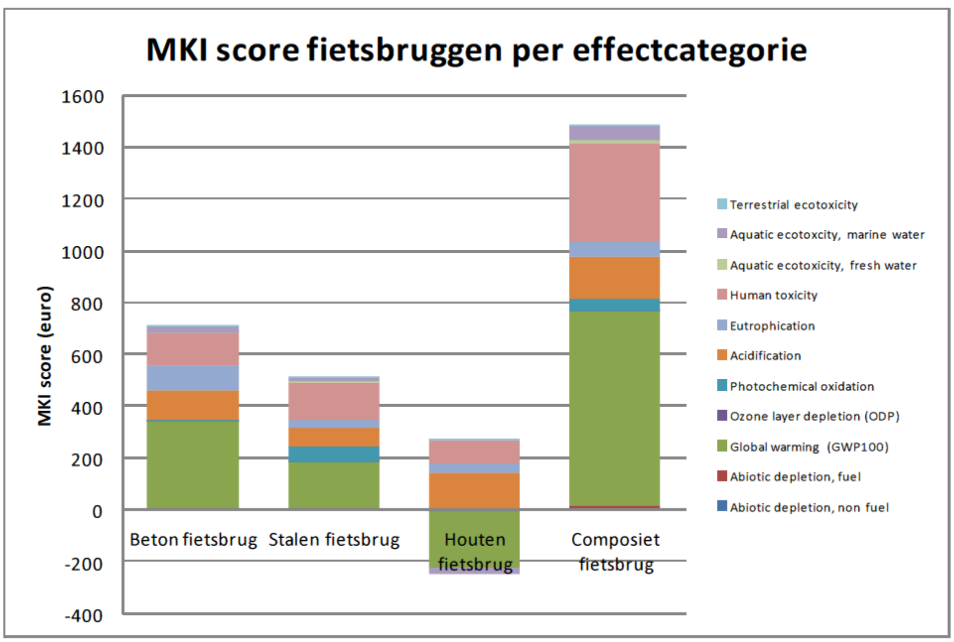

Figure 35: Environmental costs indicator for the cycle bridge, expressed in euros

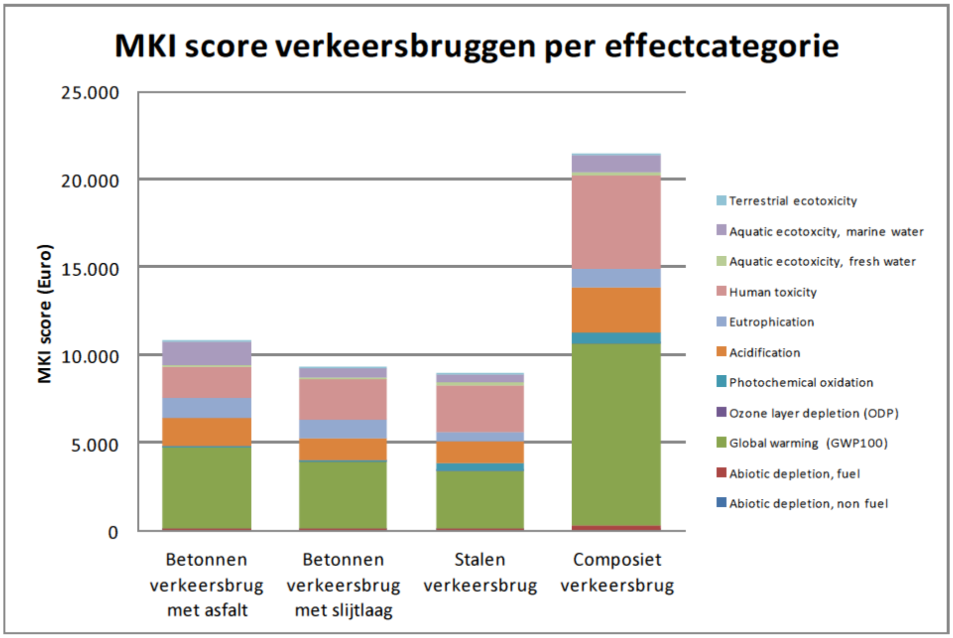

Figure 36: Environmental costs indicator for the heavy traffic bridge, expressed in euros

From this study, the exact opposite conclusion is drawn: FRP turns out to be the least sustainable for both the cycle bridge and heavy traffic bridge. The main reason for this large difference is that this study does not allow a lifetime of 100 years for composite bridges. Besides, the boundary conditions and functional requirements for these bridges are unfavourable for FRP compared to the other materials [32].

It seems that no general conclusion can be drawn on the durability of FRP compared to other materials based on these two studies. Both studies have some major drawbacks which make the results not fully representative. The uncertainties related to the lifetime of composite structures is one of the main reasons why general conclusions can not be drawn. Besides, new technologies in the relatively young FRP sector will possibly improve the sustainability of the material in the near future.

1.7. Durability

The material does not suffer from any corrosion or rotting processes. FRP does however suffer from UV-radiation and osmosis. Osmosis is the process that takes place by absorption of water. The water results in resin swelling and osmotic pressures inside the structure. The effects are degradation of technical properties due to the loss of stiffness in the resin, plasticization and debonding stresses across the fiber resin interface [10]. These properties can lead to a strength reduction of approximately 30%, which is covered by a safety factor in the CUR 96. Next to the technical degradation, also esthetical degradation takes place. The absorbed water results in blistering of the surface. Osmosis can be prevented by application of a gel coat with a thickness of 1-2 millimeters.

Figure 37: surface of a FRP-structure which is affected by osmosis [6]

UV-radiation only affects the outer surface of the FRP structure. Structures which are exposed to sunlight lose their original colour and sheen, resulting in a bad-looking surface. Technical degradation does not take place in thermosets, but to preserve the esthetics of the structure, a coating is required which consists of a pigment and UV-stabilizator. The pot life of this coating is however limited: a UV-resistant coating functions for approximately 25 years [32]. Before a new coating can be applied, the surface first need to be cleaned and dried.The old coating does not have to be removed.

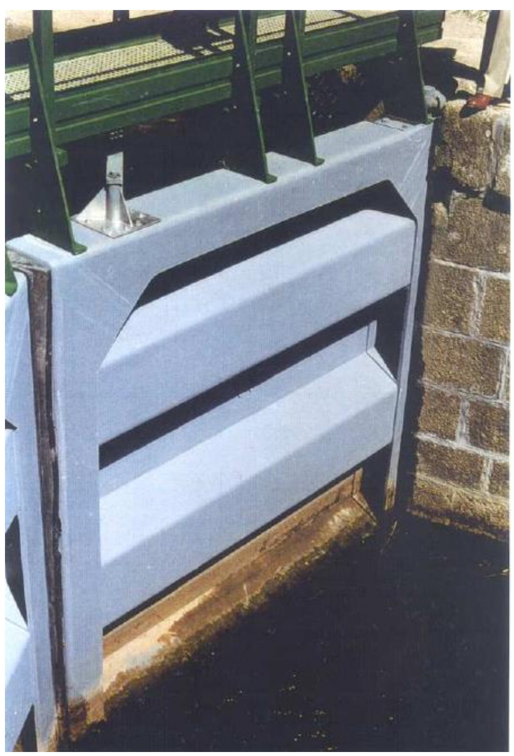

Figure 38: Example of loss of esthetics of the composite lock gate in France [5]

1.8. Monitoring

It is essential to monitor the structural behaviour of the material in order to detect risks and damages before they become vital. It is often not possible to detect anomalies in the material visually. The top layer can still be undamaged while the subsurface has failed locally, for example by delamination, wrinkling, or debonding due to impact. Several measuring techniques are available which penetrate through the material to view these subsurface failures. The following paragraphs serve as an overview of the different techniques which are available to monitor the performance of composite structures, mostly originating from the aviation industry.

Quality control during production
A large part of the anomalies can be prevented by good quality control during production. It is recommended to set up a guideline which is strictly followed by the production employees [33]. Among other things it is important to verify the correct fiber lay-up, fiber volume fraction and absence of voids during production.

Optical metrology
Optical metrology needs to be performed after production of the parts. It is essential to measure the dimensions of the manufactured parts and to see if they are in agreement with the design specifications. Optical metrology is especially important when small tolerances are required. Small adjustments to the geometry can be made by sawing, cutting or drilling.

Ultra-sonic inspection (A-scan, C-scan)
Another way to detect irregularities under the surface is by ultra-sonic inspection. This can either be done by A-scanning or C-scanning. A-scanning is a technique in which a sonic signal is transduced at a single position at the surface and penetrates through the object. The signal reflects on the object and the energy of the returned signal is registered. The result is a diagram which shows the reflected energy as a function of time. Multiplication of the time by the wave celerity results in the reflected energy over the thickness of the investigated object. Peaks or drops in the reflected energy are a sign of irregularities. C-scanning makes use of a sonic signal which is (mostly automatically) moved along the surface of the structure in a regular pattern. The result is a depth averaged echo. Strong variations in the returned signal show discontinuities in the material. This method is faster than A-scanning but also requires more expensive gear.

Batch witness panels
Another method to test the performance of the material is to attach batch witness panels to the gate which can easily be dismounted. The panel can subsequently be subjected to mechanical tests to investigate the mechanical properties and see the material performance on the long term.

Fiber optic sensors
Fiber optic sensors are mainly used in aviation for in-flight monitoring because of their low weight and low electrical power consumption. Sensors are integrated in the structure and register the performance of the structure while being in function.

Once a structure from fiber-reinforced polymers is damaged, comsetic repair can take place by vacuum injection or hand lay-up, although repair of highly loaded structures does in many cases not result in a full recovery of the original strength [6]. The watertightness of the repaired structure can still be guaranteed.

1.9. Initial costs related to application of FRP

The initial unit costs related to application of FRP depend on many variables. The most important parameters are the resin- and fiber type, fiber fraction, geometry of the structure and the selected production process. Three different sources are used to arrive at an estimation of the initial costs for application of FRP in lock gates: the thesis of Kok [14], a report of Rijkswaterstaat [34], and a bid by FiberCore [35].

Kok [14] splitted the initial material costs into resin costs, fiber costs and labour costs. The material costs are extracted from an FRP supplier while the labour costs are roughly estimated based on an expert opinion. It was concluded that the initial material costs for a combination of E-glass fibers and a polyester resin are somewhere in between €4,- and €7,- per kilogram.

The second document which has been consulted is the report on unity costs for construction and maintenance of civil structures by Rijkswaterstaat [34]. The costs extracted from this report are not very accurate because the document has been published in 2004 while recent developments in production processes and moulding technology may have resulted in changes in the unity prices. Besides, the document does not make any distinction between bridges, lock gates or other load bearing structures for the unity prices while different geometries will result in different unity costs. This report concludes that the unity prices for FRP in these load bearing structures are around €24,- per liter, which is approximately €12,- per kilogram.

The third document which has been used in order to find the initial material costs is a bid by FiberCore in which 6 options are stated for the design of two cyclist bridges near Harlem. Although the geometry and function is different to lock gates, the production process and material is the same. Based on these 6 design, an average unity price of €8,- per kilogram is found. The costs for lock gates may be a little bit higher due to a more complex geometry and a larger durability which is required because of the harsher environmental conditions.

Based on these three documents, a unit price of approximately €9,- per kilogram seems reasonable as a rough estimation of costs for application of FRP in large lock gates.

1.10. Design decisions for the case study

From an economical point of view, a combination of E-glass and polyester seems to be the most attractive material composition for composites in lock gates. Carbon- and aramyde fibers show better mechanical properties, but the initial costs are too high to be possibly competitive with steel. The manufacturing process can not be determined on beforehand. It holds close with the shape and dimensions of the gate. It seems likely that any large plates will be produced by vacuum injection. The CUR96 will serve as the design guideline for the case study. The stiffness of the material will be calculated on micro-scale by the formulations of Halpin-Tsai while the laminate properties are calculated with Kolibri, a computer program which is based on the classical laminate theory.

2. Introduction to navigation locks

This chapter serves as a general introduction to navigation locks. The primary target of this chapter is to provide general information on the functions and on the different elements of locks. The second objective of this chapter is to investigate what type of lock gate is most suitable for application of fiber-reinforced polymers in locks with a relatively large span (>20 m). The third and final objective of this chapter is to select the material to which the performance of FRP in large lock gates will be compared.

The first paragraph of Chapter 2 consists of a review on the functions of locks. This is followed by an overview of the important components of locks together with their specific functions. The third paragraph zooms in on one of the most important elements of the locks, which are the lock gates. The most frequently applied types of gates are mentioned and their specific advantages and disadvantages are discussed after which the most suitable type of gate is selected for application of FRP. This chapter is concluded with an investigation on the materials which are at present most frequently applied in lock gates.

2.1. Functions of navigation locks

A large part of the Dutch flood defence system consists of dikes and dunes. Heightening of the levees along the rivers and sea allows for higher water levels and increases the discharge capacity of rivers without flooding of the hinterland. Although this solution is in many cases very effective, at river bifurcations, confluences or road crossings construction of dikes is not an option since this would not allow for the passage of vessels or road traffic.

A solution is found in the application of storm surge barriers or locks at these positions. This report focusses on navigation locks, and particularly on their gates. In case of extreme water levels, the structure forms a barrier against the water to protect the hinterland. During regular conditions, a water level difference between the two waters which are connected by the lock are maintained while the vessels can pass by means of locking. The process of locking is visualized in Figure 39.

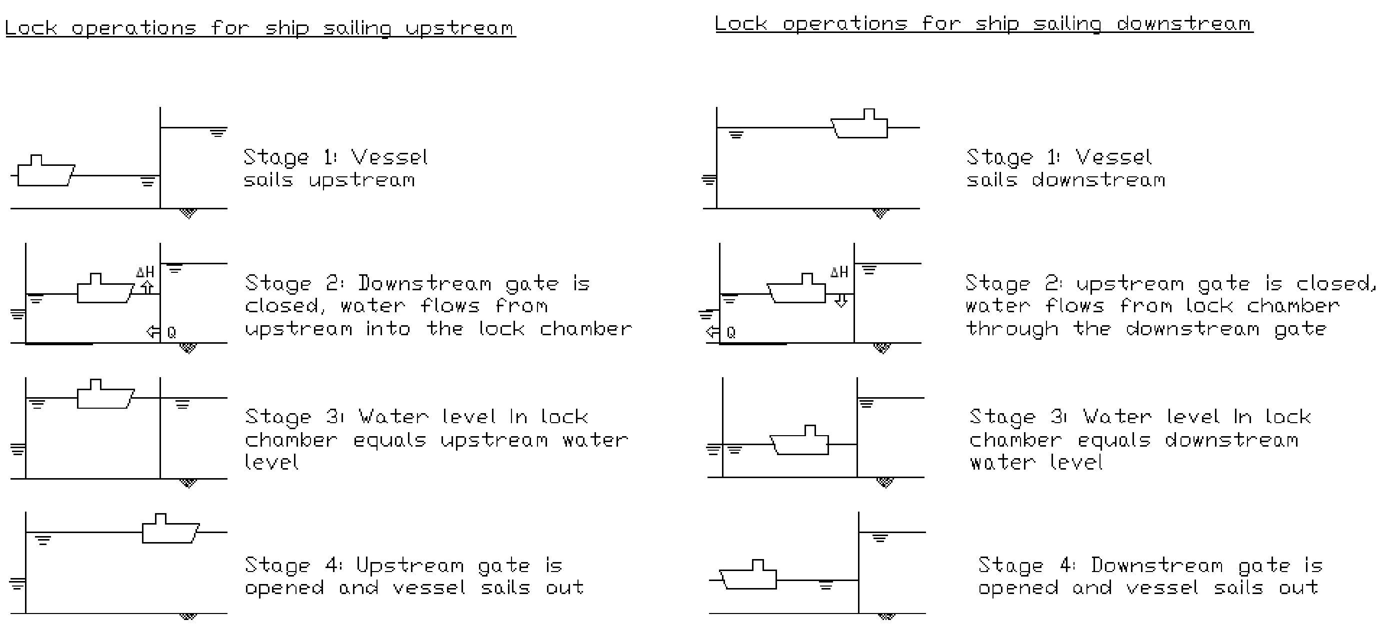

Figure 39: locking cycle for a ship sailing upstream and downstream

Locks are mostly positioned next to a weir, near a river mouth or at the border between different dike rings. Navigation locks form a special part of a larger water defence system consisting of dikes, dams, dunes and other water retaining structures. The safety level of the locks should always be considered in combination with the other failure mechanisms for dike rings, so that the prescribed safety level of the top event (which is flooding of the dike ring) is guaranteed.

Navigation locks fulfill the following three functions [36]:

- Retaining of water
- Allowing the passage of ships
- Water quality control

2.2. Main elements of navigation locks

In order to facilitate navigation while also preserving its water retaining function, a typical navigation lock consists of the following elements: a lock chamber, lock heads, seapage screens and lock gates. Besides, the lock approach is equiped with different elements to ease the navigation such as waiting berths and guide walls. The functions of the different components are furter explained in the following paragraphs. Figure 40 shows the overview of a typical lay-out of a lock complex.

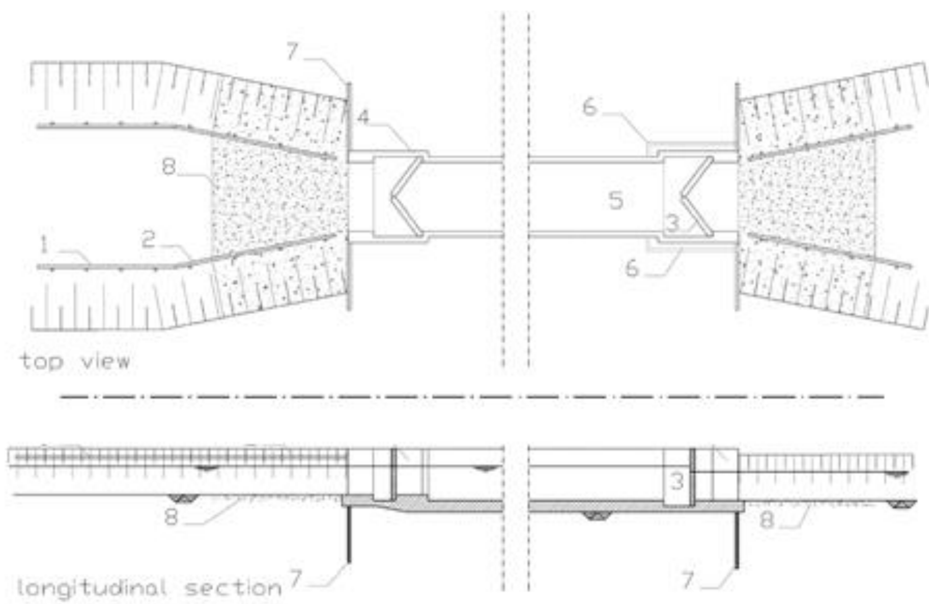

1. Waiting- or lay-by berths
2. Guard- or guide wall or lead-in jetty
3. 'Closing elements' – lock gates
4. Lock heads
5. Lock chamber
6. Filling and emptying system
7. Cut-off walls and screens (sheetpiles) to prevent piping
8. Bottom protection

Figure 40: Typical lay-out of an inland navigation lock [36]

2.2.1. Lock chamber

The function of the lock chamber is to seperate the water on the inside from the surrounding area. The walls and floor of the lock chamber need to be able to resist the forces acting on the structure during construction, in times of high water levels and in case of maintenance works. The latter stage should also be checked for floatation. Sometimes, tension piles or a thick layer of underwater concrete are required to prevent this phenomenon. For a preliminary design, the Dutch textbook “Ontwerp van Schutsluizen” [37] provides information on required dimensions of the lock chamber which is related to the CEMT-class of the lock.

2.2.2. Lock heads

The main function of the lock heads is to facilitate the gates and its associated equipment. The lock head supports the lock gate and has to resist relatively large forces. Generally, a relatively heavy structure is required to resist these forces. It should be checked whether the bearing capacity of the soil is sufficient to provide horizontal- and vertical stability and to prevent overturning of the structure. The stability can be improved by enlargement of the bottom slab, soil improvements or by placing piles underneath. Possible lay-outs and design methodologies are further elaborated in [37] and [36].

2.2.3. Seepage cut-off screens

In order to prevent a loss of stability of the structure induced to piping, locks are often equiped with seepage cut-off screens. The function of these screens is to increase the seepage length and thus increasing the resistance of theflow of water underneath and along the lock heads. The required seepage length can be determined by the relatively simple formulae of Bligh and Lane [36] or by finite element calculations for more complex geometries. The most important parameters are the design head difference, soil type and horizontal- and vertical seapage length. The position of the seepage screen also affects the upward water pressures underneath the locks. Additional bottom protection should be considered as an alternative for cut-off screens.

2.2.4. Lock gates

One of the main elements of a lock are the movable gates. Failure of locks is mostly related to the failure of the gates: either because the gates fail to close or because of structural failure of the gate (e.g. by ship impact). The lock gates should on the one hand allow for a safe and quick passage of the ships while on the other hand guarantee the structural safety during extreme (hydraulic) conditions. Besides, drainage of water needs to be possible in order to guarantee the water quality and to regulate the supply of water downstream. The different types of gates and their specific properties are further elaborated in paragraph 2.3.

2.2.5. Filling- and emptying systems

In order to fill- and empty the lock chamber, different levelling mechanisms are possible. Locking of vessels can either be achieved by discharging through valves in the gate, culverts underneath the lock head or longitudinal filling systems through culverts. This section describes the different types of filling- and emptying systems and their specific properties. The filling- and emptying system should be designed in such a way that an optimum is found between lock cycle times (or waiting costs for vessels), construction costs and mooring forces of the vessels.

The lock cycle times related to filling- and emptying of the lock chamber are a function of the initial head difference, surface area of the lock, size of the valves and lifting time of the valves. The construction costs for the system are a function of the chosen type and size of the valves, stilling chambers and culvert system.

The mooring forces are caused by translation waves, change of impulse over the length of the vessel, friction, waterjets against the bow, and density differences [37]. According to Rijkswaterstaat, these forces should be limited to a maximum of approximately 0,1% of the total mass for inland vessels. The mooring forces are a function of the type of levelling system, size of the valves, amount of valves, lifting time and the distance between gate and vessel.

The next section describes the three different types of filling- and emptying systems, together with their area of application, advantages and typical design aspects.

Valves in gate

This type of levelling system is mostly applied for gates with a small lifting height (<6m). Although this is from structural point of view the cheapest solution, the forces exerted on the vessels become very large for larger head differences. The position of the valves greatly influence the design: valves near the bottom lead to large flow velocities near the bottom and thus require a large and expensive bed protection. On the other hand, the higher the valves are placed, the larger the forces exerted on the vessels which results in larger mooring forces. An alternative can be not to moore vessels close to the gates, but this results in a reduction of the effective lock length. The valves should at least be positioned below the lowest design water level at which locking still occurs to be able to level the water.

The valves are typically opened and closed by vertical translation. The velocity with which the gates are lifted are typically in the order of 4-8 mm/s. The total lifting time of the valves is an important parameter for the lock cycle time. When the lifting time is short, the maximum discharge capacity is quickly reached which results in a short cycle time. This however also leads to large mooring forces.

The moving equipment is positioned above the water line to prevent extensive maintenance work. The valves are placed on the high water side of the gate, so that the water pressure pushes the valves against the gate to guarantee the watertightness of the connection. The valves are mostly attached to the driving equipment by cilinders. The valves move along vertical, mostly U-shaped, profiles equiped with a strip of UHMPCE to reduce the friction.

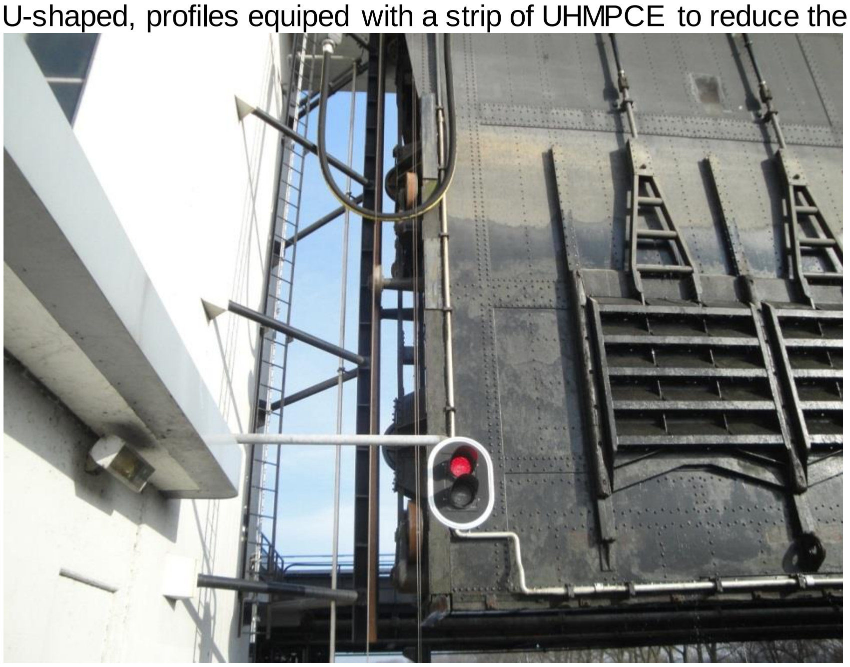

Figure 41: Valves in the gate of the existing Beatrixlock

Culverts underneath lock head

As the head difference becomes larger, the applicability of valves in the gate decreases due to large turbulence and high flow velocities. This is where culverts combined with stilling chambers come in to play. This system can only be feasible for head differences larger than 5 metres [37]. The energetic flows are reduced by construction of a stilling chamber. An intake point for the water is constructed in front of the gate. Consequently, the water is transported to the stilling chamber by means of a culvert. Usually, the stilling chamber is equiped with breaking elements such as columns or beams. These elements induce turbulance and thus dissipate the energy from the water resulting in smaller forces on the vessels.

The construction costs for this type of filling- and emptying system are a lot larger than for the valves integrated in the gate. Besides, the culverts need to be schematized as a closed conduit. This results in an additional friction and thus increases the filling time if the same cross-sectional area of the valves is applied.

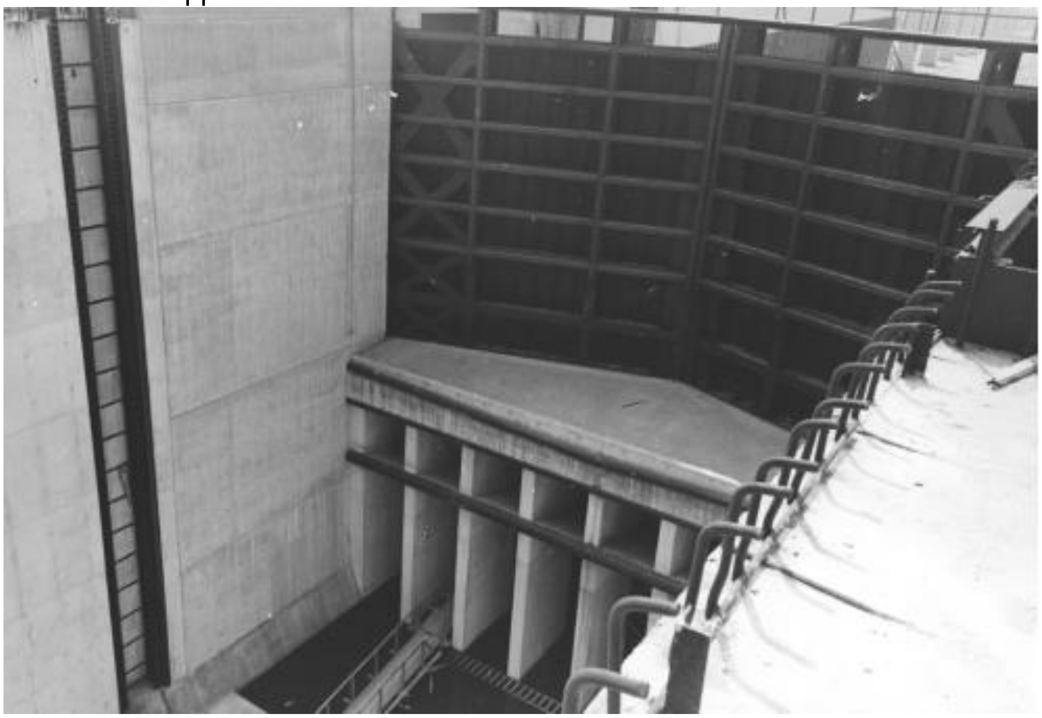

Figure 42: Culverts underneath the lock head of the lock at Maasbracht [37]

Longtitudinal culverts

For very large lifting heights (>15m), complex longitudinal culverts can be placed to distribute the discharge over the entire lock length. This system is extremely costly but leads to very quick levelling of the water with exerting large forces on the vessels. The culverts are placed near the bottom of the lock chamber, either integrated in the lock floor or lock walls. Mostly the culverts are placed opposite to each other so that the energy dissipates quickly.

Sometimes, locks with longitudinal culverts are equiped with water saving basins for example to limit the salt water intrusion. A combination of longitudinal culverts with water saving basins is used in the Panama locks.

Figure 43: Longitudinal F/E-system in the Marmet Lock, USA [36]

2.3. Types of lock gates

The water retaining gates can be constructed in different configurations with different directions of movement. Basically, there are four possible ways of movement of the gate:

- Horizontal translation
- Vertical translation
- Horizontal rotation
- Vertical rotation

Most frequently applied gate types are the mitre gate, lifting gate and rolling- or sliding gate. The selection of the gate type depends on many factors such as the lock width, available space next to the lock, type of lock, height of the vessels and whether the loads on the gates always act in the same direction or not. The following paragraphs give some more information on the different gate types and their area of application.

2.3.1. Mitre gates

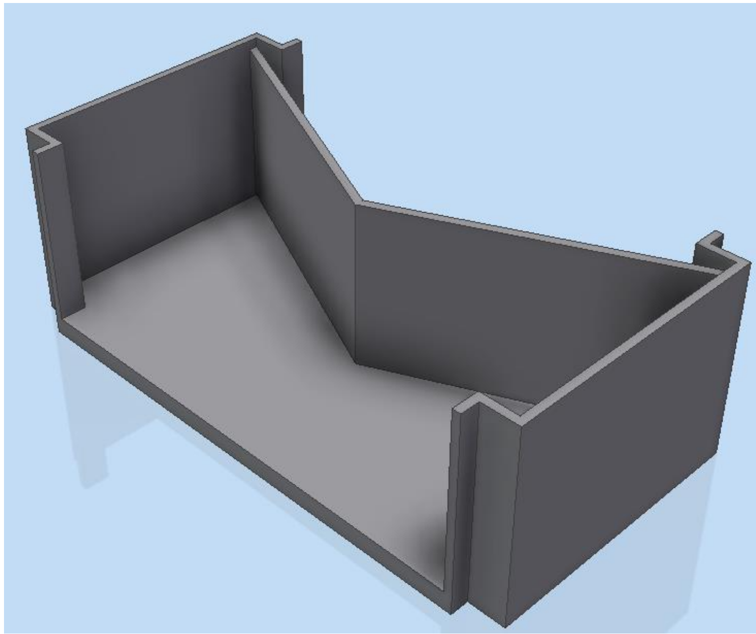

Figure 44: Graphical presentation of mitre gates (highly schematized)

The mitre gate is the most frequently applied type of lock gate for inland waterways. The water is retained by two gates which rotate around the vertical axis. The tips of the gates are connected to each other when the gates are closed.

Mitre gates are only applicable if the water pressures always act in the same direction (or in case the negative head difference is very small). The tips of the two gates connect to each other in the middle forming a mitre towards the high-water side. The hydrostatic pressure results in a compressive force between the tips of the gates. In closed position, the gates can be schematized as two simply supported beams which are connected to each other by a hinge in the middle. A large part of the hydrostatic pressure is transferred to the supports by normal forces and spalling forces. Bending of the gates only happens locally.

The gates consist most of the times of a water retaining plate with additional stiffening plates and ribs. Diagonal struts are sometimes applied in wooden gates to prevent deformations caused by the self weight of the gates. Table 16 shows the advantages and disadvantages of mitre gates.

Table 16: Advantages and disadvantages of mitre gates [36]

Advantages	Disadvantages
Loads are partly transfered to the supports by normal forces, leading to a relatively light gate	Not suitable if the gates are exposed to significant wave- or current actions when partially open
No air draught limitations	Hard to inspect the immersed parts
Opening and closing of the gates happens relatively fast	Sensitive to ice impact and debris

Especially the fact that the gates are hard to inspect is a big disadvantage for the application of FRP. Since new technologies come along with uncertainties, monitoring of the performance is very important to identify material detoriation in time. Besides, the expected weight reduction by application of FRP does not lead to (much) smaller moving equipment since the inertia forces of the water are dominant during the gate movement. The low weight does however lead to smaller loads on the hinges.

2.3.2. Rolling/sliding gates

Rolling- or sliding gates are mainly used for large, doubled-sided retaining lock gates. The gate is opened and closed by horizontal translation. When opened, the gates are positioned in a large recess in the lock head. This requires a lot of space next to the lock. The princple of a horizontally translating lock gate is schematized in Figure 45.

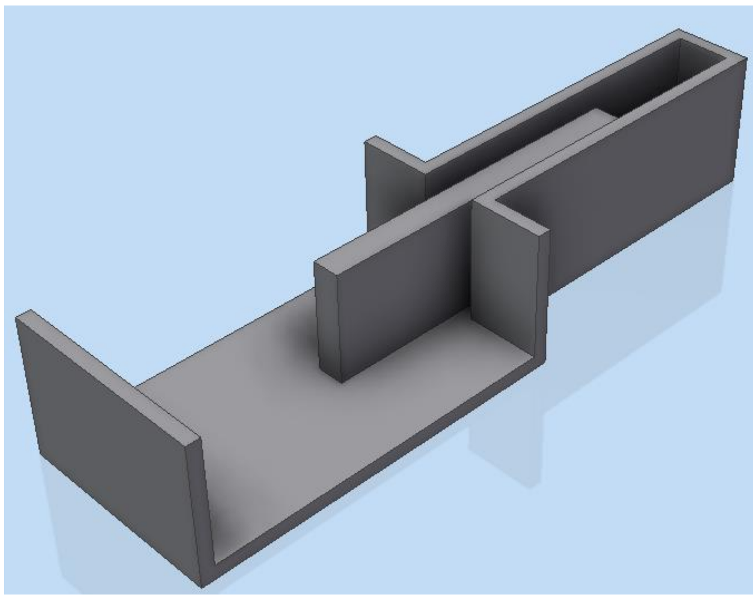

Figure 45: Graphical presentation of rolling- or sliding gate (highly schematized)

The gates are usually supported on wheels or on sliders to ease the horizontal movement of the gate. Sometimes, horitontally translating gates are equiped with a buouyancy tank to reduce the friction during movement. The gates can be inspected and maintenance work can be executed while the gate is positioned in its recess. Table 17 shows the advantages and disadvantages of rolling- or sliding gates.

Table 17: Advantages and disadvantages of horizontally translating gates [36]

Advantages	Disadvantages
Suitable for large lock widths	Forces are mainly transferred to the supports by bending moments
No air draught limitations	The risk of the gates getting jammed due to sediments or debris on rolling track
The gates can be inspected when they are positioned in their recess	A large space is required next to the lock head to construct the recess
A road connection can be placed on top of the gate	

The reduced weight for a gate made from FRP does not necessarily lead to lighter moving equipment because rolling gates can be equiped with buouyancy tanks if reduction of vertical forces is desired. The possibility to inspect the gates makes this type in principle suitable for application of FRP, although the specific advantages of the material are not fully utilized.

2.3.3. Lifting gates

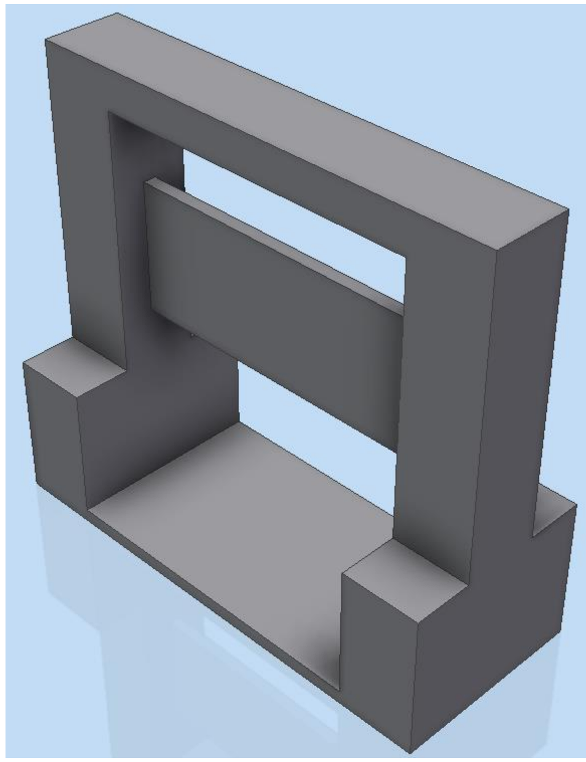

Figure 46: Graphical presentation of lifting gate (highly schematized)

Lifting gates are mainly applied in medium- to large size inland navigation locks. The gate is opened and closed by vertical translation. Lifting gates are positioned at both sides of the gate and harbor the moving equipment of the gate. The moving equipment can be connected to the gates either by cables or by chains. The mass of the gate is in most cases (partly) balanced by counterweights which are also positioned in these towers. For lifting gates, the mass of the gate is of great importance since reduction of the weight of the gate also results in a smaller counterweight, lighter lifting towers and smaller loads in the lifting cables. The gate can be schematized as a simply supported (or, in case the towers are able to withstand torsional moments, a partly fixed supported) beam for a preliminary design. Table 18 shows the advantages and disadvantages of lifting gates.

Table 18: Advantages and disadvantages of lifting gates [36]

Advantages	Disadvantages
Easy to construct	Lifting gates require a heavy lifting structure
Small lock head required	Risk of ice or debris getting attached to the gate, leading to dangerous situations for vessels passing underneath
The gates can be opened under a (small) head difference	The air draught is for vessels is limited by the lifting height of the gate
Inspection and maintenance is relatively easy	

Weight reduction of the gates will lead to great profits for the entire structure. Besides, the possibility to inspect the gate in lifted position makes this type very well suitable for application of FRP.

2.3.4. Gate type selection for the case study

The selection of the most suitable gate type depends on many factors. For very general cases, i.e. without considering the local conditions, Table 19 can be used for the selection of the most suitable gate types.

Table 19: Area of application for different lock types[3] [37]

Type of lock	Single sided water retaining inland lock			Double sided water retaining inland lock			Double sided water retaining sea lock		
Lock width	Small	Medium	large	Small	Medium	large	Small	Medium	large
Mitre gate	X	X	X						
Rolling gate						X		X	X
Lifting gate		X	X		X	X			

For more specific situations, a multi criteria analysis is recommended to select the appropriate gate configuration. This feasibility study will focus on the application of FRP in lifting gates, because the analysis performed in this chapter points out that the combination of weight reduction and inspectability leads to the largest advantages for application of FRP compared to steel for lifting gates.

2.4. Materials applied in lock gates

Traditionally, the gates are constructed from steel or timber. Extensive maintenance work required for these materials has recently resulted in application of relatively new materials like fiber-reinforced polymers (FRP) and ultra high performance concrete (UHPC). In the following paragraphs, the properties of steel, timber and UHPC are presented together with their advantages and disadvantages. More information on FRP's can be found in chapter 1 and in the literature study related to this thesis [4].

2.4.1. Steel

Steel is the most frequently applied material in lock gates. The high strength and stiffness together with the low initial costs make the material suitable for almost any type of gate. Besides, the ductile behavior of the material allows for redistribution of forces which results in a reduction of stress concentrations. Finally, the high strain at which rupture occurs (approximately 20%) means that a lot of energy can be absorbed during ship impact before failure of the gate occurs.The lock gates of the current Beatrixlock are also constructed from steel (see Figure 47).

[3] Small: <10m Medium:10-16m Large:>16m

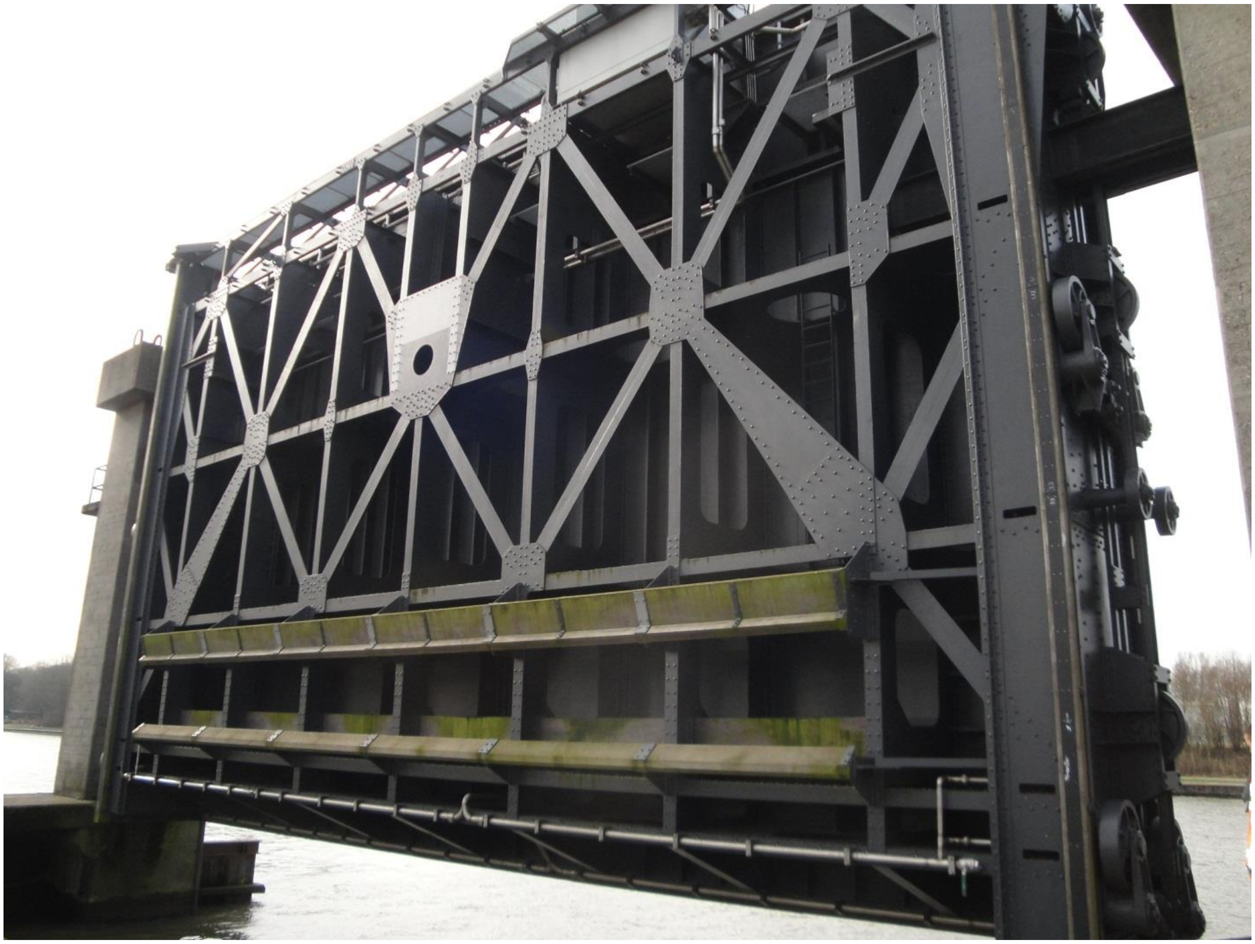

Figure 47: Spare gate of the Beatrixlock constructed from steel

One of the main drawbacks of the material is the low resistance against corrosion. Especially in the wet and oxygen-rich environment to which lock gates are suspected, corrosion leads to extensive and expensive maintenace works.

In order to prevent corrosion, a special coating can be applied to protect the steel from environmental influences. This coating is also influenced by environmental impacts and requires maintenance as well.

In case corrosion has taken place, repair is needed in order to preserve the lock gates. Typical maintenance work related to removal of corrosion from steel gates consists of the following steps [38]:

- Set up of a tent around the gate to prevent the small particles from falling into the water;
- Cleaning of the surface of the gate;
- Removal of loose rust by hand;
- Removal of remaining rust with a grinding disc;
- Surface finishing with a steel wire brush;
- Painting of the surface;
- Quality control of the work.

This laborous work leads to high maintenance costs summated over the lifetime of a lock gate. Besides, the entire lock is out of order during maintenace works unless the gates will be temporarily replaced. Maintenance usually results in a large downtime for the lock.

Except for the maintenance required by application of steel, the high specific weight of the steel is also a disadvantage. The large weight requires a powerful driving machanism, application of an air chamber for horizontal translating gates or a large counterweight for lifting gates to make the movement of the gates possible.

Table 20 shows the advantages and disadvantages of application of steel in lock gates:

Table 20: Advantages and disadvantages of application of steel in lock gates

Advantages	Disadvantages
Low initial costs	Vulnerable to corrosion
High stiffness	High specific weigth
High strength	Vulnerable to cyclic loads (fatigue)
Ductile behaviour allowing for redistribution of forces	

Table 21 shows the most important properties of steel quality S235 , the material which is for example applied in the gates of the Irenelock and in the gates of the current Beatrixlocks.

Table 21: Properties of S235

Property	Value
Young's modulus	210.000 N/mm^2
Yield stress	235 N/mm^2
Density	7850 kg/m^3
Estimated costs	5 €//kg
Yield strain	1,1‰
Strain at rupture	20%

2.4.2. Timber

Another material which is mainly applied in traditional small lock gates is timber. The size of a single component is limited resulting in a lot of joints in the gate. This feature together with the low stiffness makes the material less suitable for application in gates with larger spans. Besides, the natural origin of the material leads to a large spread in mechanical properties. This spread is often reduced by stacking many small plies together to form a laminate. In this way, the nodes, which are a weak spot in the wood, are randomly distributed over the area resulting in a higher overall strength.

Two different types of wood exist: hardwood and softwood. Softwood finds its origin in coniferous trees, while hardwoord is made out of deciduous trees. The two types differ in durability, mechanical properties, price and composition.

Just like fiber-reinforced polymers, wood consist of fibers embedded in a matrix. The fibers are made of cellulose and hemi-cellulose while the matrix is formed by lignin. The composition of the material leads to direction-dependent mechanical properties, where the weak direction is perpendicular to the fibers.

The most frequently applied type of wood in lock gates is the tropical hardwood azobé. Azobé is one of the strongest types of woods and has, compared to other wood types, a high strength/costs ratio and durability. In some situations application of timber is preferred compared to steel in terms of life-cycle costs. Another reason to apply wood can be to preserve the historical character of a lock [37].

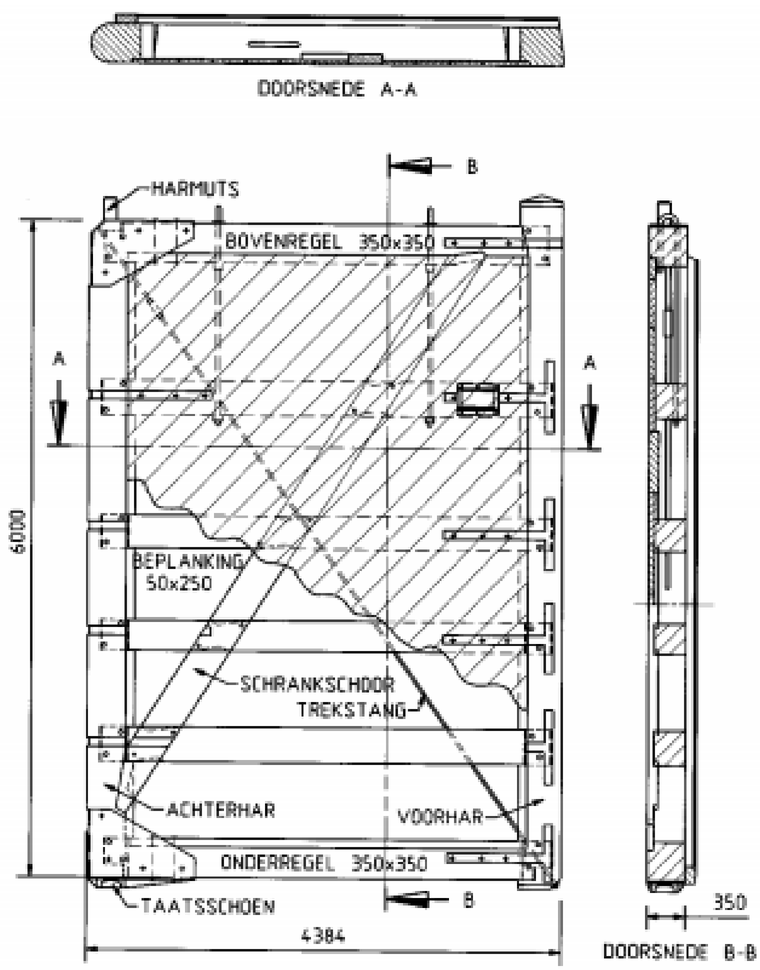

Figure 48: Overview of a wooden mitre gate [37]

When the moisture level in wood exceeds approximately 20% in an oxygenrich environment, the material is susceptible to different types of rotting processes which are induced by fungi. White rot happens when fungi break down the lingin leaving a white “fiberish” type of wood behind [39]. Brown rot takes place when the cellulose is attacked by fungi. The result is a darker piece of wood which is usually cracked. When rotten wood becomes dry again, the strength of the material is enormously decreased. Besides, the esthectics of rotten wood are very bad.

A solution is found in surface treatment of the wood. This can either be done by painting, staining or varnishing. This surface layer requires maintenance and usually contains toxic materials. The specific advantages and disadvantages for application of wood in lock gates are summarized in Table 22, while the specific material properties of azobé wood are summarized in Table 23..

Table 22: Typical advantages and disadvantages for application of wood in lock gates

Advantages	Disadvantages
Good esthetics, especially for historical locks	Relatively low stiffness
In some cases, lower maintenance costs than for application of steel	Unable to resist high local forces
Wood is renewable: chopped trees can be replanted	Size of elements is limited, many connections are required
	Surface treatment needed to prevent rotting, especially near the still water line

Table 23: Properties of azobé [40]

Property	Value
E-modulus	15.000-20.000 N/mm^2
Bending strength	75-110 N/mm^2
Density	900-1100 kg/m^3
Costs	1,20 €/kg [41]

2.4.3. Ultra high performance concrete

A relatively new developement for lock gates is the application of ultra high performance concrete. Up until now, UHPC has only been applied in lock 124 in Ijburg. These gates have a length of 6,5 meters, height of 4,5 meters and a thickness of 10 centimeters.

Figure 49: Placement of the first UHPC lock gates ever applied in IJburg [42]

Compared to ordinary concrete, ultra high performance concrete distinguishes itsself by a denser packing. Besides, steel microfibers are added to the paste to increase the ductility and tensile strength. Due to the dense packing, the resistance to intrusion of chlorides (which are harmful to the reinforcement) is a lot better than for traditional concrete.

The advantages and disadvantages for application of UHPC in lock gates are summarized in Table 24.

Table 24: Advantages and disadvantages for application of UHPC in lock gates

Advantages	Disadvantages
Less sensitive to harsh environmental conditions than steel	Risk of crushing of the concrete by ship collision
In certain situations, cheaper than application of steel **[43] [42]**	Uncertainties related to the long term properties
	No generally acknowledged design codes

Table 25 shows some of the most important properties of UHPC .

Table 25: Properties of Ultra-high performance concrete B200 [43]

Property	Value
E-modulus	50.000-60.000 N/mm^2
Bending strength	15-45 N/mm^2
Compressive strength	150-180 N/mm^2
Density	2500 kg/m^3
Costs	2 €/kg

2.4.4. Selection of reference material for the case study

The study to the different materials which can be applied in lock gates show that steel is up untill now, the only material which is applied for large lock gates. The reasons why wood is not suitable for larger lock gates is the low strength and stiffness of the material, the limited size of the elements resulting in a large amount of joints and the high material degradation near the still water level.

Ultra high performance concrete might also be feasible for large gates due to the large strength, stiffness and good durability. In order to use this material as a reference for the design of FRP, a design of UHPC should be elaborated as well since no concrete gates of these dimensions exist up to this very moment.Therefore it is decided to use a steel gate as reference to compare the design in FRP to.

3. Introduction to case study: lock gates Beatrixlock 3

In order to study the feasibility of FRP's in large lock gates, the gates of the third lock chamber of the Beatrixlock near Nieuwegein will serve as a case study. This chapter serves as a general introduction to the case study.

At first, the Beatrix lock complex is described from a historical perspective. This is followed by an overview of the current lock lay-out and an explaination why expansion of the existing complex is required. The second part of this chapter describes the functional requirements, boundary conditions and the design decisions which serve as a starting point for the design.

3.1. History of the Beatrixlock complex

The Beatrixlock has been built during the construction of the Amsterdam-Rijnkanaal and the Lekkanaal. Until the early 20st century, the only connections between the city Amsterdam and the river Lek were the Vaartse Rijn and the Kromme Rijn via the Vecht (see Figure 50). The rivers were approximately 20 meters wide and had a width of 3 meters. The rapid growth in size and number of inlands vessel resulted in large congestions, especially at the Oude Sluis near Vreeswijk. In 1892, it was decided to upgrade this lock with a second one. Although the congestion problems were temporarily solved, further growth of the inland navigation forced the government to take further measures.

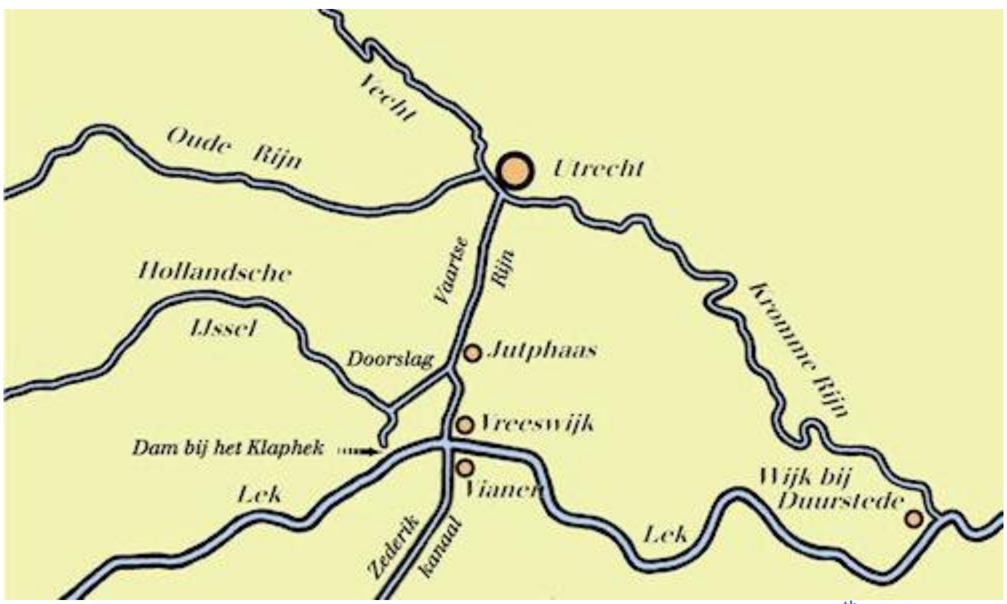

Figure 50: Waterways between Amsterdam and the Lek in the late 19th century

A study under the supervision of Lely was performed which proved the construction of a new canal to be feasible. This canal was constructed to improve the connection between Amsterdam and its hinterland. The final course of the canal was determined in 1931. The canal, at present known as the Amsterdam-Rijnkanaal, has a length of 51 kilometers and connects the city of Amsterdam to the Lek and Waal. The course of the canal is presented in Figure 51. The Irenelock is located near Wijk bij Duurstede and forms the barrier between the Amsterdam-Rijnkanaal and (the higher water level of) the Lek.

Figure 51: Location of the Amsterdam-Rijnkanaal

A small bifurcation was constructed between the Amsterdam-Rijnkanaal and the Lek at Vreeswijk to shorten the connection between Amsterdam and Rotterdam. This branch of the canal is now known as the Lekkanaal.

The water level at the Amsterdam Rijnkanaal is not influenced by the tide because the canal is fully closed off from the sea. The canal is bounded by the Irenelock at the south and by the Beatrixlock in the middle. In the north, the canal is connected to the IJ. In case of high water levels at the river Rhine, the water can be discharged through the Amsterdam-Rijnkanaal to eventually flow into the Markermeer via the Oranjelocks or into the North Sea via the locks at IJmuiden.

The Lek is directly connected to the North Sea and the water level is therefore influenced by the tide. The water level at the Lek is (except in case of an emergency) always higher than the water level at the Amsterdam Rijnkanaal. In order to prevent costly dike reinforcements at the Amsterdam Rijnkanaal, it is decided to seperate the waters by means of construction of a lock complex. This complex was finished in 1938 and is now know as the Beatrixlocks. The exact location of the lock can be found in Figure 52. More information on the lay-out and design of the locks can be found in the next subsection.

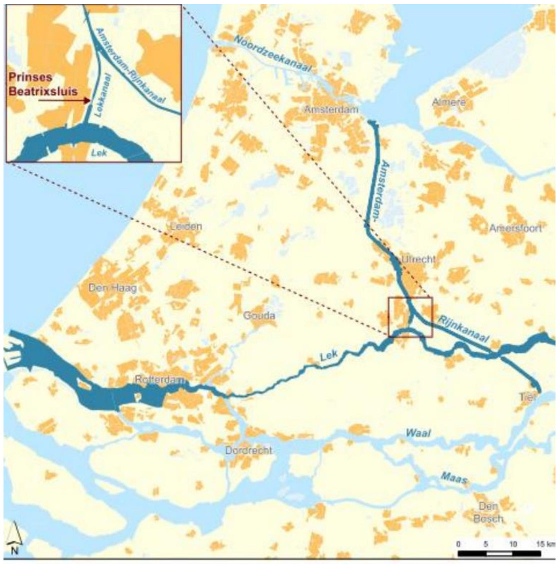

Figure 52: Location of the Beatrixlock [44]

3.2. Current lay-out of the lock complex

The current lock complex consists of two identical lock chambers, equiped with lifting gates on both sides of the lock chambers. The chambers have a length of 225 meters, a width of 18 meters and are able to handle inland navigation vessel with a draught up to 3,5 meters, which comes down to CEMT-class Vb. The lock has been built before the Lekkanaal was finished. Therefore, it could be constructed in the dry. Images of the lock complex are presented in Figure 53 and Figure 54.

Figure 53: Overview of the current Beatrixlocks [45]

Figure 54: Position of the control room [45]

The two individual lock chambers consist of continuous U-shaped cross sections which are connected toeach other in the middle. The thickness of the walls vary over the height, which leads to an efficient material use. The lock chambers and lock head are founded on piles.

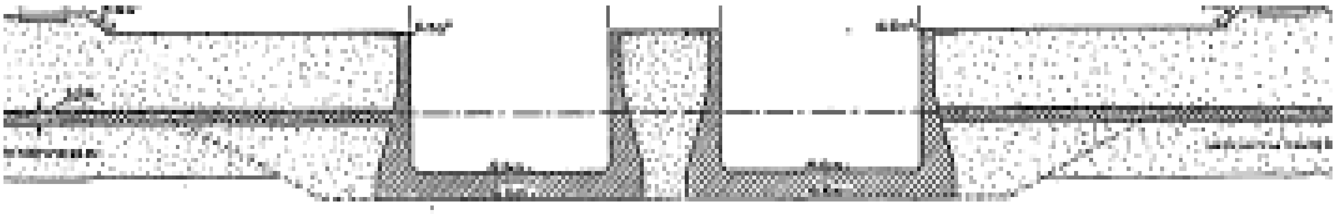

Figure 55: Cross section of the lock chamber (piles not included in the image) [45]

The gates are constructed as relatively thin plates which are made of steel and stiffened by horizontal- and vertical profiles. Diagonal struts prevent deformations of the gate by its self-weight. The current gates have a height of 12,36 meters, a length of 19,1 meters and a total thickness of 2,05 meters. The four gates are interchangeable, for the gates on the Lek side of the lock an additional part needs to be placed on top of the gate to account for the higher retaining height. A fifth spare gate is present which can be placed in case of emergency or for regular maintenance works on the gate. A picture of the gate is presented in Figure 56.

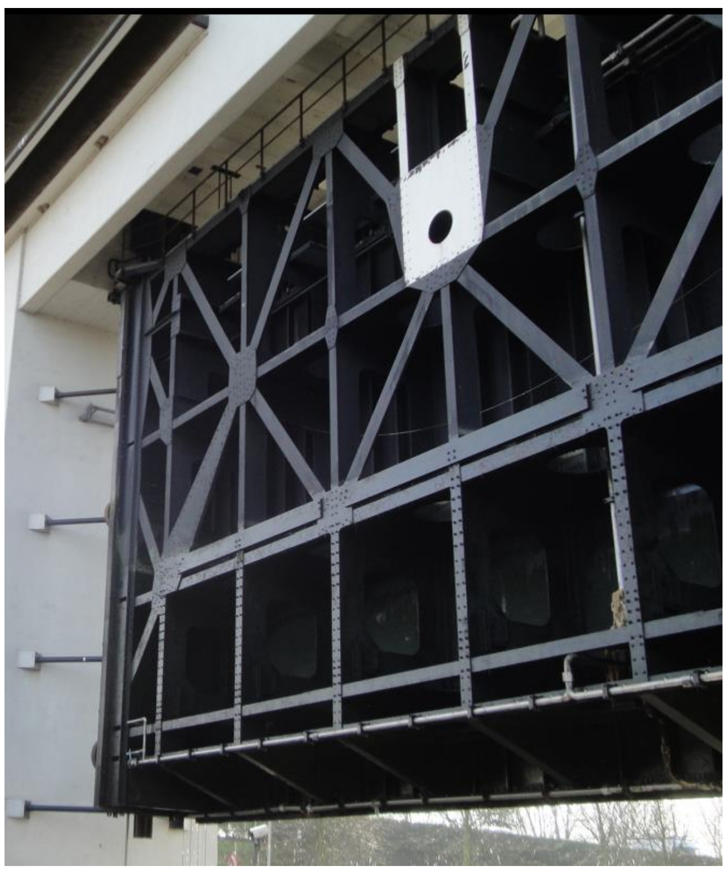

Figure 56: Lifting gates of the current Beatrix locks [45]

3.3. Recent extension plans

Studies on the average passage times for vessels combined with the expected future growth of the fleet have shown an insufficient capacity of the Beatrixlocks in the near future [46]. The average waiting time for vessels in the governing time of the year is expected to exceed the maximum allowed waiting time of 30 minutes in the year 2020. As a result, Rijkswaterstaat decided to search for alternatives to decrease the waiting time. The following concepts were considered:

- Construction of a third lock
- Enlargement of existing lock chambers
- Costruction of a second Lekkanaal
- Adjusted traffic management vessels
- Limitation of the maximum allowed vessel sizes
- Encouragement to use navigational route via Tiel

A multi criteria analysis performed by Rijkswaterstaat [46] indicated the construction of a new lock chamber as the most promising solution. The project has been tendered by Rijkswaterstaat as a DBFM-contract, in which the contractor is responsible for the maintenance of the entire Lekkanaal for a period of 35 years.

3.4. Environmental analysis

The Beatrixsluis is located in the Lekkanaal near Nieuwegein and forms the connection between the Amsterdam-Rijnkanaal (north) and the Lek (south). The Amsterdam-Rijnkanaal has a constant water level while the water level at the Lek is influenced by the tide with an average amplitude of approximately 1 meter. At present, the lock consists of two lock chambers which are closed by lifting gates. The northern lock heads also forms a road connection for cars and cyclists to cross the Lekkanaal.

The locks are located in the historical area of the “Hollandse Waterlinie”: an area which used to function as a defence system in times of war. The area could be inundated if the enemies showed up to form a barrier and protect the land. Nowadays, the area lost its original function and mainly serves as a historical recreation area. Besides, the area is marked as a wildlife corridor. This results in strict environmental requirements for the construction of the new lock. As an example, in order to preserve the historical view, lifting gates are not allowed by Rijkswaterstaat. For this feasibility study however, this requirement is ignored because this would mean that the biggest advantage of application of FRP, which is its low self weight, would not be optimally utilized.

The locks are part of dike ring 44, an area which stretches from IJmuiden to Wijk bij Duurstede (see Figure 57). The Dutch codes prescribe a safety level of 1/1250 for this dike ring, which means that a water level occuring once every 1250 years should be safely resisted [47].

Figure 57: Overview of dike ring 44 [47]

3.5. Functional requirements

Because the project is still in the tender phase, the functional requirements are not yet very acuratelydefined. Therefore, the functional requirements summarized in Table 26 shall be seen as general requirements for locks rather than site-specific requirements.

Table 26: Functional requirements

	Requirement	Origin
1	The gates shall be able to resist the head difference with an exceedance frequency of 1/1250 per year;	Rijkswaterstaat
2	The leakage of the gates shall be limited to a certain maximum (10 liters per minute per meter width is recommended in [37]);	Rijkswaterstaat
3	All the components of the gate shall be inspectable;	Rijkswaterstaat
4	Components with a lifetime shorter than the lifetime of the entire gate shall be replaceable;	Rijkswaterstaat
5	The gates shall be able to be closed by their self-weight;	Rijkswaterstaat
6	The considered load combinations shall be based on the document “ROK 1.2.”.	Rijkswaterstaat

3.6. Design decisions for the gate constructed from FRP

Several design decisions have been made which serve as a starting point for the design. These decisions are presented in Table 27.

Table 27: Design decisions for the gate made of FRP

	Design decision	Origin
1	The width of the lock equals 25 meters;	Rijkswaterstaat
2	The top of the gate in closed position is at NAP + 7,0 m;	Rijkswaterstaat
3	The bottom of the gate in closed position is at NAP - 5,8 m;	Rijkswaterstaat
4	The design shall be based on CEMT-class Vb, but 2x1 convoy vessels of CEMT-class VIb need be able to pass as well;	Rijkswaterstaat
5	Filling- and emptying of the lock chamber will happen through valves in the gate;	Own decision; see 2.2.5
6	A combination of E-glass & polyester will be used for the design of the gates;	Own decision; see 1.10
7	The material will consist of a combination of E-glass and polyester with a fiber-volume percentage of 50%;	Own decision; see 1.10
8	55% of the fibers will be placed in the main direction while the other three directions will each be equiped with 15% of the fibers;	Own decision
9	The gates will be designed for a lifetime of 100 years;	Own decision
10	The CUR 96 will serve as the guideline for the design;	Own decision
11	The maximum strain in the material shall not exceed 0,27%[4];	Own decision
12	The moulds used for production of the gates shall be reuseable for other projects in order to be cost-competative.	FiberCore

3.7. Considered load combinations

The following loads are considered for the design of the lock gates, based on the ROK 1.2.:

- Head difference with an exceedance frequency of 1/1250 y^{-1};
- Negative head difference;
- Wind waves;
- Translation waves;
- Ship collision;
- Self-weight.

Ice loads, wind loads on the lifted gate and trapped debris have been neglected during the design because these forces are all small compared to the hydrostatic forces. Table 28 shows the considered load cases together with their partial safety factors for the different load combinations. Load combinations A, B, C and D refer to the gate in closed postion while load combination E considers the lifted gate.

The load case “self-weight” of the gate is neglected for the gate in closed position for two reasons: firstly, the gravitational force is small because the density of the gate is only slightly larger than the density of water. Secondly, the self-weight is redirected to the bottom of the lock by normal forces which are spread over the entire bottom of the gate resulting in very small stresses.

[4] This requirement is relaxed during the conceptual design of the gate, see chapter 6.2.

Table 28 : Considered load combinations and load factors [48]

Load combination Load case	A	B	C	D	E
Self-weight					1,25
Design head difference **Wind waves**	1,5				
Negative head difference **Wind waves**		1,5			
Maximum operational water level **Wind waves** **Translation waves**			1,5	1,2	
Ship collision				1,0	

Load combination A: Design head difference;
Load combination B: Design head difference in opposite direction;
Load combination C: Maximum operational water level including wind- and vessel induced waves;
Load combination D: Extreme event, ship collision during the maximum operational water level difference;
Load combination E: Gate in lifted position.

The governing hydraulic boundary conditions, which are extracted from the RINK analysis performed by IV-Infra, are presented in Table 29 and Table 30.

Table 29: Hydraulic boundary conditions [49]

	Water level Lek [m+NAP]	Additional conditions Lek	Water level Lekkanaal [m+NAP]	Additional conditions Lekkanaal	Head difference [m]
Maximum locking level	5,80	Wind waves	-0,60	-	6,40
Average water levels	1,10		-0,40		1,50
Maximum retaining level	6,40	Wind waves	-0,60	-	7,00
Negative head difference	-1,15	-	-0,20	Wind waves	-0,95

Table 30: Wave characteristics at the Beatrixlock [49]

Wave type	Wave height [m]	Wave period [s]
Windwaves Lek	0,18	1,59
Windwaves Lek	0,17	1,54
Shipwaves Lek	0,66	2,60
Shipwaves Lek	0,44	2,01
Translation waves	0,30	-

The governing load situation is the combination of maximum head difference together with wind waves. The forces induced by (non breaking) wind waves are calculated by the formula of Goda. These forces are presented in Figure 58 and Figure 59.

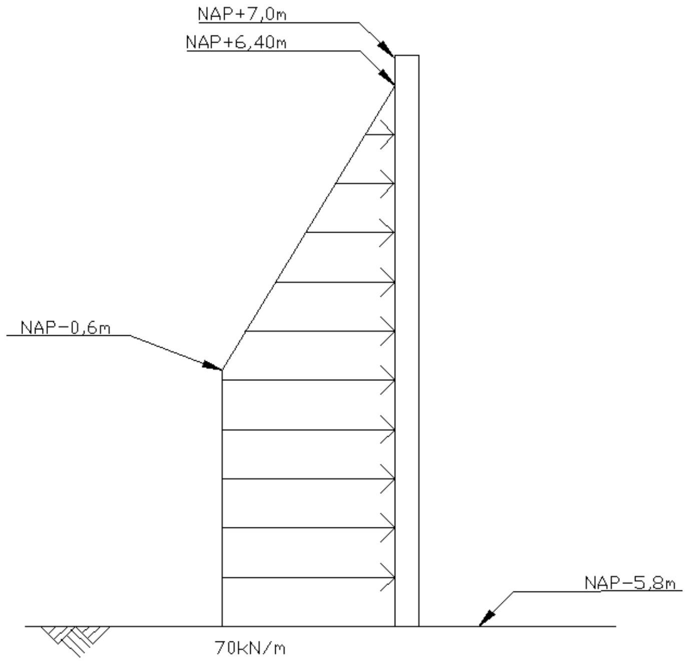

Figure 58: Resultant of horizontal hydrostatic pressures acting on the gate per unit of length

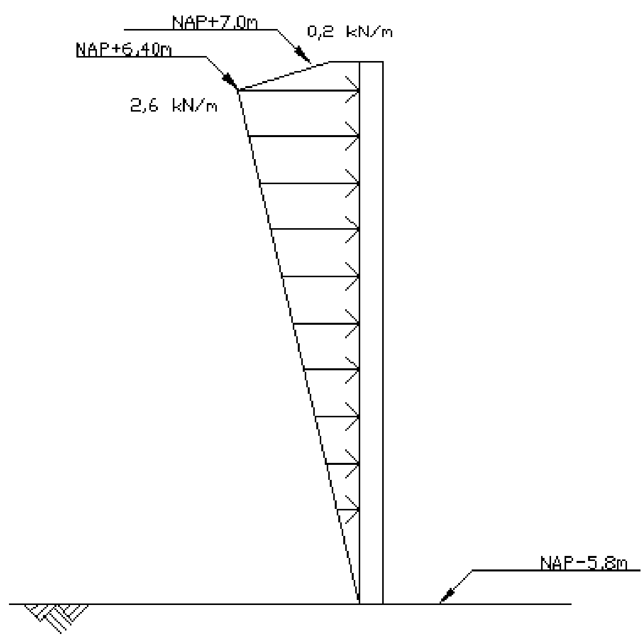

Figure 59: Forces exterted on the gate by wind waves per unit of length

The loads induced by wind waves appear to be negligible compared to the hydrostatic pressures. Therefore, only the hydrostatic pressures are considered for the gate design.

4. Study to gate alternatives constructed from FRP

The objective of this chapter is to find the optimal global shape of the gate, given the functional requirements, boundary conditions and load combinations presented in the previous chapter. The optimal shape is characterized by a maximum ratio of profits over costs. Robustness, reliability, maintainability and esthetical value are assumed to be a good measure of profits while the combination of weight and amount of joints are used as an indication of the costs of the structure.

Chapter 4 starts with an overview of the simplifications which are used in order to estimate the behaviour of the gate. Five gate alternatives are consequently elaborated based on strength- and stability requirements, after which a multi-criteria analysis has been performed in order to select the most promising alternative for furhter elaboration.

4.1. Simplifications of reality

To obtain an order of magnitude for the required dimensions, only the hydrostatic pressures related to the maximum retaining level (see Table 29) are considered for this stage of the design. Furthermore, the gates are schematized as simply supported 2-D beams, which is reasonably accurate because the properties of the gate and the loads to which the gates are exposed are more or less constant over the height . The properties of the material presented in Table 27 are found with help of the semi-empirical formulas of Halpin-Tsai (which are explained in Appendix B):

Table 31: Material properties for the applied lay-up in the preliminary design

Property	Value
$\boldsymbol{E_1}$	25800 N/mm^2
$\boldsymbol{E_2}$	15900 N/mm^2
$\boldsymbol{G_{12}}$	5600 N/mm^2
$\boldsymbol{v_{12}}$	0,32
$\boldsymbol{\varepsilon_{R;d}}$	0,27%
$\boldsymbol{\sigma_{R;d}}$	70 N/mm^2

The hydrostatic pressures presented in Figure 58 are integrated over the height of the gate in order to arrive at a 2D-schematization:

$$Q_k = \int_{z=0}^{h} q_k * dz = (h_2 - h_1) * \rho_w * g * h_1 + \frac{1}{2} * (h_2 - h_1)^2 \rho_w * g = 609\ kN/m$$

In which:

$Q_k =$ Charasteristic value of the distributed load over the length of the gate
$h_1 =$ Design water level at the Amsterdam-Rijnkanaal
$h_2 =$ Design water level at the Lek
$\rho_w =$ Density of the water
$g =$ Gravitational acceleration

This leads to the following design value for the distributed load:

$$Q_{Ed} = Q_k * \gamma_f = 609 * 1{,}5 = 913{,}5\ kN/m$$

In which:

$Q_{Ed} =$ Design value of the distributed load over the length of the gate
$\gamma_f =$ Load factor, equal to 1,5 for the hydrostatic pressures

Because of the relatively low material stiffness, the high design loads and the large span, it is important to create a large internal lever arm. Besides, the amount of joints should be reduced to a minimum. The third important requirement is that the gates need to be manufacturable. Finally, the mould(s) which will be used to produce the gate shall be reusable for other projects in order to be cost-competitive with tradtional building materials.

These requirements have resulted in five variants: the Vierendeel gate, the Warren truss gate, the curved gate, the lens-shaped gate and the stiffened plate. These different gate configurations are presented in Figure 60.

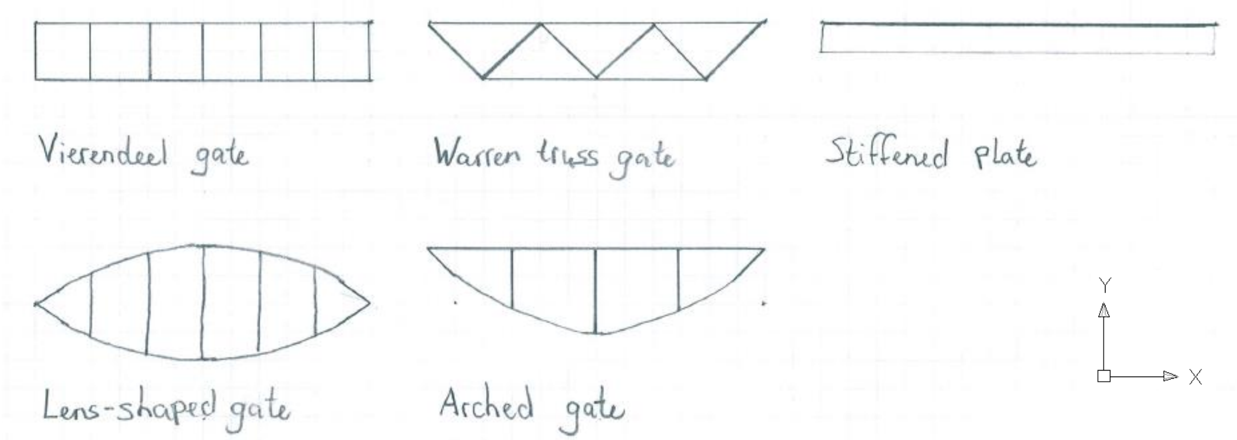

Figure 60: Overview of the five considered gate alternatives (top view)

The design approach and the final level of detail is equal for all five alternatives in order to be able to compare the different concepts. During the study to gate alternatives, the following subjects will be determined for each concept:

- Global shape
- Joint geometry
- Manufacturing technique
- Dimensions of the elements
- Total mass of the gate

The next subsections cover the structural design of the five different gate alternatives on a global scale. At first, a study has been performed to find the design parameters which are important for each gate alternative. Hereafter, each concept has been designed on maximum allowable normal stresses and stability of members. Each concept is finally optimized on weight by variation of the relevant parameters in an excel file, keeping in mind that the normal stresses stay within the limits and that the structure remains constructable and inspectable.

4.2. Gate alternative 1: Vierendeel gate

4.2.1. Introduction

The first investigated gate alternative is the Vierendeel gate. The gate can either consist of two water retaining plates which are connection by vertical and/or horizontal stiffeners or by a single water retaining plate which is connected to a truss to increase the strength and stiffness. The different options are presented in Figure 61 and Figure 62.

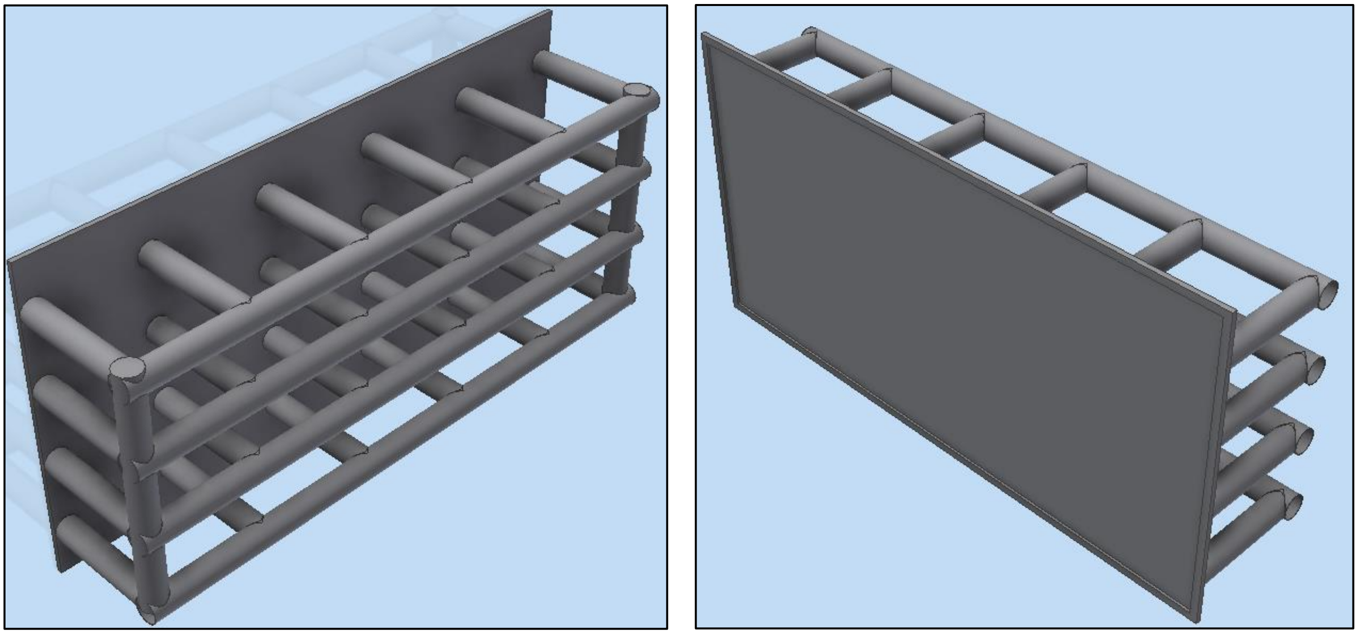

Figure 61: Vierendeel gate constructed with tubular stiffeners

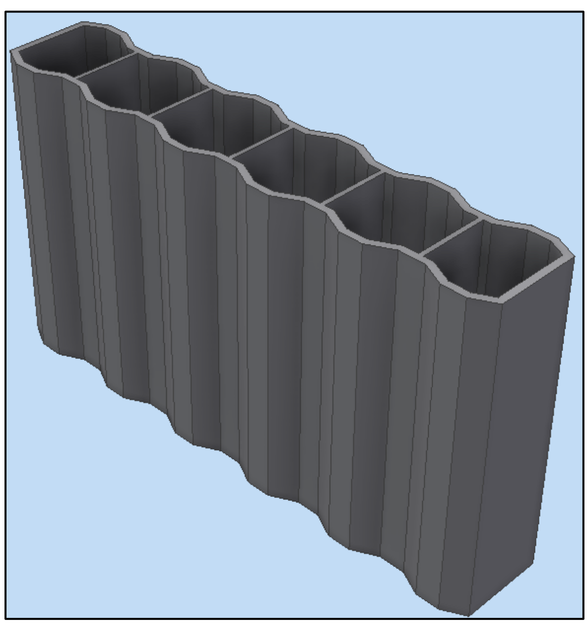

Figure 62: Vierendeel gate constructed as double plates

The function of the main plates are to retain the water and redirect the forces to the truss or webs. The required thickness of the plate depends among other things on the distance between the members of the web and the internal lever arm of the entire structure. A larger internal lever arm leads to smaller forces in the water retaining plates, but also leads to a larger buckling length for the webs.

The water retaining plate can be produced by vacuum injection. Due to the large size, the plates need to consist of multiple modules. These different modules can be connected to each other by hand lamination.

4.2.2. Static scheme

Figure 63 shows the static scheme which is used to design the variant on strength.

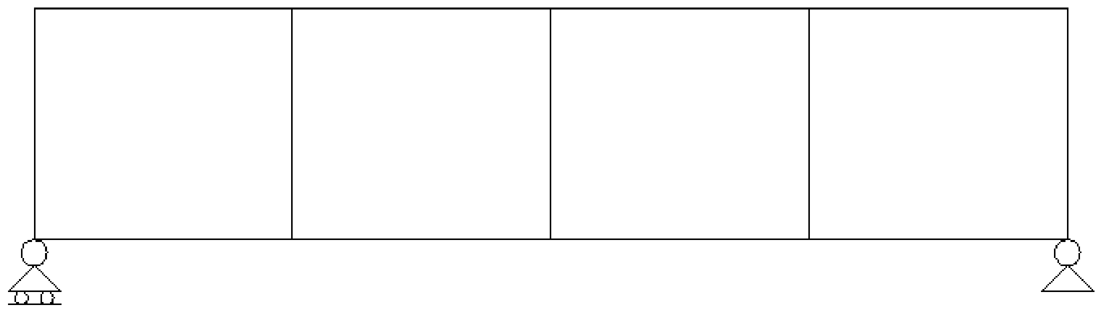

Figure 63: Static scheme for the Vierendeel gate

The members need to be connected rigidly in order for the static scheme to be kinematically determined. The parameters to be varied during the preliminary design are the number of webs, distance between the water retaining plates and the ratio of web stiffness to the stiffness of the water retaining plate.

4.2.3. Connections

The connections of the water retaining plates to the webs need to be able to resist both bending moments and normal forces. One way to reach this is by laminated T-joints.

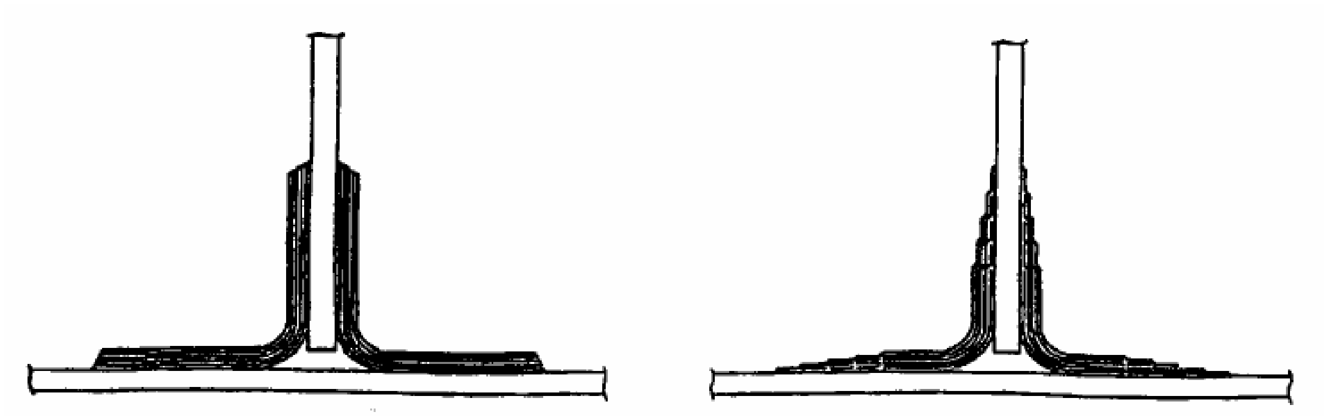

Figure 64: Possible details of the connection between water retaining plate and stiffening plate for the variant "Vierendeel truss"

The parameters which are of importance during the structural design of the connection are the thickness and radius of the overlaminate, the overlap length and the difference in stiffnesses between the connected members.Attention should be paid to delaminations of the overlaminate at the corners and edges of the joints, also in combination with a fatigue analysis.

4.2.4. Preliminary design
Because the webs are perpendicular to the gate, the forces are mainly redirected to the supports by bending moments. As a result, the bending moments in the plates become huge which has major consequences for the required plate thicknesses. Because of the unfavorable force paths through the structure, this alternative has not been structurally elaborated. As an alternative, the geometry has been improved by addition of webs under a smaller angle with the water retaining plates.This has ben further elaborated in the next paragraph, which covers the preliminary design of the Warren truss gate.

4.3. Gate alternative 2: Warren truss gate

4.3.1. Introduction
Instead of the Vierendeel gate, another option is to apply a Warren truss gate. The concept is compareable, although the Warren has a more favourable force distribution because the forces are mainly redirected through normal forces in the webs rather than bending moments.

These webs can either be constructed by beams or by plates. The main disadvantage of beams compared to plates is that the contact area is relatively small. This will result in highly concentrated stresses at the joints, which are unfavourable for FRP-structures because of the risk of delaminations. Therefore it is decided to construct the entire structure from plates. This variant is schematically presented in Figure 65.

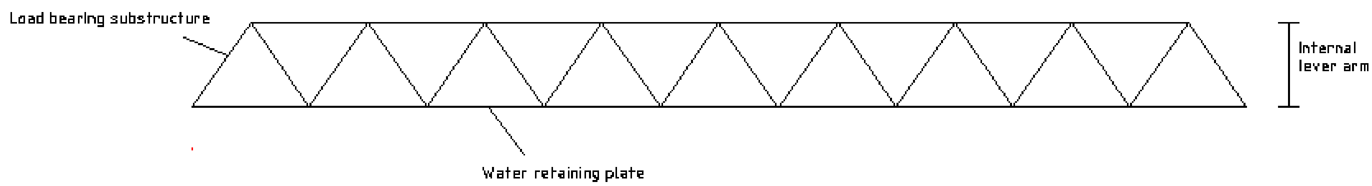

Figure 65: Variant 2: the Warren truss gate

The function of the webs is to transfer the shear from the water retaining plates to the supports. Besides, the webs need to guarantee full cooperation between the water retaining plates. The webs are loaded in compression which makes them susceptible to buckling. The internal lever arm of the structure leads to a reduction of stresses induced by the overall bending moment. The local bending moments in the plates between the webs need to be resisted by a single plate. In order to increase the strength and stiffness, these plates will be constructed as sandwich elements. The plates can be produced by vacuum injection.

The important parameters for the design are the amount of webs and the internal lever arm. More webs will results in a smaller local bending moment but the material required for the webs increases. A larger internal lever arm results in smaller overall bending moments, but also results in a larger length of the webs, which is unfavourable for the resistance against buckling.

4.3.2. Static scheme
The structure is modelled as the static scheme depicted in Figure 66, where the connections are modelled as hinges. The amount of webs and the internal lever arm of the gate has been varied to find the optimal configuration for this global concept.

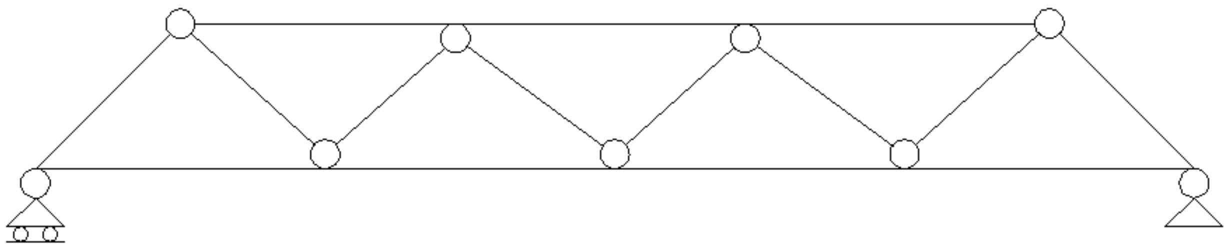

Figure 66: Static scheme for the Warren truss gate

4.3.3. Connections

Bolted connections are preferable to adhesively bonded joints in terms of replaceability. The connection of the webs to the the water retaining plates can be executed as shown in Figure 67. This connection is based on the reference project “pedestrian bridge Rijkersswoerd”. Information on this project can be found in chapter 1.1.3 .

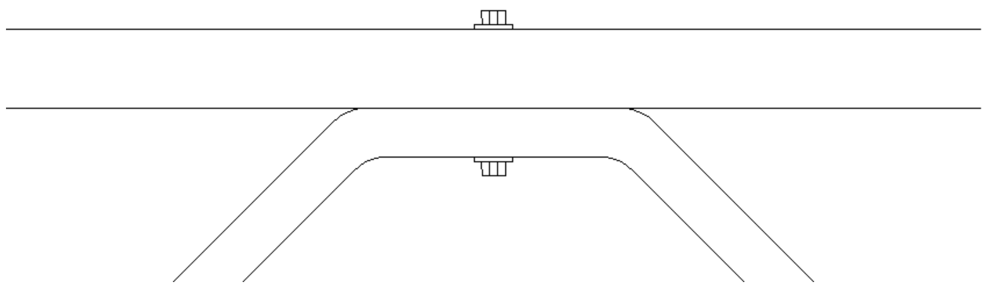

Figure 67: Detail of connection between water retaining plate and shear element

The connection should be further investigated to prove its applicability in this situation as well.

4.3.4. Preliminary design

During the preliminary design, the following parameters need to be determined:

- Number of webs
- Internal lever arm
- Skin thickness & core thickness of water retaining plates
- Skin thickness & core thickness of webs

The number of webs and internal lever arm are considered as independent variables while the plate thicknesses are determined by comparision of the governing forces with the limit state functions (maximum stress or buckling load).

According to the static scheme, the webs are only exterted to normal forces while the two water retaining plates have to resist a combination of shear forces, normal forces and bending moments. The webs close to the supports will receive the highest compressive forces and will therefore be governing for the design. The position at half of the length of the gate, where both local- and global bending moments are maximum, will be governing for the design of the water retaining plates.

The relations between loads, buckling forces and stresses in the material can be found in Appendix D). A Mathcad sheet has been set up to easily be able to process changes in the input parameters of the model. A sensitivity analysis has been performed to find the amount of webs and internal lever arm which results in the smallest mass of the structure. This has resulted in the graph which is presented in Figure 68.

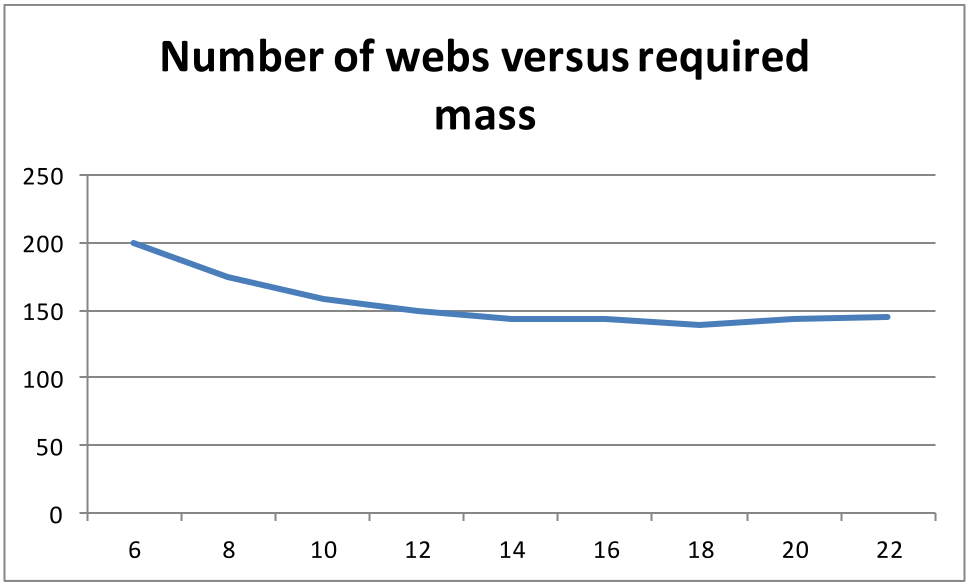

Figure 68: number of webs versus the mass of the gate for the Warren truss gate

The minimal weight is found for 18 webs and a total thickness of the gate of 3 meters. Both the water retaining plates and the webs are constructed as sandwich elements. An impression of the global design is given in Figure 69.

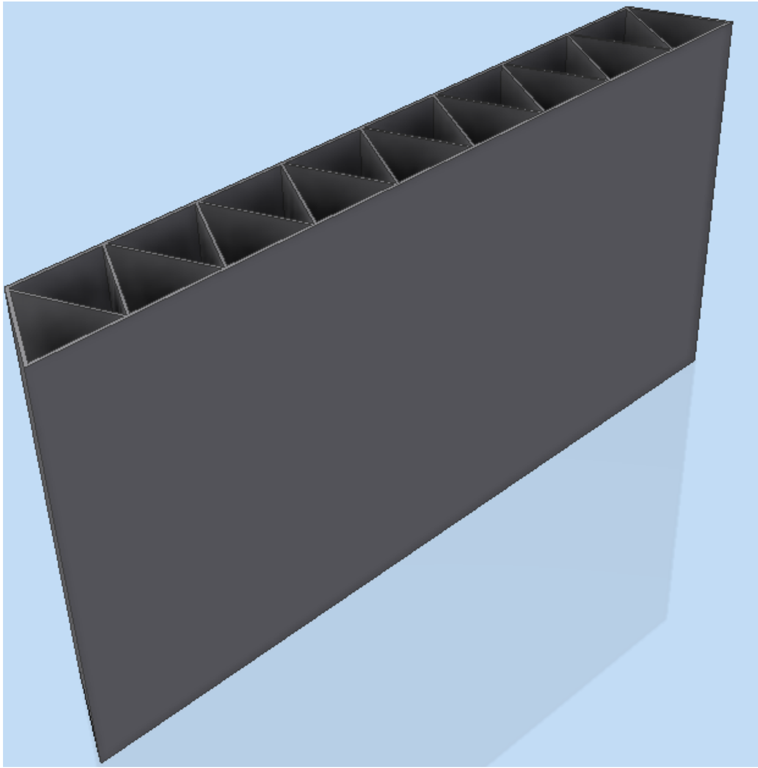

Figure 69: 3D-impression of the Warren truss gate

4.3.5. Summary of the design

- Plates are manufactured by vacuum injection;
- Plates constructed as sandwich elements to increase its strength and stiffness;
- Total mass of the gate equals 145 tons;
- The volume of the gate equals 139 cubic meters;
- Water retaining plates: thickness of 108mm, of which 54mm consisting of core material;
- Webs: 18 webs with a thickness of 88mm, of which 44mm consisting of core material;

The dimensions of the plates are presented in Figure 70.

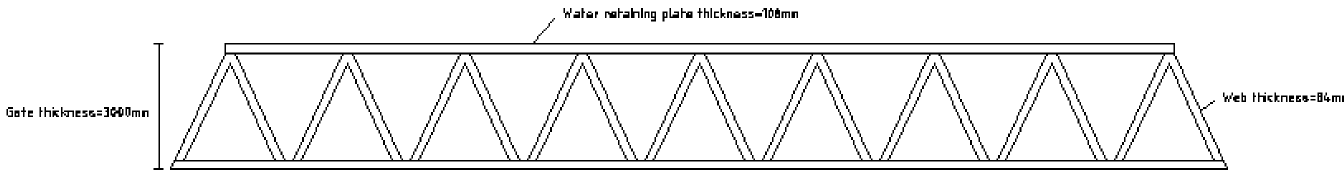

Figure 70: Global dimensions of the Warren truss gate

The specific advantages and disadvantages of this variant are summarized in Table 32.

Table 32: Advantages and disadvantages for the Warren truss gate

Advantages	Disadvantages
Large repetition in components	Small corners between plates are hard to inspect
Only flat plates, which are easy to produce	Relatively low weight savings
All the connections to the substructure are flat	Many joints required

4.4. Gate alternative 3: Stiffened plate

4.4.1. Introduction

The third alternative which is investigated is the construction of the gate as a plate stiffened by ribs. These ribs can either consist of T-profiles or solid ribs, see Figure 71.

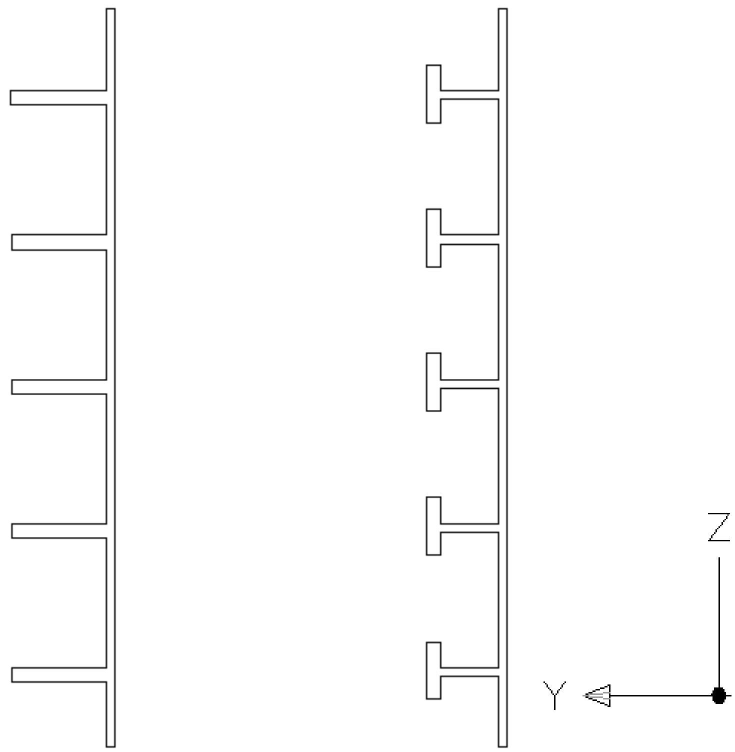

Figure 71: Two possible cofigurations for the gate consisting of a stiffened plate (side view)

If the stability of the stiffeners is at stake, the design could be improved by addition of vertical stiffeners as well, as presented in Figure 72.

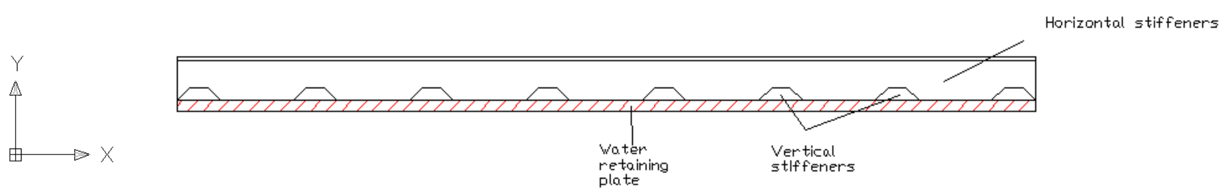

Figure 72: Top view of a plate stiffened by a combination of horizontal and vertical profiles

4.4.2. Static scheme

The gate is be schematized as a simply supported beam. The section properties are obtained by assuming full cooperation between plate and stiffeners. Therefore, the Steiner-rule applies to calculate the moment of inertia en section modulus. Figure 73 and Figure 74 show the important parameters for the design.

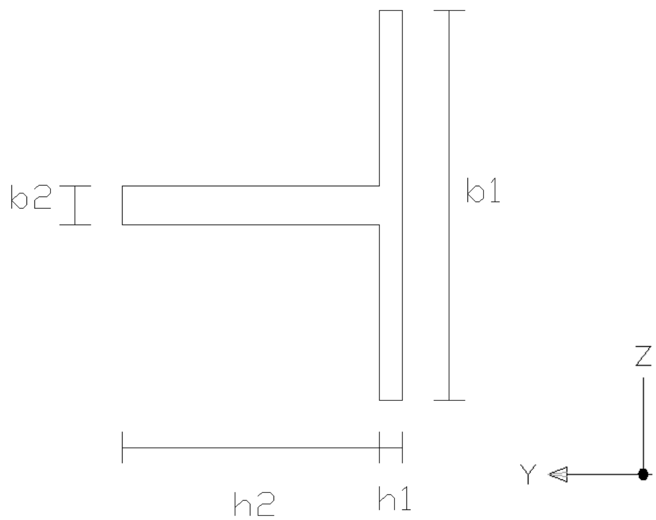

Figure 73: Side view of plate stiffened by massive profiles

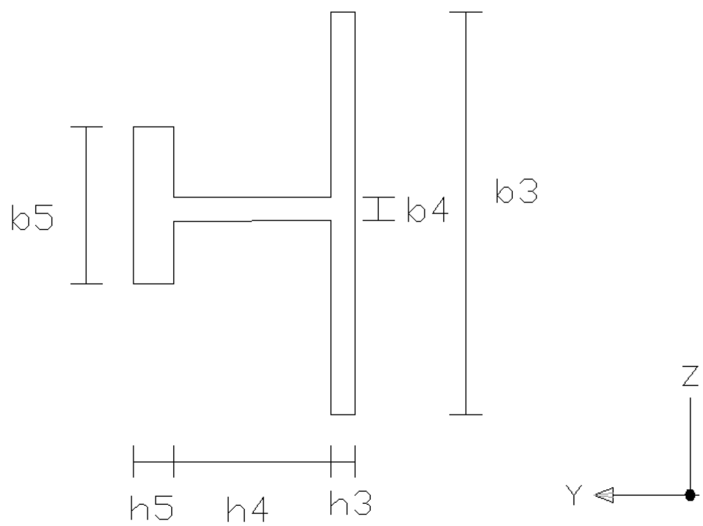

Figure 74: Side view of plate stiffened by T-profiles

4.4.3. Connections

The stiffeners can for example be attached to the water retaining plate by mechanical fastening. This principle is also applied in the Aerospace industry, as illustrated in Figure 75.

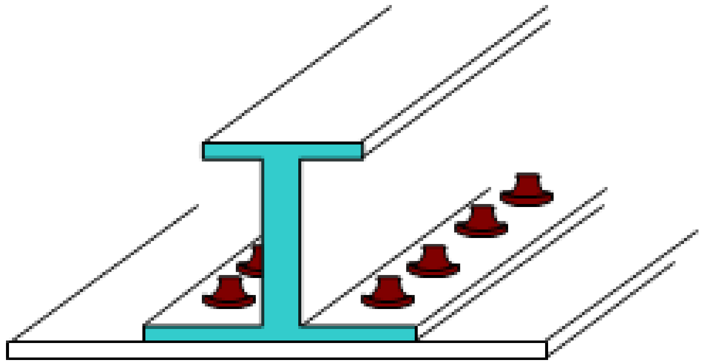

Figure 75: Attachment of the stiffeners to the water retaining gate [19]

4.4.4. Preliminary design

In order to estimate the required mass for both types of stiffened gates, a mathcad sheet has been set up. The relevant parameters are investigated and varied in order to find the minimum required mass for which the stresses in the structure do not exceed the design values of the strength. The results after optimization are presented in Table 33.

Table 33: Study to two variants for the stiffened plate

	Massive stiffeners		T-profiles
Property	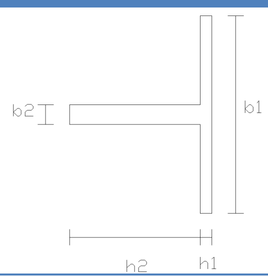	Property	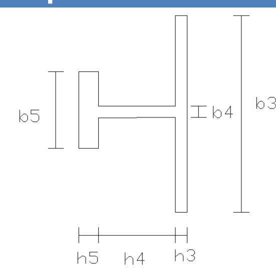
$\boldsymbol{b_1}$	2500 mm	b_3	2500 mm
$\boldsymbol{h_1}$	150 mm	h_3	100 mm
$\boldsymbol{b_2}$	250 mm	b_4	100 mm
$\boldsymbol{h_2}$	1650 mm	h_4	1000 mm
		b_5	1000 mm
		h_5	250 mm
$\boldsymbol{I_{zz}}$	0,253 m^4	I_{zz}	0,183 m^4
$\boldsymbol{z_{max}}$	825 mm	z_{max}	594 mm
$\boldsymbol{\sigma_{max}}$	67 N/mm^2	σ_{max}	67 N/mm^2
$\boldsymbol{w_{max}}$	136 mm	w_{max}	189 mm
$\boldsymbol{m_{gate}}$	197 ton	m_{gate}	150 ton

The plate which is stiffened by T-profiles performs better, because it has a larger moment of inertia compared to the internal height of the profile. T

4.4.5. Summary of the design

- Plates are manufactured by vacuum injection
- Plates are constructed as massive elements (no lightweight core is applied)

- Stiffeners are produced by pultrusion
- T-shaped profiles are preferred to massive stiffeners
- Stiffeners are attached to the plate by mechanical fastening
- Mass of the gate equals 150 tons

A 3D-impression of the stiffened gate is presented in Figure 76.

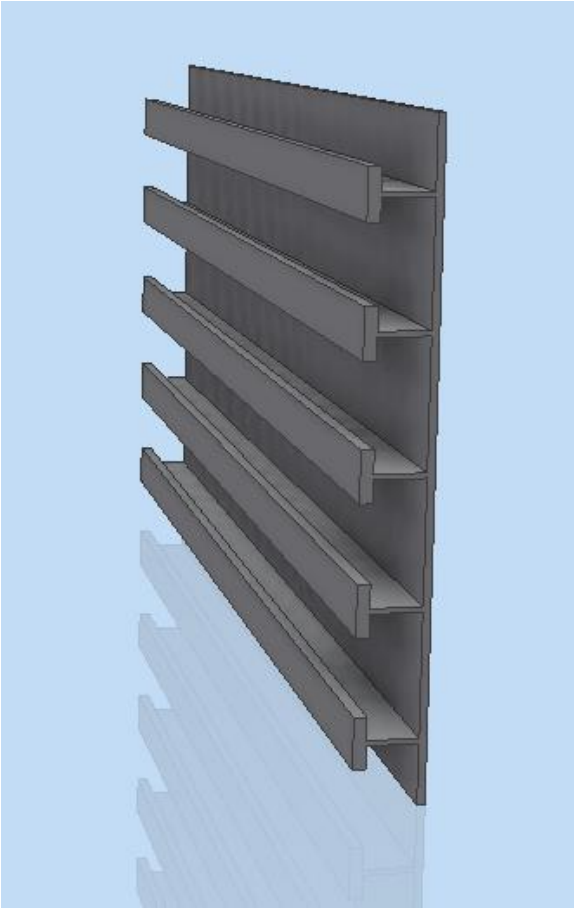

Figure 76: 3D-impression of the variant stiffened gate

In case of wave impact, this variant is not applicable due to large vertical slamming forces exerted on the stiffeners. Furthermore, the stability of individual members is not considered, which means that the calculated required mass is the lower boundary. This has been taken into account during the selection of the most promising variant.

Table 34: Advantages and disadvantages for the variant stiffened gate

Advantages	Disadvantages
This variant is easy to produce	High mass compared to the curved variants
The connection to the lock sill is flat	Little space available between the stiffeners for the valves
Higher density results in easier closure by self-weight	Sensitve to debris accumulation inside the stiffeners

4.5. Gate alternative 4: Arched gate

4.5.1. Introduction

The third considered gate configuration consists of an arched gate with its curvature towards the high-water side. Under regular conditions, this leads to high compressive forces in the arch while the straight plate connected to the arch is loaded in tension due to the thrust forces. The global geometry is presented in Figure 77.

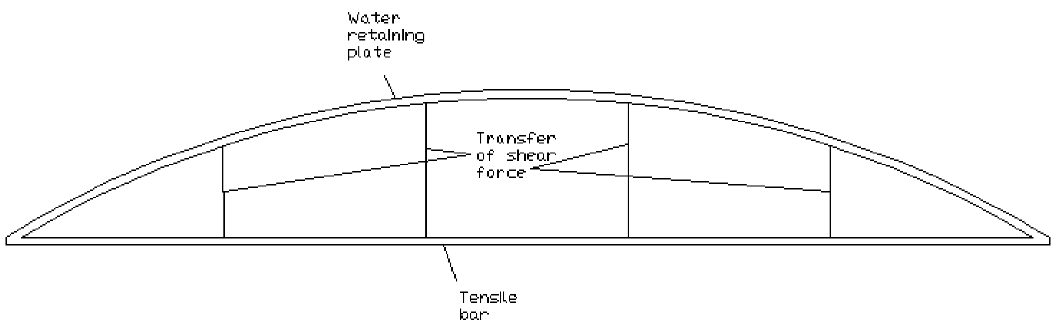

Figure 77: Overview of variant 3: Arched gate

The shape of the gate keeps close to the moment-line, which results in a good transfer of loads: The bending moments in the arch are close to zero since the loads are almost entirely directed to the supports by normal forces. Without additional measures, the thrust would lead to large, unfavourable horizontal forces at the supports. For this reason, a straight plate is connected to the arch taking care of these horizontal forces. The gate is equiped with webs to reduce the buckling length of the straight plate in case of a negative head difference.

The parameters which matter for the design are the total drape of the arch and the number of webs. Increasing the drape results in smaller tensile forces in the straight plate, but also leads to a larger length of the arch and webs. The distance between the webs is a measure for the buckling length of the straight plate connected to the arch under a negative head difference. Less webs leads to a larger buckling length which means that the tensile bar needs to be stiffer. The savings on material in the web needs to be compared to the additional material required for the plate in tension.

4.5.2. Static scheme

The selected geometry is translated into the static scheme presented in Figure 78.

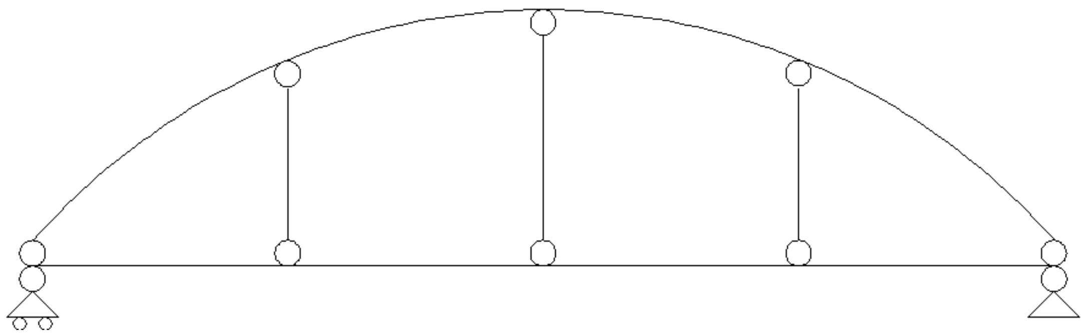

Figure 78: Static scheme of variant 3: Arched gate

4.5.3. Connections

For the sake of replaceability, also for this variant mechanically fastening is prefered. The connections can be executed as illustrated in Figure 64. Especially the connection near the support, where the arch, tensile bars and support need to be connected to each require extra attention if this configuration is selected for a more detailed design.

4.5.4. Global design

For the global design, three options are considered. The first option contains no webs, the second one contains a single web while the third variant is equiped with 3 webs.

Due to the curvature, analytical results where hard to obtain. Therefore, software program SCIA Engineer is used to obtain the internal forces in the structure. A mathcad sheet has been set-up to find the drape and number of webs which results in the smallest total mass of the gate. For the preliminary design of this variant, the negative head difference has also been taken into account because it has major effects for the stability of the straight plate.

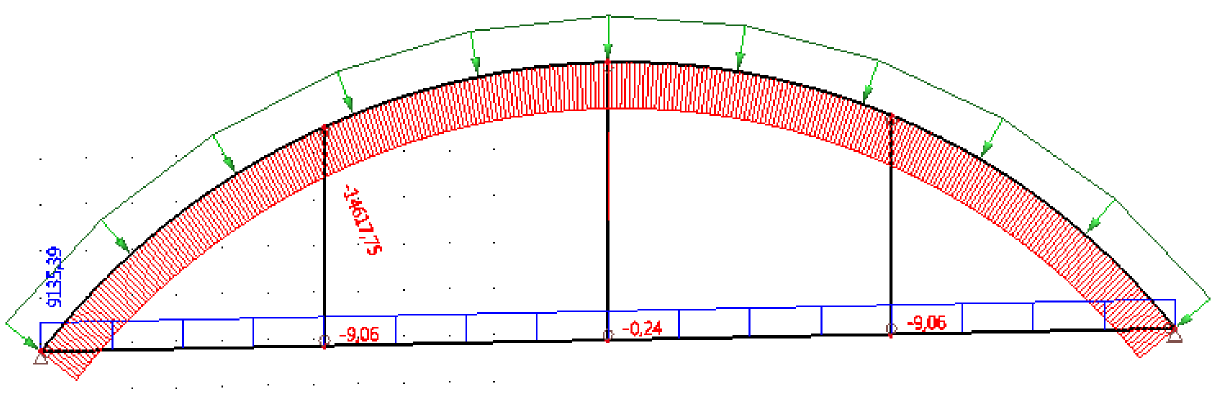

Figure 79: Normal forces for the Arched gate with 3 webs

The structural analysis (which is attached in Appendix D) has proven that the addition of webs does not result in relevant force reductions in the gate under a positive head difference. An explaination for this is that the stiffness of the arch is much larger than the stiffness of the straight plate. The webs will however result in a smaller buckling length for the straight plate in case of a negative head difference. Besides, the webs are functional in case a ship collides into the straigth plate. A total drape of 6 meters combined with 3 webs leads to the smallest mass for the gate. The entire gate will consist of sandwich elements. A 3-D impression of the gate configuration is presented in Figure 81.

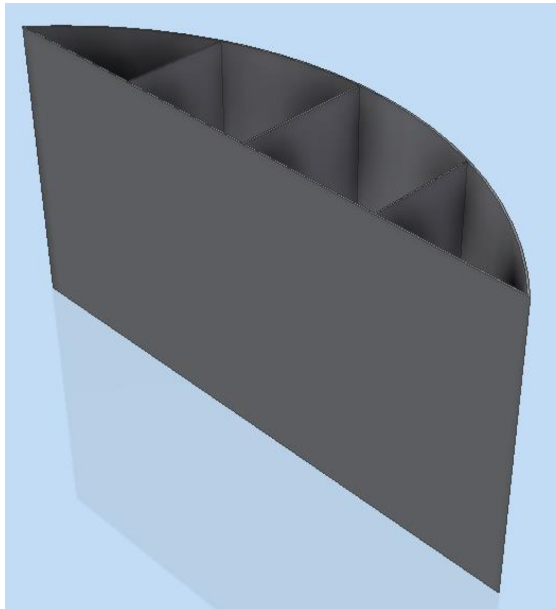

Figure 80: 3D-impression of the Arched gate

4.5.5. Summary of the design

- Plates are manufactured by vacuum injection
- Plates constructed as sandwich elements to increase the stiffness
- Mechanically fastened
- Arched plate: thickness of 80mm, of which 40mm consisting of core material
- Webs: 3 webs with a thickness of 60mm, of which 30mm consisting of core material
- Tensile plate: thickness of 68 mm, of which 34mm consisting of core material
- Mass of the gate equals 63 tons

The dimensions of the arched gate after optimization are presented in Figure 81

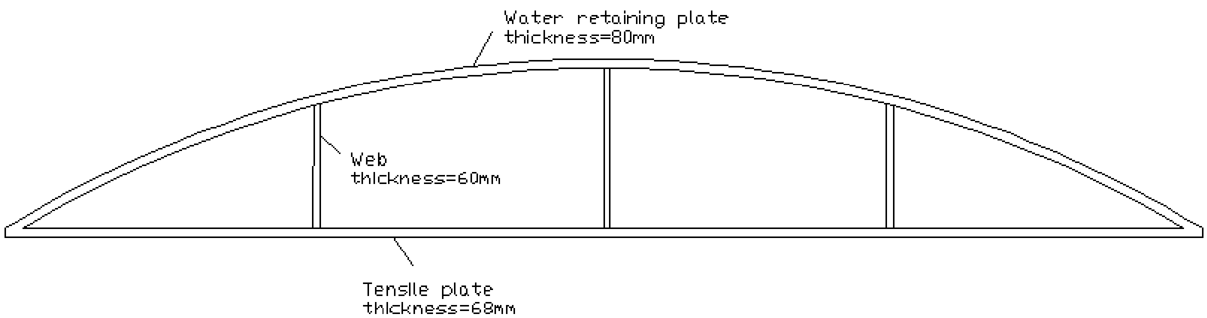

Figure 81: Global design of the Curved gate

The advantages and disadvantages for this gate alternative are summarized in Table 35.

Table 35: Advantages and disadvantages for the arched gate

Advantages	Disadvantages
Low mass due to curved shape	Structural adjustments are required to lift the gate in its centre of gravity
Small amount of joints required	Connections near support are complex

4.6. Gate alternative 5: Lens-shaped gate

4.6.1. Introduction

Instead of a single curved gate, another option is to apply two curved plates forming a lens-shaped gate. This will be beneficial in case of a negative head difference and ship impact from the downstream side. Besides, the lifting cables can easily be attached in the centre of gravity of the gate.

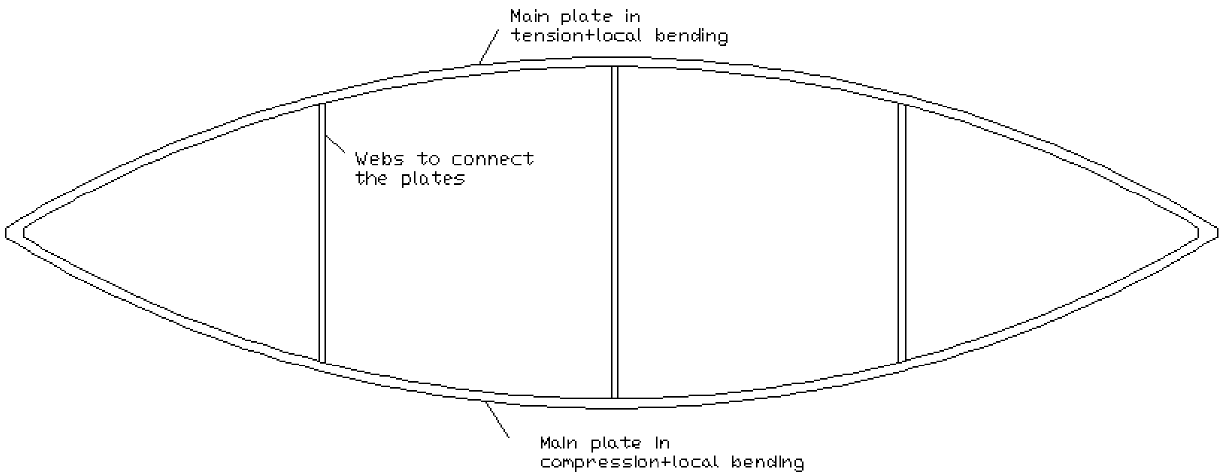

Figure 82: Concept of the lens-shaped gate

The function of the webs is to guarantee full cooperation between the two curved plates. Under the distrubuted hydrostatic load, one of the plates will be loaded in tension while the other one is loaded in compression. Except for the global forces, the plate will also be exposed local bending moments in between the webs.

The parameters which matter the most for the design are the drape of the water retaining plates and the number of webs. An increase of the drape will result in smaller normal forces in the plates due to a larger internal lever arm. This does however also result in larger lengths for the webs. The number of webs determines the local bending moments between the webs. More webs result in smaller bending moments in the curved plates, but also requires more material in the webs.

4.6.2. Static scheme

The geometry is translated into the static scheme which is depicted in Figure 83

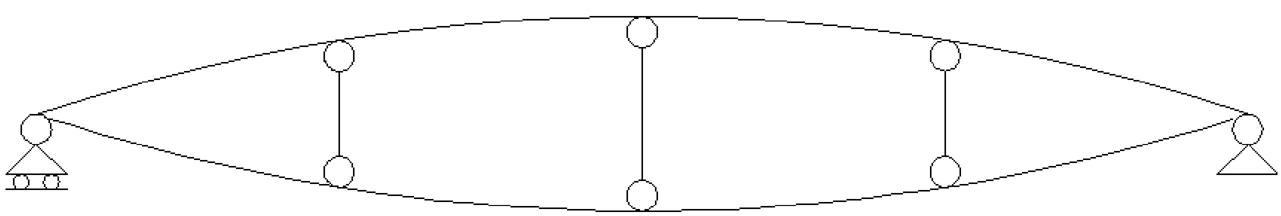

Figure 83: Static scheme for the lens-shaped gate

4.6.3. Connections

The connections of the webs to the water retaining plates can either be constructed by overlaminations or by peg-and-hole joints. The principle of overlaminations is presented in Figure 64.

4.6.4. Preliminary design

For the global design, both the drape of the main plates and the amount of webs are varied in order to obtain the optimal solution for this specific concept. Due to the curvature, analytical results are hard to obtain. Therefore, software program SCIA Engineer has been used to obtain the internal forces in the structure. A mathcad sheet has been set-up to find the drape and amount of webs resulting in the optimal gate configuration.

The main plates are designed for a combination of normal forces and bending moments while buckling was the restricting criteria for the webs. The calculations of the preliminary design can be found in Appendix D). Figure 84 shows the bending moments in the structure due to the hydrstatic pressures.

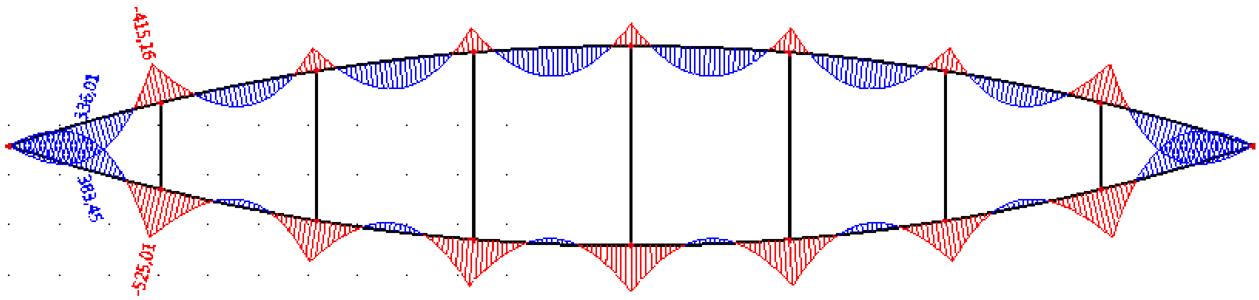

Figure 84: Moment line for the lens shaped gate with 7 webs

First of all a study is performed to find the optimal drape. An increase of the drape leads to smaller normal forces in the main plates, but also results in larger webs. An optimum is found for a drape of 4 meters. Consequently, a study to the optimal numer of webs has been carried out. These results are presented in Figure 85.

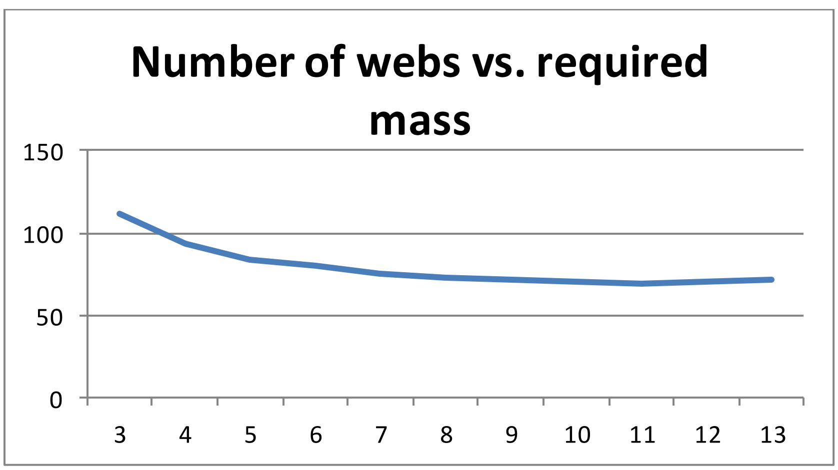

Figure 85: Number of webs versus required mass of the gate with a drape of 4 meters

A total of 11 webs leads to the lowest required mass for the entire gate. This would however also result in a very high number of joints. Besides, the compartments next to the supports would be very small, which makes inspection and maintenance to the gate difficult. It is decided to apply 7 webs instead. A 3D-impression of this variant is presented in Figure 86.

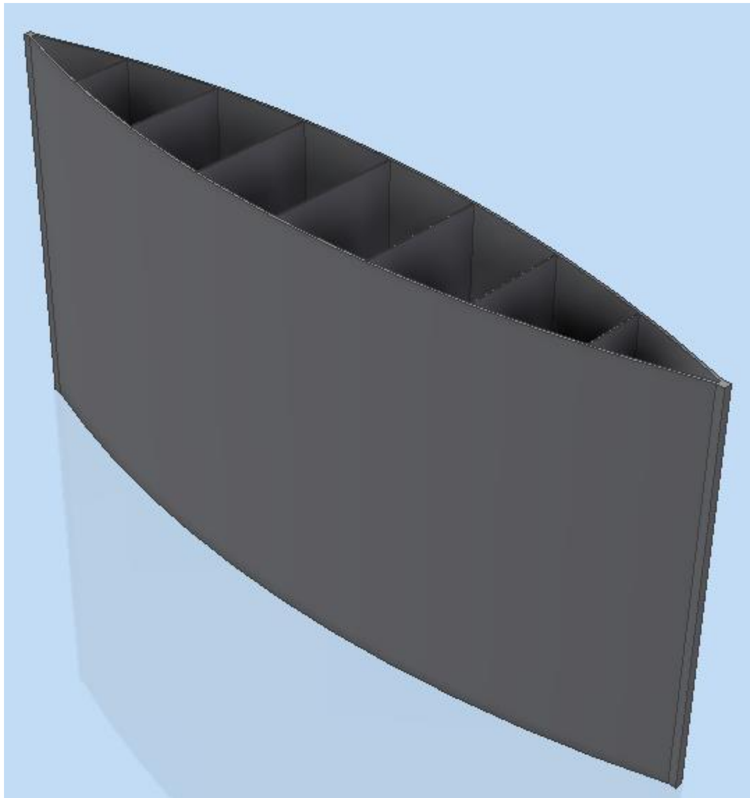

Figure 86: 3D-impression of the lens-shaped gate

4.6.5. Summary of the design

- Plates are manufactured by vacuum injection
- Plates are constructed as sandwich elements to increase the stiffness
- Connections through peg and hole joints
- Curved plates: thickness of 88mm, of which 44mm consisting of core material
- Webs: 7 webs with a thickness of 48mm, of which 24mm consisting of core material
- Mass of the gate equals 70 tons
- Shortest web has a length of 1,8m, joints can still be reached

The dimensions of the global design of the lens-shaped gate are presented in Figure 87.

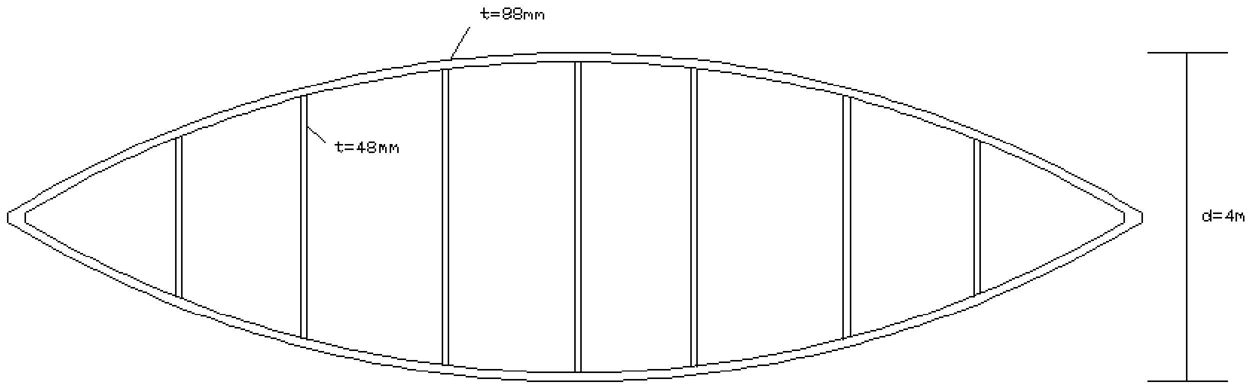

Figure 87: Global dimensions of the lens shaped gate

The specific advantages and disadvantages for the lens shaped gate are presented in Table 36.

Table 36: Advantages and disadvantages for the lens-shaped gate

Advantages	Disadvantages
Relatively low mass	Difficult to realize the joints
Easy to inspect due to the large compartments	High forces at the connection near the support
Lifting equipment can be attached in the center of gravity of the gate	Lock sill needs to be curved to guarantee watertightness

4.7. Selection of most suitable gate alternative

In order to select the most promising gate alternative for further elaboration, a multi-criteria analysis (MCA) has been performed. At first, a list of different criteria which are ought to be important for lock gates has been created by a brainstorm session. Hereafter, each criterion is given a weighting factor between 1 and 5 based on its relative importance. The four alternatives are consequently rated on how well they perform on the different criteria. The total score of each variant is the score per criterion times the weighting factor summated over all criteria. The variant with the highest score per unit of weight is selected for further elaboration.The following criteria are used during the MCA:

Resiliency: The ability to preserve the structural integrity for load situations which exceed the design situations. One can think for example about vulnerability to ship impact or the ability to resist load situations with an exceedance frequency of less than 1/1250 per year.

Reliability: The reliability holds close to the special risks which are acompanied with the design, and the difficulties which are expected to arise during a more detailed design. This includes expected stress concentrations near joints, but also the ability to connect the gate watertight to the sill and walls of the lock head.

Maintainability: The possibility to reach all the components for inspection, maintenance and repair. This criterion is related to the size of the compartments and the area of the gate which is in direct contact with the water.

Aesthetic value: The aesthetic value is rated on the way in which the structure fits in the surroundings and the possibility for the structure to become a landmark in the future.

Constructability: The ease with which the gate can be constructed. Penalties are given for complex geometries and a large number of joints. Besides, this criterion includes the possibility to attach the lifting equipment to the gate in the center of gravity.

The results of the MCA are presented in Table 37. The motivation for the ratings is given in Appendix F). The lens shaped gate is selected for further elaboration because of the best profits per unit of mass.

Table 37: Result of the multi-criteria analysis

Criterion	Weighting factor	Warren truss gate	Stiffened plate	Curved gate	Lens-shaped gate
Resiliency	4	7	4	4	7
Reliability	4	8	4	5	7
Maintainability	3	4	5	7	6
Aesthetic value	2	6	5	9	9
Constructability	3	4	8	6	6
	Total score	**96**	**81**	**93**	**110**
	Mass (t)	145	150	63	70
	Score per ton	**0,66**	**0,54**	**1,48**	**1,57**

5. Conceptual design of the lens-shaped gate

This chapter describes the further elaboration of the lens-shaped gate. Firstly, The structural shape which has been used during the study to gate alternatives in chapter 4 will be reviewed to investigate if any further optimizations are possible. Hereafter, the 2D-scheme will be converted to a 3D-design including the openings required for filling- and emptying, and a further elaboration on the connection between the gate and the walls of the lock head. The locations of these elements are presented in Figure 88 and Figure 89.

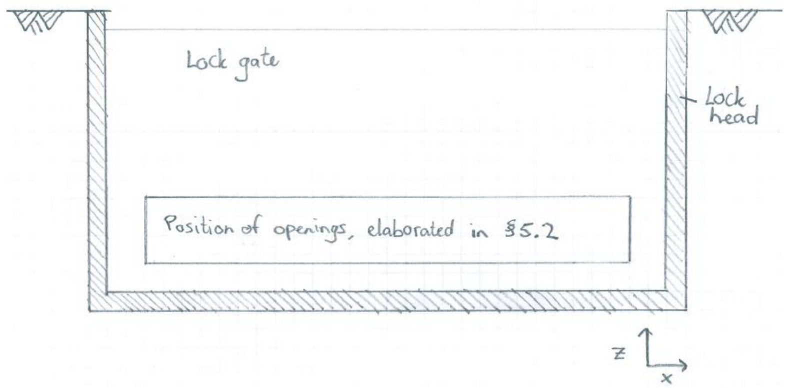

Figure 88: Location of the openings in the gate, elaborated in 5.2

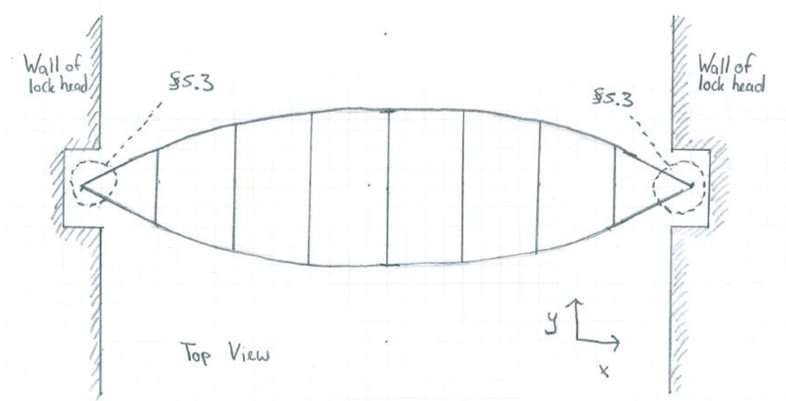

Figure 89: Location of the connection between lock gate and walls of the lock head, elaborated in 5.3

The openings in the gate will inevitably result in stress concentrations because material will be removed at the locations where the hydrostatic pressures are the largest (see Figure 58 in combination with Figure 88). The goal is to find the position, shape and size of the openings resulting in the smallest peak stresses, while also keeping in mind that the locking time for a vessel should be as short as possible.

The connection between the gate and lock head on the other hand need to be designed in such a way that the watertightness is guaranteed in a robust manner. The current 2D design does not yet fulfill these requirements, as Figure 89 shows. This subject is further elaborated in 5.3.

This chapter is concluded with a further elaboration of the production process in order to find out in what way the structure can best be produced, and what limitations are accompanied regarding the plate thicknesses, shapes and sizes of the elements.

5.1. Review of the selected structural shape

In this paragraph, the flow of forces through the gate are investigated. This is important for two reasons: firstly, founded design decisions can only be made once the structural behaviour of the gate is fully known and secondlyto see if any adjustments to the geometry will result in a more efficient use of material.

The function of the gate is to redirect the forces related to the head difference over the gate to the supports at the walls of the lock head in an efficient way. Therefore, the shape of the structure has been chosen in such a way that the form holds close to the parabolic moment line of the structure.

Just as the parabolic tendons in prestressed concrete, the curved elements can be schematized as straight plates with addition of a distributed load which is originating from the relation between normal forces in the plate and the radius of curvature. Ideally, the hydrostatic forces would be solely resisted by a single curved plate, so that the forces are redirected to the supports by normal forces only. This would however result in large thrust forces at the supports. Besides, the gate would be very vulnerable to loading situations which are different to the hyrdostatic pressures because of the slender design accompanied with the structural shape.

For those two reasons, it has been decided to design the gate as a set of two curved plates, which are connected to each other by means of webs. These webs fulfill three structural functions: Firstly they guarantee full cooperation between the two plates to increase the robustness of the structure. Secondly, the webs result in a reduction of the buckling length so that the stability of the structure is increased. Thirdly, the webs tend to smooth the distribution of stresses (see Figure 91) over the height so that a larger effective height of the gate is created. The drawback of these webs is that local forces are introduced to the curved plates, resulting in a structural shape which is not as close to the force lines in the structure anymore as it used to be. The improvement of the robustness of the gate is however considered to be more important than the additional material required to guarantee the strength of the gate. A schematizattion of the forces flowing through the gate is presented in Figure 90. The figure shows the top view on the gate, and the forces in horizontal direction are not displayed.

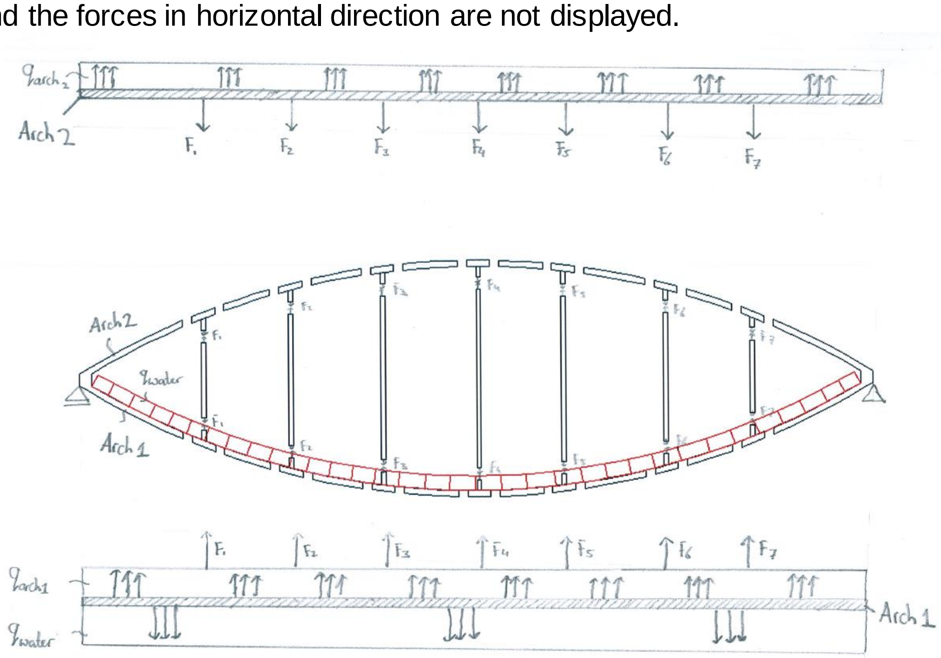

Figure 90: Flow of forces through the gate

As the water pressures are acting on the first water retaining plate (in Figure 90 named Arch 1), the gate will start to deform. The deformations result in tensile forces in both the loaded water retaining plate and the webs. Due to the curvature of the plate, the tensile forces will result in a distributed load acting in the opposite direction of the water pressure. The sum of forces from the curvature and webs need to balance the resultant of forces from the water pressures. Because the distribution of forces acting in the two directions is not exactly the same (see the schematization of Arch 1 at the bottom of Figure 90), both normal forces and bending moments will be present in the plate.

The second arch needs to resist the forces which are introduced to the plate by the webs and at the connections to the loaded arch. In the current concept, this is reached by compression in the arch, resulting in a distributed load acting in the opposite direction of the forces from the webs (see the schematization at the top of Figure 90). Again, this leads to an uneven distribution of loads in the two directions, resulting in bending moments in the plate. From a structural point of view, a faceted structure with kinks at the positions of the webs would have been more attractive. From the view of a producer however, this shape does not seem to be feasible for the selected production process elaborated in 5.4. Therefore it has been decided to preserve the structural shape consisting of two arched plates.

5.2. Design of the openings in the gate

As stated in paragraph 2.2.5, openings equiped with valves in the gate appear to be the best solution for this specific lock to allow for filling and emptying of the chamber. This does however result in major effects on the flow of forces through the gate. These openings are usually positioned close to the bottom of the gate, where the hydrostatic pressures acting on the gate are the largest (see Figure 91 on page 89). Disruptions of the curved plates, which are mainly loaded in tension or compression as explained in section 5.1, will unevitably result in peak stresses around these openings.

For the design of the openings,an optimal solution has to be found taking into account three conflicting objectives: firstly, the time required for the filling and emptying of the lock chamber needs to be as short as possible. Secondly, the forces in the mooring lines of the vessels during filling and emptying should be limited. Thirdly, the stress concentrations around the openings need to be reduced to a minimum.

During the design of these openings, the following parameters need to be determined:

- Vertical position of the openings;
- Shape of the openings;
- Surface area of the openings;
- Lifting velocity of the valves.

5.2.1. Required surface area

The first important parameter for the design is the surface area of the valves, which can be seen as a measure of the total time required for filling- and emptying of the lock chamber. Minimization of the lock cycle time is important since every additional waiting hour for a vessel costs approximately €200,- [36]. The new lock chamber will cope with about 17500 vessels on an annual basis, which means that every additional minute per locking cycle leads to approximately €60.000,- waiting costs per year. In order to minimize the lock cycle times, the openings should be as large as possible. On the other hand hoewever, larger disruptions in the water retaining plate results in higher stresses.

An indication of the required surface area is found by comparing the size of the current Beatrixlocks to the new chamber. By approximation, the ratio between surface area of the lock chamber and area of the openings needs to be constant, under the assumption that the size of the openings has been optimized for the existing lock gates.

$$\frac{A_{c1}}{A_{o1}} = \frac{A_{c2}}{A_{o2}} \rightarrow A_{o2} = \frac{A_{c2}}{A_{c1}} * A_{o1}$$

$A_{c1} =$ Surface area of the existing lock chambers
$A_{o1} =$ Area of the openings in the existing lock gates
$A_{c2} =$ Surface area of the new lock chambers
$A_{o2} =$ Required area of the openings in the new lock gates.

The chambers of the current Beatrixlocks have a surface area of $4050\ m^2$ while the third lock will cover an area of approximately $5000\ m^2$. The old gates each contain 6 openings with a width of $2{,}34\ m$ and a height of $2{,}17\ m$, resulting in a total area of the openings of $30{,}5\ m^2$. The required size of the openings in the new lock gates will thus be:

$$A_{o2} = \frac{A_{c2}}{A_{c1}} * A_{o1} = \frac{5000}{4050} * 30{,}5 = 37{,}6\ m^2$$

5.2.2. Vertical position of the valves

Another important parameter is the vertical position of the openings in the gate. If the openings are located very close to the bottom, the high flow velocities near the bottom require expensive mittigation measures to prevent erosion. On the other hand, valves which are positioned too high result in large forces on the vessels due to high flow velocities near the water surface. Based on different reference projects, the minimum distance between bottom of the gate and the valve equals 0,5 meters. The valves at least need to be beneath the lowest locking level so that levelling of the water is always possible.

The width of the valves is limited by the distance between the webs of the gate. Interruption of these webs will result in unfavourable stress concentrations. A required distance of at least 200 millimeters between the openings is assumed to be able to introduce the forces from the valves to the gate. This stll has to be verified by finite element modelling. The available area for the openings is visualized in Figure 91.

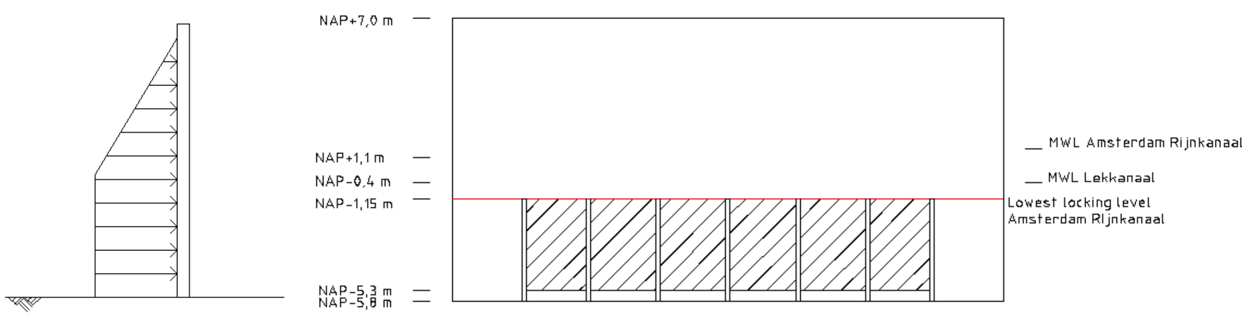

Figure 91: Available area for the openings in the gate (right) and a side view on hydrostatic forces (left)

The required area of the openings is equal to $37{,}6\ m^2$, while the available area is equal to $77{,}2\ m^2$. The study to the shape of the openings resulting in the smallest stress concentrations in the next paragraph will determine how the available area can be optimally used.

5.2.3. Shape of the openings

The shape and size of the openings determine the stress concentrations occuring in the water retaining plates. Three different shapes are considered for the openings: rectangular, circular elliptical.

Sobey [50] investigated the stress concentration factors for rectangular holes with rounded corners loaded in pure, unidirection tension. A function has been derived which relates the radii of the corners ,the height of the opening and the width of the opening to the stress concentration factor. The stress concentrations for a round opening is found in the graph at the point where $a = b = r$. An ovaloid is represented by any point on the line where $b = r$. The meaning of the governing parameters is presented in Figure 92, while the results can be found in Figure 93.

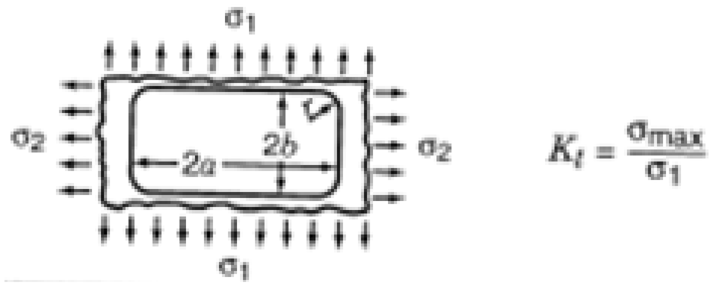

Figure 92: Definition of the different parameters of Figure 93 [50]

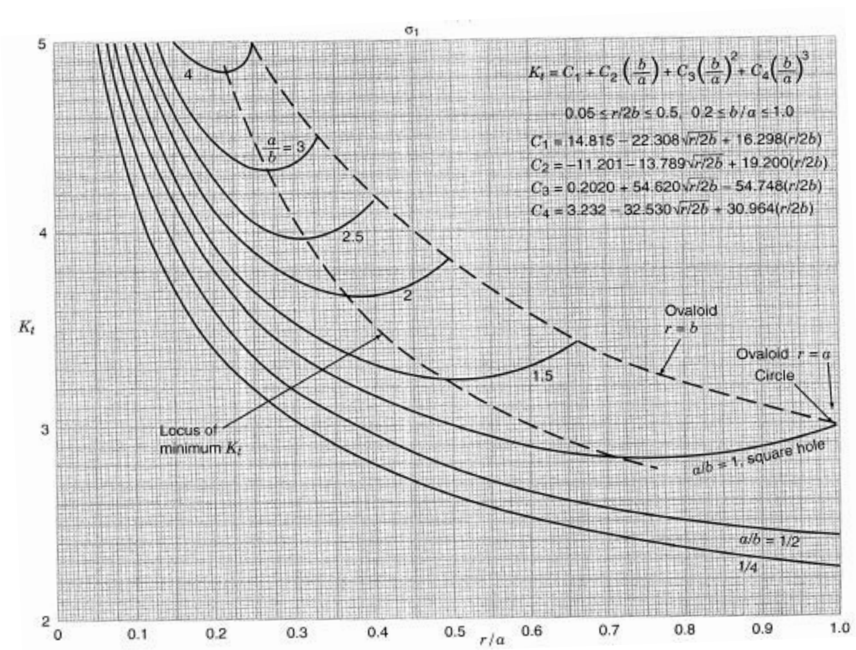

Figure 93: Stress concentration factors Kt for a rectangular opening with rounded corners, loaded in uniaxial tension ($\sigma_2 = 0$) [50]

It appears that smaller radii at the corners of the openings tend to result in higher peak stresses. Since the distance between the individual openings will be small compared to their diameter, it is fair to schematize the different small openings as being one large opening. The width of the combined openings is much larger than the height (b>>a), so the minimum stress concentration factor is found for an elliptical shape of the opening (see Figure 93).

This conclusion should however be regarded with great care for two reasons. At first, the functions for the peak stresses have been derived for plates in pure tension, while in the considered scenario the plates have to resist a combination of normal stresses and bending moments. Secondly, the expressions have been derived for homogeneous materials. The complex nature of fiber-reinforced polymers consisting of many different materials with different properties in all directions may influence the stress concentrations around the hole. It is recommended to perform a sensitivity analysis with help of finite element software during a more detailed design to find out whether the chosen shape of the openings indeed results in the optimal design.

5.2.4. Dimensions of the openings

According to Figure 93, the stress concentrations will be the smallest if the envelope of the shape of all the valves together is as close as possible to an ovaloid. This is reached if the two openings close to the support are constructed as circular openings while the other four openings are constructed as rectangular openings with rounded corners. This option is visualized in Figure 94.

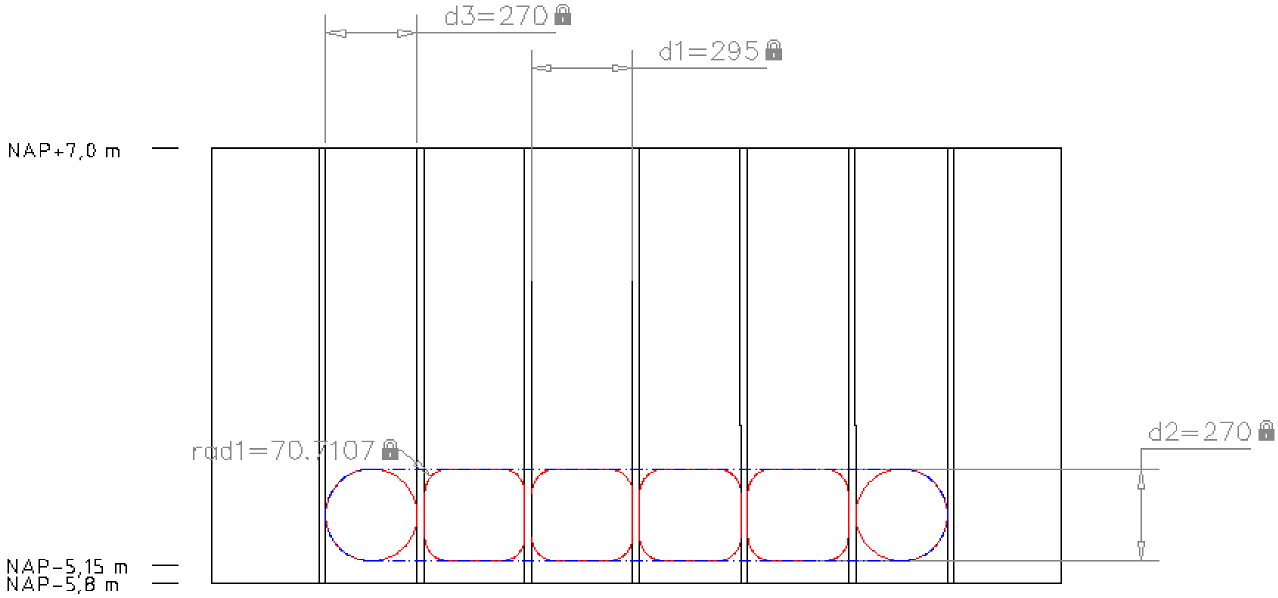

Figure 94: Shape of the openings resulting in the smallest stress concentrations

The producability however also needs to be taken into account. Short culverts need to transport the water through the gate. These culverts can easily be constructed by filament winding (see 1.3.1) if they are constructed as circular tubes. Besides, it is convenient to obtain the same size for all the valves. Not only will this lead to quicker manufacturing due to a higher repetition factor, also less spare parts need to be stored if the individual valves and culverts are interchangeable.

In order to arrive at the estimated required area of the valves, 6 openings with a diameter of 3 meters will be created. The bottom of the openings will be positioned 0,65 meters above the sill, a distance which is based on reference projects. The total area of the openings equals 42,4 m^2. The final configuration is presented in Figure 95.

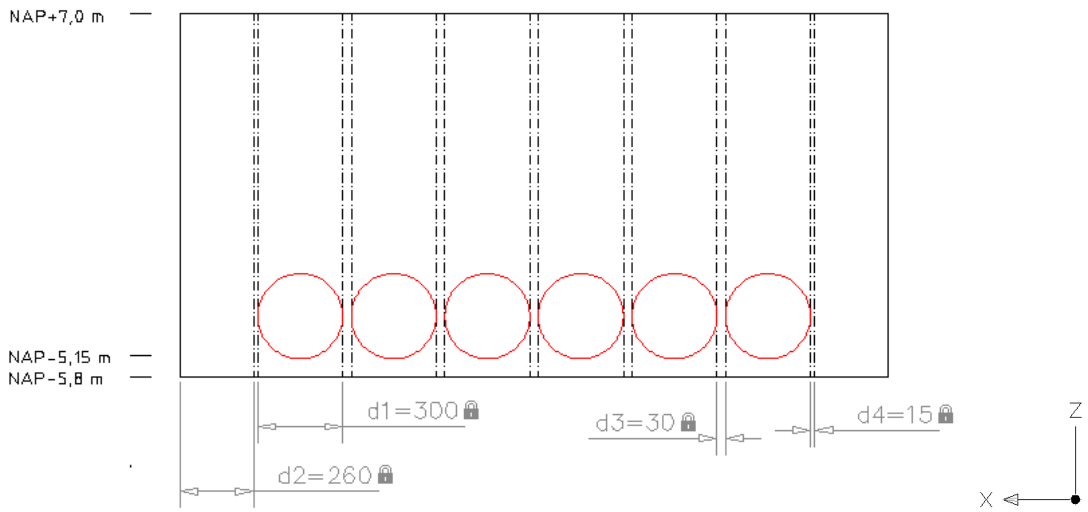

Figure 95: Final configuration of the openings in the gate (cm)

In order to study the effects of these openings on the peak stresses in the curved plates qualitatively, isolines of the forces around these oenings have been drawn. The idea beind these isolines is that the stresses multiplied by the distance in between two lines is constant. The position of the stress concentrations are obtained by determination of the positions where contraction of two adjacent lines take place. The results of this analysis are presented in Figure 96. The distribution of forces at the boundaries are estimated qualitatively, based on the distribution of hydrostatic pressures (see Figure 58) with some force redistribution of forces over the height as a result of the webs.

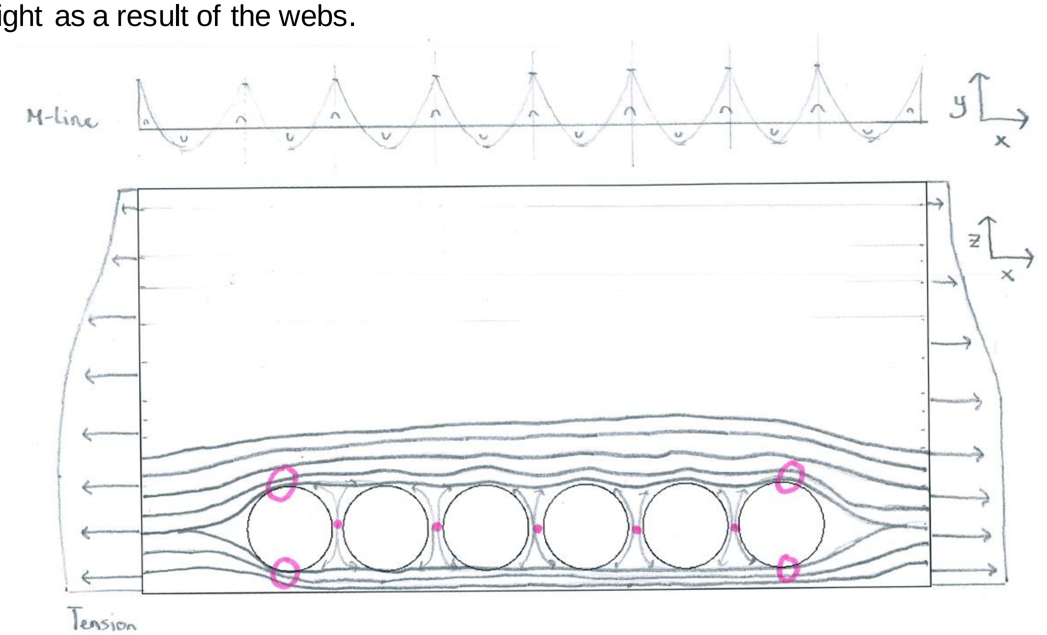

Figure 96: Isolines of the forces in the gate around the openings

This analysis shows that the largest stress concetrations are expected to occur around the openings which are the closest to the lock walls. Besides, the strips in between the openings also require further analysis since these seem to be relatively narrow to be able to resist the forces coming from the valves. These most vulnerable areas are investigated quantitatively by a finite element analysis, which is further discussed in chapter 6.

Except for the structural advantages of circular openings compared to rectangular ones, it also leads to favourable flow paterns. The discharge through the valves right after opening will happen smoother since the width of the bottom of the openings is small compared to initial width of the sharp-edged openings. This leads to a smaller initial increase in discharge right after opening of the valves and therefore results in smaller hawser forces.

The time required for filling or emptying of the lock gate during the governing head difference of 6,4 meters is calculated to be a little less than 6 minutes, which is ought to be acceptable. The underlying assumptions and the calculations itself can be found in Appendix G).

Now that the dimensions of the openings are known, it should be checked that the hawser forces do not become too large. These hawser forces consist of 4 different components [37]:

- Translation waves
- Difference in impulse over the vessel length
- Friction
- Waterjet against the bow

Translation waves are supposed to be the governing contributors to the hawser forces. These forces are calculated in Appendix G) and turn out to be approximately 1,5‰ of the mass of mass of the governing vessel, which is equal to 142 kN. Inland navigation vessels are usually moored by two hawsers [36], resulting in a force of 71kN per cable for the governing locking cycle. This is smaller than the heaviest cables which can still be operated manually[5]. More accurate calculations of these forces can for example be obtained by making use of Lockfill, a software tool developed by Deltares.

Large hawser forces due to a water jet against the bow of the vessel can be prevented by application of beams to dissipate the energy of the water by turbulence. Design of these beams is however left out of the scope of this project.

The valves required to control the discharge will be constructed as rectangular plates with a width and height of approximately 3,2 meters. This will result in an overlap of 10 centimeters around all four sides of the openings. Hollow tubes will be connected to the openings to take care of the transport of water through the gate. The structural design of the valves is elaborated in 7.6, the tubes are further elaborated in 7.5.

5.3. Connection between gate and walls of the lock head

In order to guarantee the watertightness at the vertical connection to the lock head, flat contact surfaces are preferred. Therefore, two massive blocks over the full height of the gate will be constructed to connect the two curved plates at the supports. Not only will this be favorable for the watertightness, the additional material also helps to resist the forces at the connection between the two water retainng plates, where the shear forces are the largest. Two small recesses in the lock head need to be created to accommodate these blocks. The design of these blocks are further elaborated in section 7.3. An overview of the lay-out of the global structure is presented in Figure 97. Elements such as valves, lifting equipment and vertical sliding profiles are not yet included in the drawing.

[5] i.e. steel cables with a diameter of 22 millimeters and a fracture load of circa 105 kN [33]

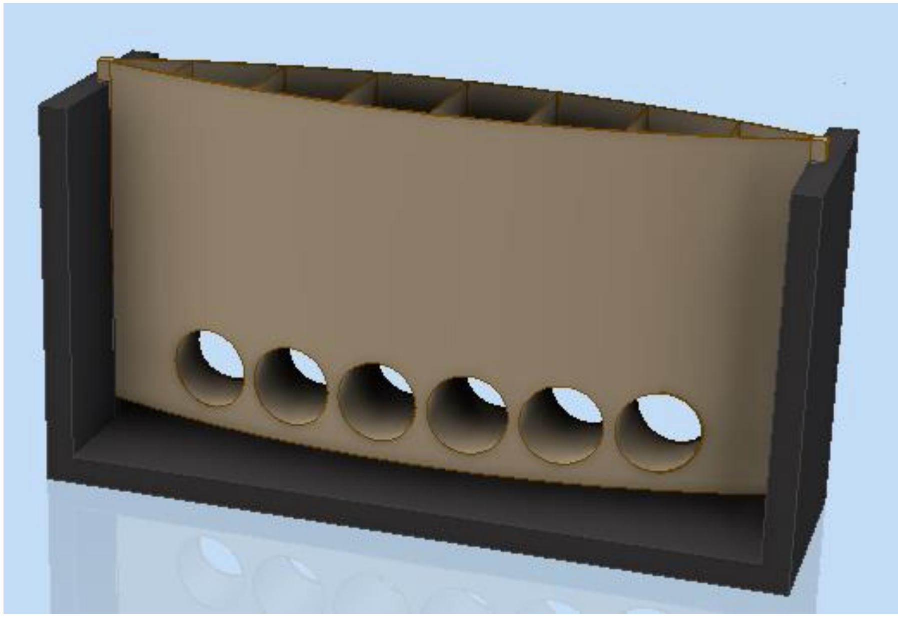

Figure 97: Visualization of the global design of the lens shaped gate

5.4. Production process

Since the global geometry has yet been defined, the production process can now be further elaborated. As already stated in the study to gate alternatives, the plates will be produced by vacuum injection. Special attention needs to be paid to the infusion strategy, design of the mould, curvature of the plates and special details of the plates. These subjects will be covered in this section.

At present, the largest available mould for the civil sector is owned by FiberCore. This mould has a length of 25 meters, a width of 6 meters [51] and is used in combination with the vacuum injection technique. The mould consists of a flexible, steel plate supported by many poles which are individually adjustable in height to create the desired curvature. This makes the mould flexible and usable for multiple structures. The costs of such a mould, which is able to produce around 100 structures over its lifetime, are approximately €100.000,- [51]. FiberCore is planning to construct a much larger mould with a length of 50 meters.This mould will be large enough to produce the individual plates of the design of the lens-shaped gate in one piece.

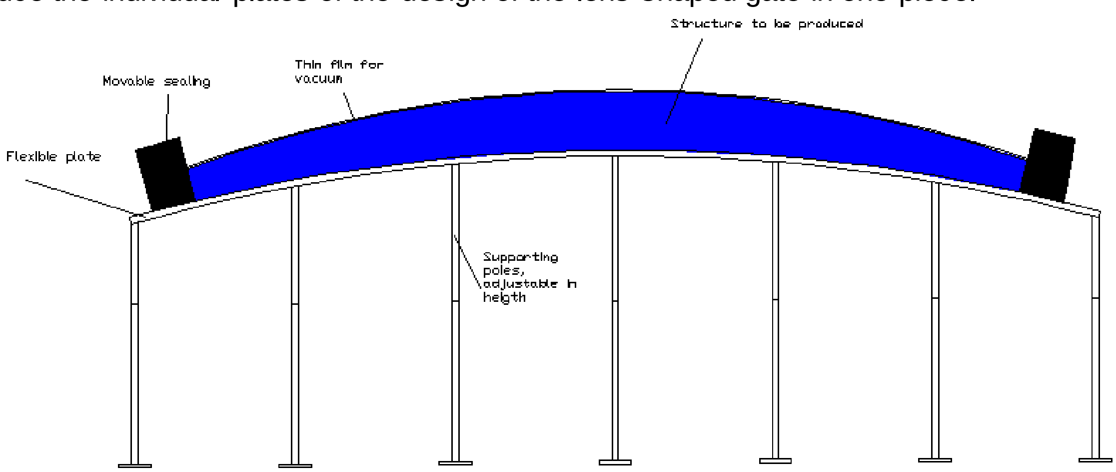

Figure 98: Impression of the moulding system

The resin will be injected at many injection points, each taking care of an area of approximately 2 m^2 of the structure. This is a standard procedure for the production of large FRP elements, resulting in a good quality control during production [32]. The resin is injected at the bottom of the plate and flows to the top of the plate by the vacuum. The thickness of the structure is the restricting factor for this production technique: the vacuum injection technology functions for sandwich structures up to a total construction thickness of 1,2 meters, while the skin thickness should not exceed 33 millimeters [32]. For larger thicknesses, the resin is unable to reach the top skin of the sandwich, which means that other production techniques are required.

Core material is only available in straight blocks. Curved elements need to be produced by placement of the blocks under an angle with respect to each other. This leads to additional space between the cores and results in larger amounts of resin to be injected. A single foam block usually has a width of approximately 100 millimeters. The core is only functional during production of the elements to create the internal lever arm between the skin plates. Once the resin is cured, the core does not contribute to the mechanical properties of the laminate. The shear forces between the skin plates are solely resisted by the Z-structure of the fibers instead.

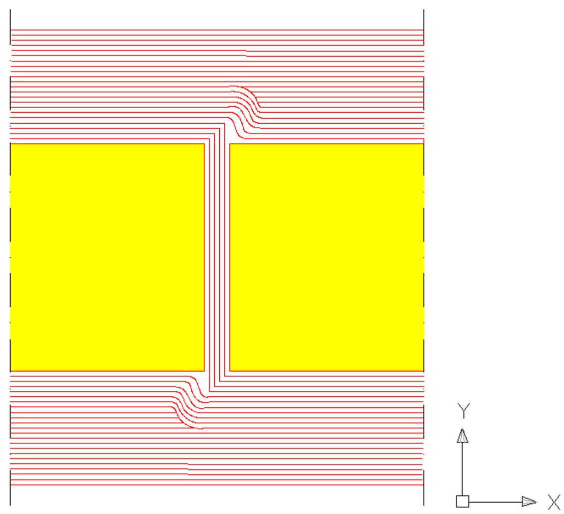

Figure 99: Impression of Z-structure of the fibers around the cores

As a starting point for the structural design, a space of approximately 3 millimeters is assumed in between the cores every 100 millimeters, based on an interview with FRP-expert Peeters [51]. An impression of this principle is presented in Figure 99. The principle is somewhat compareable to H- and I-profiles in the steel industry, where the flanges take care of the bending moments and the webs provide shear resistance.

These spaces in between the core which are filled with FRP result in an additional weight of the structure of nearly 2 tons, which is approximately 3% of the total structural weight. The determination of the volumes in between the cores can be found in Appendix G).

6. Structural design of the lens-shaped gate

6.1. Introduction

In order to study the effects of the conversion from 2D to 3D on local stress concentrations quantitatively, to study the stability of individual members and to study the possible optimizations to the structure, the structure has been modelled with help of the finite element software ANSYS.

At first, a relatively simple model has been set up in SCIA Engineer and compared to the (simplified) calculations made during the study to gate alternatives. Hereafter, the complexity of the model has been gradually increased and the results have been compared in order to be able to validate the correctness of the finite element model. The scheme which has been used to arrive at the structural design is presented in Figure 100.

This chapter starts with an overview of the differences in boundary conditions and starting points of the design between the study to gate alternatives and the structural design in 3D. Secondly, the set-up and results of the finite element models are presented. Thirdly, an analysis has been performed to find out in what ways the design can be improved by structural adjustments to the finite element model. This chapter is concluded with a review of the creep deformations and fatigue resistance of the structure.

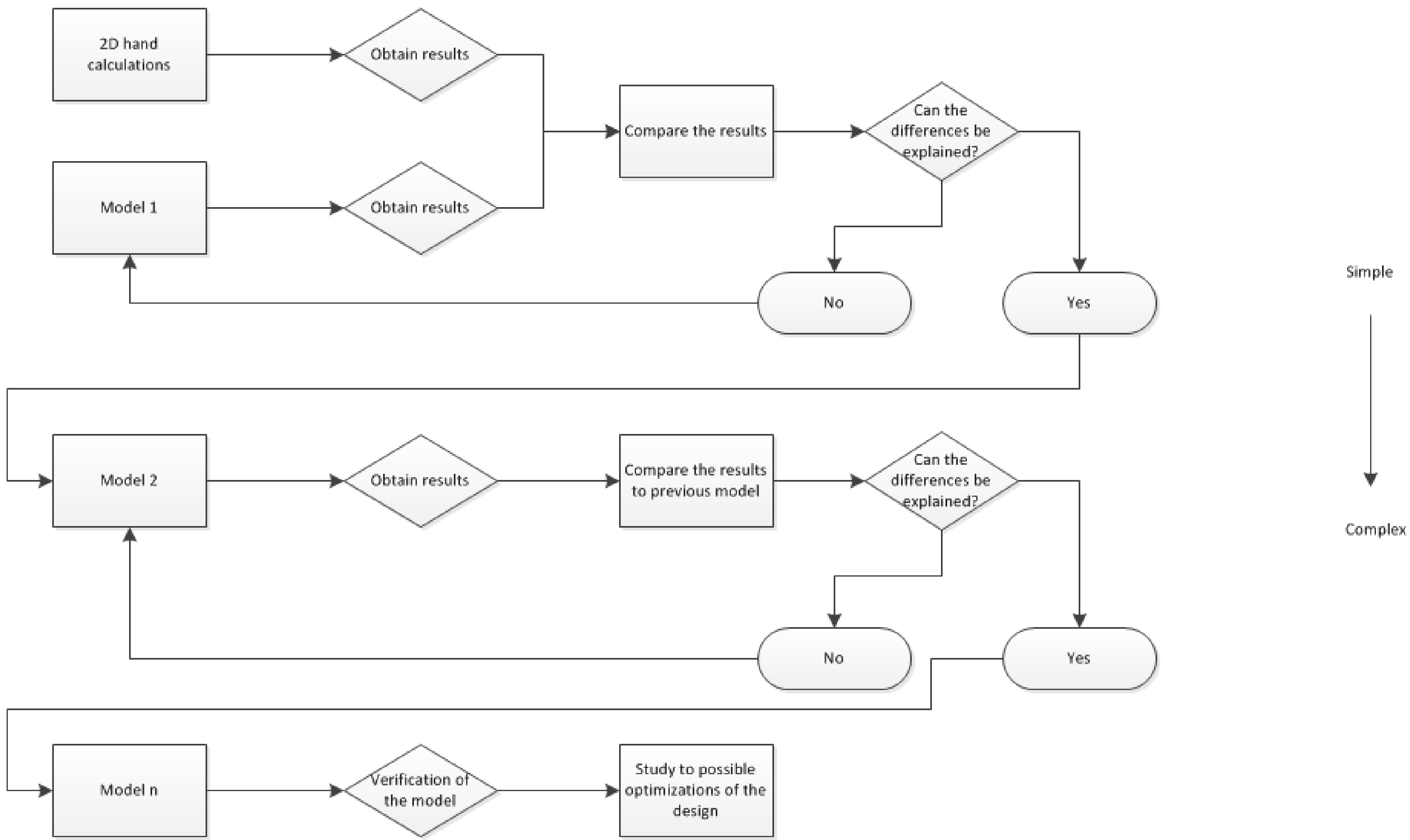

Figure 100: Scheme which has been used in order to arrive at the structural design

6.2. Differences to the study to gate alternatives

During the study to gate alternatives, the loads related to the maximum head difference of 7,0 m have been placed on the gate in such a way that the webs are loaded in compression. This is not correct, as Figure 101 shows. The maximum head difference of 7,0 meters only has to be retained by the upstream gate (at the Lek side of the lock), where the hydrostatic pressures are acting in the opposite direction. For the downstream gate, the loads acting on the structure are in the same direction as considered during the study to gate alternatives, but this gate only needs to retain the head difference related to the maximum locking level, which is equal to 6,4 meters. In this chapter, the load case for the upstream gate has been considered as governing for the structural design due to the larger hydrostatic pressures related to the head difference.

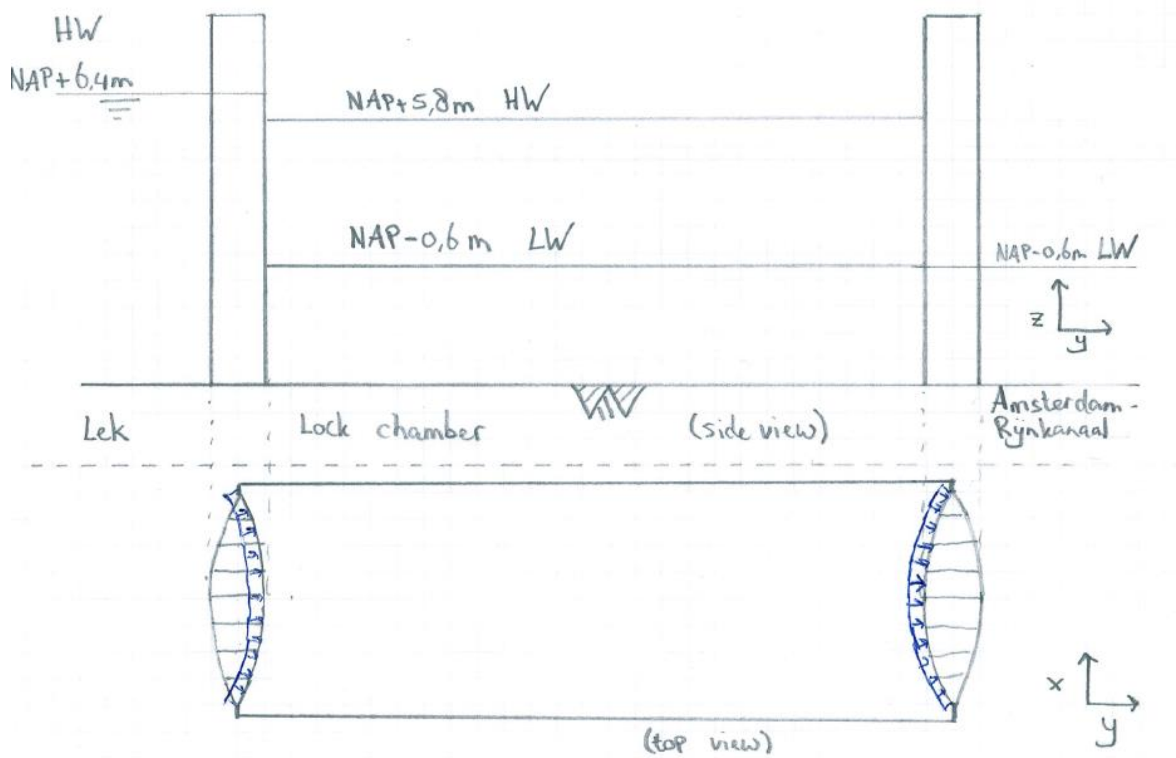

Figure 101: Overview of the water levels and directions of loading for the upstream- and downstream lock gate

From the failure tree which is presented in Figure 24, only the failure mechanisms buckling, delaminations and fiber rupture have been incorporated in the design. Wrinkling and crippling can be prevented by a suitable distance between the z-structures of the fibers (which is further explained in section 1.4.2). Besides, failure of joints is also not considered due to a lack of available literature on this subject. Finally, matrix yielding, fiber pull-out and matrix cracking are not considered because for the selected combination of fibers and resin, rupture of fibers will happen before these failure mechanisms take place.

The way to arrive at the ultimate strain in the material has changed compared to the study to gate alternatives. During the study to gate alternatives, the maximum strain in the material has been limited to 0,28%, which is based on micro-failure of the fibers induced by strains perpendicular to the fiber-direction. After consultancy of FRP-expert Peeters from FiberCore Europe, this criterion has been changed. According to Peeters, micro-cracking of the fibers does not harm the water retaining function of the gate as long as the remaining fibers are still able to resist the governing forces [32]. During this stage of the design, the maximum allowable strain in the SLS has therefore been set to 1,2%, which is in accordance with the CUR 96. This charasteristic value has been divided by conversion factors for temperature effects, moisture effects, creep effects and fatigue effects to obtain the design value of the strength (ULS). For the selected fiber type, design lifetime and fiber orientation the difference between the two criteria is negligible .Therefore, this adjustment does not result in differences to the optimal shape. The following design values for maximum stresses and strains have now been obtained:

$$\varepsilon_{R;d} = \frac{\varepsilon_{R;c}}{\gamma_m * \gamma_c}$$

$$\varepsilon_{R;c} = 1{,}2\%$$

$$\gamma_m = \gamma_{m1} * \gamma_{m2} = 1{,}35 * 1{,}2 = 1{,}62$$

$$\gamma_c = \gamma_{ck} * \gamma_{cv} * \gamma_{ct} * \gamma_{cf} = 1{,}44 * 1{,}3 * 1{,}1 * 1{,}1 = 2{,}27$$

$$\varepsilon_{R;d} = \frac{1{,}2\%}{1{,}62 * 2{,}27} = 0{,}33\%$$

In order to prevent delaminations, the shear stresses in the structure should not exceed the design value of the interlaminar shear strength, which is calculated by division of the charasteristic values of strengths by the material factors [52]:

$$\tau_{R;d} = \frac{\tau_{R;c}}{\gamma_m}$$

$$\tau_{R;c} = 20\ N/mm^2$$

$$\gamma_m = \gamma_{m1} * \gamma_{m2} = 1{,}35 * 1{,}2 = 1{,}62$$

$$\tau_{R;d} = \frac{20\ N/mm^2}{1{,}62} = 12{,}35\ N/mm^2$$

Besides, the structure has to be checked for local stability of the plates. The safety factor on buckling should at least be 2,5, as stated in the CUR 96 [25]. This safety factor consists of a combination of a load factor and a material factor.

The fiber lay-up consists of UD-lamellas with a fiber fraction volume of 50%. For the curved water retaining plates, 55% of the fibers will be placed in the main direction of loading, while the other 45% of the fibers will be evenly distributed over the -45°/+45°/0° directions. This is reached by placement of 11 layers of fibers in the main direction per skin while the other three direction each are equiped with 3 layers of fibers. The thickness of a single ply equals 1,1 millimeters. The core thickness will become 44 millimeters for these plates, resulting in a total plate thickness of 88 millimeters.

The laminate properties are obtained by application of the semi-empirical formulae of Halpin-Tsai (which are explained in Appendix B) combined with the classical laminate theory (which is explained in Appendix C). With help of computer program Kolibri, the following stiffness matrix has been obtained for the water retaining plates:

$$[ABD] = \begin{bmatrix} 1.2117 \cdot 10^{9} & 2.3895 \cdot 10^{8} & 0 & 0 & 0 & 0 \\ 2.3895 \cdot 10^{8} & 7.4672 \cdot 10^{8} & 0 & 0 & 0 & 0 \\ 0 & 0 & 9.0640 \cdot 10^{8} & 0 & 0 & 0 \\ 0 & 0 & 0 & 1.3684 \cdot 10^{6} & 2.6986 \cdot 10^{5} & 0 \\ 0 & 0 & 0 & 2.6986 \cdot 10^{5} & 8.4330 \cdot 10^{5} & 0 \\ 0 & 0 & 0 & 0 & 0 & 3.8475 \cdot 10^{5} \end{bmatrix} \text{N, m}$$

Figure 102: Stiffness matrix of the water retaining plates

The following Young's moduli are obtained if the skins of the sandwich elements are schematized as a homogeneous plates:

$$E_x = 25.800\ GPa$$
$$E_y = 15.900\ GPa$$

As already mentioned in the introduction, the complexity of the model has been increased stepwise in order to be able to check the correctness of the outcomes of the model. The different steps are presented in Table 38.

Table 38: Overview of the models used during the structural design

Step	Model	Applied software
1	2D-schematization, $q = 70kN/m^2$	Hand calculations and SCIA Engineer framework
2	Model 1 extruded to 3D-model, poisson ratio of 0	SCIA Engineer
3	Model 2, with poission ratio of 0,3	SCIA Engineer
4	Model 3, modelled in ANSYS	ANSYS Static Structural
5	Model 4, including openings and tubes	ANSYS Static Structural
6	Model 5, with realistic water pressures and load factors	ANSYS Static Structural
7	Model 6, with layered plates	ANSYS Static Structural
8	Model 7, including forces from valves	ANSYS Static Structural

The results of the different models and an explanation of the differences between the models can be found in Appendix I). The following paragraphs will discuss the set-up, results of the final model and recommendations on structural adjustments in order to fulfill the requirements.

6.3. Set up of the model in ANSYS

The set-up of the final model (Model 8) consisted of 7 steps, which are presented in Table 39.

Table 39: Steps to arrive at the final model in ANSYS

Step	Explanation
1	Modelling of the structure as body elements (draw and extrude)
2	Conversion from body elements into surfaces, to save on calculation times
3	Assignment of the charasteristic material properties
4	Conversion of the surfaces into layered plates
5	Defining the boundary conditions and loads
6	Creation of the mesh
7	Obtain results

The plates are modelled as sections consisting of three layers, which are the two skin plates and a core. The skin plates are assumed to be homogeneous and anisotropic. The material properties of the skins are presented in section 6.2. The core is modelled as a layer with longitudinal stiffness close to zero, and is only able to provide shear resistance. The Z-structure of the fibers around the core has not been included in the model. As the first 4 steps do not require any further explanations, only steps 5, 6 and 7 are discussed in this chapter.

At the boundaries, the gate is only simply supported by two line supports at the connection to the lock walls, as Figure 103 shows. The schematization of these supports is in line with the 2D-model depicted in Figure 83. Furthermore, the connections between the plates are assumed to be rigid, which is also in line with earlier schematizations.

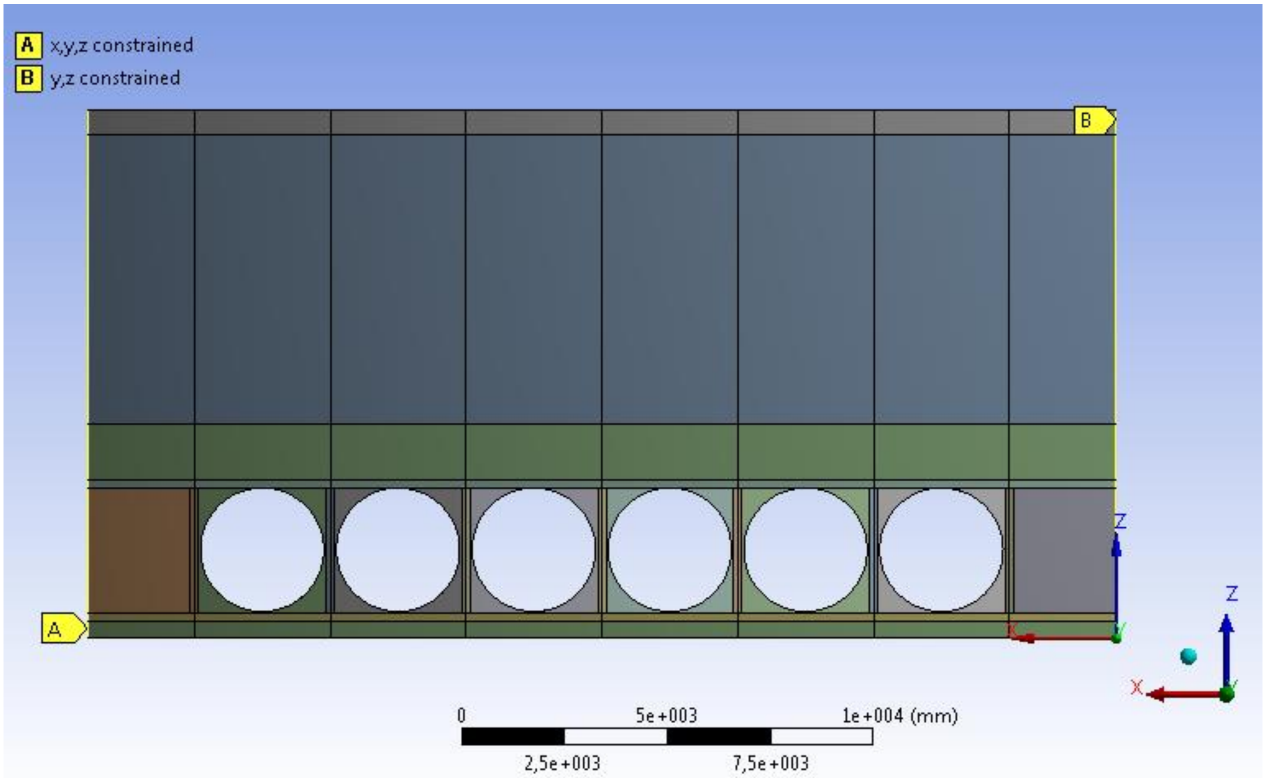

Figure 103: Schematization of the line supports at the lock walls

The design values of the hydrostatic pressures acting on the gate are presented in Figure 104, based on the hydrostatic pressures in the servicability limit state (SLS) presented in section 4.1 multiplied by a load factor of 1,5.

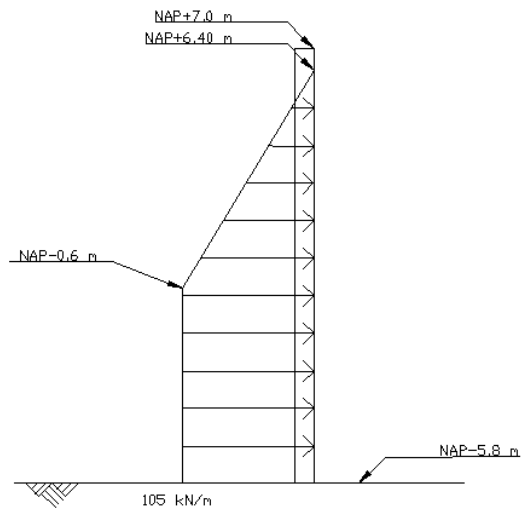

Figure 104: Design values of the hydrostatic pressures acting on the upstream gate per unit of width

The schematization of these pressures in the finite element model is presented in Figure 105. Please note the difference in units between the two figures (MPa versus kN/m^2) and the fact that the colour schemes for the constant part of the load and the variable part do not match in Figure 105.

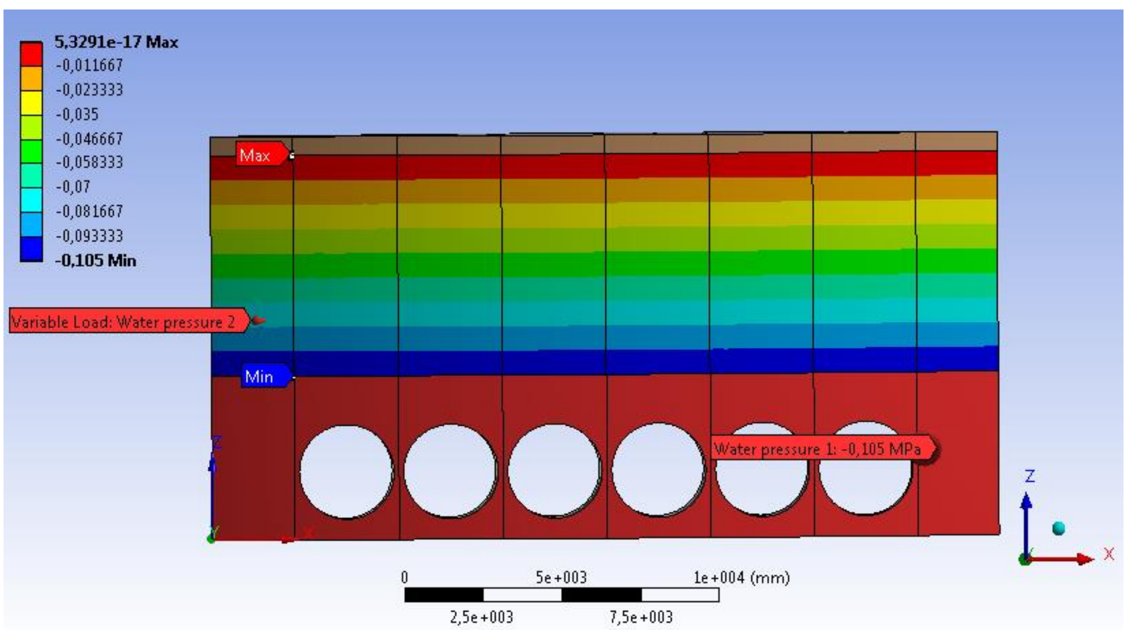

Figure 105: Hydrostatic pressures related to the design head difference (MPa)

The valves are placed at the high water side of the gate (opposite to the plate which is loaded by the hydrostatic pressures). This will result in a compressive force between gate and valve, providing a watertight connection. A uniform distribution of forces has been assumed over the four edges at which the valves are supported. The pressure of 105 kN/m^2 has been multiplied with the surface area of the valves and divided by the area of the line supports at the edges to obtain a value for the pressures acting on the gate itself.

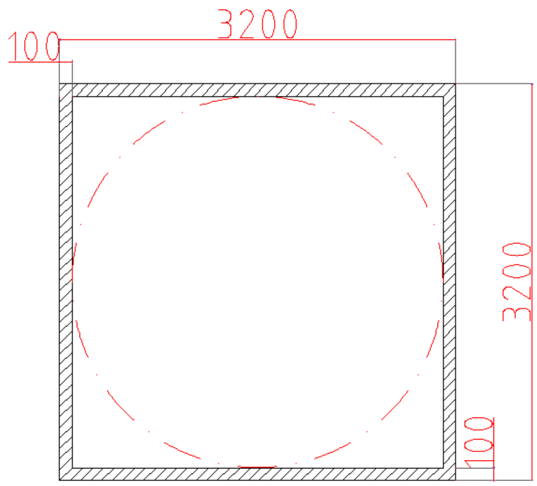

Figure 106: Dimensions of the valves, line supports and the tubes [mm]

$$q_{support} = q_{valve} * \frac{A_{valve}}{A_{support}} = 105 * \frac{(3,2)^2}{3,2^2 - 3^2} = 867\ kN/m^2 = 0,867\ MPa$$

The way in which these loads acting on the gate are schematized in the finite element model is visualized in Figure 107.

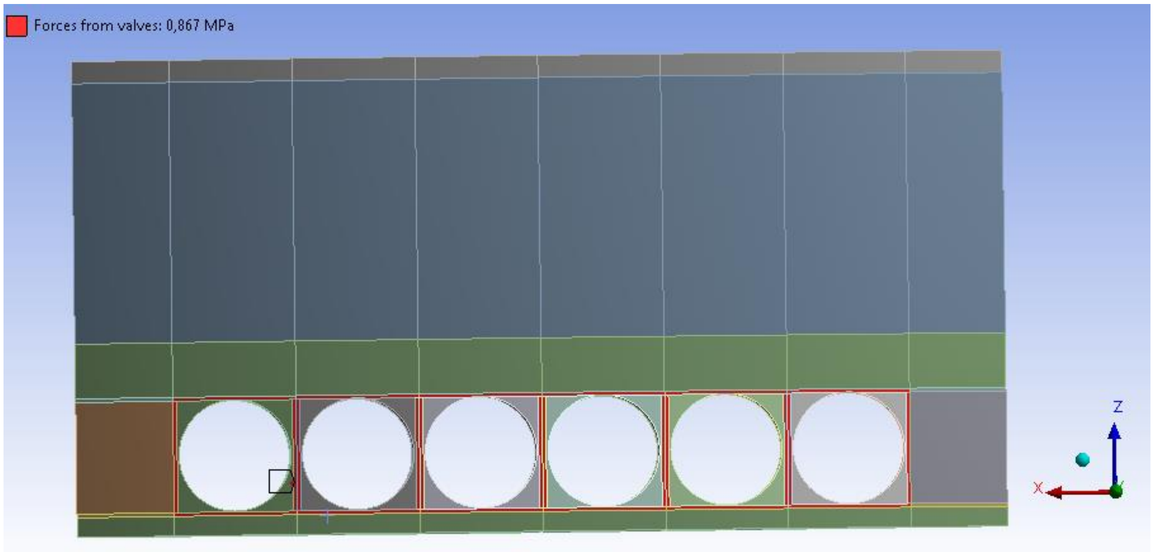

Figure 107: Forces from the valves on the low-water side of the gate [MPa]

The mesh which has been applied is presented in Figure 108. The mesh seems to be of good quality, which is supported by the fact that verification of the model did not result in unexplanable results compared to less complex schematizations.

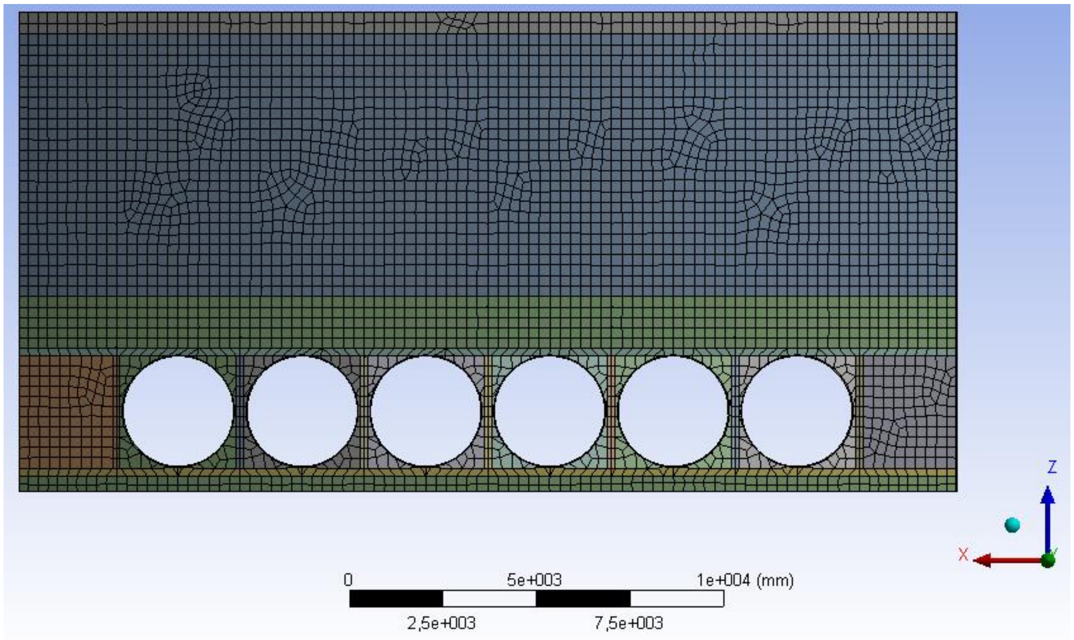

Figure 108: Mesh of the model in ANSYS

6.4. Results of the final model in ANSYS

This paragraph discusses the results of the finite element calculations. The structure has been checked for deformations, normal strains, shear stresses and local stabilities of the plates. The deformations are checked for the servicability limit state (SLS) while the three other subjects are analyzed in the ulitimate limit state (ULS). The limit states regarding strains, shear stresses and plate stabilities to which the results of the finite element caluclations are compared can be found in section 6.2.

Firstly, the initial deformations are investigated to check if these will endanger the water retaining function of the gate. The results are presented in Figure 109, Figure 110 and Figure 111.

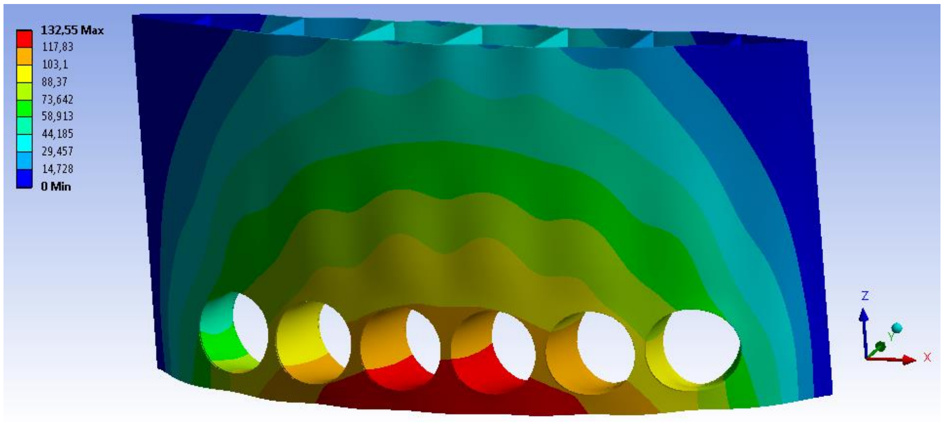

Figure 109: Global deformations of the water retaining plate loaded by hydrostatic pressures (SLS) [mm]

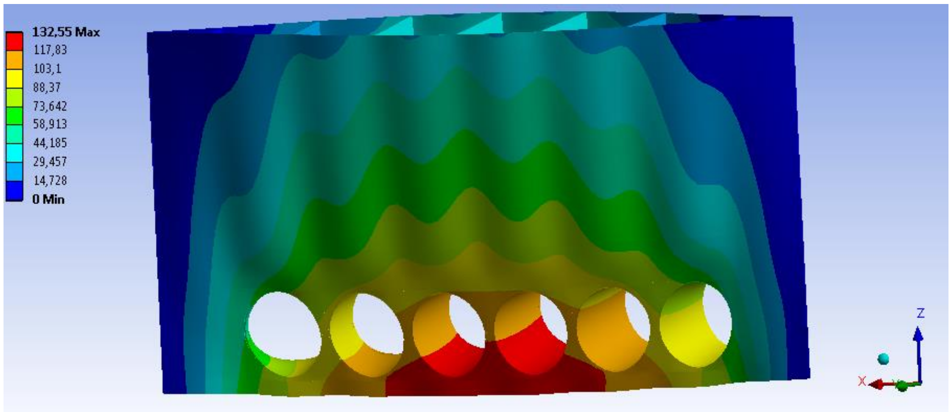

Figure 110: Global deformations of the water retaining plate loaded by the valves (SLS) [mm]

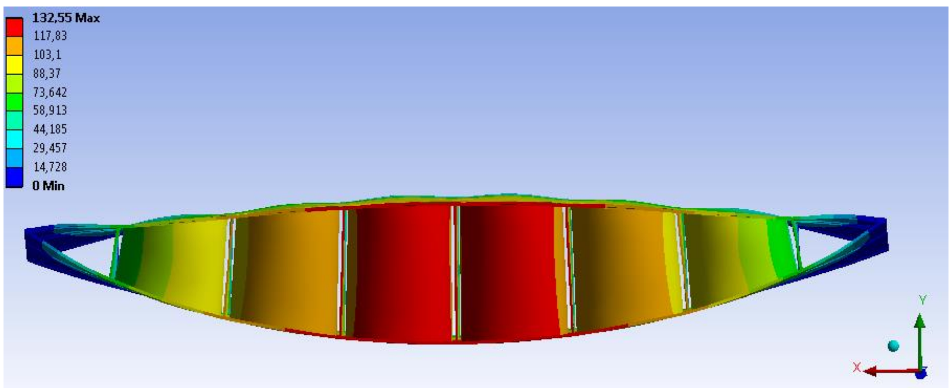

Figure 111: Bottom view on the deformed gate (SLS) [mm]

The maximum elastic deformations are equal to 133 millimeters, which is approximately 1/200 of the length of the gate. These deformations take place at the bottom of the gate right in the middle between the supports. This is as expected, because the loads are the highest at the lower part of the gate, and the 2D-schematization already pointed out that the deflections would be the largest at the middle of the gate.

The deflections of 1/200 of the length of the span are in line with the criterion which has been applied at the Spieringsluis [2]. To find out if these relative deformations will not cause leakages for this gate as well, it is recommended to perform a more detailed analysis to the deformations around the vertical connection to the lock walls and at the connection between valves and gate.

Secondly, the normal strains are investigated to check if rupture of the fibers occurs. The results are presented in Figure 112 and Figure 113. At the red areas in Figure 112 and at the dark blue area in Figure 113, the safety regarding rupture of fibers is not sufficient.

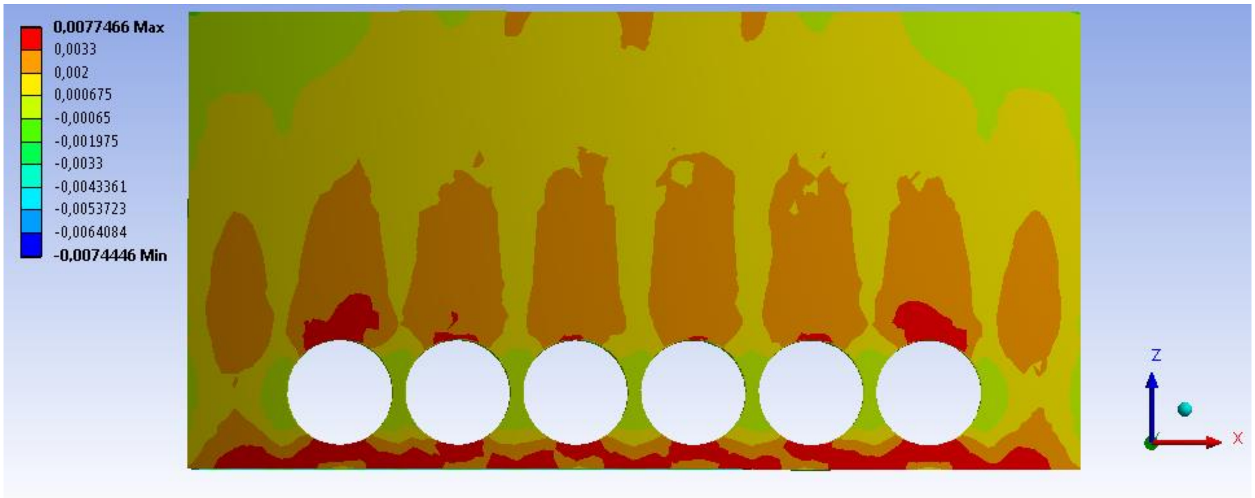

Figure 112: Maximum prinical elastic strains at the plate loaded by hydrostatic pressures [-]

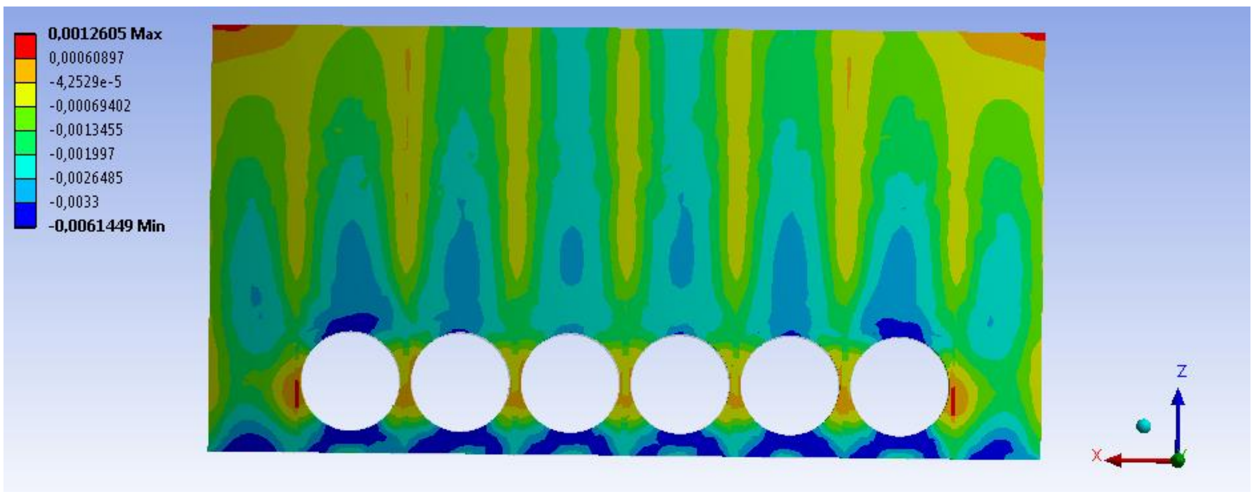

Figure 113: Normal strains at the plate loaded by the valves [-]

On a global scale, the structure fulfills the structural requirements regarding normal strains: the design strain of 0,33% has not been exceeded in the largest part of the gate. Nevertheless, stress concentrations adjacent to the openings result in a structure which is not able to resist the design values of the forces. The locations where the design values of the normal strains are exceeded are in line with the qualitative analysis performed in section 5.2.4, as Figure 96 shows.

During the 2D-schematization, the structure has been designed on strength under the assumption that the stresses are constant over the height. The openings in the gate, which are located at the positions where the hydrostatic pressures are the highest, result in peak stresses adjacent to these openings which were not incorporated during the preliminary design of the structure. As the figures prove, structural adjustments are required to guarantee the safety of the gate under design conditions.

The third failure mode which has been analyzed is delaminations due to an exceedance of the interlaminar shear strength. The shear stresses in the gate during the design load case are presented in Figure 115 and Figure 116. The dark red and dark blue colors indicate the positions where the design value of the interlaminar shear stress is exceeded.

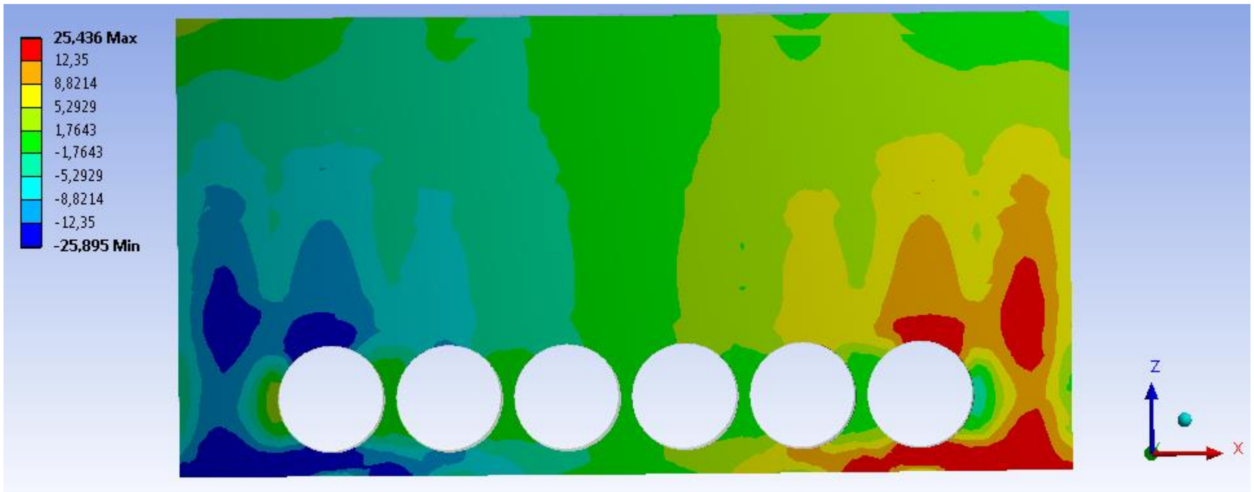

Figure 114: Shear stress at the plate loaded by hydrostatic pressures [N/mm2]

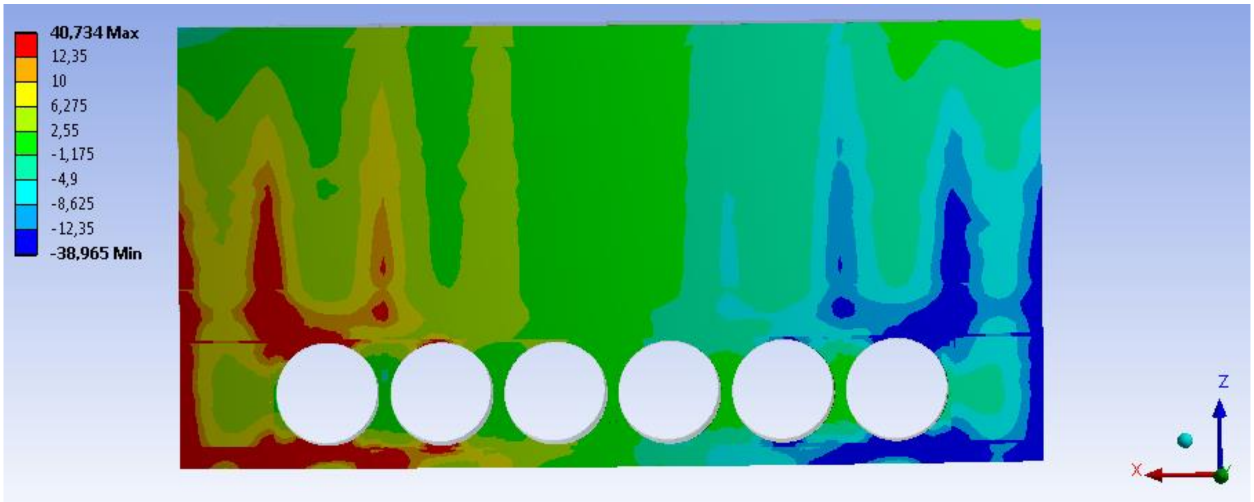

Figure 115: Shear stress at the plate loaded by the valves [N/mm^2]

As the figures show, delaminations are expected to occur at substantial parts of the water retaining plates during the design conditions. Structural adjustments are required to reduce the shear stresses in the structure to prevent delaminations.

The fourth and final subject which has been analyzed is the local stability of the plates. The resulting stresses and deformations found by the static calculation performed above forms the input for the linear buckling analysis in ANSYS. The program performs a modal analysis, after which the load multiplication factor is determined which leads to instabilities in the plates. The first mode (related to the lowest buckling load) is presented in Figure 116.

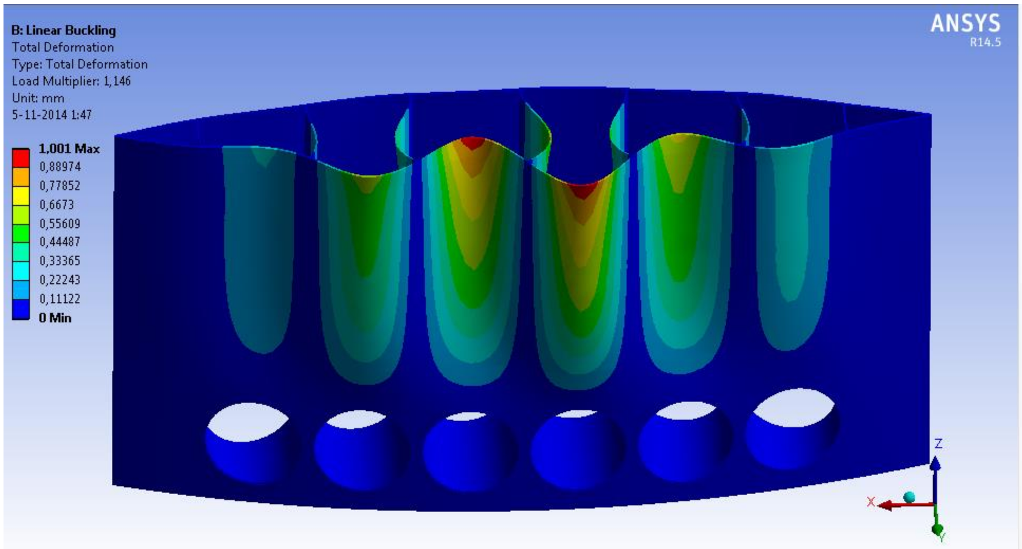

Figure 116: Safety against local instabilities for the first modal shape [-]

The first buckling mode of the gate is related to instabilities of the plate loaded by the valves. This is as expected since this is the only plate which is loaded in compression. It appears that the safety factor on buckling of the plates is only 1,15 instead of the minimum value of 2,5 which is recommended by the CUR 96. Structural adjustments are also required to provide the desired safety level regarding stability of the gate.

6.5. Analysis to the required structural adjustments

As the previous paragraph pointed out, the structure does not fullfill the functional requirements regarding normal strains, shear stresses and plate stability during the design load case. Therefore, structural adjustments are required to improve the strength and stability of the structure.

The following possible adjustments are considered:

- Overall thickening of the skins (1)
- Overall thickening of the cores (2)
- Increase of the fiber volume fraction (3)
- Local reinforcements of the plates (4)
- Construction of a horizontal support at the sill (5)
- Stiffening of the tube (6)
- Addition of stiffeners to the curved plates (7)
- Adjustments to the openings (8)

The first 3 options describe overall strengthening of the structure without a change of the loading paths through the structure: the strength and stability of the structure will only be improved by addition of extra material. The fourth option describes local strengthening of the structure there where the peak stresses occur. The options 5-8 describe a change of flow of forces through the gate by changes to the static scheme. These adjustments should take place in such a way that they lead to more preferable loading paths resulting in smaller peak stresses in the gate.

The first considered solution, which is an overall increase of the thickness of the skins will result in a reduction of strains, shear stresses and deflections because more material becomes available to resist the forces acting on the gate. The cross sectional area of the skins will become larger, which results in a reduction of normal strains induced by normal forces. Besides, a larger cross sectional area will also reduce the shear stresses. Next to this, also the moment of intertia of the plates will be increased, resulting in lower stresses due to bending moments and an increase of plate stabilities. Overall strengthening will however be financially unattractive because the limit state functions were online exceeded locally. Overall strengthening of the structure to decrease the local strains and stresses will result in a gate which is heavily overdimensioned and leads to an uneconomical use of materials.

The second considered solution, which is an overall increase of the core thickness, will result in a larger internal lever arm between the skin plates. The stiffness, member stability and resistance to bending moments will be increased significantly. The shear stresses and strains induced by normal forces will however barely change because the effective area which provides resistance against these forces has not been increased. Besides, an increased core thickness may also require additional ballast to prevent floatation of the gate due to its low density. Therefore, this solution does not seem to be feasible.

The third possibility is to increase the fiber volume fraction in the plates. This would result in higher Young's moduli in the two directions without changes to the maximum strains in the material. This solution would have been feasible if the initial fiber fraction would have been lower. As stated in the CUR 96, vacuum assisted resin injection is only suitable for production of elements up to a fiber fraction volume of 60%. The peak stresses in the material exceed the strength by a larger factor than the additional strength provided by the extra 10% of fibers compared to the current design.

The fourth alternative is local reinforcements of the plates at the locations where peak stresses occur. These reinforcements can be in the form of adjustments of fiber volumes and directions, adjustments of skin thicknesses or even by local application of other structural materials such as steel or concrete. Because of the large number of variables which can be adjusted, the structure can be fully tailored to arrive at the most economical design. Two negative side effects are accompanied with this solution however. Firstly, attention should be paid that local reinforcements do not just result in a relocation of peak stresses. Secondly, the production process becomes more complex since the mould needs to be locally adjusted as well to follow the shape of the structural adjustments.

The fifth considered option is a redirection of forces by construction of a horizontal support at the lock sill. The result will be that the forces, which are now all directed to the lock walls, will have alternative (and shorter) paths to follow. The deflections, normal strains and shear stresses will all decrease due to the creation of a lock sill. Besides, the stability of the plate in compression will be increased as well.The results of the finite element calculations are presented after construction of this additional support In Appendix J) . Although this solution is very favourable to the structural performance under regular load conditions, it also comes with large costs and additional risks. Firstly, the construction tolerances become very small because the shape of the bottom of the gate needs to be very similar to the shape of the sill to guarantee full contact. Secondly, the structural shape has been optimized for the situation where there is no support present at the bottom. Adjustments of the static scheme may result in changes to the optimal shape. Thirdly, construction of a lock sill will result in sediment collection in front of the sill, requiring regular maintenance works. Finally, the connection between gate and sill will be vulnerable to entrapment of hard objects, endangering the water retaining function and resulting in very large local forces induced by the object.

The peak stresses around the openings are caused by a redirection of the forces around these, as Figure 96 pointed out. A sixth possible solution to reduce these stress concetrations is by construction of very stiff tubes which are placed inside these holes. The stiff tubes will attract the forces so that the stresses do not have to be redirected around the holes anymore.

Another solution would be to add stiffeners to the plates in order to reduce the deformations and increase the stability of the plates. This solution can be seen as a combination of the stiffened gate and the lens shaped gate, which are both elaborated in the study to gate alternatives (see chapter 4). This solution may be feasible, but also results in a whole different design. The forces through the gate will be redirected via the plates to the stiffeners which will in the end lead the forces to the supports. Due to a lack of time, an elaborated study to the effects of this solution has not been performed.

The final option to improve the design is by adjustments to the openings. These openings could for example be scaled down to reduce the forces from the valves and thereby reduce the peak values of shear stresses and normal strains. The time required for filling and emptying of the lock chamber will however be increased. Second possible adjustment to the openings in by a change of their shape. In section 5.3, only three shapes are investigated, while other shapes may actually result in preferable loading paths through the gate. The third and most extreme adjustment could be by a change of the entire filling- and emptying system. Instead of openings in the gate, also culverts underneath the lock head or longitudinal culverts could be considered. These systems are all described in section 2.2.5.

6.6. Fatigue analysis

Next to the problems related to strength, stiffness and stability of the gate, this paragraph investigates whether fatigue failure at the positions where peak stresses occur may also form a threat to the structural safety. A general introduction to the processes behind fatigue failure of FRP structures is presented in section 1.4.3.

For the fatigue analysis of this specific design, the following assumptions are made:

- The water level at Amterdam Rijnkanaal side is constant and equals NAP -0,40 m;
- A single day consists of 20 locking cycles;
- The water levels at the Lek are based on lit. [49]. The duration of a high water is one day;
- The lock is in use for 365 days a year;
- The lifetime of the gate is 100 years;
- The average stress in the gate is equal to zero;
- Wave impacts are neglected due to the low stress amplitude.

The performed analysis has the following limitations:

- The fatigue analysis has been based on stresses in the x-direction; multi-axial stress states are not included in the model due to a lack of available literature;
- Head differences with an exceedance frequency of less than 10^{-2} per year are excluded;
- Sea level rise and changes in trend of discharge of the river Rhine are not incorporated in the model;
- Fatigue failure is investigated for the positions in the plates itsself, while connections between members may be more vulnerable to this phenomenon;
- Waves induced by wind and vessels are neglected.

So in fact, only the stress variations related to the locking process are investigated. The accumulated result of the stress-cycles with variable amplitudes are calculated by the Miner's sum, which reads as follows:

$$N_f = \left(\frac{\sigma_{amp}}{\sigma_{Rd}}\right)^k$$

$$D = \sum n/N < 1$$

$$\sigma_{Rd} = \frac{\varepsilon_{max} * E}{\gamma_{m1} * \gamma_{m2} * \gamma_{ct} * \gamma_{cv}} = \frac{0{,}012 * 25600}{1{,}35 * 1{,}2 * 1{,}1 * 1{,}3} = 106{,}2\ N/mm^2$$

$N_f =$	Number of load cycles up until failure for a certain stress-amplitude
$\sigma_{amp} =$	Stress amplitude during a loading cycle
$\sigma_{Rd} =$	Charasteristic value of the maximum fatigue stress
$k =$	Coefficient related to the slope of the S-N curve, equal to -9 for polyester
$n =$	Number of load cycles during the lifetime of the structure
$D =$	Damage number. Structure fails if D equals 1.
$\gamma_{m1} =$	Safety factor related to the uncertainties in material properties
$\gamma_{m2} =$	Safety factor related to the production process
$\gamma_{ct} =$	Safety factor related to temperature effects
$\gamma_{cf} =$	Safety factor related to moisture effects

The position at which fatigue failure is investigated has been marked in Figure 117 with a red dot. The normal strains are shown for the daily head difference of 1,5 meters.

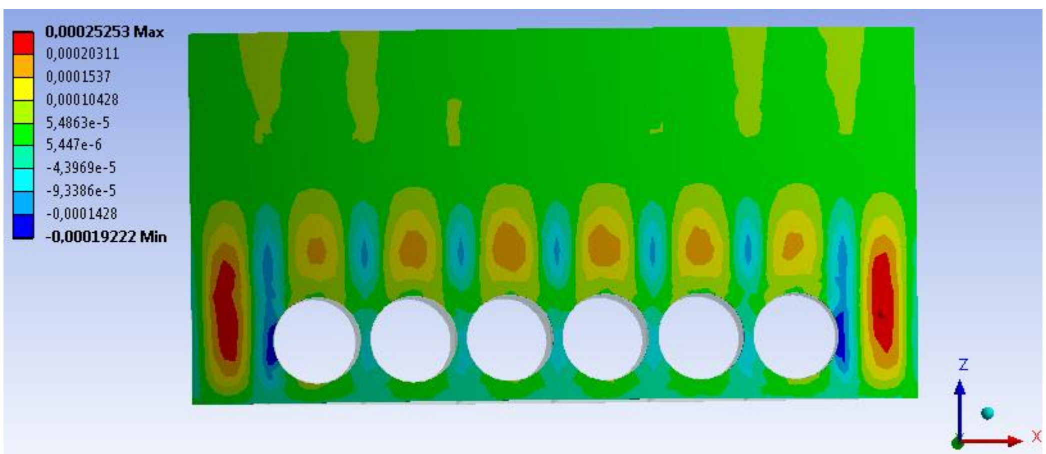

Figure 117: Position at which fatigue failure has been investigated

The results of the fatigue analysis are presented in

Table 40. The stress amplitudes obtained for the fatigue analysis are based based on FE-calculations and are presented in Appendix J).

Table 40: Fatigue analysis of the gate

Head difference (m)	Frequency (days/year)	Total cycles n during lifetime	Stress amplitude [N/mm^2]	N_f	n/N_f
1,5	365	730000	6,5	$8,3 * 10^{10}$	$8,8 * 10^{-5}$
3,18	1	2000	13,9	$8,8 * 10^{7}$	$2,3 * 10^{-5}$
3,71	0,5	1000	16,0	$2,5 * 10^{7}$	$4,0 * 10^{-5}$
3,99	0,33	667	17,5	$1,12 * 10^{7}$	$6,0 * 10^{-5}$
4,16	0,25	500	18,1	$8,24 * 10^{6}$	$6,1 * 10^{-5}$
4,30	0,2	400	18,8	$5,86 * 10^{6}$	$6,8 * 10^{-5}$
4,78	0,1	200	20,9	$2,26 * 10^{6}$	$8,9 * 10^{-5}$
5,27	0,04	80	22,5	$1,16 * 10^{6}$	$6,9 * 10^{-5}$
5,59	0,02	40	23,7	$7,28 * 10^{5}$	$5,5 * 10^{-5}$
5,87	0,01	20	25,3	$4,05 * 10^{5}$	$4,9 * 10^{-5}$
				$D = \sum n/N_f$	$5,2 * 10^{-4}$

It appears that on a global scale, sufficient safety factors are applied during the design so that fatigue failure on a global scale is prevented. This does not necissarrily have to be the case for every lock gate however. This specific lock gate has a large difference between design head difference (which isequal to 7,0 meters) and the daily head difference of 1,5 meters. This results in a large margin between daily stresses in the structure and the design strength. For lock gates where this difference is smaller, fatigue failure can not be ruled out on beforehand.

Besides, the connections are not considered in the fatigue analysis. Due to a lack of available literature on the flow of stresses through these details, it is impossible to tell anything about the fatigue performance of these details. Physical testing of these details is recommended, and may result in worse fatigue performance than assumed in this analysis.

6.7. Creep analysis

Under influence of the long term loadings, the gate are susceptible to creep deformations. These creep displacements may result in difficulties for the vertical movement of the valves along the plates. In this paragraph, the creep deformations are investigated for the area of the gate where the valves need to slide along. The results will be used for the valve design in section 7.6. Calculations on the creep deformations consist of the following steps:

- Calculate the initial deflections $w_{o;I}$ for the governing long term load case;
- Determine which fibers are aligned with the direction of the long term stresses, leave all other fibers out of the calculation;
- Determine the stiffness of the reduced laminate;
- Find the initial deflections $w_{o;R}$ of the reduced laminate for the long term load situation;
- Multiply the initial deflections $w_{o;R}$ with creep factor $\gamma_{ck}(t)$ to find the total deflections $w_{\infty;R}$ at the end of the lifetime of the structure;
- The creep deformations are found by subtracting $w_{o;I}$ from $w_{\infty;R}$.

The intial displacements of the gate during the long term load situation (which is a head difference of 1,5 meters) are presented in Figure 118 for the area which is important to guarantee the vertical movement of the valves.

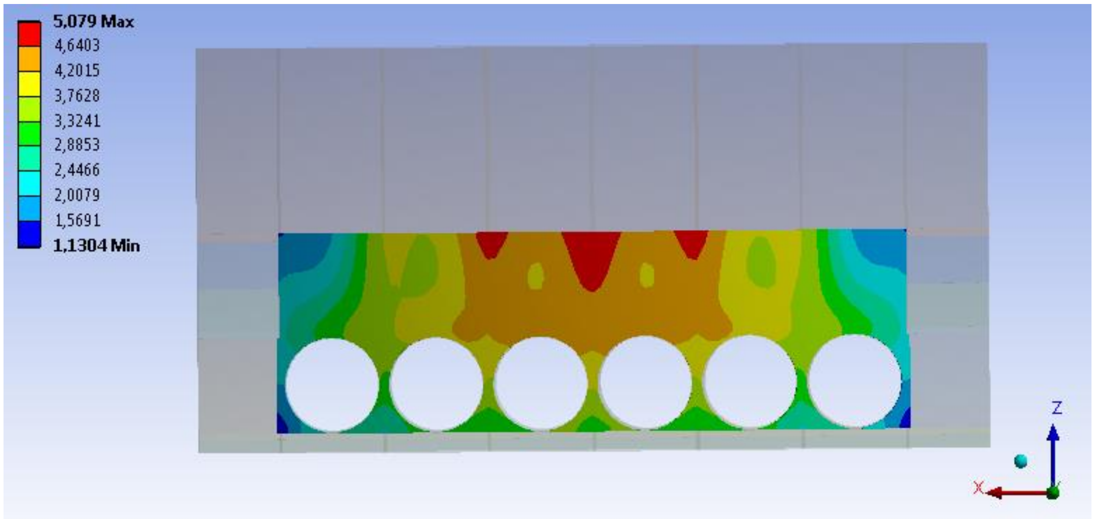

Figure 118: Elastic gate displacements during the long term load case at the position of the valves [mm]

The initial Young's modulus $E_{x;0}$ is calculated with help of Halpin-Tsai (see Appendix B) and is equal to $25600\ N/mm^2$. For the long term loading, only the fibers which are oriented in the main loading direction will contribute to the stiffness. This means that the long term loads are resisted by only 55% of the fibers. The stiffness of the reduced laminate is calculated as follows:

$$E_{X;R;UD;0} = \frac{h_{UD;0°}}{h_{skin}} * E_{X;R;UD} = 0{,}55 * 37{,}7 = 20{,}7\ GPa$$

In which:

$E_{X;R;UD;0} =$	Reduced stiffness of the UD-plies
$h_{UD;0°} =$	Total thickness of the UD-plies oriented in the 0° direction
$h_{skin} =$	Total skin thickness
$E_{X;R;UD} =$	Initial stiffness of the UD-plies

In order to find the creep deformations at the end of the structural lifetime, the values calculated above are divided by a creep factor which depends on the type of reinforcement, and lifetime of the structure. The lowest creep factor is found for UD-plies, followed by woven fabrics. Mats are showing the worst creep performance of the three types of reinforcements. For the assumed lifetime of 100 years, this coefficient y_{ck} equals 1,15 for UD-rovings The stiffness of the reduced laminate at t=100 years is calculated as follows:

$$E_{X;R;\infty} = \frac{E_{X;R;UD;0}}{y_{ck;UD}(t)} = \frac{20{,}7}{1{,}15} = 18\ \mathrm{GPa}$$

The deformation caused by creep is calculated by the following formula:

$$w_c = w_0 * (\frac{E_{x;0}}{E_{X;R;\infty}} - 1)$$

In this specific situation, the creep deformations are approximately 42% of the initial deformations of the structure during long-term loading. This comes down to an additional deformation of 2 millimeters, which needs to be added to the elastic deformations during the govering short term load case. The creep deformations are relatively small because the loads for the ULS design on strength are much larger than the daily loads.

7. Detailed design of the lens-shaped gate

In the previous chapter, the risks and problems related to the design were investigated on a global scale. The next section focusses on the detailed design of the structure, to find out what problems may be involved with detailing of the structure.

7.1. Critical details of the gate

The following details are further elaborated in this chapter:

Detail 1: Attachment of webs to water retaining plates
Detail 2: Vertical connection between gate and lock head
Detail 3: Attachment of lifting equipment to the gate
Detail 4: Design of the tubes
Detail 5: Design of the valves

The locations of the most critical details are presented in Figure 119.

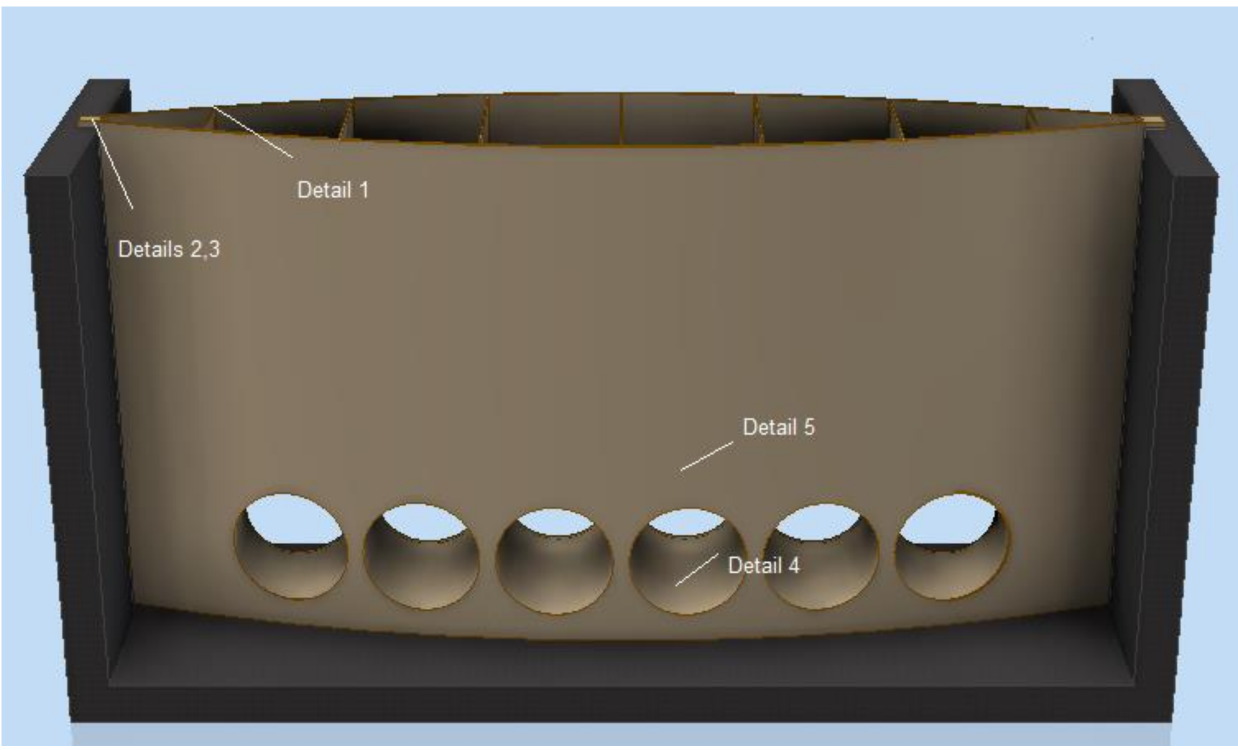

Figure 119: Critical details of the design

The next subsections cover the design of each of the details mentioned above. The possible fastening techniques which are taken into consideration are presented in Appendix L). The details will only be elaborated qualitatively, because too little information is publicly available on calculation methods to provide all the required dimensions. In many cases, physical tests are still required to prove the feasibiity of a certain connection.

7.2. Detail 1: Connection of webs to water retaining plates

The watertightness of the structure needs to be preserved, which means that bolts which penetrate the water retaining plates are undesirable. Besides, the webs are connected to the water retaining plates at the positions where the loads in the curved plates are the highest. Additional stress concentrations need to be prevented, which means that the application of laminated T-joints seems to be the most favourable solution. The forces exerted on the governing connection between web and curved plate are presented in Figure 120, based on the simplified 2D-calculations in SCIA Engineer. These forces are distrubuted over the full height of the gate of 12,8 meters. The location of this most highly loaded connection between web and water retaining plate is indicated in Figure 119.

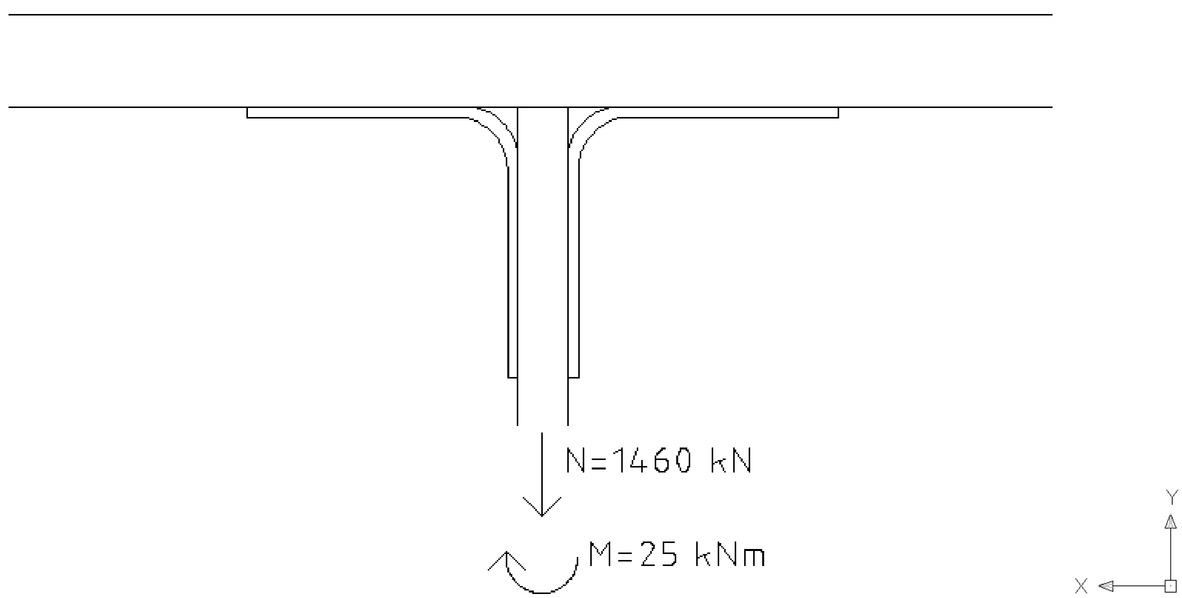

Figure 120: Estimated design values of the forces which have to be resisted by the connection

The calculations on the required overlap length, mat thickness and radius of the overlaminate are not elaborated due to a lack of available literature on this subject. Physical testing or consultancy of an FRP-expert is recommended to design the connection on strength.

7.3. Detail 2: Connection of water retaining plates to support

The second detail which has been elaborated qualitatively is the connection between the two curved water retaining plates. Because the watertightness of the connection needs to be guaranteed, both bolted connections and peg-and-hole joints are not recommended. As a result, overlaminations are advised to connect the members. The forces which have to be resisted by the joints are presented in Figure 121.

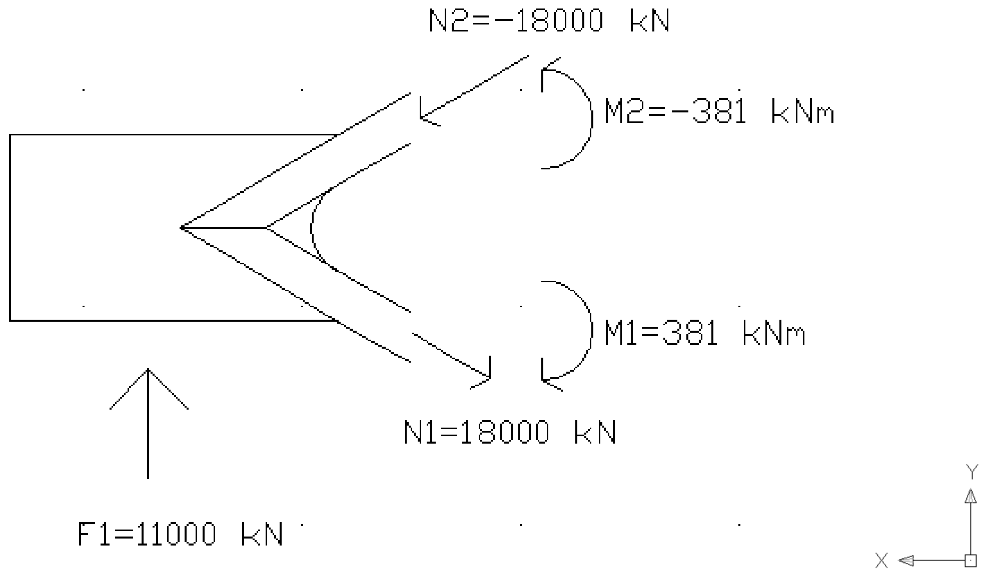

Figure 121: Forces acting on the connection between the two curved plates

For the same reasons as stated in the previous paragraph, calculations on the detailed design of the joint have not been performed. If required, the curved plates can be locally reinforced around the supports, especially to resist the large shear forces.

7.4. Detail 3: Attachment of lifting equipment

In order to lift the gate, cables or chains need to be attached to the gate. The most usual way to do so is by application of lifting eyes made out of steel. This principle is for example also applied in the current gates of the Beatrixlock.To prevent high interlaminar tensile stresses, which are one of the weak spots of fiber-reinforced polymers, the gate needs to be supported at the bottom so that the self weight is redirected to the supports by compression instead of tension.

Asuming that the self-weight is evenly distributed over the two supports, both details need to be able to resist a force of nearly 50 tons in the serviceability limit state. The most appropiate way to do so is by co-curing of a steel pin with the support block which has been elaborated in the previous paragraph. The bottom of the pin consists of a plate to distribute the forces over a larger area, while the top of the pin will be equiped with an eye to attach the lifting equipment to. This detail is visualized in Figure 122. Further analysis to design the detail on strength is required.

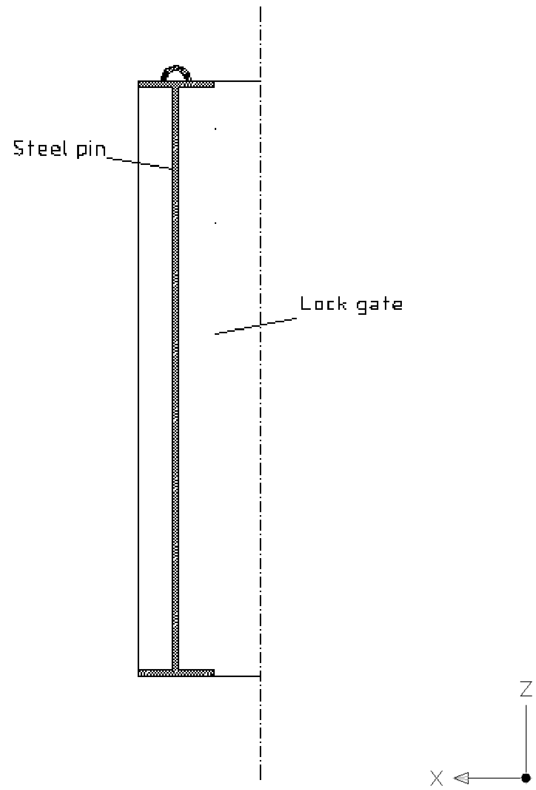

Figure 122: Visualization of the lifting eye on the left hand side of the gate

7.5. Detail 4: Culvert design

In order to transport the water trough the gates during filling and emptying of the lock chamber, culverts are required. These culverts basically need to fulfill two requirements: firstly the watertightness of the connection with the curved plates needs to be guaranteed, and secondly the producability needs to be considered during the design. These requirements have resulted in two variants, of which the solution involving a shoe around the tube to connect it to the curved plates turned out to be the most promising. These two solutions are further elaborated in the next subsections.

7.5.1. Option 1: Culverts fastened by screwing

In the first concept, the culvert consists of twoidentical components. Both components consist of a tube with flange on one end. The other end is equiped with screw thread. The two parts are are placed through the openings in the water retaining plates and connected in the middle by screwing of the entire tubes. Rubber sealings are required between flanges and water retaining plate and at the connection between the two parts to guarantee the watertightness. An impression of this variant is presented in Figure 123.

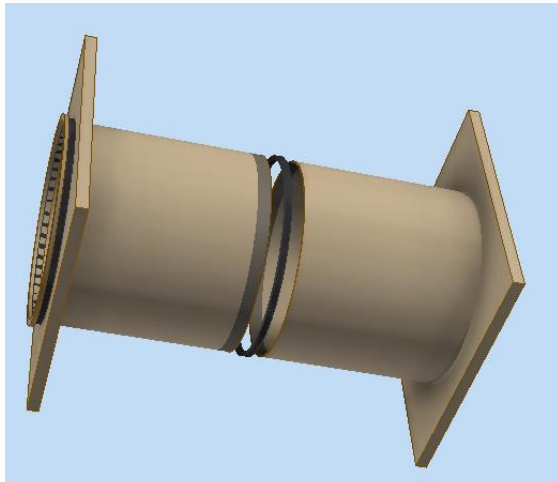

Figure 123: Visualization of the culvert which is fastened by screwing

This concept contains a lot of risk. Especially the connection between the two components is fragile and can easily lose its watertightness. Because this connection is located in between the water retaining plates, inspection is not easy. Besides, special equipment is needed to screw these two large elements to connect them to each other. For these reasons, this concept is not selected.

7.5.2. Option 2: Culverts fastened by a shoe around the tube

The second concept also consists of two components: one component is the tube with a flange attached to the end and the other component is a shoe which is placed around the tube at the free end. The tube is placed through both openings of the water retaining plates. The shoe is attached to the tube by adhesive bonding. A combination of glueing and mechanical fastening takes care of the connection between shoe and water retaining plate. The bolts guarantee a solid connection while the glue takes care of a reduction of stress concentrations around the bolts. The fastener is prestressed so that the rubber and glue between shoe and plate is permanently loaded in compression. The concept is visualized in Figure 124.

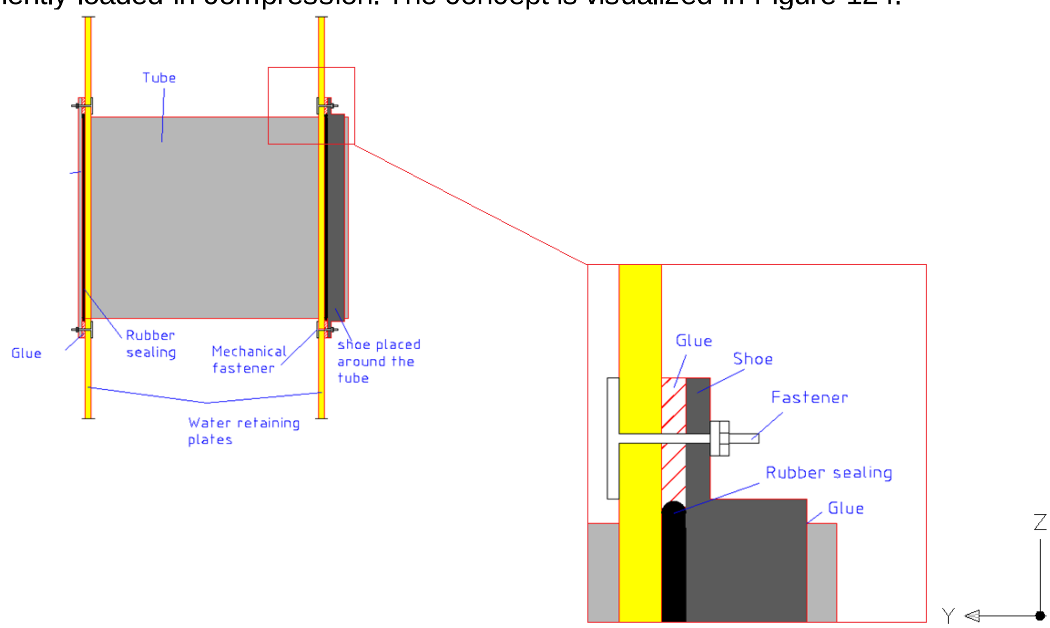

Figure 124: Visualization of the second concept

The large advantage of this concept is that the most vulnerable parts are well-reachable. This makes inspection and maintenance to these parts fairly easy. The flange will be placed on the high-water side of the gate so that the valves are still able to slide along the openings. The side where the shoe will be placed extents further than the water retaining plate since overlap is needed to transfer the forces between the tube and the shoe. This is visualized in Figure 125.

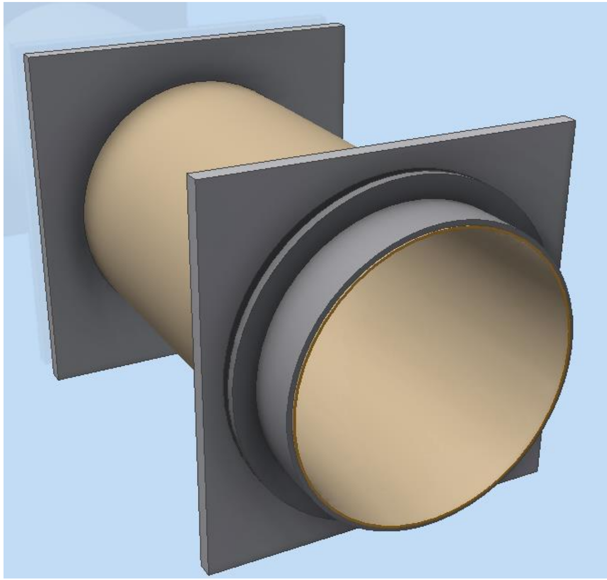

Figure 125: 3D-impression of the second concept (fasteners are not included in the sketch)

The tubes should be designed on the following failure modes:

- Adhesive failure between tube and shoe;
- Failure of the mechanical fasteners;
- Pull through of the mechanical fasteners;
- Shear failure of the flange;
- Failure of the tube itself(due to instabilities or stresses under extreme conditions)

The forces acting on the culverts can be extracted from the ANSYS model presented in section 6.4. Furthermore, physical testing is recommended to prove the strength of the connections.

7.6. Detail 5: Valve design

A structural design of the valves has been elaborated in FRP to find out whether this material is feasibile for this purpose or if application of steel is prefered. The valves in FRP have been fully designed on strength and stiffness while the reference design in steel has been based on available data on the valves in the current gates of the Beatrixlocks.

Two situations are investigated for the structural design of the valves: The maximum head difference of 7 meters acting on a fully closed, on four edges supported valve and the maximum head difference of 6,4 m where locking is still allowed, right after opening of the valves. In this second situation, the valve is only supported at the vertical edges.

Furthermore, the fiber orientations and volumes are assumed to be the same as for the the rest of the gate. This results in a Young's modulus in the main (horizontal) direction E_1 of $25.800\ N/mm^2$, while the E_2 equals $15.900\ N/mm^2$. The maximum allowable stress in the valves equals $85\ N/mm^2$.

The structural design of the valves, which have resulted in the valve lay-out presented in Figure 126 and Figure 127, is to be found in Appendix N).

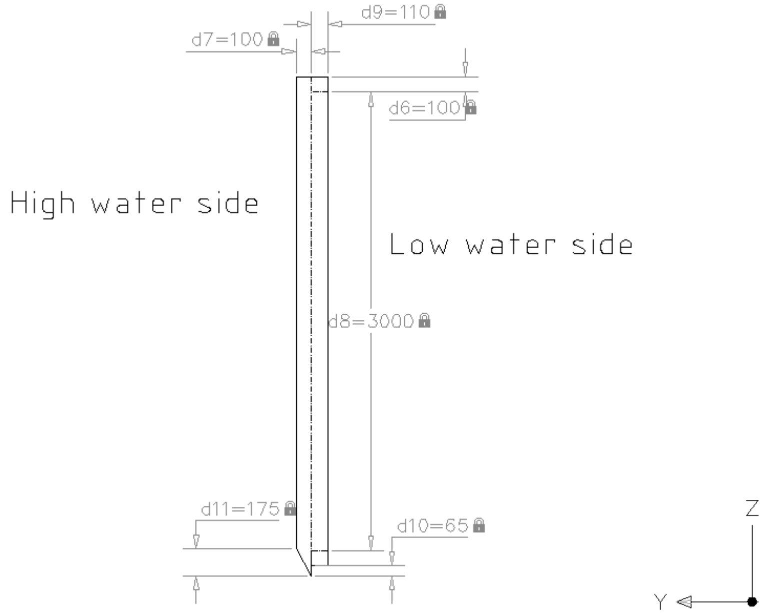

Figure 126: Side view with dimensions of the valves

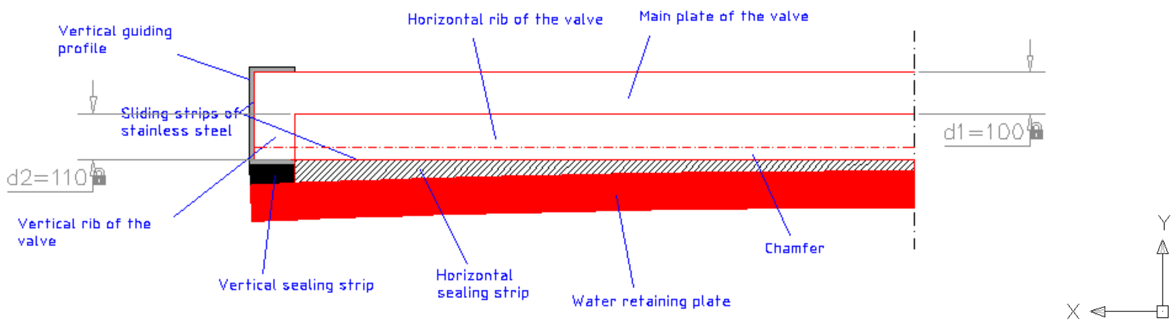

Figure 127: Top view of the valves including the vertical guiding profiles

The final design of the valves in FRP has a mass of approximately 2 tons, with a height and width of 3,2 meters. As a comparison: the valves of the current Beatrixlocks comstructed from steel have a mass of approximately 1,8 tons, are 2,39 meters wide and have a height of 2,61 meters [45]. If the mass is assumed to be linearly dependent on the surface area, application of FRP results in a weight reduction of nearly one third compared to a valve constructed from steel (which would weight nearly 3 tons per valve).

Further research is recommended to find out what the effects of this reduced weight will be on the dynamic behaviour of the gate during openings and closings, especially in combination with fatigue failure.

7.7. Final lay-out of the gate

The current design of the gate, including valves and sliding strips is presented in Figure 128. Possible structural adjustments which are described qualitatively in section 6.5 are not yet incorporated in this figure.

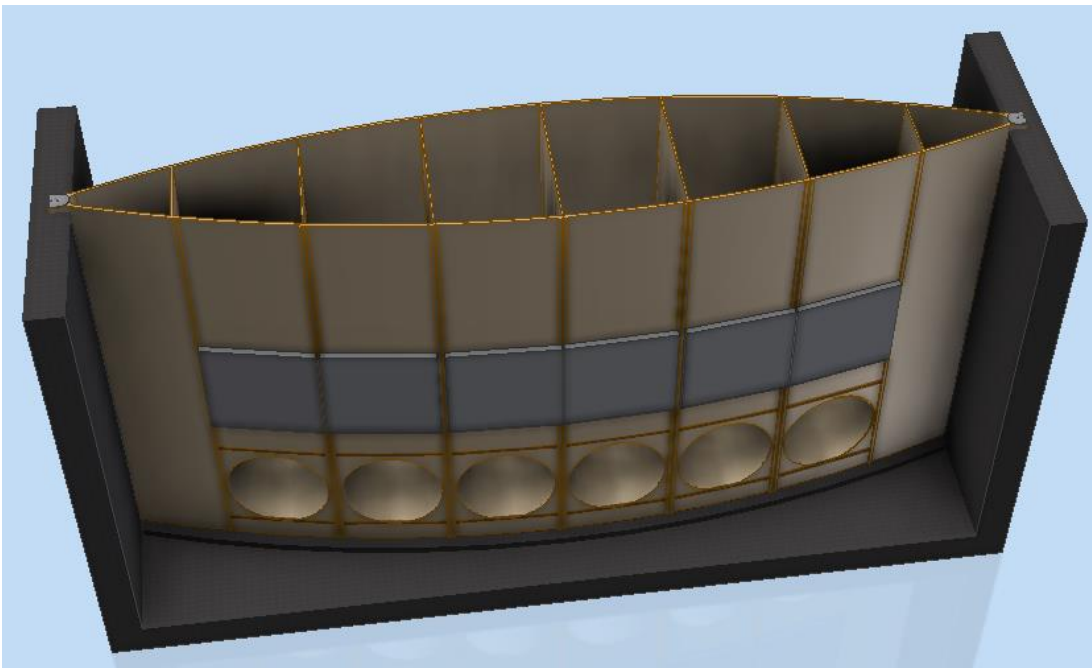

Figure 128: Final design of the gate in FRP

The gate has a length of 25 meters, a height of 12,8 meters and the distance between the curved plates right in the middle equals 4 meters. The gate will be constructed from a combination of E-glassfibers and polyester, around a core of foam. The fibers are placed in multiple layers of unidirectional plies, where 55% of the fibers are placed in the main direction of loading. The total fiber volume fraction equals 50% of the total skin volume.

During the structural design, the cuved plates turned out to require a total thickness of 88 millimeters, consisting of two 22 millimeter skin plates with a 44 millimeter core in the middle. The webs are formed by a 24 millimeter core surrounded by two skin plates of 12 millimeters each. The design of the gate, including valves, tubes and sliding strips, has a mass of nearly 100 tons.

Since the structural adjustments which are required to reduce the peak stresses are not yet quantified, very accurate values for the final mass of the gate are not yet possible. Based on the surface areas where the strength of the gate is not yet sufficient (see section 6.4), it is assumed that the final mass of the gate will be approximately 20% higher than stated above. The final design of the gate constructed from FRP is therefore estimated on 120 tons.

8. Comparison of the FRP gate to a gate constructed from steel

The feasibility of FRP compared to steel will be based on a combination of weight, life-cycle costs and specific risks related to application of both materials. The environmental impact of both materials is left outside of the scope of this research.

The first paragraph discusses the structural design in steel to which the FRP gate will be compared. Secondly, the total mass of both gates are compared, which forms the basis of the estimation of the life-cycle costs for both designs elaborated in the third paragraph. Finally, the specific risks related to both designs are investigated.

8.1. Reference design from steel quality S235

In order to study the relative feasibility of the two materials, a global design in steel has been elaborated in this paragraph. The material properties in the finite element model presented in section 6.4 have been changed from FRP to structural steel. After changements to the material properties, the plate thicknesses have been adjusted until the Von-Mises stress in the structure has reached the limit state value of $235\ N/mm^2$. Besides, the minimum required safety factor on stability has been set to 2,5, which is in accordance with the eurocodes. The gate has not been designed on fatigue, nor have the connections been designed on a detailed level.

A drawback of this approach is that the structure has been optimized for application of FRP, while a structure from steel may have a somewhat different optimal structural shape. It can not be ruled out that the design in steel can be further optimized, for example by stiffening of the plate with horizontal- and vertical profiles or by application of a single water retaining plate in combination with a truss structure, similar to the Hartelkering. It is however assumed that this approach at least provides results which are sufficiently accurate to compare the design in FRP to.

The following structural adjustments have been made:

- Web thickness has changed from 48 mm to 10 mm;
- Thickness of the tubes has changed from 48 mm to 25 mm;
- Thickness of the curved plates has changed from 88 mm to 33 mm;

At first, the deformations are investigated and compared to the deformations in the gate design in FRP. The results are presented in the figures below.

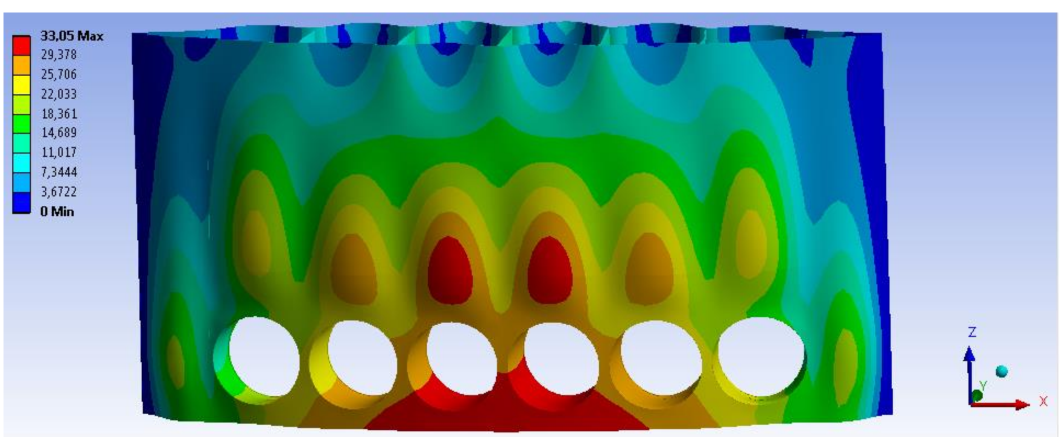

Figure 129: Deformations in the plate loaded by hydrostatic pressures constructed from steel

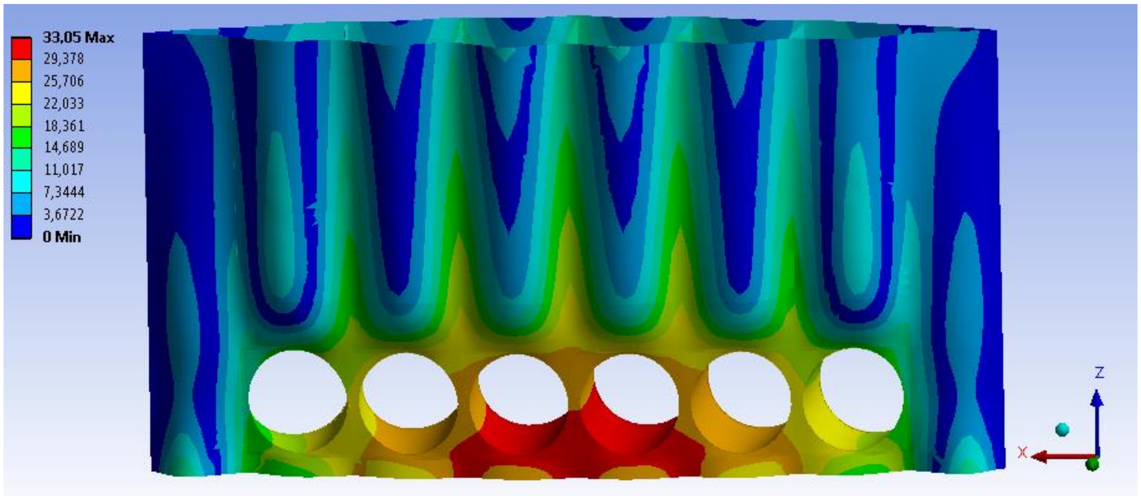

Figure 130: Deformations in the plate loaded by the valves constructed from steel

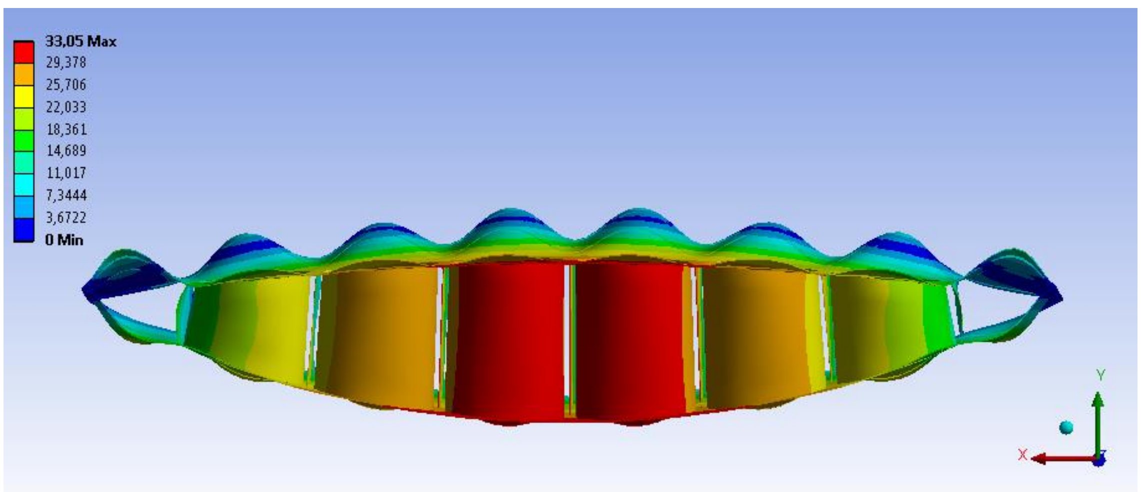

Figure 131: Bottom view on the deformations in the gate constructed from steel

The deformations of the gate constructed from steel are smaller than those at the gate designed in FRP, as the results of the finite element calculations point out. Next to the elastic deformations, a second advantage of steel compared to FRP is that the material does not suffer from creep deformations. At gates where the stiffness is a governing criterion for the design, for example because of strict leakage requirements or because of very large spans, it seems more attractive to apply steel instead of FRP due to the larger Young's modulus.

Where for the normal strains and shear stresses where mainly important for the gate constructed from FRP, for steel only the Von-Mises stresses have to be checked for the static analysis on strength. This criterion reads as follows for a two-dimensional stress state:

$$\sigma_{1,2} = \frac{\sigma_x + \sigma_z}{2} \mp \sqrt{\left(\frac{\sigma_x + \sigma_z}{2}\right)^2 + \tau_{xz}^2} \leq f_{yd} = 235\ N/mm^2$$

$\sigma_{1,2} =$ Prinicipal stress [N/mm^2]
$\sigma_x =$ Stress in the x-direction [N/mm^2]
$\sigma_z =$ Stress in the z-direction [N/mm^2]
$\tau_{xz} =$ Shear stress in the plain of loading [N/mm^2]

Figure 132 and Figure 133 show the results of the finite element model related to the Von-Mises stresses in the structure.

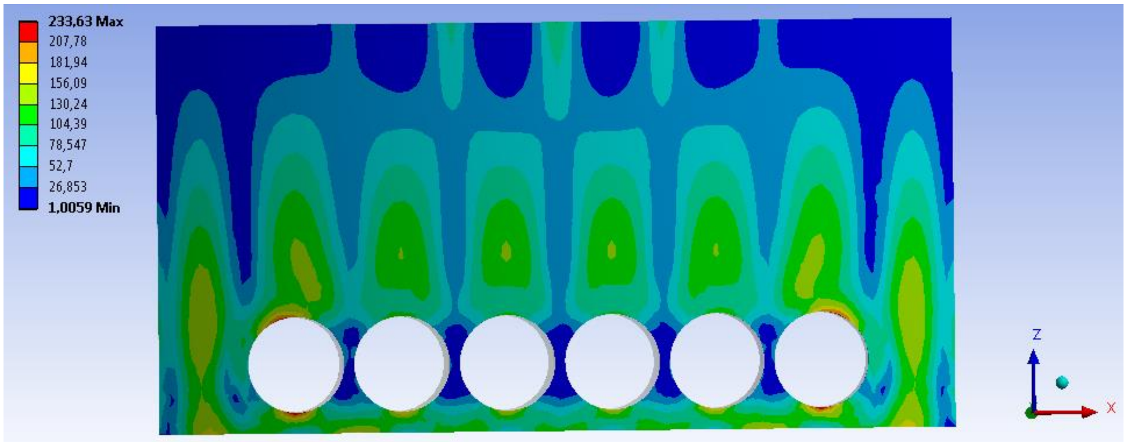

Figure 132: Von-Mises stress in the plate loaded by hydrostatic pressures constructed from steel

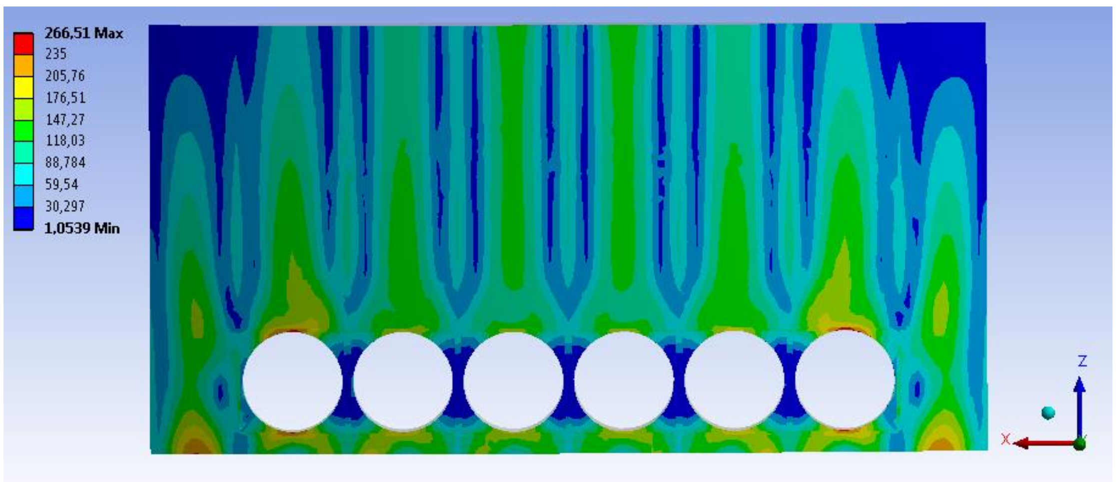

Figure 133: Von-Mises stress in the plate loaded by the valves constructed from steel

The figures show that the structure mostly fullfills the requirements on strength, except for the very small red area around the openings at the plate loaded by the valves. This minor problem can for example be solved by local strengthening of the plate, or stiffening of the tubes. These adjustments have not been elaborated quantitatively.

The final criterion which has been analyzed is the local stability of the plates loaded in compression. Just like for the analysis on the stability of the gate constructed from FRP, the output of the static analysis formed the input for the linear buckling analysis performed with help of ANSYS. The resulting load multiplication factor and modal shape which results in local instabilities for the first mode is presented in Figure 134.

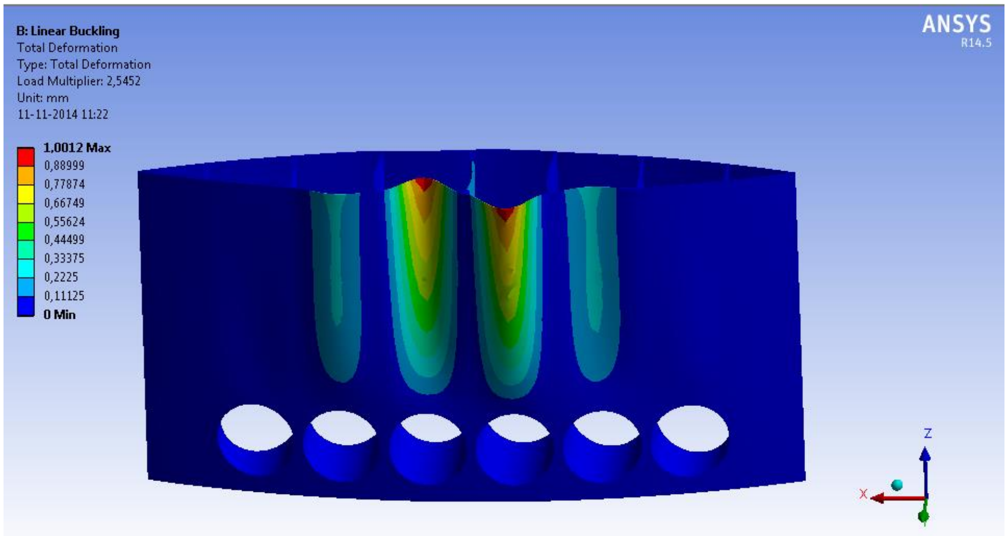

Figure 134: Modal shape and load multiplication factor related to the first mode at which instabilities are expected

Just as expected, the modal shape related to the first buckling mode is the same as for the gate constructed from FRP (see Figure 116), because of the similar geometry and load case. The plate loaded by the valves is the most vulnerable to instabilities, which is also as expected according to the study to gate alternatives. For this specific design in steel, the safety factor on local buckling is equal to 2,55, meaning that the requirement on stability is just met. Because the stability turns out to be governing for this specific design, application of steel quality S355 instead would not result in a lighter structure because the stiffness of both steel qualities is the same. Adjustments to the design, such as including stiffeners to the plate in combination with application of a steel quality with a higher yield strength , could result in a more economical design. Optimizations to the steel gate have however been left out of the scope of this research.

8.2. Comparison of mass of the design in FRP and steel

The final mass has increased by approximately 60% compared to the study to gate alternatives, which is mainly caused by the stress concentrations related to the openings in the gate. The decomposition of the mass of the gate in FRP is presented in Table 41.

Table 41: Decomposition of the mass of the Beatrixlock 3 made of FRP

Element	mass
Mass after study to gate alternatives	75 tons
Additional blocks of FRP at the supports	3 tons
Additional FRP in curved plates around webs	4 tons
Additional FRP in webs around curved plates	2 tons
FRP on top- and bottom of the gate	1 ton
Additional mass due to the Z-structure of fibers	1 ton
Sliding strips	1 ton
Material savings due to openings in the gate	-4 tons
Valves	12 tons
Culverts	2 tons
Adjustments required to fulfill the requirements as described in section 6.5	24 tons
Total mass of the gate	**120 tons**

The mass of the gate from steel is directly extracted from the ANSYS model described in section 8.1, and equals 202 tons. Please notice that further optimizations on mass for the design in steel might be possible, and that the extra masses required at the connections are not included.

The total mass of the gate constructed from FRP is approximately 40% less than of the design of the gate in steel. This reduced mass will have a postive effect on the mass of the counterweights, required power of the moving equipment and required strength of the lifting cables. The monetary value of this advantage has not been elaborated and could be an interesting topic for a follow up study.

8.3. Comparison of life-cycle costs for the design in FRP and steel

A life-cycle analysis has been performed in order to estimate the total costs over the lifetime of the gates constructed from steel and FRP. These life cycle costs can be split up into six different components [53]:

- Design costs;
- Construction costs;
- Maintenance and repair costs;
- Operational costs;
- Social costs;
- Environmental costs.

In this study, the design and construction costs are incorporated in a price per kilogram related to the initial costs. The annual maintenance, repair and operational costs are incorporated in the life-cycle costs as a percentage of the initial costs. The social costs and environmental costs are assumed to be very much compareable for both gate alternatives and are therefore not con

Furthermore, a technical lifetime for the gate of 50 years has been assumed. The estimations on costs are only related to the gate itsself: the influence of the mass on the surrounding structures and driving equipment has been excluded from this study. The future costs are translated to a net present value by application of a discount rate to account for inflation and risks. Because of the discount rate, future costs are of less importance than the present costs. The formula to convert future costs to present costs reads as follows:

$$NPV = \sum_{t=o}^{n} \frac{C}{(1+r)^t}$$

In which:

$C =$	Costs [€]
$r =$	Discount rate [-]
$t =$	Time [years]
$NPV =$	Summation of net present value of costs over the considered lifetime [€]

PIANC Workgroup 42 recommends a discount rate in between 2,5% and 10% for infrastructure projects in Europe, depending on the risks involved [54]. For this study on the life cycle costs, a discount rate of 4% has been assumed.

Unity prices for the initial costs related to application of FRP in lock gates are investigated in section 1.9. The unity prices found in literature are ranging from €4,-/kg (Kok [14]) to as much as €12,-/kg (Rijkswaterstaat [34]). These costs consist of the following components:

- Design costs;
- Raw material costs;
- Production costs;
- Costs of the mould;
- Transportation costs;
- Assembly costs;
- Overhead and risks.

The large variations in unity prices found in literature are caused among other things by differences in production processes, fiber fractions, structural geometries and fiber- and resin types. For this study, a unity price of €9,-/kg has been assumed, which is a weighted average of the unity prices found in literature.

The maintenance to FRP structures is limited to application of a new top coating every 25 years to protect the structure from UV-radiation [51]. The most frequently applied coating is ISO NPG, which is pigmented so that it takes care of both protection of the structure and good esthetics. In order to apply the coating, the structure has to be cleaned and dried. Opposite to steel, the old coating does not have to be removed however.

Although maintenance may be less than for steel gates, more frequent inspections are required. Because delaminations can generally not be detected by eye, special equipment is needed to inspect the structure on a regular basis (see section 1.8 for an overview of the available techniques). Estimations on the yearly costs for the design elaborated in this report are based on the thesis by Kok [14] and are assumed to be equal to 0,5% of the initial costs. An overview of the build-up of the life-cycle costs related to application of FRP is presented in Table 42.

Table 42: Life cycle costs related to application of FRP

Subject	Value
Mass of the gate	120 tons
Unity price related to initial costs	€9,-/kg
Total initial costs	€1,1 M
Ratio annual costs/ initial costs	0,5%
Total annual costs	€5.400,-
Net present value of costs over a lifetime of 50 years	**€1,2 M**

Secondly, the life-cycle costs related to the design in steel have been analyzed, which have also been split up into initial costs and annual costs.

The initial costs related to application of steel consist of the following components:
- Design costs;
- Production costs;
- Transportation costs;
- Assembly costs;
- Costs of opplication of a coating;
- Overhead and risks.

For an estimation on these combined costs, cost-expert Michel Koop and Merlijn Zewald (Iv-Infra) have been consulted for advise. For the selected geometry, mass and type of structure, a unity price of €5,-/kg is assumed to be reasonable.

The second part of the life-cycle costs related to application of steel consists of maintenance, repair and operation costs. For steel structures, it is recommended to have a preventive maintenance strategy [34]. This means that the structure will have maintenance periods after a certain time interval or a certain amount of load cycles. According to Rijkswaterstaat, for movable barriers it is common practice to have small maintenance works every 5 to 7 years, while steel barriers usually undergo large maintenance every 13 to 23 years [34].

During the small maintenance periods, approximately 1 to 5% of the surface area of the structure needs to be maintained [34]. The small maintenance consists of the following steps:

- Set up of a tent around the gate to prevent the small particles from falling into the water;
- Removal of the loose conservation layer;
- Local application of a new primer;
- Application of a new top coat.

During large maintenance works, 20 to 100% of the coating needs to be maintained, depending on the state of the structure. The large maintenance consists of the following steps:

- Set up of a tent around the gate to prevent the small particles from falling into the water;
- Full removal of the top coat and primer at the damaged area;
- Application of a new primer and top coat.

PIANC workgroup 26 investigated the life-cycle costs for construction of a new weir in the Meuse, equiped with steel lifting gates [55]. Due to the similarities with the lifting gates of the Beatrixlock regarding the type of structure and environmental conditions, the results of this study have been used to arrive at estimates on the relation between initial costs and yearly maintenance costs.

The initial costs related to construction of the weir on the Meuse mentioned above are estimated on €36 million, while the maintenance, repair and operation costs are expected to be €340.000,- on annual basis [55]. Based on this report, the large and small maintenance works for conservation of steel gates re assumed to be 1% of the initial costs if these are translated to yearly costs. This percentage is also supported by the lecture notes of the course Hydraulic Structures 2, published at the Delft University of Technology [56]. The build-up of the life cycle costs for the gate constructed from S235 are presented in Table 43.

Table 43: Life cycle costs related to application of S235

Subject	Value
Mass of the gate	202 tons
Unity price related to initial costs	€5,-/kg
Total initial costs	€1,0 M
Ratio annual costs/ initial costs	1%
Total annual costs	€10.000,-
Net present value of costs over a lifetime of 50 years	**€1,2 M**

The net present value of the costs related to application of both S235 and FRP over the life time is presented in Figure 135.

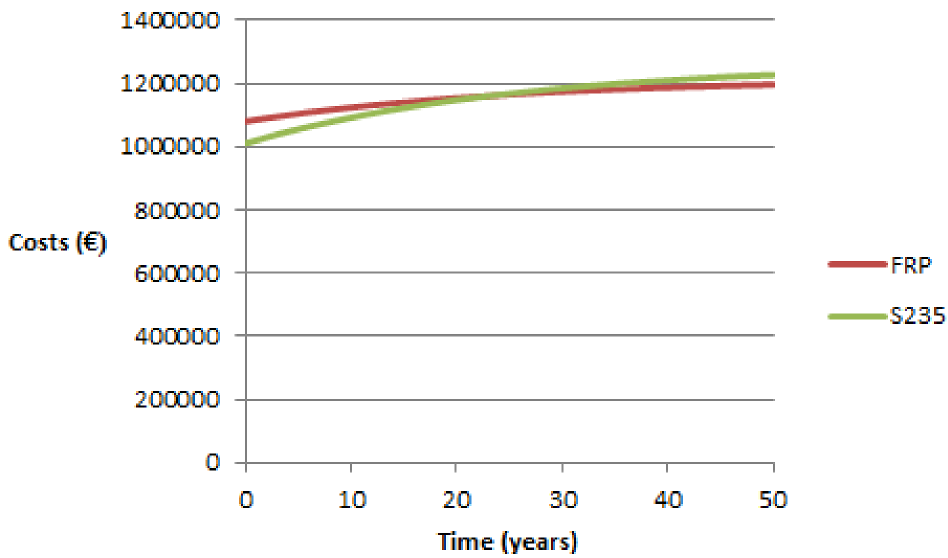

Figure 135: Net present value of the costs related to application of S235 and FRP in time

As Figure 135 shows, the expected life-cycle costs related to application of FRP and steel for the gates of the Beatrixlock 3 are very much compareable over the considered lifetime of 50 years. The slightly higher initial costs related to application of FRP are compensated by the maintenance costs which are expected to be lower over the lifetime of the structure.

It should however be kept in mind that this cost-analysis contains relatively large uncertainties. The large scatter in unity prices found in literature related to the initial costs and maintenance costs, together with the uncertainties related to the final mass of both gates after detailing make that this conclusion should be approached with some care. Besides, it may be more appropriate to relate the maintenance costs to the surface area of the gate instead of to the mass. Further analysis to the costs of reference projects is recommended to arrive at more reliable estimations on the unity prices.

8.4. Comparison of risks for the design in FRP and steel

The final criterion on which the large lock gates in FRP and steel are compared are the specific risks related to application of both materials. These risks are identified by the case study elaborated in this report, the performed literature study [4], recommendations on further research in the CUR 96 [22] [25], recommendations by Kok [14] and consultancy of FRP-expert Peeters [32] [51]. The risks analysis only considers the gate itself: failure of the driving mechanism or lifting towers have not been considered.

The following risks are identified for the gate constructed from FRP:

- *Fatigue damage*: small cracks are formed which accelerate the moisture absorption. This moisture absorption may lead to structural degradation by means of osmosis.
- *Impact damage*: Due to the high kinetic energy related to ship impact, combined with a lack of ductility in the material, ship collision forms a serious threat for the lock gate constructed from FRP. The relevant failure mechanisms and the extents of the damaged area require further investigation.
- *Valve vibrations*: The lower mass of the valves compared to valves made of steel may induce vibrations which can result in fatigue failure of the gate

- *Errors during production:* Trapped voids, anomalies or bad positioning of the fibers during production may lead to a structure which is not as strong or stiff as designed.
- *Design errors:* The designer's lack of experience with the material in combination with the absence of
- *Moisture absorption in core:* If the core is saturated with water due to leakages in the skin plates, expansion due to frost may lead to undesirable stresses in the structure.
- *Strength of connections:* A detailed calculation on the design of the connections is not performed. The strength of these overlaminated connections still contains a lot of uncertainties.

The probabilities and consequences of these risks are assessed in a qualitative way, based on the available literature on these subjects in combination with making use of common sense. Hereafter, the recommended mitigation measures are determined in order to manage these risks. The results are presented in Table 44.

Table 44: Overview of risks related to application of FRP in large lock gates

Event	Probability	Consequence	Mitigation measures
Fatigue failure at the connections	Low	High	Monitoring of the structure on a regular basis
Failure due to ship impact	Moderate	Very high	Further investigation required, possibly external protection required
Vibration of valves	Moderate	Moderate	Further investigation required, response analysis i.c.w. fatigue
Errors during production	Low	High	Quality control during production and after production by scans
Design errors	Moderate	High	Review of the design by an FRP-expert
Moisture absorption in core	Moderate	Unknown	Further investigation required to the extents of these effects
Failure of the connections	Moderate	High	Further investigation required, mainly by physical testing

The risk analysis has indicated that joint failure and ship impact are the largest risks for application of FRP in large lock gates.

At this very moment, too little information is publicly available on the detailed design of FRP structures to be able to say anyting useful about the risks related to this topic. Production companies may be in posession of more knowledge on the strength of the connections in FRP but keep this information to theirselves to preserve their strong competitive position. It is recommended to invest in physical- and numerical tests in order to arrive at design standards for joints in composite structures.

The second main risk related to application of FRP in large lock gates is failure of the structure due to ship impact. The low strains at which rupture of the fibers occurs together with a lack of ductility in the material limits the ability to absorp the kinetic energy of vessels colliding into the gate. It is questionable whether the water retaining function is still preserved and to what extend the damage is repairable with preservation of strength. This subject is further elaborated in the next chapter.

Since steel has already been applied for centuries in civil prjects, a lot of experience on the material performance has been gathered throughout the decades. Physical testing, numerical analysis and experience with real life projects constructed from steel have resulted in design codes which cover the risks related to application of the material very well, both on a global level and on a detailed level. One of the few subjects which has not been very well defined in the avaiable design codes is how a lock gate from steel needs to be designed for ship impacts. This subject together with the uncertainties related to the hydraulic boundary conditions forms the largest risks for application of steel in lock gates. The effects of a ship collision into the steel gate will also be elaborated in the next chapter.

9. Structural response to ship impacts

During the risk analysis performed in section 8.4, ship impact turned out to be one of the largest risks both for the design in FRP and steel. The uncertainties related to such an event are twofold: firstly, the governing input parameters related to an impact (such as mass, velocity and shape of the hull of the vessel) are not very well defined in litetature. Secondly, the structural response related to a predefined impact is hard to predict due to non-linear effects both in geometry (plate stabilities) and material properties (ductility). Besides, the effects of friction between bow and gate and added mass of water still contain uncertainties.

During an impact, the kinetic energy of the colliding vessel needs to be balanced by deformations in the gate resulting in a reaction force to absorp the kinetic energy. Ideally, the gate should be able to resist small collisions without damages resulting in unavailabilities of the lock, while the water retaining function should be preserved during extreme collisions. As section 9.1 will prove, most (hazardous) collisions take place at the second lock gate while the first gate is still in lifted position. This means that once the water retaining function is lost during an impact, the other gate needs to be closed in strong flow conditions, which is usually not possible.

This chapter has been divided into 3 different parts. The first part focusses on a determination of the input parameters for the elaboration of a ship collision, based on a probabilistic study on the risks of ship collisions to lock gates by Deltares [57]. The second part of this chapter serves as an overview of the different methods to assess the structural response due to a ship collision. Finally, a full dynamic approach has been performed with finite element software ANSYS to assess the effects of the governing impact on the gates designed in FRP and steel.

9.1. Study on the kinetic energy related to the governing collision

In order to assess the effects of a ship collision to both the design in FRP and steel, the governing kinetic energy needs to be determined first. The formula to determine the kinetic energy of a ship collision reads as follows:

$$E_{kin} = \frac{1}{2} * m * v^2$$

In which:

$E_{kin} =$	Kinetic energy related to a ship impact
$m =$	Mass of the vessel, together with the added mass of water
$v =$	Sailing velocity of the vessel at the moment of impact

The determination of the governing energy has been based on the report by the Dutch “Waterloopkundig Laboratorium” (now known by the name Detalres). In 1992, this organization performed a study to the risks of ship collisions into lock gates [57]. The aim of this study was to draw a probability density function of the kinetic energy related to an impact for lock gates constructed for different CEMT-classes. Data on registered accidents in the period 1985-1989 in The Netherlands formed the basis for this probabilistic study.

Firstly, the registered accidents in this period have been divided into collisions to the first- and second gate and a distinction has been made between collisions to opened- and closed gates. Subsequently, the collisions have been subdivided into different causes. The distribution of the collisions over the two gates, the status of the gate and the different causes is presented in

Figure 136. Please note that this study is not restricted to lifting gates: ship collisions to mitre gates and rolling/sliding gates have also been incorporated in this study.

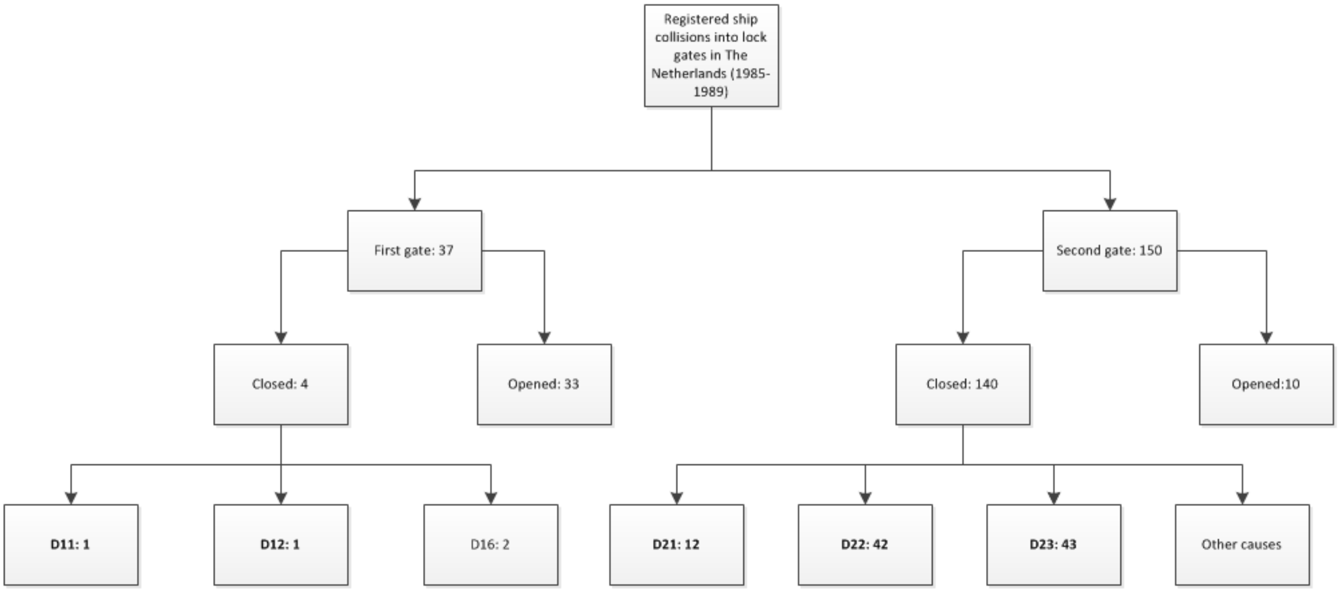

Figure 136: Registered collisions in The Netherlands in the period 1985-1989 divided into different categories, basedon [57]

The symbols in Figure 136 represent the following causes:

D11: The captain is unable to reduce the velocity and the ship collides into the first gate;
D12: The rudder of the ship can not be put into reverse, the engine is turned off but the ship collides with reduced velocity into the first gate;
D16: The captain puts the rudder accidently in reverse while trying to exit the lock after filling- or emptying of the chamber has taken place. The ship collides into the first gate reversed.
D21: The captain is unable to reduce the velocity and the ship collides into the second gate;
D22: The rudder of the ship can not be put into reverse, the engine is turned off but the ship collides with reduced velocity into the second gate;
D23: The rudder is put into reverse too late, the ship collides into the second gate with a reduced velocity.

The scenarios D11, D12, D21, D22 and D23 have been selected as governing because of relatively high impact velocity or a high reoccurance rate. This means that a total of 2 collisions are considered for the first gate and 97 collisions are considered for the second gate during the considered timespan of 5 years. The total amount of locking cycles for the 40 most important navigation locks in The Netherlands is estimated to be 650.000 per year [57]. This brings the probability of a ship colliding into the first gate to 1/1.600.000 per locking cycle while the probability of a ship colliding into the second gate is on average 1/33.000 per locking cycle [57]. As an example, a navigation lock which performs 20 locking cycles a day will encounter a ship collision every 5 years on average.

Hereafter, the registered masses and sailing velocities of the vessels have been investigated in a similar way. For the results of these studies, reference is made to the original report [57]. By combining the probabilities of a ship impact with the distribution of masses and sailing velocities of the vessels for a certain CEMT-class, curves can be drawn to assess the probability of exceendance of a certain kinetic energy related to a ship collision. Figure 137 shows the exceedance curve for the impact energy for different types of vessels for a CEMT-class Vb lock with water depth of 3,90 meters, given that an accident occurs.

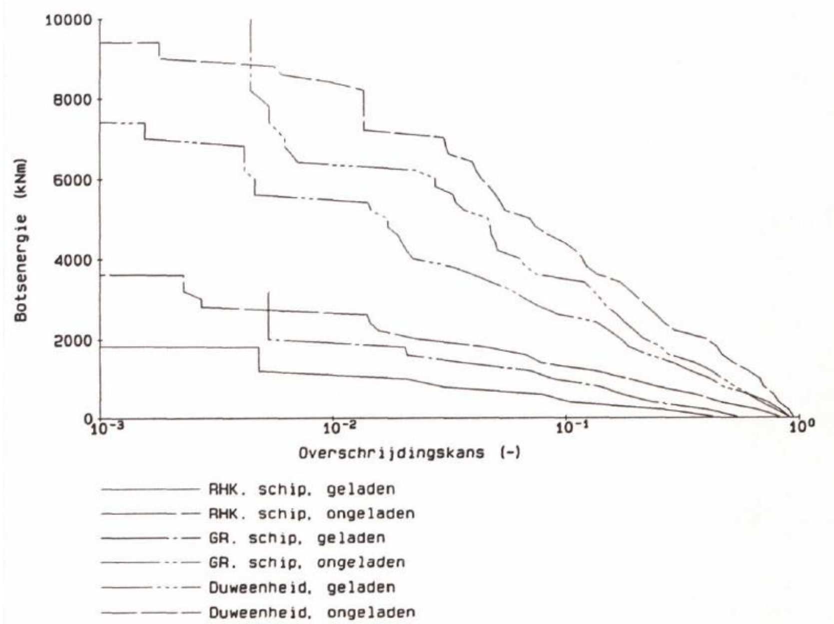

Figure 137: Kinetic energy versus exceedance frequencies for the second lock gate of a CEMT-class Vb lock [57]

In order to determine the energy related to the maximum collision which has to be resisted by the gate, the exceedance frequency of such an impact has been set equal to the frequency of the considered design water levels of 1/1250 per year. This is not fully correct, because this would not result in the required safety level for the entire dike ring of 1/1250 per year. Therefore, actually a higher safety level for the individual failure mechanisms should be considered to arrive at the required safety level for the top event. On the other hand, an underestimation of the collision energy is still very useful for this investigation: if the gate is not able to resist a 1/1250 years impact, it is definitely not able to provide the required safety level for the entire dike ring either.

Based on a collision frequency of 0,2 per year, the governing impact energy which has to be resisted by the gate with a loss of the water retaining function has been set to 8 MJ, based on Figure 137. In order to arrive at this energy, a ship with a mass of 8000 tons and a velocity of 1 m/s has been considered as representative.

9.2. Overview of approaches to investigate the effects of an impact

Basically, the following three methods can be used to investigate the effects of ship collision:

- Empirical approach
- Energy approach
- Full dynamic approach

The empirical approach makes use of physical tests in order to find the maximum static forces related to ship impact. The results of physical tests are normalized in tables which can be used for the (preliminary) design of the structure. An example of such a table can be found in the NEN-EN 1991-1-8. This table relates the CEMT-class of the waterway to the the collision force between a vessel and a rigid structure. Although this method is very easy to use, it does not give very reliable results. Effects of variation of velocities and local geometries of both the waterway and collision area are not incorporated in the model. Therefore, these tables can only be applied for a preliminary design.

The results which are obtained by an energy approach are already a lot more accurate. During such an analysis, the gate is schematized by a certain force-displacement diagram related to the location and area of impact. The effects of the added mass of water, rigidity of the ships and confined water between ship and gate are typically accounted for by coefficients. The kinetic energy of the vessel is compared to the energy stored in the spring to obtain the maximum deflections, which are subsequently translated to static forces. The structural respons to these maximum forces are finally investigated in a static analysis. This method has two drawbracks: the force-displacement relation is not easy to find if plasticity and stability of members needs to be included and the damping due to friction is hard to incorporate in the model.

The third and most accurate approach is the full-dynamic approach. Both the vessel and the gate are modelled with FE-software. The equations of motion are consequently solved in the time-domain so that the deformations and forces on the gate are obtained at every single timestep of the model. The disadvantage of this method is that it is computationally heavy to obtain results from such a calculation and that it might be hard to verify the correctness of the results of the calculation without expensive physical tests.

Because of the accurate results which are achieved by a full dynamic calculation in combination with the relatively little effort that it takes to change the static finite element calculations in ANSYS (which are presented in sections 6.3 and 8.1) into a dynamic calculation, it has been decided to select this approach for an investigation of the effects of the governing ship collision.

9.3. Elaboration of the dynamic approach to ship impact

As already mentioned in the previous paragraph, the Ansys Transient Structural module has been used to investigate the effects of a ship collision. This module makes use of an implicit method to solve the set of equations.The large advantage of an implicit method compared to an explicit method is that it is unconditionally stable, which means that the time steps do not have to be within predefined limits to arrive at a solution, resulting in less calculation times. For more information on the differences between implicit- and explicit methods and information on when to apply which type of solver, reference is made to [58].

9.3.1. Set-up of the model

The gate geometry for the dynamic analysis has been extracted from the model which is described in chapter 6 (FRP) and chapter 8.1. (steel). Schipperen (TNO) advised to refrain from sharp edges for the model of the ship to obtain better results [59]. therefore, the ship has been modelled as a small tube with conical head. The cone of the vessel has been given a radius of 1,5 meters, so that the contact area matches the bow shape of a large rhine vessel. The density of the vessel has been adjusted until the governing mass of 8000 tons has been reached. The vessel has been given an initial velocity of 1 m/s, and the contact area has been given a friction coefficient of 0,3. Furthermore, the ship is assumed to be fully rigid.

In order to investigate the structural response to the design impact, firstly an impact right in the middle between two webs is investigated. If an impact at this location can not be resisted without a loss of function, it is clear that additional measures are required to preserve the structural integrity of the gate. If the gate is able to resist the impact however, further analysis is required to find the location of impact where the damage will be largest to find out if this impact can be resisted as well. The structural response of the gate to impact has not been investigated in combination with the hydrostatic pressures. The schematization of the vessel, position of impact and geometry of the gate is presented in Figure 138.

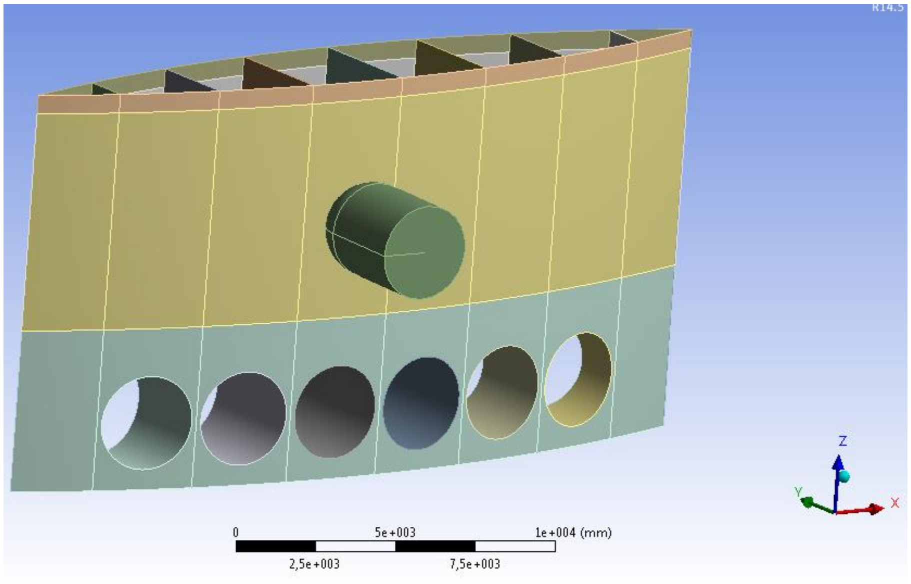

Figure 138: Overview of the model and representation of the vessel

The ANSYS Transient Structural module makes use of an iterative solver to include geometrical non-linearities and non-linearities in material properties. The position of the vessel is estimated in advance of each timestep, and compared to the force afterwards given the estimated deformations during the timestep. The initial estimation of the position is corrected for the forces found related to the deformations after the timestep. The Newton-Raphson method is used to converge to a solution where the difference between estimated displacements on beforehand and the displacement related to the force after a timestep are within predefined limits. Once the result of a timestep has converged, a new timestep is started. This principle is presented in Figure 139. A single run takes approximately 5 minutes of calculation time.

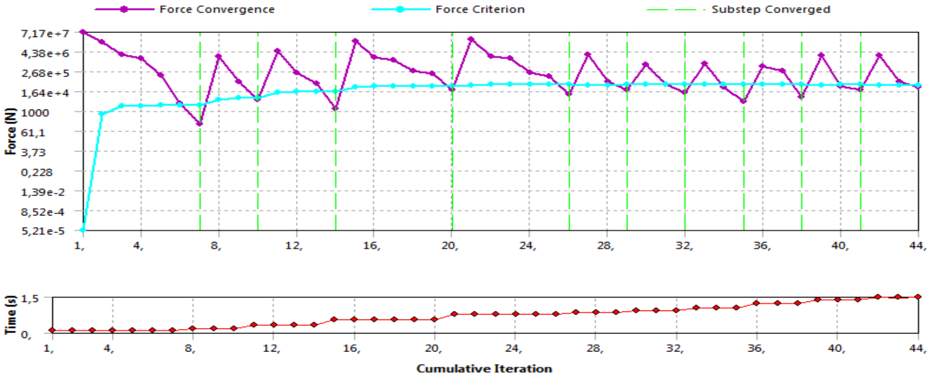

Figure 139: Chart of the force convergence during the calculations

9.3.2. Results of the dynamic approach for the gate constructed from FRP

In order to check the effects of the ship collision to the gate in FRP, the resulting maximum deformations, shear stresses and normal strains are investigated. The results are presented in the figures below. The proposed structural adjustments described in section 6.4. to fulfill the requirements related to the static approach have not been included in the model.

Firstly, the deformations are investigated. The results are presented in Figure 140.

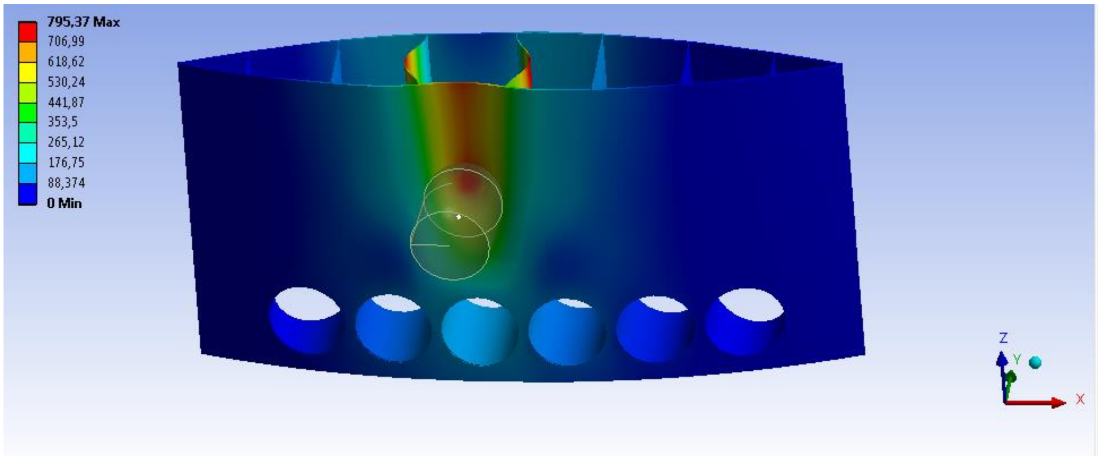

Figure 140: Maximum deformations of the gate (mm)

The maximum deformations appear to be nearly 800 millimeters, while It takes approximately 1,15 seconds for the gate to reach these maximum deformations related to impact. The deformations are relatively local: only the area between two webs is involved with resistance of the impact. Due to the large compressive forces in the webs accompanied with the impact, these elements have the tendency to become instable.

Secondly, the normal strains in the gate are investigated. For this load case, FRP-expert Tromp (Royal HaskoningDHV) recommended to divide the maximum strain of 1,2% in the SLS by the material factors y_{m1} and y_{m2} and by the conversion factors for moist- and temperature effects y_{cv} and y_{ct}. This results in a maximum allowable strain of 0,52% in the ULS. The resulting strains around the impact zone caused by ship impact are presented in Figure 141 and Figure 142.

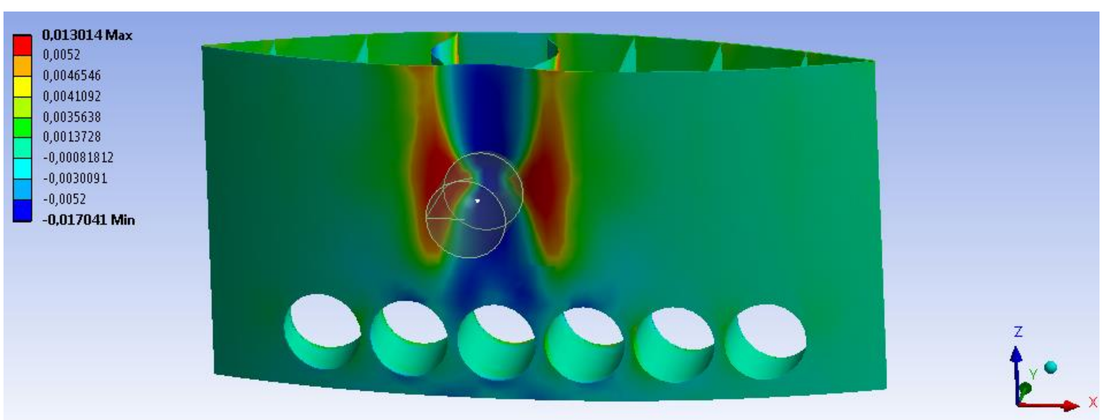

Figure 141: Normal strains at the top skin (-)

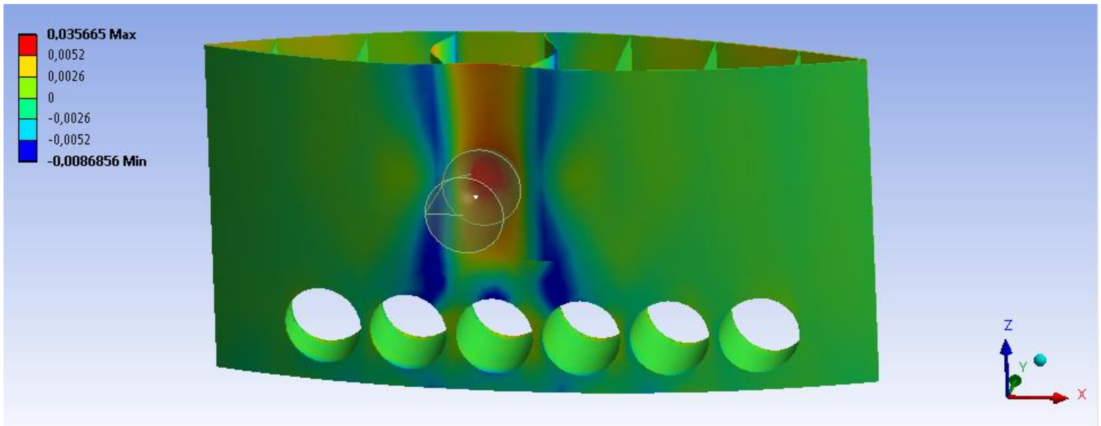

Figure 142: Normal strains at the bottom skin (-)

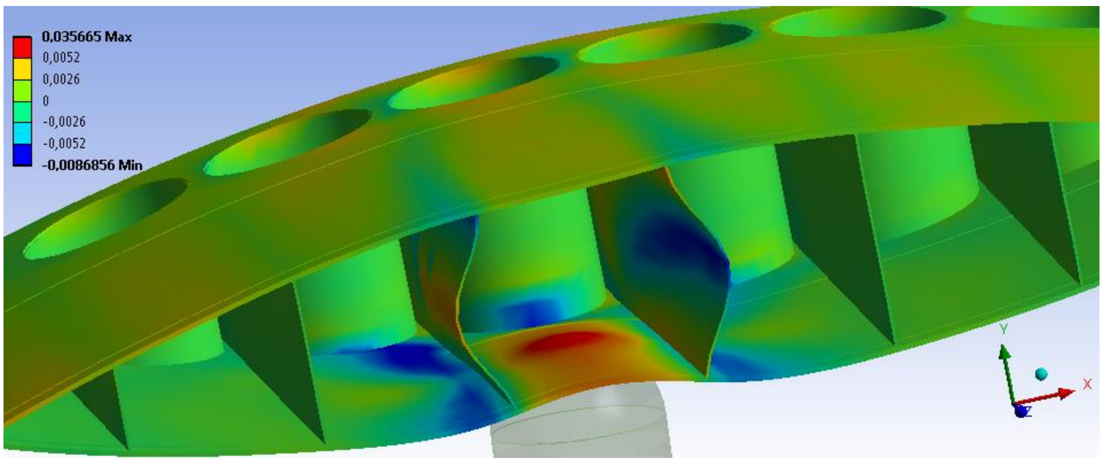

Figure 143: Top view on the normal strains at the bottom skin (-)

The red and dark blue areas in the previous pictures represent the areas where rupture of fibers is expected to occur. Not only will a large area of the gate be crushed during the collision, the water retaining function is not preserved either. The unity check on fiber rupture for the worst damaged part is even as high as 7, as Figure 144 shows. Next to that, Figure 143 shows that not only the curved gate gets crushed, the culvert will become leaky as well. This means that there is a direct connection between the two sides of the gate, resulting in a loss of the water retaining function of the gate as a whole.

Thirdly, the interlaminar shear stresses in the structure are investigated to see if next to fiber ruptures, delaminations between the plies is expected to occur as well. The limit state shear stress at which delaminations are expected to occur is equal to 12,35 N/mm^2 for the selected type of resin. The results are presented in Figure 146 and Figure 145.

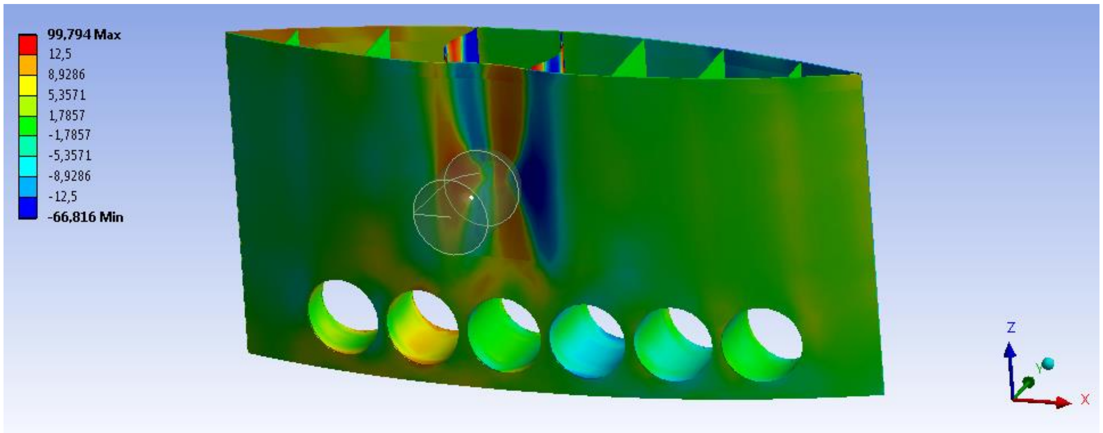

Figure 146: Maximum shear stresses (MPa)

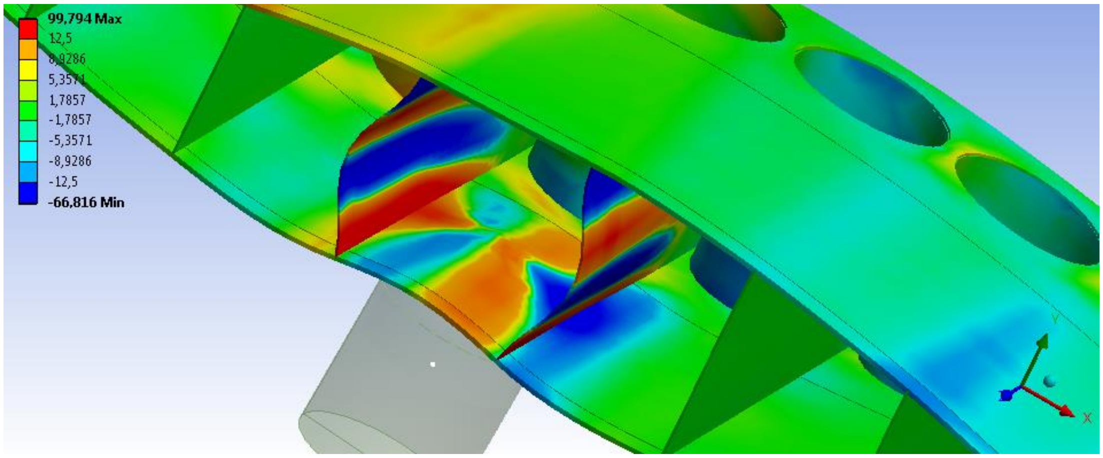

Figure 147: Top view on the maximum shear stresses in the gate (MPa)

Again, the dark blue and red colours indicate the locations where delaminations are expected to occur. The webs appear to be the most vulnerable to delaminations. The unity check on shear strength is equal to 8,1.

9.3.3. Results of the dynamic approach for the gate constructed from steel

The same collision has been modelled for the design in steel which has been designed on static strength in chapter 8.1. A bilinear stress-strain diagram is assumed with a yield strength of 235 N/mm^2. The considered stress-strain diagram is presented in Figure 148.

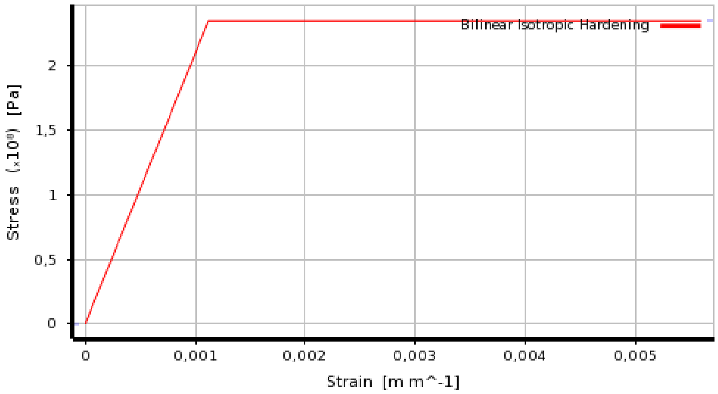

Figure 148: Schematized stress-strain relation for the applied steel quality S235

To assess the effects of the governing ship collision to the lock gate constructed from steel, the deflections, equivalent stresses and the maximum strains are investigated. The results are presented in the section below.

Firsty the deformations are investigated. The results are presented in Figure 149.

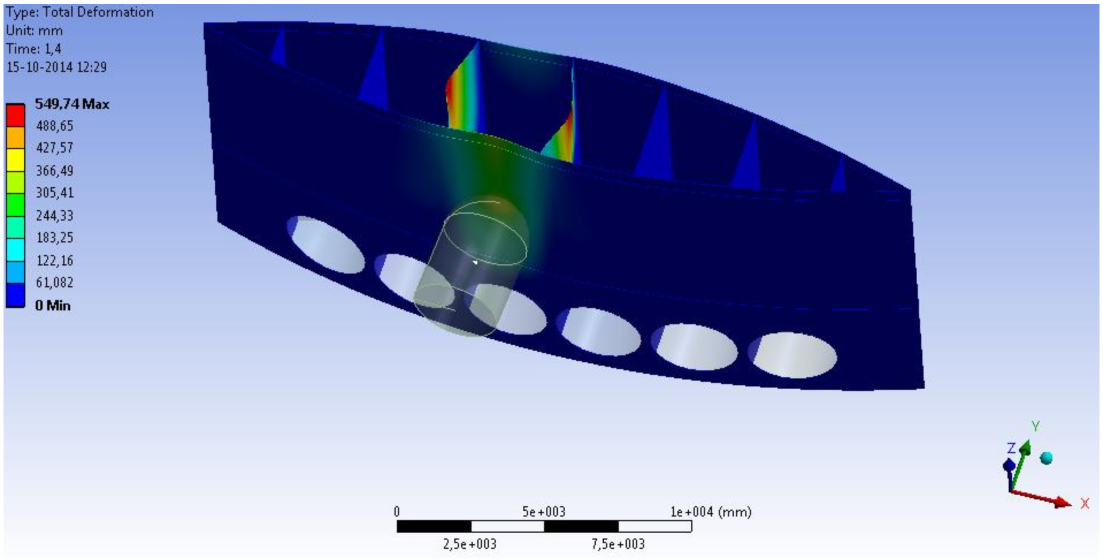

Figure 149: Maximum deformations for the steel gate during ship impact

Just as expected from the static calculations, the total deformations during impact turn out to be less for the steel gate than for the gate of FRP because of the higher stiffness. The time between impact and maximum deformations takes about 0,9 seconds. Just as for the gate constructed from FRP, also for this design the stability of the webs appear to be a problem as Figure 149 shows.

Secondly, the equivalent stresses have been investigated. The results are presented in Figure 150.

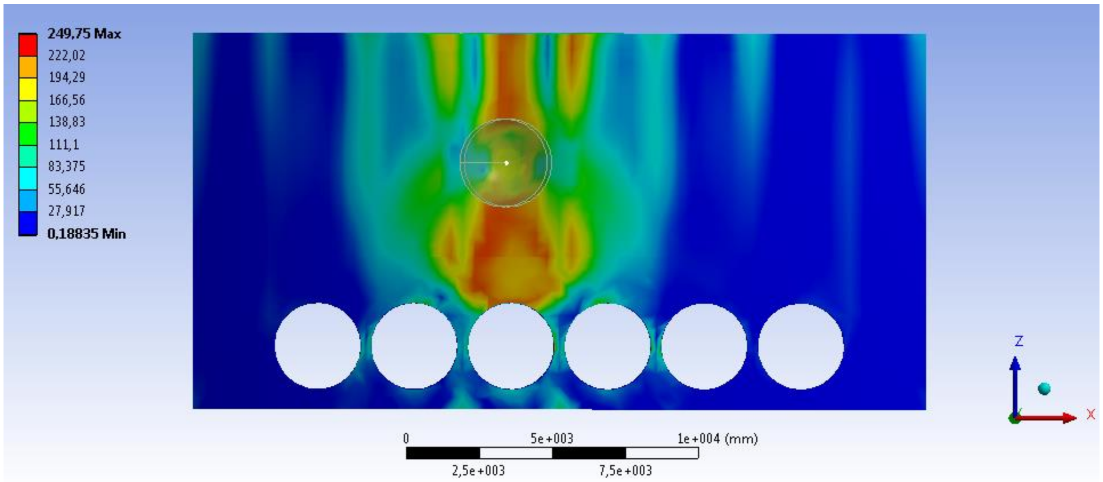

Figure 151: Maximum normal stresses in the steel gate during ship impact

Due to the ductile behaviour of the material, the effective area which is active to absorb the impact is much larger than the one at the FRP gate. As Figure 152 shows, a large area will deform plastically. This means that permanent deformations are expected to take place. Plastic deformations do not endanger the structural performance of the gate as long as the valves can still be opened and closed. In order to find out whether the water retaining function of the gate is still preserved, the maximum strains in the plates have been investigated and compared to the ultimate strain of 15% for S235. The results are presented in Figure 153.

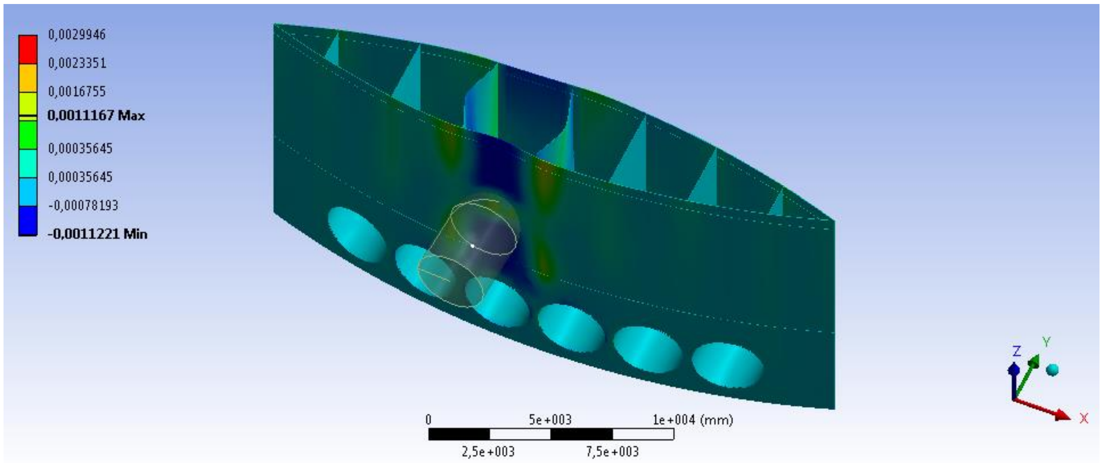

Figure 154: Strains at the steel gate due to ship impact

The maximum equivalent strain in the gate of 0,3% is much less than the failure criterion of 15%. Therefore, the water retaining function is still guaranteed. Please note that the connections between the plates have not been investigated in this study.

9.4. Conclusion on ship impact for the gates in FRP and steel

According to the dynamic analysis to the ship impact performed in this chapter, the gate in steel appears to be much more resistant to ship impact than the gate in FRP. For the steel gate, the stability of the webs and the operateability of the valves due to plastic deformations of the gate seem to be the largest problems. This is easiliy be solved by increasing the web thickness or application of additional stiffeners to the gate.

For the gate in FRP however, both fiber rupture and delaminations are expected to take place, resulting in a loss of the water retaining function. Besides, the unity checks on strains and shear stresses turn out to be such high that adjustments to the gate itself do not seem to be feasible. A better solution would be to install an external protection device to absorb the kinetic energy of the incoming ship. Such a device could be one of the following concepts [60]:

- Protection devices attached to the gates
-
- Shock-absorbing beams
- Shock-absorbing swing beams
- Shock protecting grids
- Frame supporting cables
- Cable retaining devices

The analysis performed in thischapter only focussed on the preservation of the water retaining function for huge impact energies. An interesting topic for future research would be to investigate what kinetic energy could be resisted by the gates without the need to repair, to investigate the unavailablity of the gates due to required maintenance after impact.

10. Conclusion

The objective of this study was to assess the feasibility of fiber-reinforced polymers (FRP) for application in large lock gates as an alternative for steel. The criteria which were applied to assess the feasibility are the required mass (as a measure for the forces on the supporting structure and driving equipment), the life-cycle costsof the gate and the risks related to application of both materials.

In order to compare the feasibility of both materials, structural designs of the gates of the new “Beatrixlock 3” have been elaborated and optimized both in steel and in FRP. The gate spans a length of 25 meters, a height equals 12,8 meters while the design head difference equals 7 meters. Lifting gates were selected for this purpose based on the large advantages of a low mass in combination with a good inspectability. A study to five different alternatives regarding the gate geometry showed that the lens-shaped gate was the most promising option, due to an efficient use of materials in combination with a good producability an maintainability. E-glass has been selected as fiber type while the resin consists of polyester, based on minimization of costs.

The design in FRP turned out to be considerably less heavy than the design in FRP due to its higher specific strength : 120 tons versus 202 tons. The life-cycle costs for both designs over the considered life-time of 50 years were in the same order of magnitude: the slightly higher initial costs for application of FRP are compensated by the expected lower maintenance costs, resulting in life-cycle costs for both designs of approximately €1.200.000,-. These costs are only related to the gate itself, driving equipment and supporting structures are excluded.

However, application of FRP in large lock gates also contains some downsides compared to application of steel. Firstly, FRP shows linear elastic behaviour up until fiber rupture. Not only does this mean that structural failure happens abruptly, it is also at the expense of the robustness of the design because no redistribution of forces can take place during unexpected extreme load conditions. Secondly, the low interlaminar shear strength makes FRP structures vulnerable to delaminations, which are mostly impossible to detect by eye. This does not only require special attention for the design of the spots where high shear forces are expected, but also requires regular inspection with special equipment to detect delaminations. Thirdly, the low Young’s modulus of the material in combination with high creep deformations (in the order of 50% of the elastic deformations during daily load conditions) makes a large lock gate constructed from FRP vulnerable to leakage gaps between gate and lock head. Fourthly, the little experience with the material so far have not yet resulted in globally acknowledged design codes. Especially information on the detailed design is missing.

Finally, a dynamic approach has been applied to study the structural response to a large ship impact for the designs in steel and FRP. The design from steel showed some plastic deformations but the water retaining function was still preserved. Due to the low strains at which fiber rupture occurs, the gate from FRP turned out to be unable to resist the impact without a loss of the water retaining function. The unity checks on shear strength and principal strains were such high (the ultimate limit states on strains and interlaminar shear stresses were exceeded by a factor 8) that structural adjustments do not seem to be feasible: external devices to resist ship impacts are therefore recommended for large lock gates constructed from FRP.

Based on the life-cycle costs, application of FRP appears to be a promising alternative for steel for application in large lock gates. However, the robustness of designs for large lock gates in FRP is still questionable.

11. Recommendations

In order to prove the feasibility of FRP in large lock gates, further investigation is required on the robustness, durability and detailed design of FRP structures. The following subjects are recommended for follow-up studies:

Static strength of connections between members

The CUR 96, which is at present the only design document available for the design of FRP structures, does not provide any information on the strength of connections. It is recommended to perform physical tests on different joint geometries. The results of these test can be generalized an converted into design rules on the connections.

Fatigue resistance of connections between members

Up until now, very little information is available on the fatigue performance of the material, especially compared to the abundance of literature available for fatigue in steel structures. It is recommended to perform physical tests where details vulnerable to fatigue are exposed to repeated loading cycles until failure.

Study on combined degradation mechanisms of FRP

The conversion factors stated in the CUR 96 to account for moisture absorption, temperature effects, creep effects and fatigue effects are based on isolated tests. It is not yet clear whether combination of different degradation mechanisms will result in accelerated degradation, which would imply that the different safety factors can not be simply multiplied with each other. For lock gates, it would be interesting to investigate the combination of moisture absorption with fatigue, moisture absorption with creep and structural degradations after damages to the structure.

Study on the vibrations of FRP valves in lock gates

Due to the light weight and easy installation, FRP seems to be a good alternative for steel for application in valves of lock gates. The combination of high flow velocity and a low specific weight may however result in dangerous vibrations to these valves, especially if considered in combination with fatigue. It is recommended to investigate the dynamic behavior of valves during rapid flow conditions analytically. The most useful result would be a study to the frequency response function. Finite element modeling can be used to verify the analytical results.

Study on the life-cycle costs of FRP compared to steel

The analysis performed in this report on the life-cycle costs are based on rough estimates. More detailed information on the costs is desired to make well-founded design decisions during an early stage. It is recommended to set up a model which relates the mass, geometry, production method and the applied materials to the costs of a structure. This subject can for example be studied by back-analysis of the costs of recently finished projects involving application of FRP in civil structures.

Study on the environmental impact of FRP compared to steel

Studies on the environmental impact of FRP compared to traditional building materials show large differences in results [30] [31]. Because of the growing importance of sustainability in the construction branche, this is an interesting study for further elaboration. The emphasis of this study should be on the gathering of accurate source data and on an elaboration of designs in different materials based on the same functional requirements.

Study on ship impacts to lock gates constructed from FRP
This study has proved that the design in FRP is not able to resist (very) large impacts. Another interesting subject to study is its resistance to small impacts, and to investigate what impact energies can be resisted without unacceptable damage to the gate. The results can be used to assess the availability of locks equiped with gates from FRP.

Study on the optimal inspection and maintenance strategies for FRP structures
Because of the uncertainties related to this relatively new material, decent monitoring of FRP structures is required. An interesting subject is to study the most promising maintenance strategy (preventive versus corrective maintenance) and the optimal inspection strategy (technique, intervals, processing of data) resulting in the lowest life-cycle costs. This is best reached by a probabilistic approach to the strength of the structure over its lifetime.

Bibliography

[1] M. Kolstein, Fibre-reinforced polymers (FRP) in composites for structural applications, Delft: Faculty of Civil Engineering and Geosciences, Delft University of Technology, 2008.

[2] Bouwdienst Rijkswaterstaat, „Kunststof Puntdeuren voor de Spieringsluis," *Product Innovatieblad,* 2001.

[3] Bouwdienst Rijkswaterstaat, „Kunststof schuif in de Kreekraksluizen," *Product Innovatieblad,* 2000.

[4] A. Zorgdrager, „Feasibility study on the application of fibre-reinforced polymers: Literature study," Amsterdam, 2014.

[5] M. Kolstein, „CT5128: Projects Netherlands," Delft University of Technology, Faculty of Civil Engineering and Geosciences, 2004.

[6] R. Nijssen, Composieten basiskennis, Hogeschool Inholland, 2013.

[7] C. Kassapoglou, Design and Analysis of Composite Structures, Wiley book publishing, 2013.

[8] „Modern airliners," [Online]. Available: http://modernairliners.com/Boeing787_files/Specifications.html. [Geopend 17 June 2014].

[9] R. Evenblij, Technobis, „Monitoring techniques for composite structures," in *Round table conference: Monitoring of composite structures*, Hogeschool van Amsterdam, 2014.

[10] Lecture notes MT816: Composite materials in marine structures, Delft: Faculty of 3mE, Delft University of Technology, 2005.

[11] Lightweight Structures, „Vacuum infusion strategies for yacht hulls," 1999. [Online]. Available: http://www.lightweight-structures.com/nl/vacuum-infusion-strategies-for-yacht-hulls/index.html. [Geopend 11 July 2014].

[12] Decentlab, Artist, *Stork Bridge in Winterthur.* [Art]. http://www.decentlab.com/storchenbruecke.

[13] PIANC, „Report no.106 - Innovations in navigation lock design," 2009.

[14] L. Kok, „Feasibility study for FRP in large hydraulic structures," Faculty of Civil Engineering and Geosciences, Delft University of Technology, Delft, 2013.

[15] H. Tuin, „New canalization of the Nederrijn and Lek: Design of a weir equipped with fibre reinforced polymer gates which is designed using a structured design methodology based on Systems Engineering,” Faculty of Civil Engineering, Delft University of Technology, Delft, 2013.

[16] J. Veraart, „Glasvezelversterkte kunststof schuiven als alternatief voor de schuiven in de Oosterscheldekering,” Faculty of Civil Engineering, Delft University of Technology, Delft, 1998.

[17] R. v. Straten, „Feasibility study on fibre reinforced polymer slides in the Eastern Scheldt storm surge barrier,” Faculty of Civil Engineering, Delft University of Technology, Delft, 2013.

[18] N. Bantia, ISIS Educational Module 2: An introduction to FRP Composites for Construction, Department of Civil Engineering, Queen's University, 2006.

[19] C. Kassapoglou, Powerpoint presentations AE4509: Advanced Design and Optimization of Composite Structures I, Delft: Faculty of Aerospace Engineering, Delft University of Technology, 2013.

[20] „Fibercore Europe,” 2014. [Online]. Available: www.fibercore.com.

[21] N. Bantia, „ISIS Educational Module 8: Durability of FRP composites for construction,” Department of Civil Engineering, Queen's University, 2006.

[22] CUR-commissie C124, „CUR 2003-6: Achtergrondrapport bij CUR-Aanbeveling 96,” Civieltechnisch Centrum Uitvoering Research en Regelgeving, 2003.

[23] Bouwen met Staal, Construeren B, 1996.

[24] Eurocode, „NEN-EN 1993-1-9,” 2012.

[25] CUR-commissie C124, „CUR 96: Vezelversterkte kunststoffen in civiele draagconstructies,” Civieltechnisch Centrum Uitvoering Research en Regelgeving, 2003.

[26] C. Qian, „Multi-Scale Modeling of Fatigue of Wind Turbine Rotor Balde Composites,” Delft University of Technology, Delft, 2010.

[27] R. Nijssen, „Fatigue Life Prediction and Strength Degradation of Wind Turbine Rotor Blade Composites,” Delft University of Technology, Delft, 2006.

[28] D. Duthinh, „Connections of Fiber-Reinforced Polymer (FRP) Structural Members: A Review of the State of the Art,” National Institute of Standards and Technology, Gaithersburg, 2000.

[29] J. Clarke, Eurocomp: Structural Design of Polymer Composites, Taylor & Francis e-library, 2005.

[30] beco, „LCA composietbrug," Rotterdam, 2009.

[31] beco, „Vergelijkende LCA studie bruggen," Rotterdam, 2013.

[32] J. Peeters, Interviewee, *Founder of Fibercore Europe.* [Interview]. 25 July 2014.

[33] P. Kortbeek, „Non-destructive testing techniques by Fokker," in *Round table conference: Monitoring of composite structures*, Amsterdam, 2014.

[34] Bouwdienst Rijkswaterstaat, „Referentiedocument kengetallen onderhoud," Rijkswaterstaat, 2004.

[35] FiberCore Europe, „Offerte InfraCore fietsbruggen," 2011.

[36] W. Molenaar, Lecture notes CT3330: Hydraulic Structures, locks, Delft: Faculty of Civil Engineering and Geosciences, Delft University of Technology, 2011.

[37] Bouwdienst Rijkswaterstaat, Ontwerp van schutsluizen deel 1 & 2, Rijkswaterstaat, 2000.

[38] Rijkswaterstaat, „Oosterscheldekering: onderhoud aan de schuiven," Rijkswaterstaat, [Online]. Available: http://www.rijkswaterstaat.nl/water/plannen_en_projecten/vaarwegen/oosterschelde/conserveren_van_de_schuiven/index.aspx. [Geopend 03 june 2014].

[39] Rijksdienst voor de Monumentenzorg, „Schimmels in hout: oorzaken en oplossingen," 2001. [Online]. Available: http://www.vhn.org/pdf/rdmz_21-schimmels.pdf. [Geopend 22 July 2014].

[40] H. B. J.W.G. van de Kuilen, „Mechanical properties of azobé (Lophira alata)," Springer-Verlag, 2004.

[41] Vraag en aanbod, „Richtprijzen 5 mie 2011," 05 may 2011. [Online]. Available: http://www.vraagenaanbod.nl/download/Richtprijzen%20Week%2018%20-%2005-05-11_29.pdf. [Geopend 10 june 2014].

[42] Cementbetom, „Eerste hsb-sluisdeuren ter wereld op hun plek," 2010. [Online]. Available: http://www.cementenbeton.nl/nieuws/187-nieuws-uit-de-pres/1633-eerste-hsb-sluisdeuren-ter-wereld-op-hun-plek. [Geopend 11 July 2014].

[43] A. Reitsema, „Ontwerp van een VVUSHB sluisdeur," TU Eindhoven, Eindhoven, 2012.

[44] Bouwdienst Rijkswaterstaat, „Factsheet ontwerp 3e kolk Beatrixsluis," [Online]. Available:

http://www.rijkswaterstaat.nl/images/Factsheet%20Ontwerp_tcm174-355263.pdf. [Geopend 23 mei 2014].

[45] O. d. Horde, „RINK 2011: Analyserapport werktuigbouw Beatrixsluis," Iv-Infra, Amsterdam, 2011.

[46] Rijkswaterstaat, „Trechteringsnotitie 3e kolk Prinses Beatrixsluis," Rijkswaterstaat, 2011.

[47] C. H. C. Bisschop, „VNK2: Overstromingsrisico Dijkring 44 Kromme Rijn," Ministerie van Infrastructuur en Milieu, 2011.

[48] Bouwdienst Rijkswaterstaat, „Richtlijnen Ontwerp Kunstwerken 1.2," Rijkswaterstaat, 2013.

[49] R. Nooij, „RINK 2011: Analyserapport Waterbouw - Beatrixsluis," Iv-Infra, Papendrecht, 2011.

[50] D. P. W.D. Pilkey, Stress Concentration factors, Hoboken, New Jersey: John Wiley & Sons, 2008.

[51] J. Peeters, Interviewee, *Founder of Fibercore Europe.* [Interview]. 16 may 2014.

[52] L. Tromp, Interviewee, *Advisor on fiber-reinforced polymers, Royal HaskoningDHV.* [Interview]. 29 September 2014.

[53] D. Ros, „Technische innovaties voor het verlagen van integrale kosten en milieubelasting," 2003.

[54] PIANC, „Report no. 42: Life Cycle Management of Port Structures Recommended Practice for Implementation," 2007.

[55] PIANC, „Report no. 26: Design of movable weirs and storm surge barriers," 2006.

[56] A. v. d. T. e. J. de Gijt, Lecture notes CIE-5313: Structures in Hydraulic Engineering 2, Delft: Delft University of Technology, faculty of Civil Engineer and Geosciences, 2003.

[57] Waterloopkundig laboratorium, „aanvaarrisico's voor sluisdeuren," Ministerie van Verkeer en Waterstaat, 1992.

[58] H.-H. Lee, Finite Element Simulations with ANSYS Workbench 14, 2012.

[59] I. Schipperen, Interviewee, *Senior researcher TNO.* [Interview]. 17 August 2014.

[60] PIANC, „PIANC report no.151: Design of lock gates for ship collision," PIANC Secretariat General, Bruxelles, 2014.

[61] T. J. P.A. Kolkman, Dynamisch gedrag van waterbouwkundige constructies deel A, B en C.

[62] L. Tong en J. White, Photo-oxidation of thermoplastics in bending and uniaxial compression, Elsevier, 1996.

[63] Sorathia, „Effects of fire," in *Gap analysis for Durability of FRP composites in Civil Infrastructure*, New York, American Society of Civil Engineers, 2001, pp. 100-121.

[64] V. Karbhari, Durability of composites for civil structural applications, Boca Raton, Florida: Woodhead Publishing Limited, 2007.

[65] X. Jiang, „Mechenical behaviour and durability of FRP-to-steel adhesively-bonded joints," Faculty of Civil Engineering, Delft University of Technology, Delft, 2013.

[66] C. Honselaar, vm 119: Vezelversterkte kunststoffen in constructieve toepassingen, Vereniging FME-CWM, 1999.

[67] M. Chlosta, „Feasibility study on fiber reinforced polymer cylindrical truss bridges for heavy traffic," Faculty of Civil Engineering, Delft University of Technology, Delft, 2012.

[68] H. W. C. Hartsuijker, Mechanics of Structures: Module: Introduction into Continuum Mechanics, Delft: Faculty of Civil Engineering and Geosciences, Delft University of Technology, 2007.

[69] C. Bakis, „Fiber-Reinforced Polymer Composites for Construction," in *Journal of Composites for Construction*, 2002.

[70] M. T. J. Weijers, Lecture notes CT5314: Flood Defences, Delft: Faculty of Civil Engineering and Geosciences, Delft University of Technology, 2009.

[71] T. Gernay, „Optimization and analysis of lock gates in the framework of the "Seine-Escaut-Est" waterway upgrading," *PIANC Magazine 'On Course' no 141,* pp. 11-26, October 2010.

[72] TATA Steel, „Steelconstruction info: corrosion of sturctural steel," [Online]. Available: http://www.steelconstruction.info/Corrosion_of_structural_steel. [Geopend 03 June 2014].

[73] Eurocode, „NEN-EN 1990," 2010.

[74] R. Groves, „Health monitoring of composite structures," in *Round table conference: Monitoring of composite structures*, Amsterdam, 2014.

[75] M. Pelt, „Ultrasonic verification," in *Round table conference: Monitoring of composite structures*, Amsterdam, 2014.

[76] T. Versteeg, „Monitoring of composite structures at Arkefly," in *Round table conference:*

Monitoring of composite structures, Amsterdam, 2014.

[77] NEN, „NEN-EN 1991-1-7+C1," 2011.

Appendices

Appendix A) CUR 96

The CUR 96 is the only available design guideline for FRP structures which is not originating from a manufacturing company. Although designers are not obliged to follow the CUR guideline, RWS does acknowledge it to be correct. A design which is in correspondence with the CUR 96 is assumed to be safe. This paragraph touches upon the safety factors and design philosophy of the document.

The general design philosophy is in accordance with the eurocodes:

$$S * \gamma_f \leq \frac{R}{\gamma_m * \gamma_c}$$

In which:

$S =$ Loads on the structure
$R =$ Strength of the structure
$\gamma_f =$ Load factor
$\gamma_m =$ Material factor
$\gamma_c =$ Environmental factor

According to the CUR 96, at least 15% of the fibers should be present in each direction when lamellas are applied. The idea behind this rule is that fatigue, creep and impact effects are not solely received by the resin. The most common fiber orientation are showed in the table below.

Table 45: Most common fiber orientations in laminates

angle	0º	90º	45º	-45º
One main direction	55%	15%	15%	15%
Two main directions	35%	35%	15%	15%
Quasi isotropic	25%	25%	25%	25%

Under these conditions, it is allowed to use one overall strain limit to predict failure of the material. CUR 96 recommends to use a charasteristic value of the ultimate strain of 1,2%. The charasteristic strength of the structure is found by multiplication of of the maximum strain by the E-modulus of the material, which is calculated by Halpin-Tsai (see Appendix B) and the classical laminate theory (see Appendix C). The design values are found by devision of the charasteristic strength by a material factor γ_m and and environmental factor γ_c.

The material factor γ_m is divided into two different components:

$$\gamma_m = \gamma_{m1} * \gamma_{m2} \geq 1{,}5$$

γ_{m1} represents the partial safety factor related to the uncertainties in the material properties while γ_{m2} represents the partial safety factor related to the manufacturing process.

CUR 96 indicates the following values for γ_{m1} and γ_{m2}:

$$\gamma_{m1} = 1{,}35$$

Table 46: Recommended values for ym2

	Post-cured	Not post-cured

Spray-up	1,6	1,9
Hand laminating	1,4	1,7
Vacuum- or pressure injection	1,2	1,4
Filament winding	1,1	1,3
Vacuum-assisted resin injection	1,1	1,3
Pultrusion	1,1	1,3

The environmental factor γ_c is divided into four different terms:

$$\gamma_c = \gamma_{ct} * \gamma_{cv} * \gamma_{ck} * \gamma_{cf}$$

$\gamma_{ct} =$ Temperature factor
$\gamma_{cv} =$ Factor related to moisture absorption
$\gamma_{ck} =$ Creep factor
$\gamma_{cf} =$ Fatigue factor

Table 47 shows when to apply which conversion factor.

Table 47: situations in which conversionfactors γc should be applied

	Ultimate limit state			Servicability limit state		
	Strength	Stiffness	Fatigue	Deformation	Vibrations	Cracking
γ_{ct}	X	X	X	X	X	X
γ_{cv}	X	X	X	X	X	X
γ_{ck}	X	X	-	X	-	X
γ_{cf}	-	X	-	X	X	X

CUR recommends the following value for temperature effects (regardless the range of temperatures to which the actual structure is exposed):

$$\gamma_{ct} = 1{,}1$$

Table 48 shows which partial factor for moisture effects should be applied.

Table 48: values for γcv

Environment	γ_{cv}
Dry	1,0
Wet/Dry	1,1
Wet	1,3

The reduction factor for stiffness due to fatigue is stated in CUR 96 as follows:

$$\gamma_{cf} = 1{,}1$$

$$\gamma_{ck} = (t * 8760)^n$$

$t =$ Duration of the load in years

The recommended value for n depends on the type of reinforcement:

Table 49: Values for n for different fabrics

Type	n
UD-lamella	0,01
Woven	0,04
Mat	0,1

Figure 155: graphical representation of values for γc over the duration of long term loading

Fatigue failure can be predicted by comparing the amplitude of the stress during a load cycle by the design value of the strength. The following formula can be used:

if $\sigma_{mean} = 0 \rightarrow N_f = \left(\frac{\sigma_{amp}}{\sigma_{t,Rd}}\right)^k$

if $\sigma_{mean} < 0 \rightarrow N_f = \left(\frac{\sigma_{amp}}{\sigma_{t,Rd} * (1 - \frac{\sigma_{mean}}{\sigma_{c,Rd}})}\right)^k$

If $\sigma_{mean} > 0 \rightarrow N_f = \left(\frac{\sigma_{amp}}{\sigma_{t,Rd} * (1 - \frac{\sigma_{mean}}{\sigma_{t,Rd}})}\right)^k$

The k-value depends on the selection of resin material:

Table 50: k factors for different compositions

Load type	Material	k
Constant amplitude	Glass/epoxy	10
	Glass/polyester	9

For different amplitudes of load cases, the unity check for fatigue reads as follows:

$$D = \sum_{i=1}^{n} \frac{n_i}{N_i} \leq 1$$

$$n_i = number\ of\ load\ cycles$$

$$N_i = maximum\ number\ of\ load\ cycles\ before\ failure$$

The structure collapses if $D = 1$.

Appendix B) Calculation of lamella properties

The semi-empirical formulae of Halpin -Tsai can be used to calculate the material properties for the combination of fibers and resin given the fact that the material properties of the individual contents are known. The formulae are valid for fiber volumes between 40%-70%. A parallel- and serial schematization of the lamella's are the base of the model, where several coefficients are introduced to account for the difference between the model and the real geometries.

The following formulae can be used [22].

$$E_1 = E_R + (E_F - E_R) * V_f$$

$E_1 =$ Laminate stiffness in the main direction [N/mm^2]
$E_R =$ Young's modulus of the resin [N/mm^2]
$E_F =$ Young's modulus of the fibers [N/mm^2]
$V_f =$ Fiber fraction volume [-]

$$E_2 = E_R \frac{1 + \xi * \eta * V_f}{1 - \eta * V_f}$$

$E_2 =$ Laminate stiffness perpendicular to the main direction [N/mm^2]
$\xi =$ Factor related to the shape of the fibers, packing geometry and load conditions [-]

$$\eta = \left(\frac{E_F}{E_R} - 1\right)\left(\frac{E_F}{E_R} + \xi\right)$$

$$G_{12} = G_R \frac{1 + \xi * \eta * V_f}{1 - \eta * V_f}$$

$G_{12} =$ Transverse shear modulus [N/mm^2]
$G_R =$ Shear modulus of the resin [N/mm^2]

$$\eta = \left(\frac{G_F}{G_R} - 1\right)\left(\frac{G_F}{G_R} + \xi\right)$$

$$v_{12} = v_R - (v_R - v_f)V_f$$

$v_{12} =$ Poisson coefficient of the laminate [-]
$v_R =$ Poisson coefficient of the resin [-]
$v_f =$ Poisson coefficient of the fibers [-]

The following values for the different parameters are indicative for fiber reinforced polymers consisting of a combination of E-glass and polyester:

$$v_R = 0{,}35$$

$$v_f = 0{,}22$$

$$G_R = 1{,}3\ GPa$$

$$G_F = 30GPa$$

$$E_R = 3{,}4\ GPa$$

$$E_f = 72\,GPa$$

$$\xi = 1$$

Specific properties of UD-lamellas, woven fabrics and mats are presented in the Figure 156, Figure 157 and Figure 158.

V_f	E_1 [GPa]	E_2 [GPa]	G_{12} [GPa]	ν_{12}
40%	30,8	8,9	2,8	0,30
45%	34,3	10,0	3,1	0,29
50%	37,7	11,3	3,5	0,29
55%	41,1	12,8	3,9	0,28
60%	44,6	14,6	4,5	0,27
65%	48,0	16,7	5,1	0,27
70%	51,4	19,3	6,0	0,26

Figure 156: Material properties for UD-plies with different fiber volume fractions [22]

V_f	E_1 [GPa]	E_2 [GPa]	G_{12} [GPa]	ν_{12}
25%	13,4	13,4	2,1	0,21
30%	15,5	15,5	2,3	0,20
35%	17,6	17,6	2,5	0,20
40%	19,8	19,8	2,8	0,19
45%	22,1	22,1	3,1	0,19
50%	24,5	24,5	3,5	0,19
55%	27,0	27,0	3,9	0,18

Figure 157: Material properties for balanced woven fabrics with different fiber fraction volumes [22]

V_f	E_1 [GPa]	E_2 [GPa]	G_{12} [GPa]	ν_{12}
10%	6,2	6,2	2,3	0,33
12,5%	6,9	6,9	2,6	0,33
15%	7,6	7,6	2,9	0,33
17,5%	8,3	8,3	3,1	0,33
20%	9,1	9,1	3,4	0,33
25%	10,6	10,6	4,0	0,33
30%	12,2	12,2	4,6	0,33

Figure 158: Material properties for mats with different fiber fraction volumes [22]

Appendix C) Classical laminate theory

This appendix explains the classical laminate theory and is based on CUR 2003-6: achtergrondrapport bij CUR 96.

The calculation of the laminate properties usually consists of 3 steps. Firstly the properties E_1, E_2, G_{12} and v_{12} of all the lamellas need to be obtained by the formula of Halpin Tsai (see Appendix Appendix B). Hereafter, these properties need to multiplied by a factor to acount for the direction of the lamella compared to the main axis. Finally, the contributions of the individual lamellas are integrated over the height of the laminate to find the stiffness matrix which relates the forces and bending moments to the strains and curvatures of the laminate.

The classical laminate theory will be derived in this appendix. The theory is only valid under the following conditions:

- Plates are thin
- The thickness of the plates is constant
- Straight sections remain straight

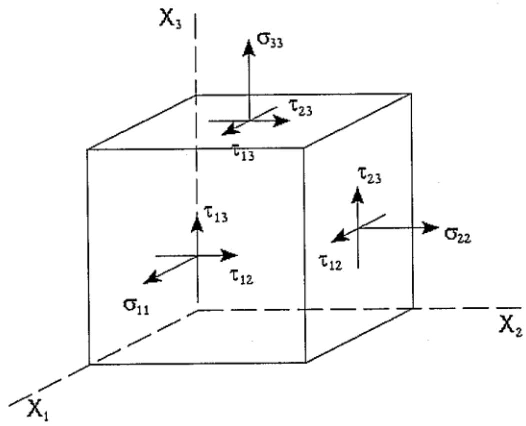

Figure 159: Stresses in 3D [22]

Under these conditions, the relations between forces and strains in the material are described by Hooke's law:

$$\begin{Bmatrix} \sigma_1 \\ \sigma_2 \\ \sigma_3 \\ \tau_{23} \\ \tau_{31} \\ \tau_{12} \end{Bmatrix} = \begin{bmatrix} Q_{11} & Q_{12} & Q_{13} & 0 & 0 & 0 \\ Q_{21} & Q_{22} & Q_{23} & 0 & 0 & 0 \\ Q_{31} & Q_{32} & Q_{33} & 0 & 0 & 0 \\ 0 & 0 & 0 & Q_{44} & 0 & 0 \\ 0 & 0 & 0 & 0 & Q_{55} & 0 \\ 0 & 0 & 0 & 0 & 0 & Q_{66} \end{bmatrix} \begin{Bmatrix} \varepsilon_1 \\ \varepsilon_2 \\ \varepsilon_3 \\ \gamma_{23} \\ \gamma_{31} \\ \gamma_{12} \end{Bmatrix}$$

The following relations between matrices and engineering constants hold:

$$Q_{11} = \frac{E_1}{1 - v_{12} * v_{21}}$$

$$Q_{22} = \frac{E_2}{1 - v_{12} * v_{21}}$$

$$Q_{12} = \frac{v_{21} * E_1}{1 - v_{12} * v_{21}}$$

$$Q_{66} = G_{12}$$

$$S_{11} = \frac{1}{E_1}$$

$$S_{22} = \frac{1}{E_2}$$

$$S_{12} = -\frac{v_{12}}{E_2}$$

$$S_{66} = \frac{1}{G_{12}}$$

$$\frac{v_{12}}{v_{21}} = \frac{E_1}{E_2}$$

Because the thickness of the lamella's is assumed to be small, the forces perpendicular to the plain of the cross-section can be neglected. This results in a simplification of the model from 3D to 2D.

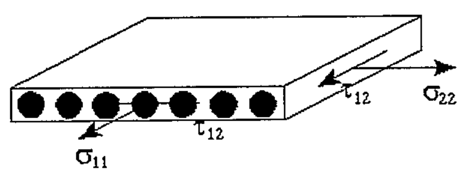

Figure 160: Simplification to 2D

The result is the following simplified matrix for the 2D-schematization:

$$\begin{Bmatrix} \sigma_1 \\ \sigma_2 \\ \tau_{12} \end{Bmatrix} = \begin{bmatrix} Q_{11} & Q_{12} & 0 \\ Q_{12} & Q_{22} & 0 \\ 0 & 0 & Q_{66} \end{bmatrix} \begin{Bmatrix} \varepsilon_1 \\ \varepsilon_2 \\ \gamma_{12} \end{Bmatrix}$$

$$\begin{Bmatrix} \varepsilon_1 \\ \varepsilon_2 \\ \gamma_{12} \end{Bmatrix} = \begin{bmatrix} S_{11} & S_{12} & 0 \\ S_{12} & S_{22} & 0 \\ 0 & 0 & S_{66} \end{bmatrix} \begin{Bmatrix} \sigma_1 \\ \sigma_2 \\ \tau_{12} \end{Bmatrix}$$

$[Q] =$ Stiffness matrix

$[S] =$ Compliance matrix

The subscript 1 indicates the direction of the main axis while subscript 2 indicates the direction perpendicular to the main axis. To account for the angle between fibers and main axis, the transformation matrix [T] is introduced. The following relations now hold:

$$\begin{Bmatrix} \sigma_1 \\ \sigma_2 \\ \tau_{12} \end{Bmatrix} = [T] \begin{Bmatrix} \sigma_x \\ \sigma_y \\ \tau_{xy} \end{Bmatrix}$$

$$\begin{Bmatrix} \varepsilon_1 \\ \varepsilon_2 \\ 1/2\gamma_{12} \end{Bmatrix} = [T] \begin{Bmatrix} \varepsilon_x \\ \varepsilon_y \\ 1/2\gamma_{xy} \end{Bmatrix}$$

$$[T] = \begin{bmatrix} \cos^2\theta & \sin^2\theta & 2\sin\theta\cos\theta \\ \sin^2\theta & \cos^2\theta & -2\sin\theta\cos\theta \\ -\sin\theta\cos\theta & \sin\theta\cos\theta & \cos^2\theta - \sin^2\theta \end{bmatrix}$$

$$[T]^{-1} = \begin{bmatrix} \cos^2\theta & \sin^2\theta & -2\sin\theta\cos\theta \\ \sin^2\theta & \cos^2\theta & 2\sin\theta\cos\theta \\ \sin\theta\cos\theta & -\sin\theta\cos\theta & \cos^2\theta - \sin^2\theta \end{bmatrix}$$

Or in short notation:

$$[T] = \begin{bmatrix} c^2 & s^2 & 2sc \\ s^2 & c^2 & -2sc \\ -sc & sc & c^2 - s^2 \end{bmatrix}$$

$$[T]^{-1} = \begin{bmatrix} c^2 & s^2 & -2sc \\ s^2 & c^2 & 2sc \\ sc & -sc & c^2 - s^2 \end{bmatrix}$$

Where:

$$s = \sin\theta$$

$$c = \cos\theta$$

$\theta =$ Angle between main direction of lamella and main axis.

From linear algebra follows:

$$\begin{Bmatrix} \sigma_x \\ \sigma_y \\ \tau_{xy} \end{Bmatrix} = [T]^{-1}[Q][T] \begin{Bmatrix} \varepsilon_x \\ \varepsilon_y \\ 1/2\,\gamma_{xy} \end{Bmatrix}$$

Or in different notation:

$$\begin{Bmatrix} \sigma_x \\ \sigma_y \\ \tau_{xy} \end{Bmatrix} = \begin{bmatrix} \overline{Q_{11}} & \overline{Q_{12}} & \overline{Q_{16}} \\ \overline{Q_{12}} & \overline{Q_{22}} & \overline{Q_{26}} \\ \overline{Q_{16}} & \overline{Q_{26}} & \overline{Q_{66}} \end{bmatrix} \begin{Bmatrix} \varepsilon_x \\ \varepsilon_y \\ \gamma_{xy} \end{Bmatrix}$$

Where:

$\overline{Q_{ij}} = [T]^{-1}\left[Q_{ij}\right][T]$

Under the assumption that straight section remain straight, the following relations hold:

$$\varepsilon_x = \varepsilon_x^0 + z * k_x$$

$$\varepsilon_y = \varepsilon_y^0 + z * k_y$$

$$\gamma_{xy} = \gamma_{xy}^0 + z * k_{xy}$$

Where:
$\varepsilon_i =$ Strain in the i-direction
$k_i =$ Curvature in the i-direction
$\gamma_i =$ Shear in the i-direction

The superscript 0 represents the position of the neutral axis. After rearrangement of the formulae the following matrix is found:

$$\begin{Bmatrix} \sigma_x \\ \sigma_y \\ \tau_{xy} \end{Bmatrix} = [\bar{Q}][\varepsilon_0] + z * [\bar{Q}][k]$$

Where:

$$[\varepsilon_0] = \begin{Bmatrix} \varepsilon_x^0 \\ \varepsilon_y^0 \\ \gamma_{xy}^0 \end{Bmatrix}$$

$$[k] = \begin{Bmatrix} k_x \\ k_y \\ k_{xy} \end{Bmatrix}$$

Under the assumption that the centre of gravity of the laminate is located at z=h/2 the following relations hold for the relations between stresses, forces and moments:

$$N_x = \int_{-h/2}^{h/2} \sigma_x * dz$$

$$N_y = \int_{-h/2}^{h/2} \sigma_y * dz$$

$$N_{xy} = \int_{-h/2}^{h/2} \tau_{xy} * dz$$

$$M_x = \int_{-h/2}^{h/2} \sigma_x * zdz$$

$$M_y = \int_{-h/2}^{h/2} \sigma_y * z dz$$

$$M_{xy} = \int_{-h/2}^{h/2} \tau_{xy} * z dz$$

The next step is to discretize the cross-section into an amount of n lamella's, ranking from k=1 to k=n.

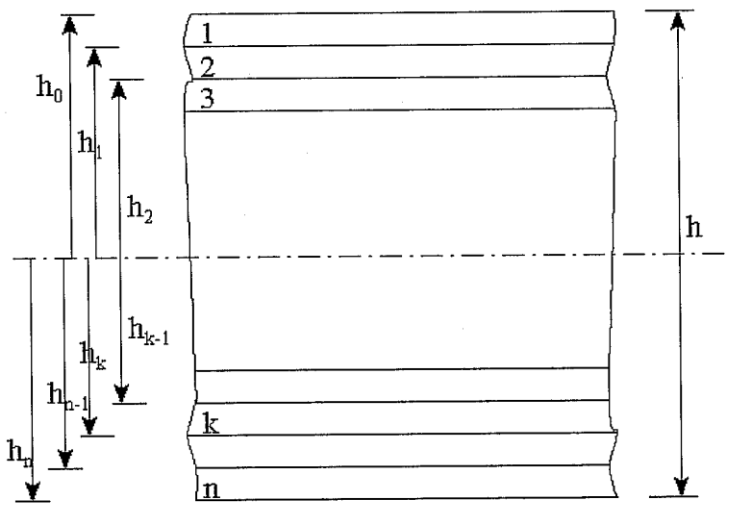

Figure 161: Discretization of the laminate into n lamellas [22]

The external forces on the cross section are balanced by internal stresses. The indivual contributions of the stresses in the plies are integrated over the height and must be in balance with the external forces:

$$\begin{Bmatrix} N_x \\ N_y \\ N_{xy} \end{Bmatrix} = \sum_{k=1}^{n} \int_{h_{k-1}}^{h_k} \begin{Bmatrix} \sigma_x \\ \sigma_y \\ \tau_{xy} \end{Bmatrix}_k dz$$

The external bending moments are in balance with the product of the stress in a ply and the distance to the neutral axis integrated over the height:

$$\begin{Bmatrix} M_x \\ M_y \\ M_{xy} \end{Bmatrix} = \sum_{k=1}^{n} \int_{h_{k-1}}^{h_k} \begin{Bmatrix} \sigma_x \\ \sigma_y \\ \tau_{xy} \end{Bmatrix}_k zdz$$

Substitution leads to the following system of equations:

$$\begin{Bmatrix} N_x \\ N_y \\ N_{xy} \end{Bmatrix} = \sum_{k=1}^{n} \left\{ \int_{h_{k-1}}^{h_k} \begin{bmatrix} \overline{Q_{11}} & \overline{Q_{12}} & \overline{Q_{16}} \\ \overline{Q_{12}} & \overline{Q_{22}} & \overline{Q_{26}} \\ \overline{Q_{16}} & \overline{Q_{26}} & \overline{Q_{66}} \end{bmatrix}_k \begin{Bmatrix} \varepsilon_x^0 \\ \varepsilon_y^0 \\ \gamma_{xy}^0 \end{Bmatrix} dz + \int_{h_{k-1}}^{h_k} \begin{bmatrix} \overline{Q_{11}} & \overline{Q_{12}} & \overline{Q_{16}} \\ \overline{Q_{12}} & \overline{Q_{22}} & \overline{Q_{26}} \\ \overline{Q_{16}} & \overline{Q_{26}} & \overline{Q_{66}} \end{bmatrix}_k \begin{Bmatrix} k_x \\ k_y \\ k_{xy} \end{Bmatrix} zdz \right\}$$

$$\begin{Bmatrix} M_x \\ M_y \\ M_{xy} \end{Bmatrix} = \sum_{k=1}^{n} \left\{ \int_{h_{k-1}}^{h_k} \begin{bmatrix} \overline{Q_{11}} & \overline{Q_{12}} & \overline{Q_{16}} \\ \overline{Q_{12}} & \overline{Q_{22}} & \overline{Q_{26}} \\ \overline{Q_{16}} & \overline{Q_{26}} & \overline{Q_{66}} \end{bmatrix}_k \begin{Bmatrix} \varepsilon_x^0 \\ \varepsilon_y^0 \\ \gamma_{xy}^0 \end{Bmatrix} zdz + \int_{h_{k-1}}^{h_k} \begin{bmatrix} \overline{Q_{11}} & \overline{Q_{12}} & \overline{Q_{16}} \\ \overline{Q_{12}} & \overline{Q_{22}} & \overline{Q_{26}} \\ \overline{Q_{16}} & \overline{Q_{26}} & \overline{Q_{66}} \end{bmatrix}_k \begin{Bmatrix} k_x \\ k_y \\ k_{xy} \end{Bmatrix} z^2 dz \right\}$$

The following assumptions are made in order to simplify the system of equations above:

- The zero-strains are assumed to be independent of the z-coordinate
- The curvatures are assumed to be independent of the z-coordinate (sections remain straight)

The result is that all the terms except for the z are just constants when the integrals are computed. The following result is now obtained:

$$\begin{Bmatrix} N_x \\ N_y \\ N_{xy} \end{Bmatrix} = \begin{bmatrix} A_{11} & A_{12} & A_{16} \\ A_{12} & A_{22} & A_{26} \\ A_{16} & A_{26} & A_{66} \end{bmatrix} \begin{Bmatrix} \varepsilon_x^0 \\ \varepsilon_y^0 \\ \gamma_{xy}^0 \end{Bmatrix} + \begin{bmatrix} B_{11} & B_{12} & B_{16} \\ B_{12} & B_{22} & B_{26} \\ B_{16} & B_{26} & B_{66} \end{bmatrix} \begin{Bmatrix} k_x \\ k_y \\ k_{xy} \end{Bmatrix}$$

$$\begin{Bmatrix} M_x \\ M_y \\ M_{xy} \end{Bmatrix} = \begin{bmatrix} B_{11} & B_{12} & B_{16} \\ B_{12} & B_{22} & B_{26} \\ B_{16} & B_{26} & B_{66} \end{bmatrix} \begin{Bmatrix} \varepsilon_x^0 \\ \varepsilon_y^0 \\ \gamma_{xy}^0 \end{Bmatrix} + \begin{bmatrix} D_{11} & D_{12} & D_{16} \\ D_{12} & D_{22} & D_{26} \\ D_{16} & D_{26} & D_{66} \end{bmatrix} \begin{Bmatrix} k_x \\ k_y \\ k_{xy} \end{Bmatrix}$$

With:

$$A_{ij} = \sum_{k=1}^{n} \left(\overline{Q_{ij}}\right)_k (h_k - h_{k-1})$$

$$B_{ij} = \frac{1}{2} \sum_{k=1}^{n} \left(\overline{Q_{ij}}\right)_k (h_k^2 - h_{k-1}^2)$$

$$D_{ij} = \frac{1}{3} \sum_{k=1}^{n} \left(\overline{Q_{ij}}\right)_k (h_k^3 - h_{k-1}^3)$$

Or in short notation:

$$\begin{Bmatrix} N \\ M \end{Bmatrix} = \begin{bmatrix} A & B \\ B & D \end{bmatrix} \begin{Bmatrix} \varepsilon^0 \\ k \end{Bmatrix}$$

In case of a symmetric stacking of the lamellas, there is no coupling between normal forces and moments which means that the matrix [B] equals zero. This results in much easier calculations.

Software packages like Kolibri or LAP can save a lot of calculations. The properties of the laminates are calculated when the properties per layer are known.

Appendix D) Conversion from Kolibri to SCIA Engineer

Kolibri is a freely available computer program which calculates the laminate- and plate properties as soon as the properties of the different plies are known. First of all the ply properties are required as input. The following properties are required:

- E_1
- E_2
- E_3
- G_{12}
- G_{23}
- G_{31}
- v_{12}
- v_{23}
- v_{31}

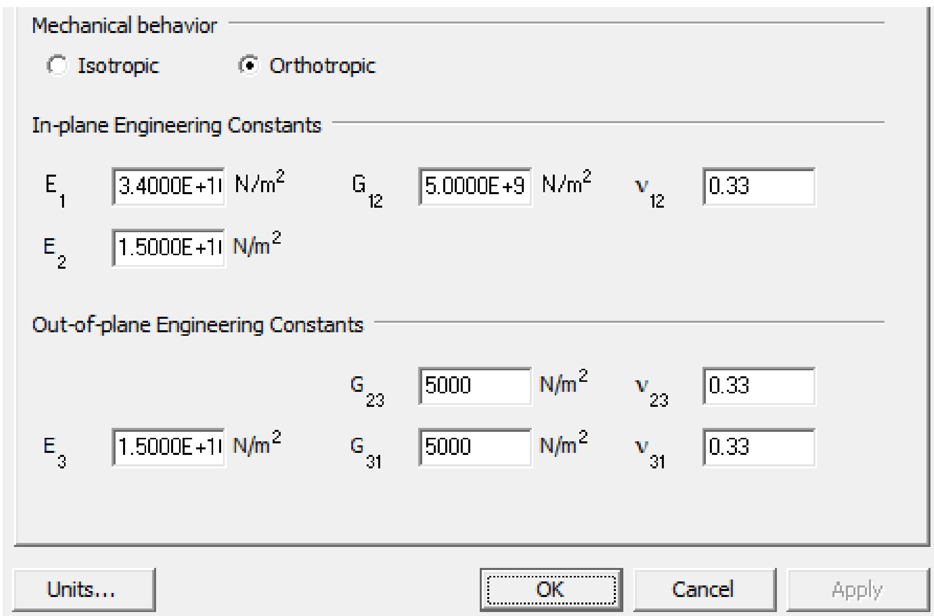

Figure 162: Input of ply properties in Kolibri

These properties are calculated with help of the empirical relations found by Halpin & Tsai. Some examples of material properties can be found in [25]. If it is decided to apply a sandwich structure, also the core properties are needed as input for the program. The same input parameters are required as for a ply. Hereafter, the stacking sequence, thicknesses and orientation of the individual plies need to be specified in order to obtain the laminate properties.

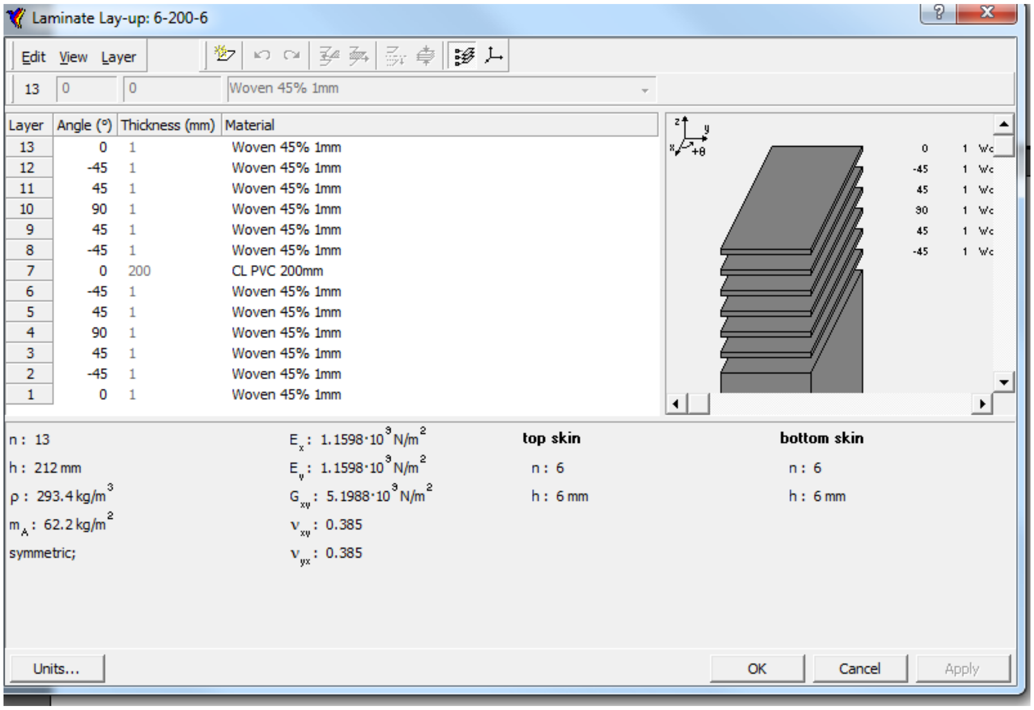

Figure 163: Input of laminate lay-up in Kolibri

The program converts the input with help of the classical laminate theory to the stiffness matrices [A], [B] & [D] for the entire laminates. The result is a 6x6 matrix which is shortly notated as $\begin{bmatrix} A & B \\ B & D \end{bmatrix}$.

In case of a symmetrical stacking, the [B] equals zero.

Laminate Stiffness Matrix

$$[ABD] = \begin{bmatrix} 2.8867\cdot10^{8} & 1.1114\cdot10^{8} & 0 & 0 & 0 & 0 \\ 1.1114\cdot10^{8} & 2.8867\cdot10^{8} & 0 & 0 & 0 & 0 \\ 0 & 0 & 1.1021\cdot10^{9} & 0 & 0 & 0 \\ 0 & 0 & 0 & 2.9202\cdot10^{6} & 1.1271\cdot10^{6} & -59.877 \\ 0 & 0 & 0 & 1.1271\cdot10^{6} & 2.8953\cdot10^{6} & -59.877 \\ 0 & 0 & 0 & -59.877 & -59.877 & 4.4130\cdot10^{6} \end{bmatrix} \text{N, m}$$

Figure 164: Example of a stiffness matrix as output of the Kolibri calculations

These matrixes are required as input for the SCIA calculation. SCIA however uses another notation. Instead of the [ABD] matrix as input, SCIA requires the following parameters to account for the orthotropy of the component:

- D_{11}
- D_{22}
- D_{33}
- D_{44}
- D_{55}
- D_{12}
- d_{11}

- d_{22}
- d_{12}
- d_{33}

A symmetric lay-up is assumed in SCIA Engineer, which means that [B] is alway equal to zero in the stiffness matrix. Table 51 shows the difference in notations for the stiffness matrix between Kolibri and SCIA Engineer. Please be aware of the difference in unities between SCIA Engineer and Kolibri ([MN,m] versus[N,m]).

Table 51: translation from Kolibri output tot SCIA input

SCIA Engineer [MN,m]	Kolibri [N,m]
$\boldsymbol{D_{11}}$	D_{11}
$\boldsymbol{D_{22}}$	D_{22}
$\boldsymbol{D_{12}}$	D_{12}
$\boldsymbol{D_{33}}$	D_{33}
$\boldsymbol{D_{44}}$	D_{13}
$\boldsymbol{D_{55}}$	D_{23}
$\boldsymbol{d_{11}}$	A_{11}
$\boldsymbol{d_{22}}$	A_{22}
$\boldsymbol{d_{12}}$	A_{12}
$\boldsymbol{d_{33}}$	A_{33}

Appendix E) Structural design of the gate alternatives

This appendix covers the structural calculations on which the design of the variants is based. The considered variants are the warren truss gate, the arched gate, the lens-shaped gate and the stiffened plate.

a) Variant 2: Warren truss gate

The webs of the warren truss gate are designed on buckling loads while the water retaining plates are designed on a combination of normal forces and bending moments.

The governing compressive force in the web can be found by considering the free body diagram at the support. Let α be the angle between the water retaining plate and the web. The normal force in the web is calculated by the following formula:

$$N = \frac{F_{v;Ed}}{\sin \alpha}$$

$N =$ Normal force in the governing web
$F_v =$ Support reaction
$\alpha =$ Angle between water retaining plate and web

The support reaction is calculated with the following formula:

$$F_{v;Ed} = \frac{q_{Ed} * l}{2}$$

$q_{Ed} =$ Design value of the distributed load due to the water level difference
$l =$ Length of the gate (25 m)

The buckling load is calculated as follows, where the connections between web and water retaining plates are assumed to be hinged:

$$N_{buckling} = \frac{\pi^2 EI}{l_k^2}$$

$E =$ long term Young's modulus of the material
$I =$ Moment of inertia
$l_k =$ Length of the governing web

The webs should also be tested for maximum stress. This is calculated by the following formula:

$$\sigma_{max} = \frac{N}{A}$$

$A =$ Area of the skin plates of the web

The web fulfills the requirements if the normal force does not exceed the buckling load and if the maximum stress does not exceed 70 N/mm^2.

The water retaining plates are exposed to a combination of a global bending moment and a local bending moment. The global bending moment is resisted by full cooperation between the two plates while the local bending moment between in the plate near the connection to the web is resisted by a single plate. For the local bending moment, the plate is schematized as a (statically indetermined) beam on multiple supports (which are the connections of the webs). The following values are obtained for the moments in the plates:

$$M_g = \frac{1}{8} * q_{Ed} * l^2$$

$M_g =$ Design value of the global bending moment
$l =$ Length of the gate

$$M_l = \frac{1}{10} q_{Ed} * d_{webs}^2$$

$M_l =$ Design value of the local bending moment at the connection with a web
d_{webs} =Distance between the webs

$$\sigma_{max} = \frac{M_g * z_g}{I_g} + \frac{M_l * z_l}{I_l}$$

$z_g =$ Distance between neutral axis en outer fiber
$l_g =$ Global moment of intertia
$z_l =$ Distance between center of gravity of a single plate and outer fiber
$I_l =$ Moment of inertia of a single plate

The water retaining plates fulfill the requirements when the stresses do not exceed 70 N/mm^2.

b) Variant 3: Arched gate

Due to the curved shape of the gate, analytical results were hard to obtain, especially where the arche was combined with webs. Finite element program SCIA Engineer has been used to obtain the forces in the structure. The normal forces and bending moments are visualised in Figure 165 and Figure 166.

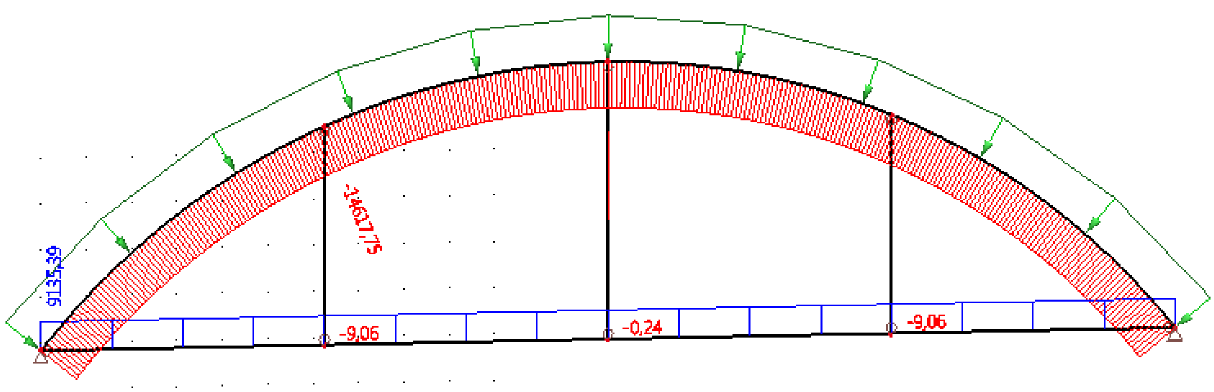

Figure 165: Normal forces for the curved gate with 3 webs

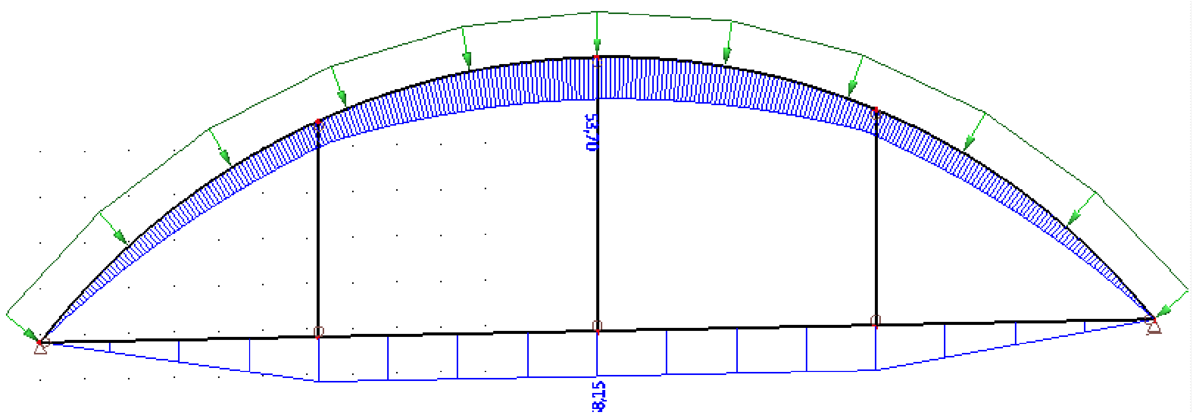

Figure 166: Bending moments for the curved gate with 3 webs

Next to the maximum head difference, also the results of a positive head difference (where the straight plate is loaded in compression) and an estimation of the effects of a ship impact are investigated.

To account for ship impact, a 2000 ton vessel sailing with a velocity of 1 m/s is considered as representative. The effect of added mass of the water is neglected. The impact is modelled as a point force positioned at the middle of the straight plate. An energy balance results in a maximum force exerted on the gate. This force is subsequently translated into a bending moment and maximum compression of the material.

$$E_{kin} = \frac{1}{2} * m_{ship} * v_{ship}^2$$
$$E_{spring} = \frac{1}{2} * k * u_{max}^2$$
$$u_{max} = \frac{1}{48} \frac{F * l^3}{EI}$$

$$k_1 = \frac{F}{u_{max}} = \frac{48EI}{l^3}$$

$$E_{kin} = E_{spring} \rightarrow u_{max} = v_{ship} \sqrt{m_{ship}/k}$$

$$F_{max} = k * u_{max} = v_{ship} \sqrt{m_{ship} * k} = v_{ship} \sqrt{m_{ship} * \frac{48EI}{l^3}}$$

$$M_{max} = \frac{1}{4} * F_{max} * l$$
$$\sigma_{max} = \frac{M_{max} * z}{I}$$

The full results of the simulations are summirized in Table 52.

The different members are numbered as follows:
1 = Arched water retaining plate
2 = Straight water retaining plate

3 = Web in the center
4 = Remaining webs

Table 52: Results of variation in number of webs

Variant		No web	Single web	Tripple web
	Static scheme		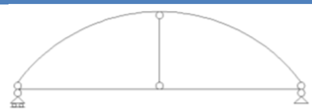	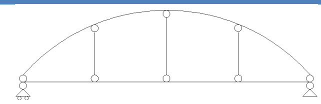
Load case				
Water	N1	9146 kN	9136 kN	9135 kN
	M1	0	76 kNm	58 kNm
	N2	-14622 kN	-14612 kN	-14612 kN
	M2	50 kNm	46 kNm	51 kNm
	N3	0	-12 kN	0
	N4	0	0	-9 kN
Ship collision	N1	3880 kN	3735 kN	3881 kN
	M1	0	1171 kNm	3849 kNm
	N2	-4613 kN	-4403 kN	-4827 kN
	M2	7970 kNm	7671 kNm	4114 kNm
	N3	0	-187 kN	-1979 kN
	N4	0	0	1364 kN

If also a negative head difference is considered, it appears that application of three webs results in the lowest mass for this concept.

c) Variant 4: Lens-shaped gate

Also for this variant, force distributions are found with help of SCIA Engineer. A study is done to the variation of the drape of the lens and the number of webs in order to minize the mass of the gate.

A larger drape results in smaller forces in the water retaining plates due to a larger lever arm. The length of the webs will however also increase which results in more material required in the webs because of the decrease of buckling loads. An optimum is found for a drape of 4 meters (see Table 53).

Table 53: Study to the effects of variation of drape

	4m	6m	8m	12m
N1	17881 kN	12024 kN	9082 kN	5937 kN
M1	-1367//1960 kNm	-1429//1909 kNm	-1484//1886 kNm	-1950//2048 kNm
N2	-19139 kN	-13933 kN	-11655 kN	-10140 kN
M2	-1771//1462 kNm	-1824//1472 kNm	-1838//1508 kNm	-2024//1962 kNm
N3	-2556 kN	-2434 kN	-2268 kN	-1347 kN
N4	-3237 kN	-3220 kN	-3188 kN	-3116 kN

Hereafter, the optimal amount of webs is investigated. The forces, which are found with help of SCIA, are translated to required cross-sections. Buckling was governing for the webs while the water retaining plates were dimensioned on strength. An impression of the force lines is presented in Figure 167 and Figure 168.

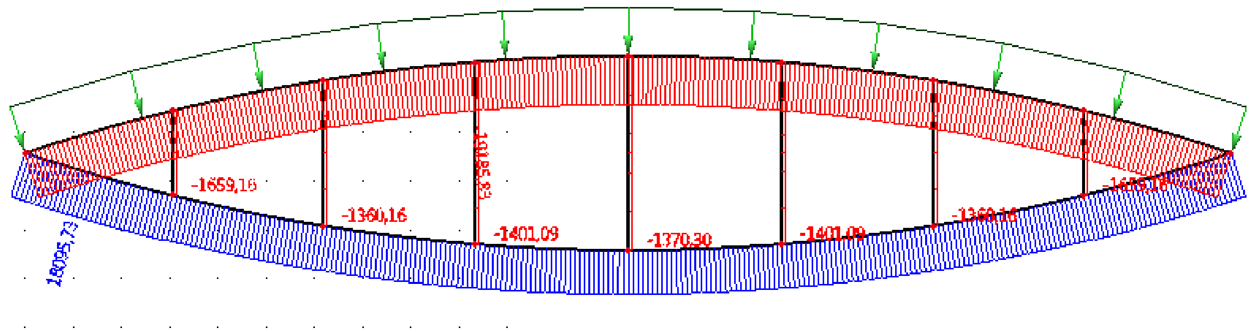

Figure 167: Normal forces for the lens-shaped gate with 7 webs

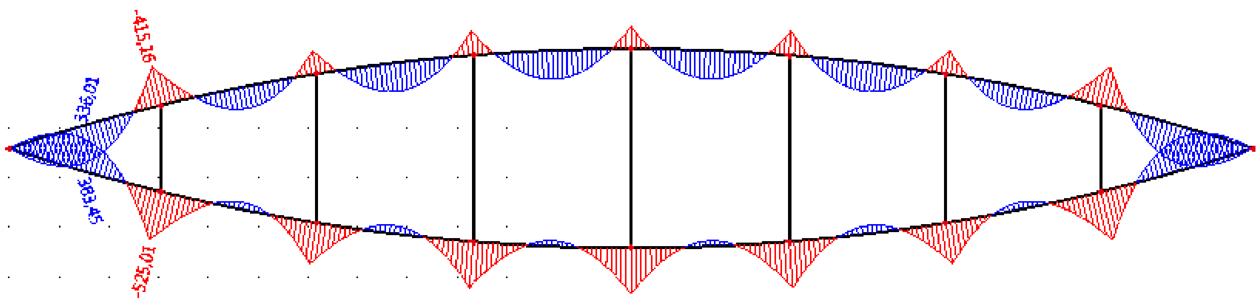

Figure 168: Moment line for the lens shaped gate with 7 webs

The full results of the analysis are summarized in Table 54 and Table 55.

Table 54: Study to the effects of variation of number of webs

Variant		No web	Single web	Tripple web
			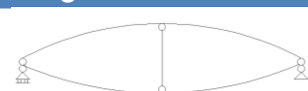	
Load case				
water	N1	9146 kN	9136 kN	9135 kN
	M1	0	76 kNm	58 kNm
	N2	-14622 kN	-14612 kN	-14612 kN
	M2	50 kNm	46 kNm	51 kNm
	N3	0	-12 kN	0
	N4	0	0	-9 kN
Ship collision	N1	3880 kN	3735 kN	3881 kN
	M1	0	1171 kNm	3849 kNm
	N2	-4613 kN	-4403 kN	-4827 kN
	M2	7970 kNm	7671 kNm	4114 kNm

N3	0	-187 kN	-1979 kN
N4	0	0	1364 kN

Table 55: Study to the effects of variation of number of webs

Component	Number of webs	3	4	5	6	7	8	9	10	11	12	13
Arch												
	Larch (m)	25,4	25,4	25,4	25,4	25,4	25,4	25,4	25,4	25,4	25,4	25,4
	Tskin (mm)	37	30	26	24	22	21	20	19	18	18	18
	Tcore (mm)	70	60	52	48	44	42	40	38	36	36	36
	Vfrp (m^3)	48,1	39,0	33,8	31,2	28,6	27,3	26,0	24,7	23,4	23,4	23,4
	Vcore (m^3)	45,5	39,0	33,8	31,2	28,6	27,3	26,0	24,7	23,4	23,4	23,4
Web												
	Ltot (m)	10	12,8	15,5	18,3	21,0	23,7	26,4	29,0	30,7	33,3	36
	Tskin (mm)	15	14	13	13	12	11	11	11	11	11	11
	Tcore (mm)	30	28	26	26	24	22	22	22	22	22	22
	Vfrp (m^3)	3,8	4,6	5,2	6,1	6,5	6,7	7,4	8,2	8,6	9,4	10,1
	Vcore (m^3)	3,8	4,6	5,2	6,1	6,5	6,7	7,4	8,2	8,6	9,4	10,1
Total												
	Vfrp (m^3)	52,0	43,6	39,0	37,3	35,1	34,0	33,4	32,9	32,1	32,8	33,5
	rhoFRP (ton/m^3)	1,95	1,95	1,95	1,95	1,95	1,95	1,95	1,95	1,95	1,95	1,95
	Mfrp (ton)	101	85	76	73	68	66	65	64	63	64	65
	Vcore (m^3)	49,4	43,6	39,0	37,3	35,1	34,0	33,4	32,9	32,1	32,8	33,5
	Rhocore (ton/m^3)	0,2	0,2	0,2	0,2	0,2	0,2	0,2	0,2	0,2	0,2	0,2
	Mcore (ton)	10	9	8	8	7	7	7	7	6	7	7
	Vtotal	101	87	78	75	70	68	67	66	64	66	67

	(m^3)										
	Mtotal (ton)	111	94	84	80	75	73	72	71	69	71	72

d) Variant 5: Stiffened plate

A mathcad sheet has been set up to find the minimum mass for the stiffened gate. Both a variant equiped with massive stiffeners and a variant equiped with T-profiles as stiffeners has been investigated. The gate is schematized as a simply supported beam where the properties are calculated with help of the Steiner rule. The results are presented below. The meaning of the parameters can be found in section 4.4.

Massive profiles as stiffeners

$$q := 70\frac{kN}{m^2}$$

$$\gamma_S := 1.5$$

$$l := 25m$$

$$b_1 := 2500mm$$

$$h_1 := 150mm$$

$$b_2 := 250mm$$

$$h_2 := 1650mm$$

$$h_{gate} := 12800mm$$

$$E := 25800MPa$$

$$M_{max} := \left(\frac{1}{8}\right)\cdot q\cdot\gamma_S\, b_1\cdot l^2 = 2.051\times 10^4\cdot kN\cdot m$$

$$d_z := \frac{\left[b_1\cdot h_1\cdot\left(h_2+\frac{h_1}{2}\right)+b_2\cdot\frac{h_2^{\,2}}{2}\right]}{b_1\cdot h_1+b_2\cdot h_2} = 1.254\times 10^3\cdot mm$$

$$d_1 := \left|\left(h_2+\frac{h_1}{2}\right)-d_z\right| = 471.429\cdot mm$$

$$d_2 := \left|\left(\frac{h_2}{2}\right)-d_z\right| = 428.571\cdot mm$$

$$I_{zz} := \left(\frac{1}{12}\right)\cdot b_1\cdot h_1^{\,3}+b_1\cdot h_1\cdot d_1^{\,2}+\left(\frac{1}{12}\right)\cdot b_2\cdot h_2^{\,3}+b_2\cdot h_2\cdot d_2^{\,2} = 0.253\cdot m^4$$

$$a := \max\left(\left|d_1-d_z\right|,\left|d_2-d_z\right|\right) = 825\cdot mm$$

$$\sigma_{max} := M_{max} \cdot \frac{a}{I_{zz}} = 66.769 \cdot \frac{N}{mm^2}$$

$$\rho_{FRP} := 1950 \frac{kg}{3}$$

$$w_{max} := \left(\frac{5}{384}\right) \cdot b_1 \cdot q \cdot \frac{1^4}{E \cdot I_{zz}} = 136.15 \cdot mm$$

$$V_{gate} := \left(\frac{h_{gate}}{b_1}\right) \cdot \left(b_1 \cdot h_1 + b_2 \cdot h_2\right) \cdot 1 = 100.8 \cdot m^3$$

$$m_{gate} := V_{gate} \cdot \rho_{FRP} = 1.966 \times 10^5 \, kg$$

T-profiles as stiffeners

$b_3 := 2500mm$

$h_3 := 15mm$

$b_4 := 100mm$

$h_4 := 1000mm$

$b_5 := 1000mm$

$h_5 := 40mm$

$$d_{z2} := \frac{\left[\left(\frac{h_5}{2}\right) \cdot h_5 \cdot b_5 + \left(h_5 + \frac{h_4}{2}\right) \cdot h_4 \cdot b_4 + \left(h_5 + h_4 + \frac{h_3}{2}\right) \cdot h_3 \cdot b_3\right]}{h_3 \cdot b_3 + h_4 \cdot b_4 + h_5 \cdot b_5} = 530.035 \cdot mm$$

$$d_3 := \left|-d_{z2} + h_5 + h_4 + \frac{h_3}{2}\right| = 517.465 \cdot mm$$

$$d_4 := \left|h_5 + \left(\frac{h_4}{2}\right) - d_{z2}\right| = 9.965 \cdot mm$$

$$d_5 := \left|\left(\frac{h_5}{2}\right) - d_{z2}\right| = 510.035 \cdot mm$$

$$I_{zz2} := \left[\left(\frac{1}{12}\right) \cdot b_3 \cdot h_3^3 + d_3^2 \cdot b_3 \cdot h_3 + \left(\frac{1}{12}\right) \cdot b_4 \cdot h_4^3 + d_4^2 \cdot b_4 \cdot h_4 + \left(\frac{1}{12}\right) \cdot b_5 \cdot h_5^3 + d_5^2 \cdot b_5 \cdot h_5\right] = 0.029 \cdot m^4$$

$$a_2 := \max(d_3, d_5) = 517.465 \cdot mm$$

$$M_{max2} := \left(\frac{1}{8}\right) \cdot q \cdot 1.5 b_3 \cdot 1^2 = 2.051 \times 10^4 \cdot kN \cdot m \qquad \rho_{steel} := 7850 \frac{kg}{m^3}$$

$$\sigma_{max2} := M_{max2} \cdot \frac{a_2}{I_{zz2}} = 368.525 \cdot \frac{N}{mm^2}$$

$$m_{gate2} := \left(\frac{h_{gate}}{b_3}\right)\cdot\left(b_3\cdot h_3 + b_4\cdot h_4 + b_5\cdot h_5\right)\cdot 1\cdot\rho_{steel} = 178.352\cdot 10^{3}kg$$

$$V := \left(\frac{1}{2}\right)\cdot q\cdot\gamma_S\cdot 1\cdot b_3 = 3.281\times 10^{3}\cdot kN$$

$$S_{afgeschoven} := \left(\frac{1}{2}\right)\cdot h_3\cdot h_3\cdot b_3 = 2.812\times 10^{5}\cdot mm^{3}$$

$$\tau_{plaat} := V\cdot\frac{S_{afgeschoven}}{b_3\cdot I_{zz2}} = 0.013\cdot\frac{N}{mm^{2}}$$

$$w_{max2} := \left(\frac{5}{384}\right)\cdot b_3\cdot q\cdot\frac{1^{4}}{E\cdot I_{zz2}} = 1.198\times 10^{3}\cdot mm$$

Appendix F) Motivation of the MCA ratings

Resiliency

During negative head differences, the curved gate has the tendency to buckle. The stiffened gate may also face serious stability problems as soon as the stiffeners are loaded in compression. The Warren truss gate and Lens-shaped gate score well on resiliency because these configurations are (nearly) symmetrical, meaning that these options are well able to resist negative head differences.

Reliability

The Warren truss gate apears to be relatively free of risks. The joints are not highly loaded and the high repetition factor of the individual elements reduces the chance of possible mistakes during production. The stiffened plate has not been designed for stability of the stiffeners, which may cause serious problems. Besides, the large lengths of the connections between stiffeners and plate also induce a high risk profile. Finally, the T-shape of the stiffeners are also vulnerable to collection of sediments and mud, which may induce material degradation. The curved gate contains highly loaded connections between the curved- and the straight plate. This connection requires much attention during detailing of the structure. Besides, the structural safety of the straight plate during negative head differences is not guaranteed.The main challenge of the lens-shaped gate will be the connection of the two curved plates to each other. This connection is however not as highly loaded as for the previous gate alternative. The stabily of individual components has been incorporated in the design.

Maintainability

The Warren truss gate consists of a lot of small compartments which are hard to reach for maintenance and inspection. The stiffened gate is sensitive to collection of sediments and debris requiring regular cleaning of the gate. The lens-shaped gate also consists of compartments but the sizes are sufficiently large so that a human can enter. The arched gate is easiliy accessible due to its open structure without small corners and holes.

Aesthetic value

The Warren truss gate and stiffened plate are somewhat like regular lock gates. These designs are similar to designs which are constructed from steel. The curved gate and lens-shaped gate are very futuristic and can really serve as a tourist attraction. Besides, these shapes fit very well with the design of the arched bridge a few kilometer north of the lock.

Constructability

The Warren truss gate consists of a large amount of connections which is at the expanse of the constructability. The stiffened plate is easily constructed, due to the simple geometry. The only difficulty will be the attachment of stiffeners to the water retaining plate. The curved gate and lens-shaped gate may be difficult to connect to the lock sill due to the curvature of the plates. For the curved gate, additional elements are required to attach the lifting equipment in the center of gravity. The lens-shaped gate however has more elements and thus requires more connections.

Appendix G) Required size of the openings

To calculate the time which is required for filling- and emptying of the lock chamber, the circular openings are schematized as rectangular to ease the calculations. The difference between the schematized relation between area of the opening and lifting height (blue dotted line) of the gate and the real relation (red) is relatively small, as illustrated by Figure 169.

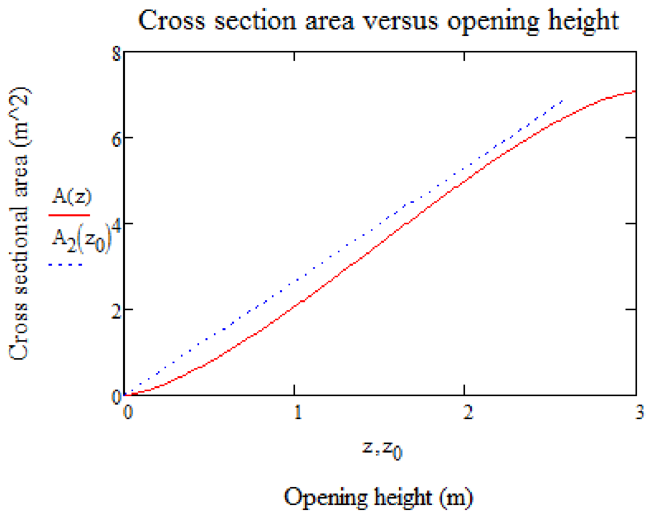

Figure 169: Difference between schematization (blue) and reality (red)

The following assumptions are made to calculate the time required for levelling of the lock chamber:

- The water level outside the lock chamber is constant;
- The lifting velocity is constant until fully opened;
- The lifting time equals the total filling or emptying time;
- The discharge through the round openings equals the discharge through rectangular openings with the same surface area.

Under these assumptions, the total time required for filling or emptying the lock chamber under the maximum operational water level difference is a little less than 6 minutes, which is ought to be acceptable. The calculations can be found in Appendix G).

Under the assumptions mentioned in 5.2.4, the following function holds for the time required for filling- or emptying of the lock chamber [36]:

$$T = \sqrt{\frac{4A\sqrt{\Delta H} * t_h}{m_s * f * \sqrt{2g}}}$$

$A =$ Surface area of the lock chamber
$\Delta H =$ Design head difference
$t_h =$ Lifting time
$m_s =$ Discharge coefficient
$f =$ Area of the openings
$g =$ Gravitational acceleration.

The following values are filled in:

$$A = L_{lock} * B_{lock} = 200 * 25 = 5000\ m^2$$

$$\Delta H = 6{,}4\,m$$

$$t_h = \frac{h_{valve}}{v_{lift}} = \frac{2 * r_{opening}}{9} = 333\ s$$

$h_{valve} =$ Height of the valves
$v_{lift} =$ Lifting velocity
$r_{opening} =$ Radius of the openings

$$m_s = 0{,}80$$

$$f = 6 * \pi * r_{opening}^2 = 42{,}4\,m^2$$

$$g = 9{,}81 \frac{kgm}{s^2}$$

$$T = 346\,s$$

$$i(t) = \frac{dQ}{dt} * \frac{1}{g * (A_v - n)}$$

With A_v the cross sectional area of the lock chamber (width x water height) and n the cross sectional area of the governing vessel (width x draught).

The formula for the discharge in time is derrivated in [36] and reads:

$$Q(t) = \frac{m_s f \sqrt{2g\Delta H}}{t_h} * t - \frac{m_s^2 f^2 g}{2At_h^2} t^3$$

Now the discharge is derrivated with respect to t:

$$\frac{dQ}{dt} = \frac{m_s f \sqrt{2g\Delta H}}{t_h} - \frac{m_s^2 f^2 g}{At_h^2} t^2$$

The rate of change of the discharge is maximum for t=0:

$$i(0) = \frac{m_s f \sqrt{2g\Delta H}}{t_h} * \frac{1}{g * (A_v - n)} = 1{,}5 * 10^{-3}$$

This means that the hawser forces due to translation waves are approximately 1,5‰ of the mass of the vessel. This force equals 142 kN, which comes down to 71 kN per hawser.

Appendix H) Additional weight induced by the Z-structure

In this Appendix, the additional mass related to the Z-structure of the fibers around the core is investigated.The space between the cores is determined by the amount of fibers in between the cores and the curvature of the plate.

Geometric relations are found which relate the angle between the blocks to the radius of curvature and width of a single block. The formula reads as follows:

$$\theta = 2 * \tan^{-1}(\frac{w_{block}}{2 * r})$$

$\theta =$	Angle between individual core blocks [degrees]
$w_{block} =$	Width of a single block of foam [m]
$r =$	Radius of curvature of the plate [m]

For the radius of the gate of 39 meters, an angle between the indivual cores of $0{,}29°$ is obtained. The curvature is constant for the entire plate. Therefore, the angle between two sequential blocks is also equal for the entinre plate. The angle is required to calculate the volume of FRP between two cores. An impression of these gaps is presented in Figure 170.

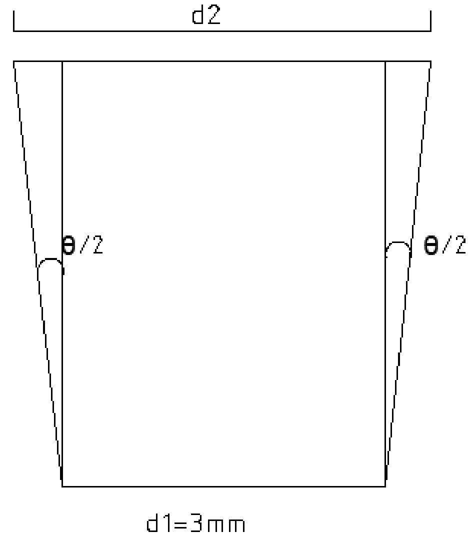

Figure 170: Impression of the area between two cores which needs to be filled with resin

The length d_2 follows from simple geometry:

$$d_2 = d_1 + 2 * h_{core} * \tan\left(\frac{\theta}{2}\right)$$

The total added mass of the gate is calculated by multiplication of the area presented in Figure 170 by the height of the gate and the number of transitions between blocks of core material. This additional mass of the curved plates is equal to approximately 1700 kilograms. Because of the small curvature of the gate, the additional mass due to the curvature is only 2% of the total added mass caused by the spaces in between the cores. The extra mass of the webs due to the spaces in between the cores is approximately 300 kilograms. This makes the total added mass of the gate due to spaces between the cores equal to 2 tons.

Appendix I) Verification of the structural model

This Appendix shows the verification of the final finite element model. The results after each step of increase in complexity are presented and compared to the results of the previous step.

Model 1

Software	SCIA Engineer
Type of model	2D-frame
Joint type	Rigid
Loads	Constant q-load of $70\frac{kN}{m^2} * 12{,}8m = 896kN/m$
Plate thickness	Curved plates: $87{,}2\ mm$, webs:$48\ mm$ (no core)
Youngs modulus	E= $25.800\ N/mm^2$

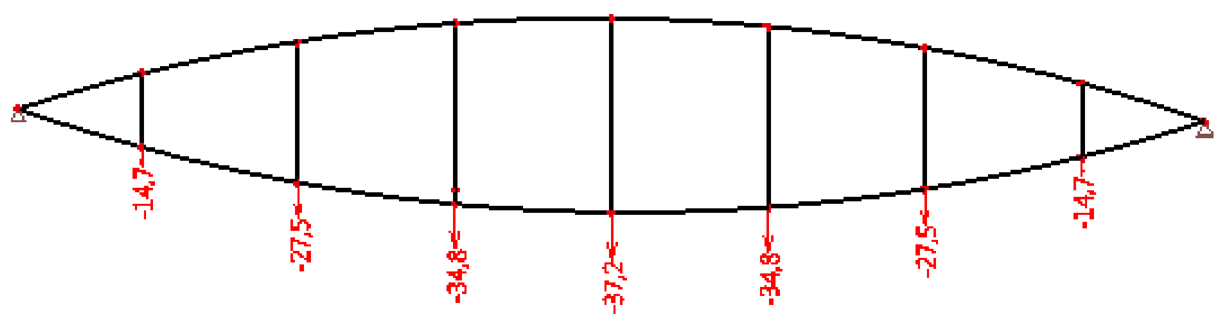

Figure 171: Model 1, displacement of nodes

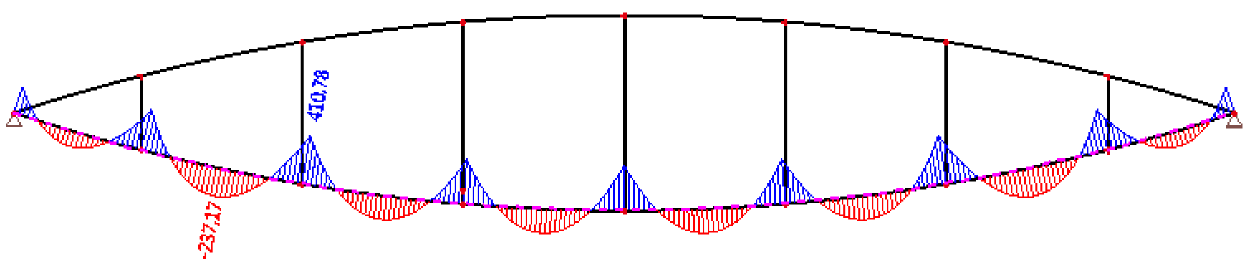

Figure 172: Model 1, momentline

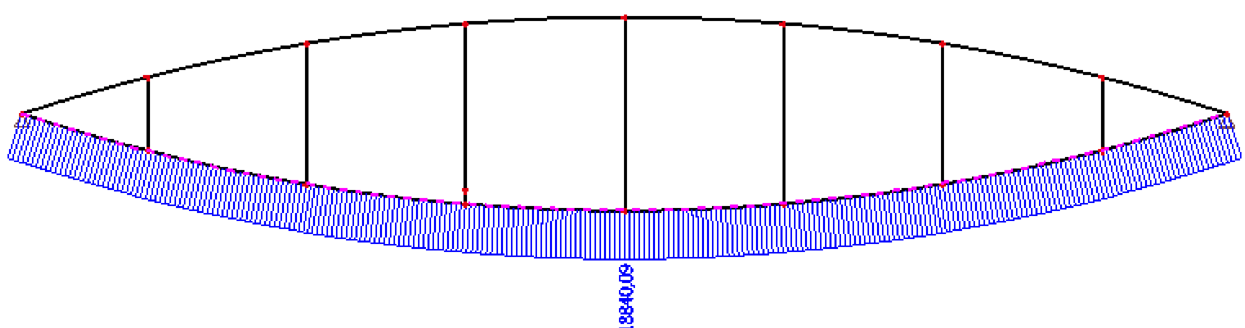

Figure 173: Model 1, normal forces

$$M_1 = 411\ kNm$$

$$M_2 = -237\ kNm$$

$$N = 18840\ kN$$

$$A = b * h = 12{,}8 * 0{,}0872 = 1{,}12\ m^2$$

$$I_{zz} = \frac{1}{12} * b * h^3 = 7{,}07 * 10^{-4} m^4$$

$$z = \frac{h}{2} = 43{,}7\ mm$$

$$\sigma_{1;top} = \frac{N}{A} + \frac{M_1 * z}{I_{zz}} = 16{,}9 + 25{,}4 = 42{,}3\ N/mm^2$$

$$\sigma_{2;top} = \frac{N}{A} + \frac{M_2 * z}{I} = 16{,}9 - 14{,}6 = 2{,}3\ N/mm^2$$

$$\sigma_{1;bottom} = \frac{N}{A} - \frac{M_1 * z}{I} = 16{,}9 - 25{,}4 = -8{,}5\ N/mm^2$$

$$\sigma_{2;bottom} = \frac{N}{A} + \frac{M_2 * z}{I} = 16{,}9 + 14{,}6 = 31{,}5\ N/mm^2$$

Model 2

Difference to first model: 3D-model instead of 2D-frame. Constant properties over the height. Coefficient of lateral contracttion equals 0. The model should give the same results as model 1.

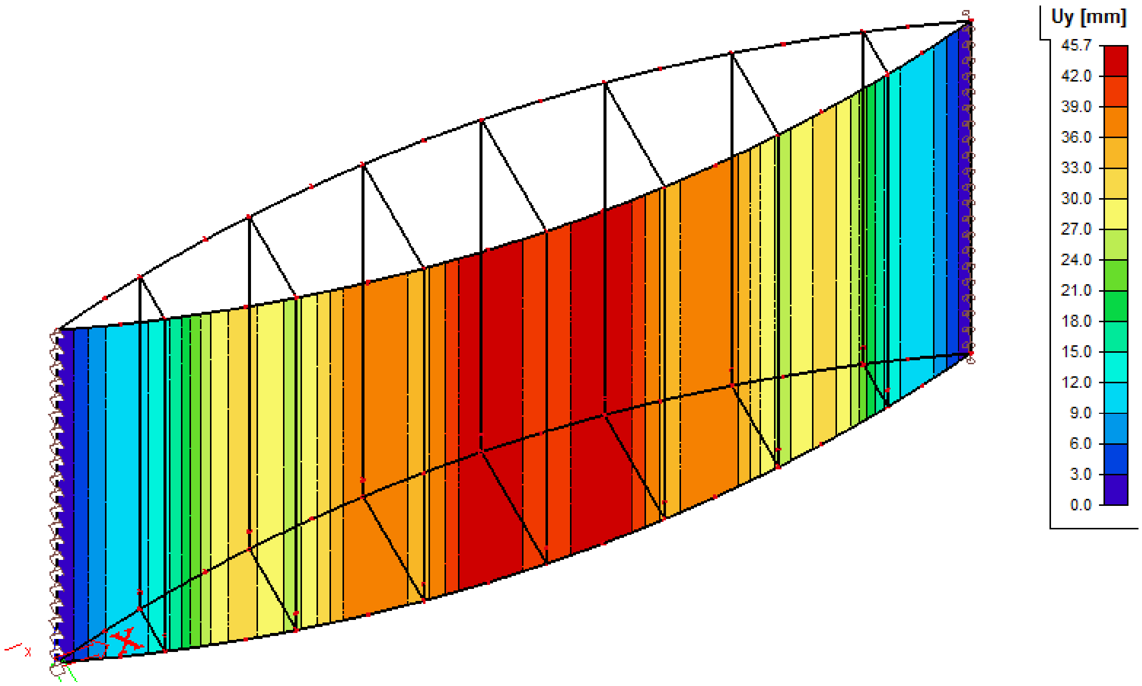

Figure 174: Model 2, displacement of nodes

,

Figure 175: Model 2, stresses at the top side of the plate

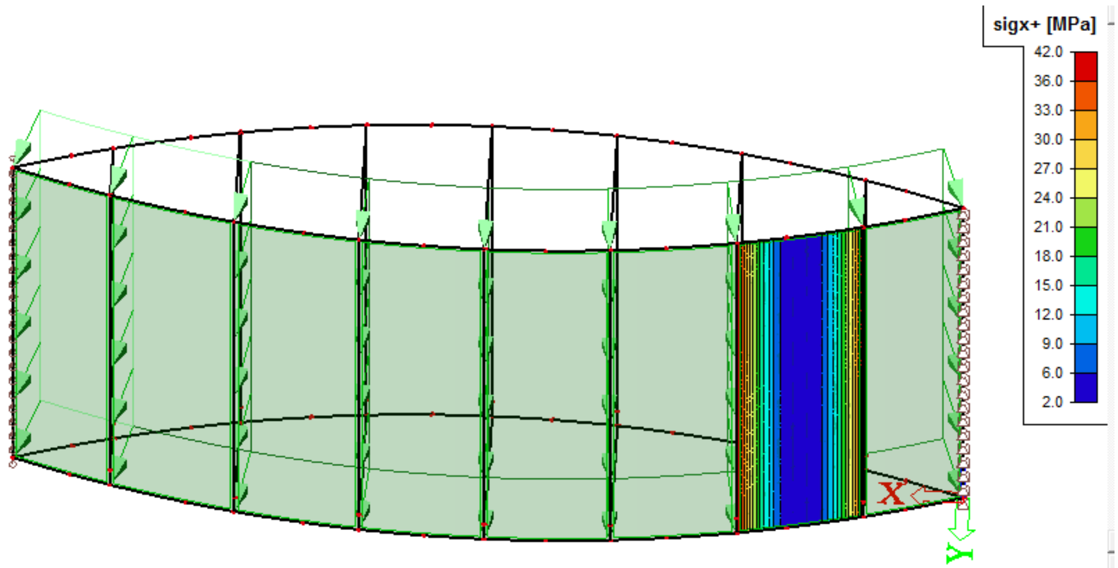

Figure 176: Model 2,, stresses at the top of the plate at the governing section

Figure 177: Model 2, stresses at the bottom side of the plate

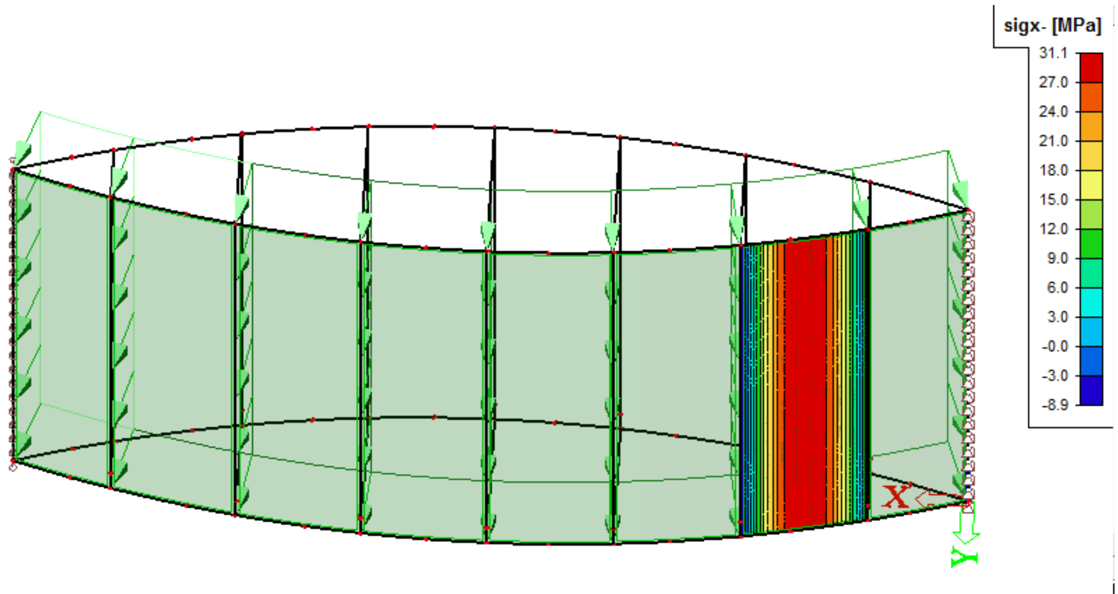

Figure 178: Model 2, stresses at the bottom of the plate at the governing section

Position of maximum stresses is equal to the 2D-model. The difference in values is within a acceptable range. (At the bottom side: $31{,}1\ N/mm^2$ & $-\ 8{,}9\ N/mm^2$ versus $31{,}5\ N/mm^2$ & $-8{,}5\ N/mm^2$. At the top side: $42{,}0\ N/mm^2$ & $2{,}0\ N/mm^2$ versus $42{,}3\ N/mm^2$ & $2{,}3\ N/mm^2$.

Model 3

Equal to model 2, the only difference is that the coefficient of lateral contraction is now equal to 0,3.

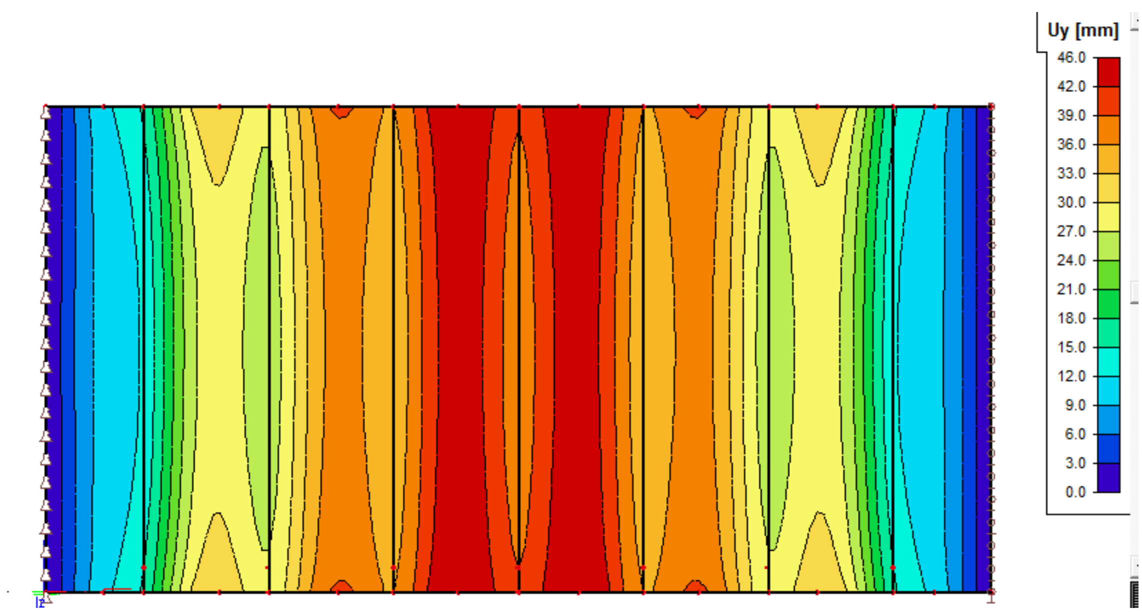

Figure 179: Model 3, deformations of the plate

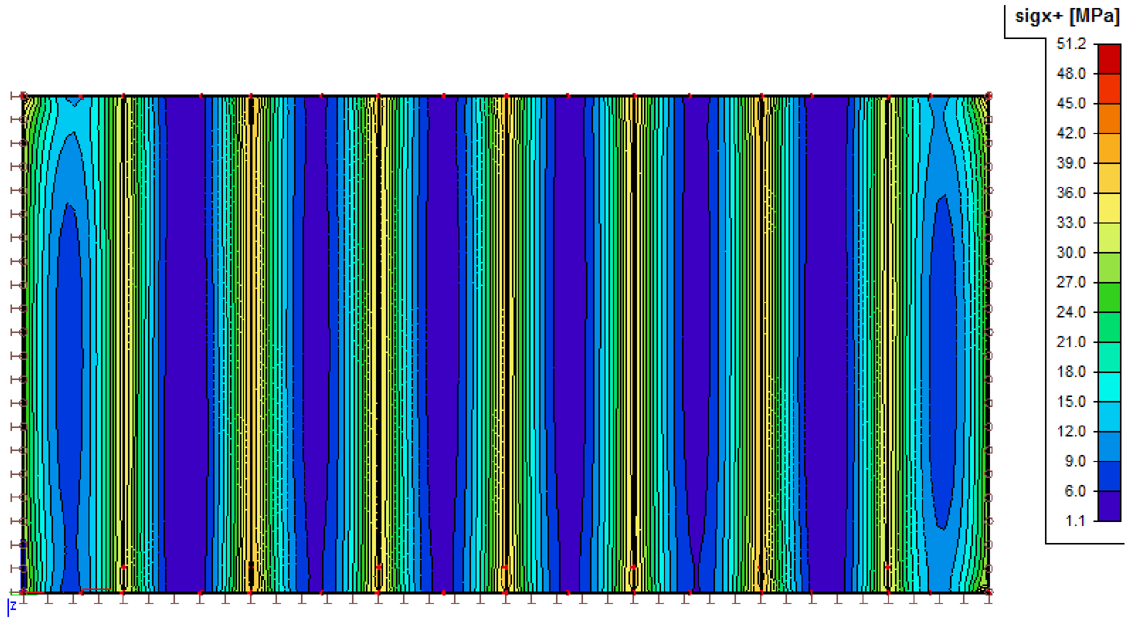

Figure 180: Model 3, global stresses at the top of the plate

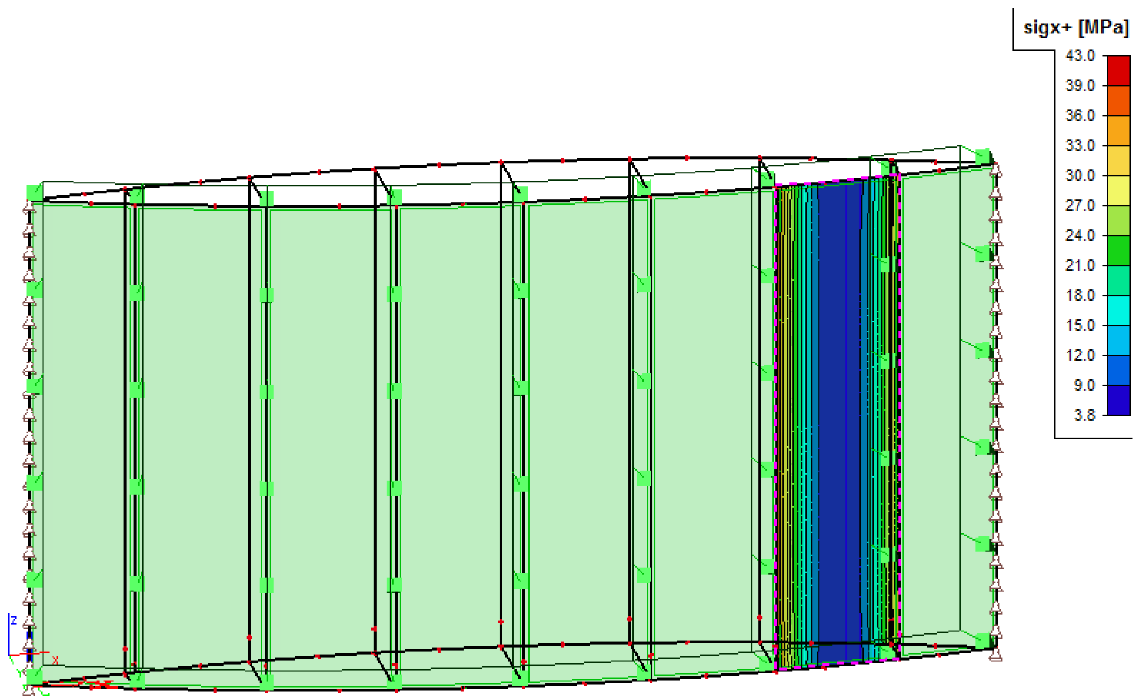

Figure 181: Model 3, stresses at the top of the governing section of the plate

Figure 182: Model 3, global stresses at the bottom of the plate

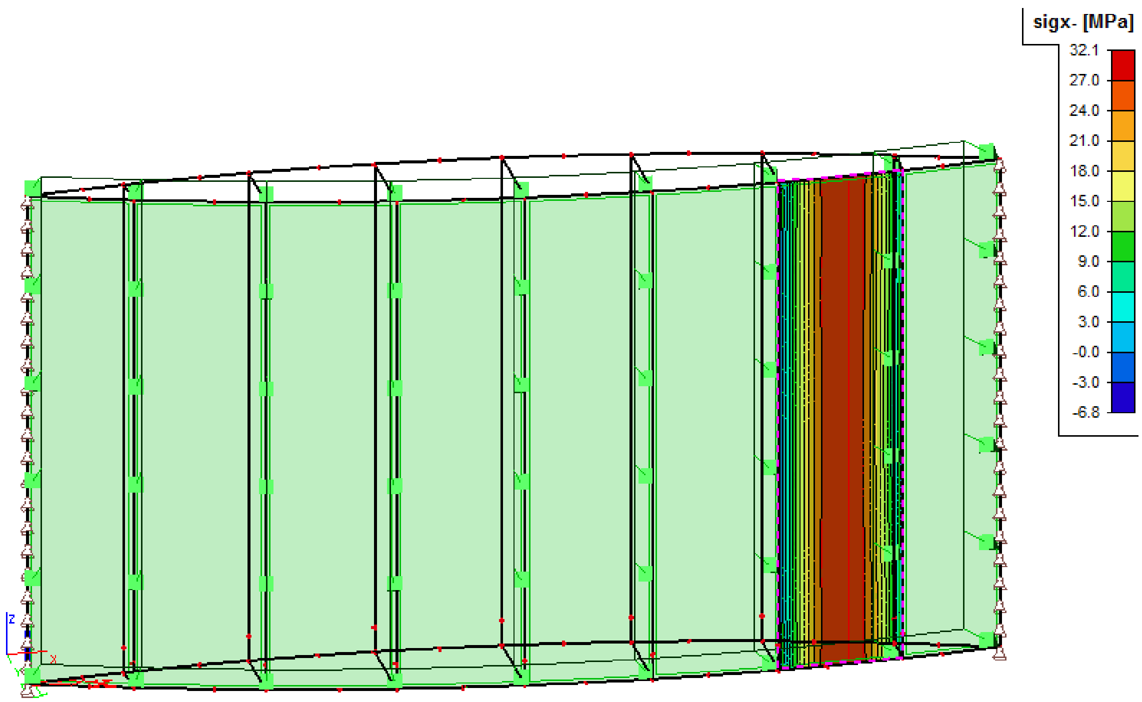

Figure 183: Model 3, stresses at the bottom of the governing section of the plate

The properties are not constant over the height of the gate anymore. This is caused by lateral contraction: the normal forces in x-direction result in stresses in the z-direction. The top- and bottom edge of the gate are only supported by neigbour material on one side. This is why the deflections at the edges is larger than in the middle.

Model 4

The geometry, loads and material properties of model 3 have now been assigned in ANSYS instead of SCIA Engineer.

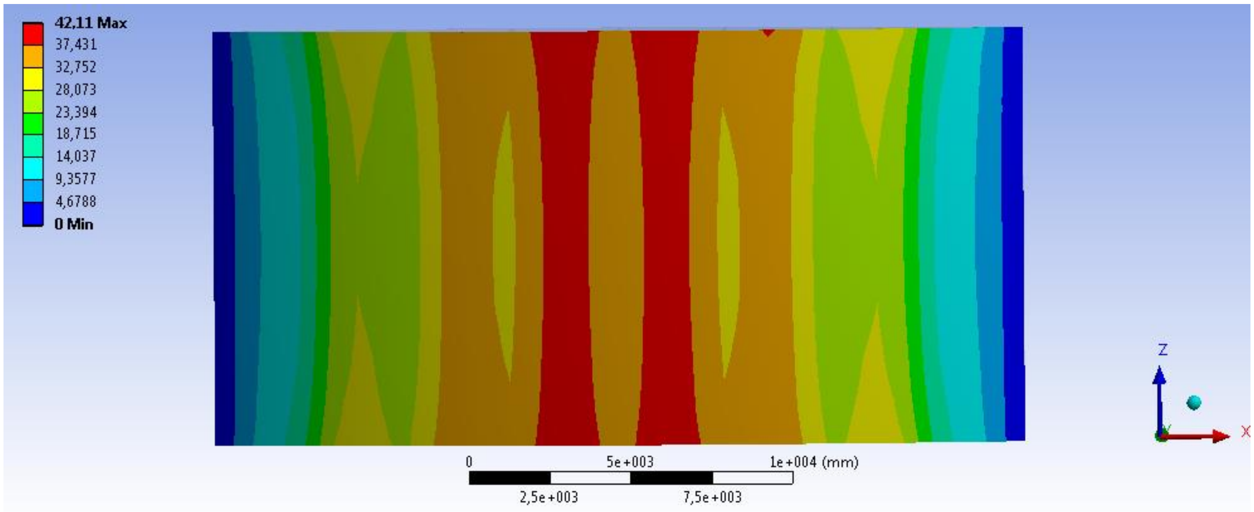

Figure 184: Model 4, global deformations of the gate

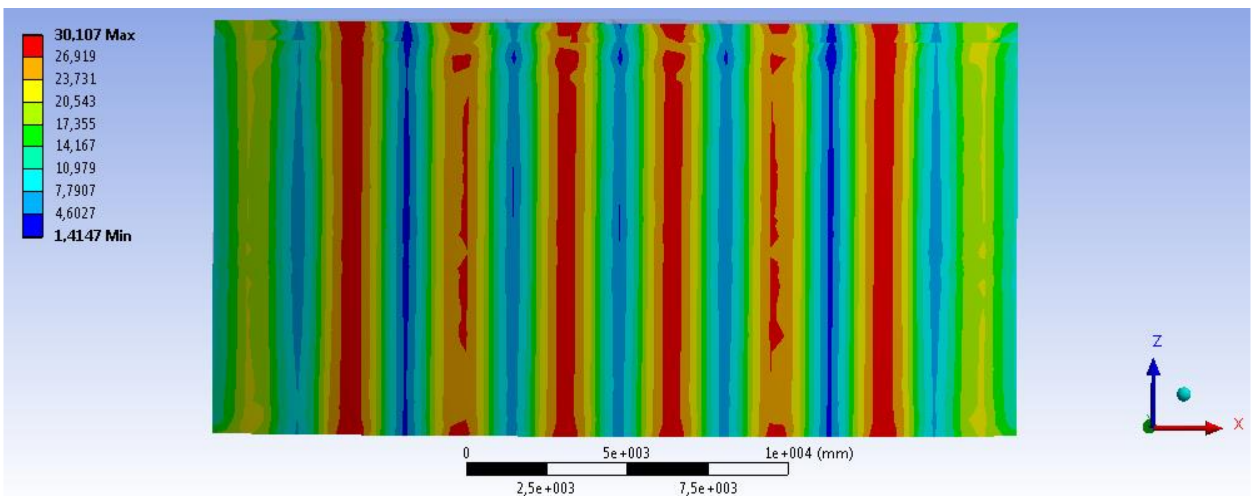

Figure 185: Model 4, global stresses at the top of the plate

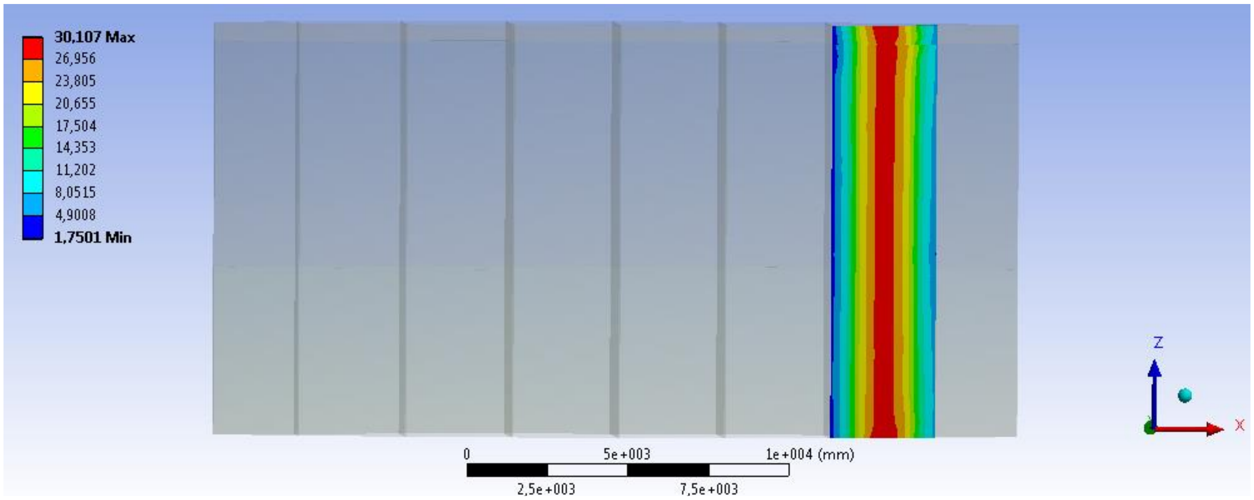

Figure 186: Model 4, stresses at the top of the governing section of the plate

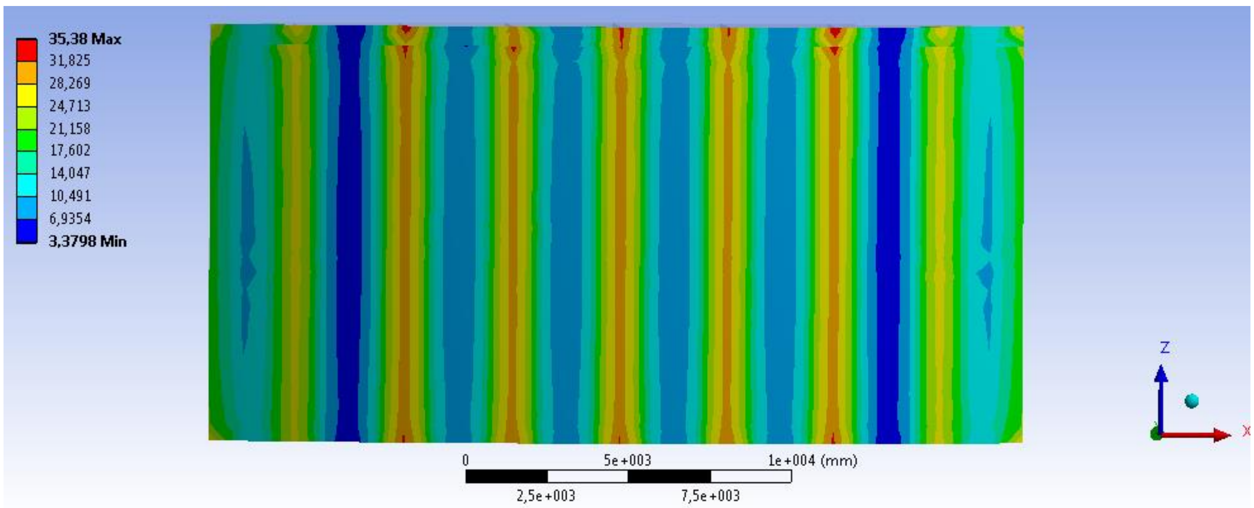

Figure 187: Model 4, global stresses at the bottom of the plate

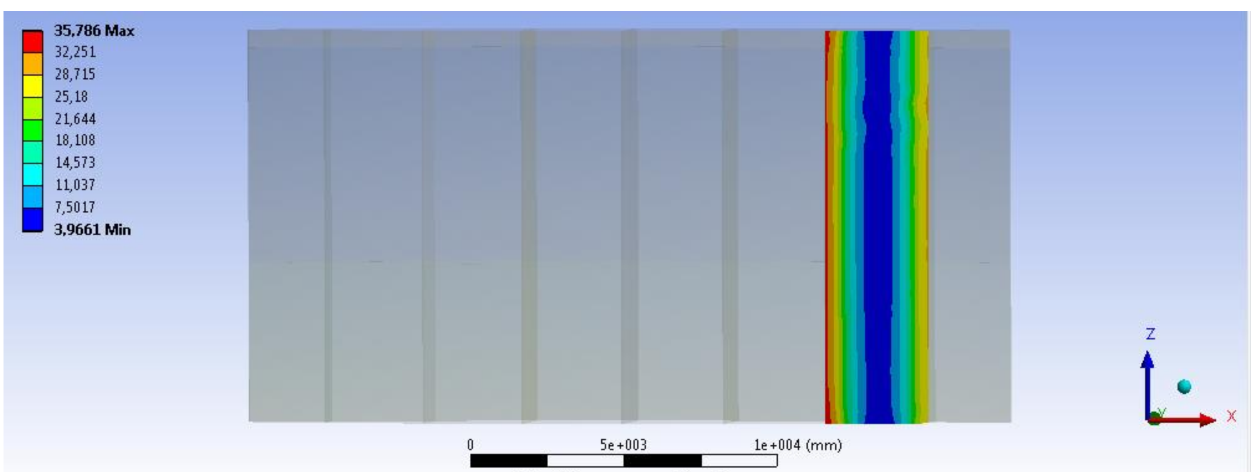

Figure 188: Model 4, stress at the bottom of the governing section of the gate

The difference in deformations are acceptable. The difference in stresses are however not neglicable. In SCIA Engineer, the webs are schematized as 2D plates with 0 thickness while ANSYS uses the real thickness which will give more accurate results. The peaks of the momentline are topped off, resulting in smaller stresses in the curved plates near the webs. Difference in stresses in the fields between the webs are neglicable.

Model 5

The difference to model 4 is that this model is now equiped with openings and tubes which are required for the filling- and emptying of the lock chamber.

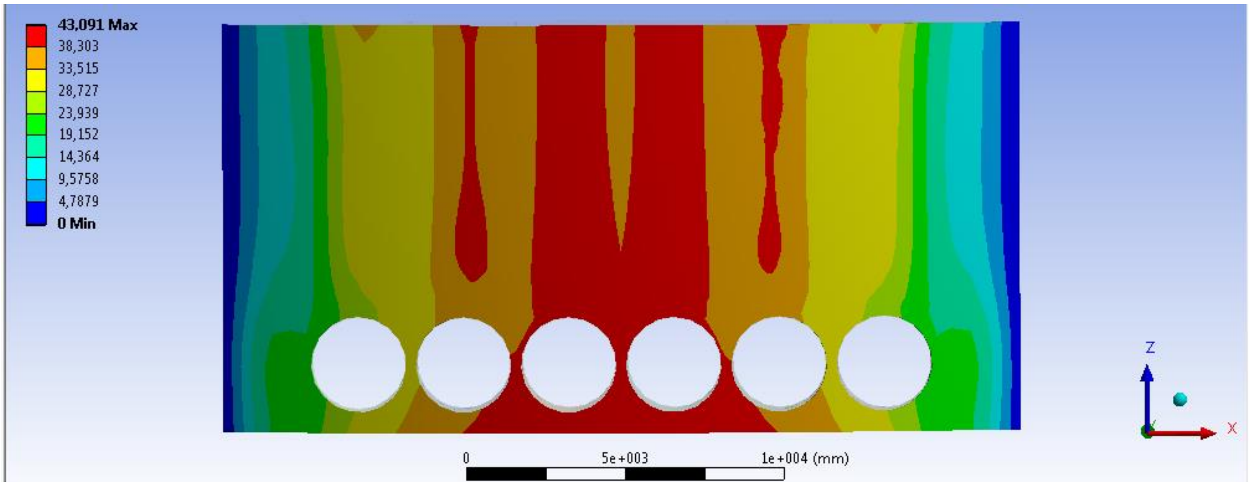

Figure 189: Model 5, deformations of the gate

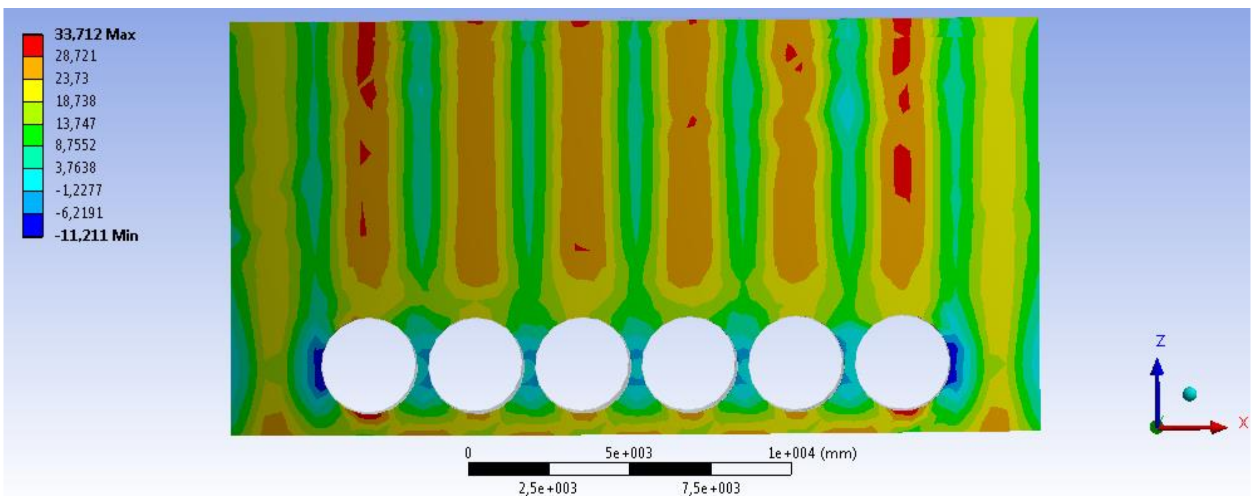

Figure 190: Model 5, global normal stresses at the top of the water retaining plate

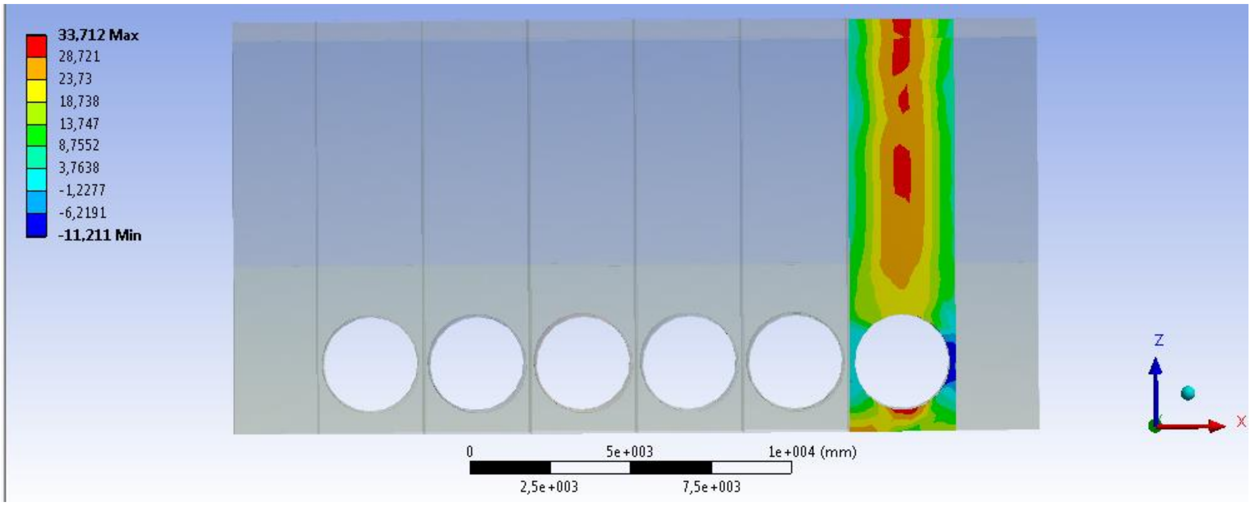

Figure 191: Model 5, local normal stresses at the top of the water retaining plate

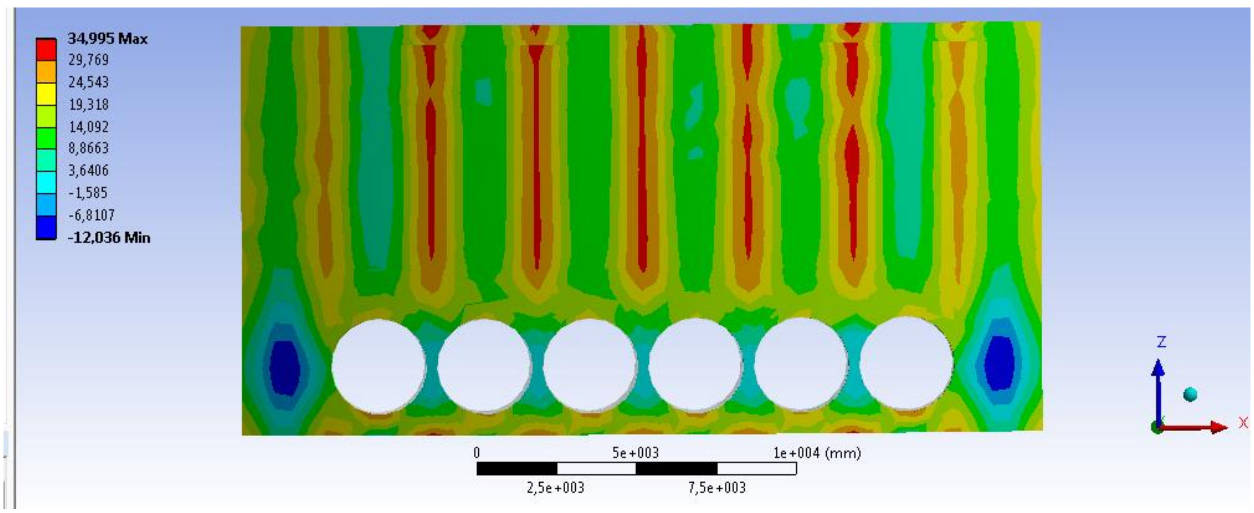

Figure 192: Model 5, global normal stresses at the bottom of the water retaining plate

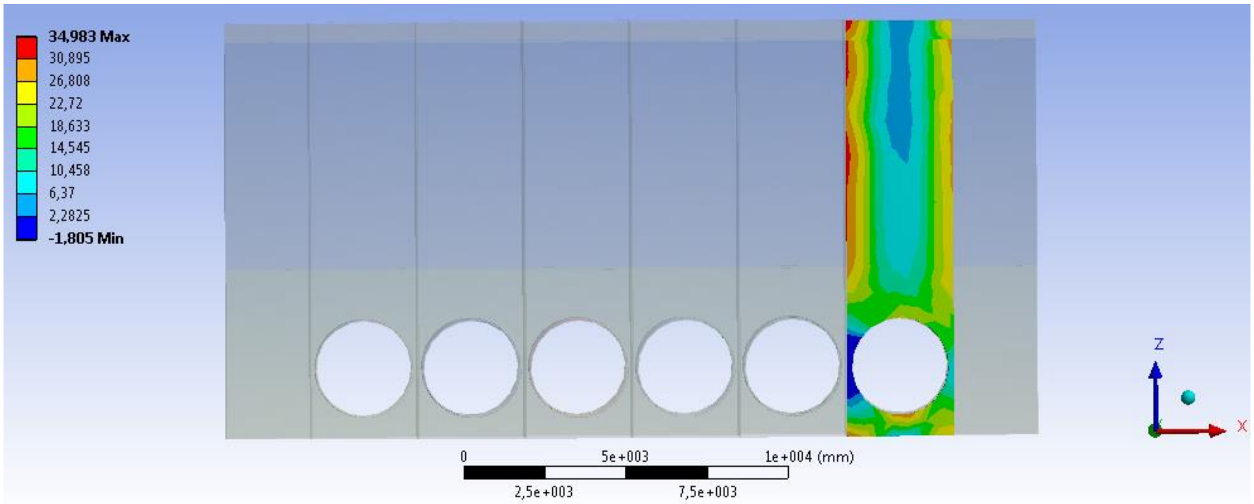

Figure 193: Model 5, local normal stresses at the bottom of the water retaining plate

Model 5 shows stress concentrations around the openings at the positions where they were expected to occur. The stresses in the unadjusted zone at the top of the gate are still compareable to the stresses at model 5.

Model 6

The water pressures in this model are in line with the hydrostatic pressures presented in Figure 58, multiplied with a load factor of 1,5 (instead of a distributed load of 70 kN/m^2 over the entire plate).

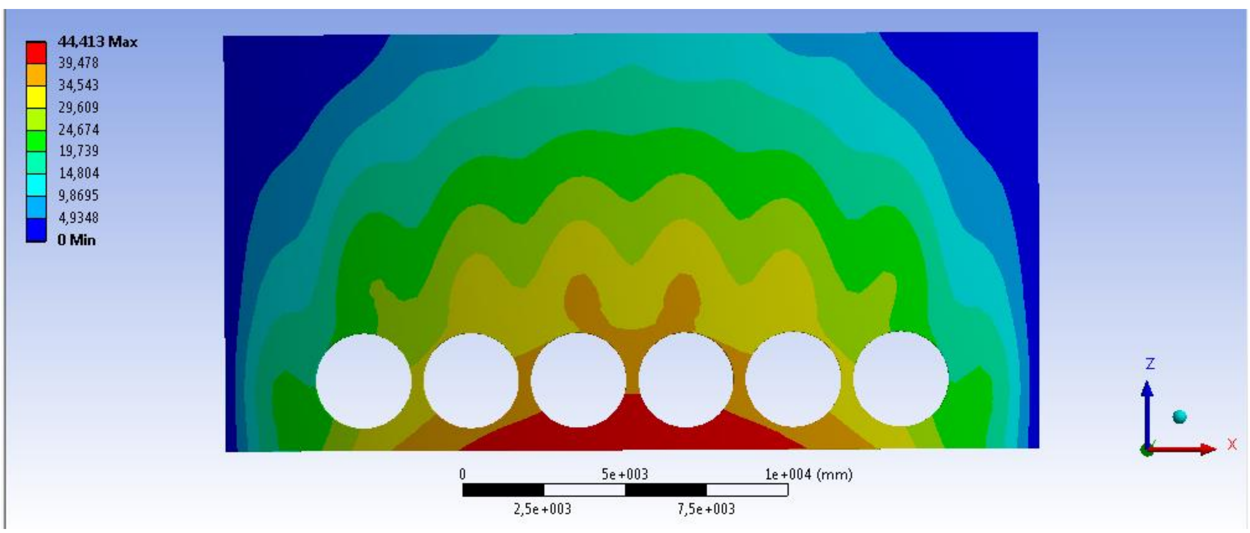

Figure 194: Model 6, deformations of the gate

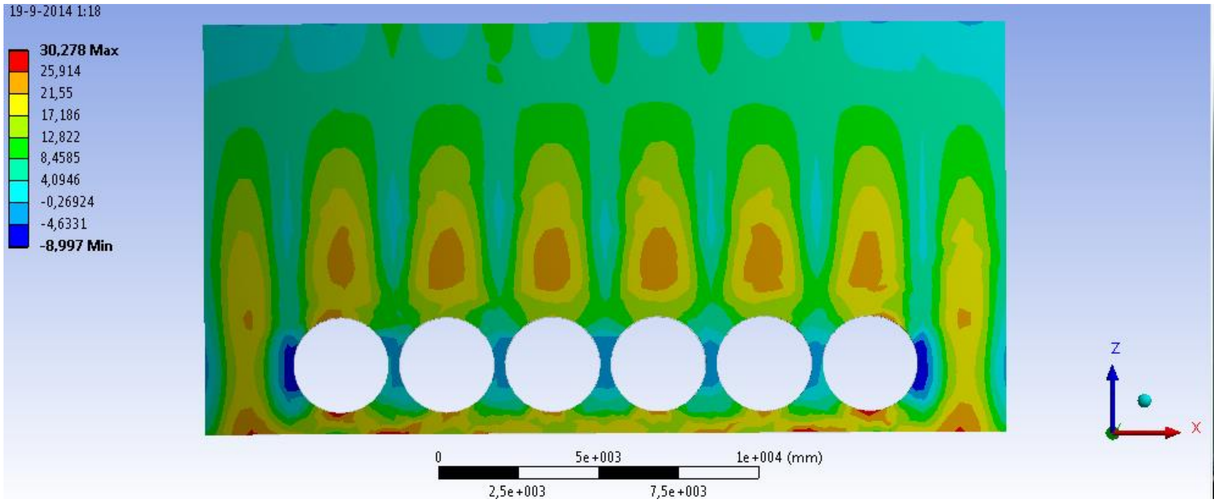

Figure 195: Model 6, global stresses at the top of the water retaining plate

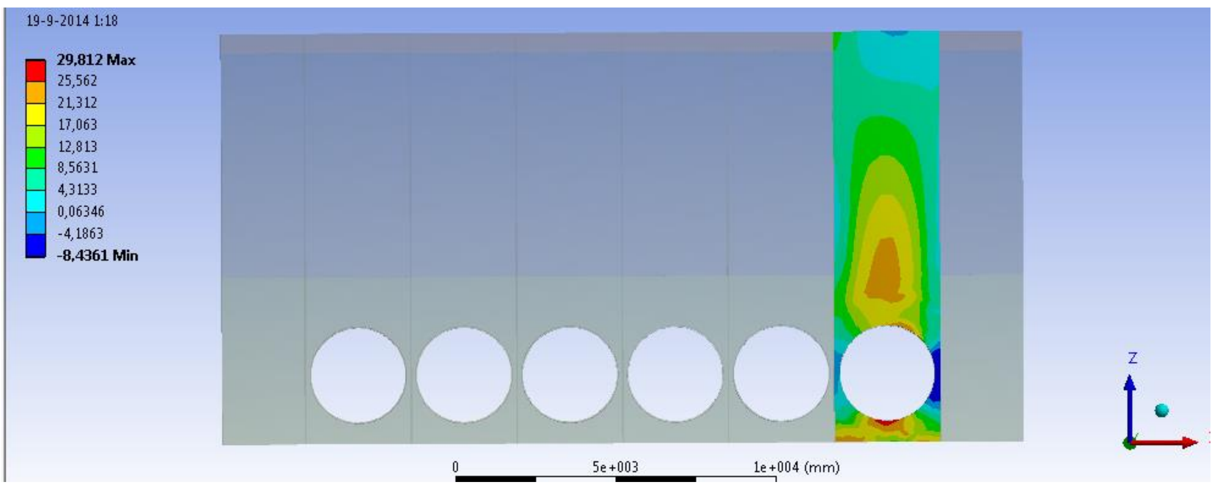

Figure 196: Model 6, local stresses at the top of the water retaining plate

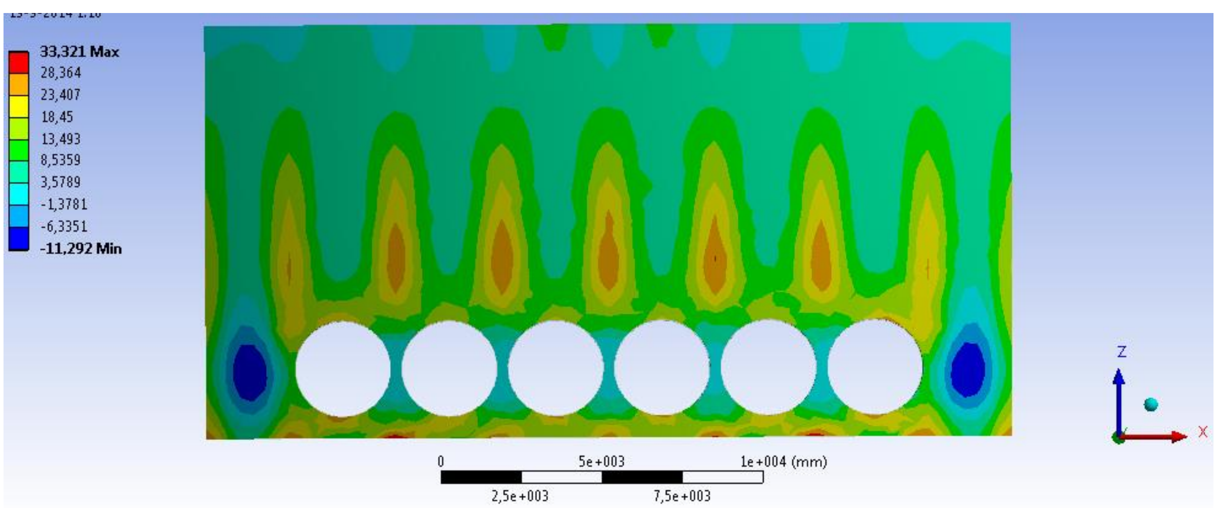

Figure 197: Model 6, global stresses at the bottom of the water retaining plate

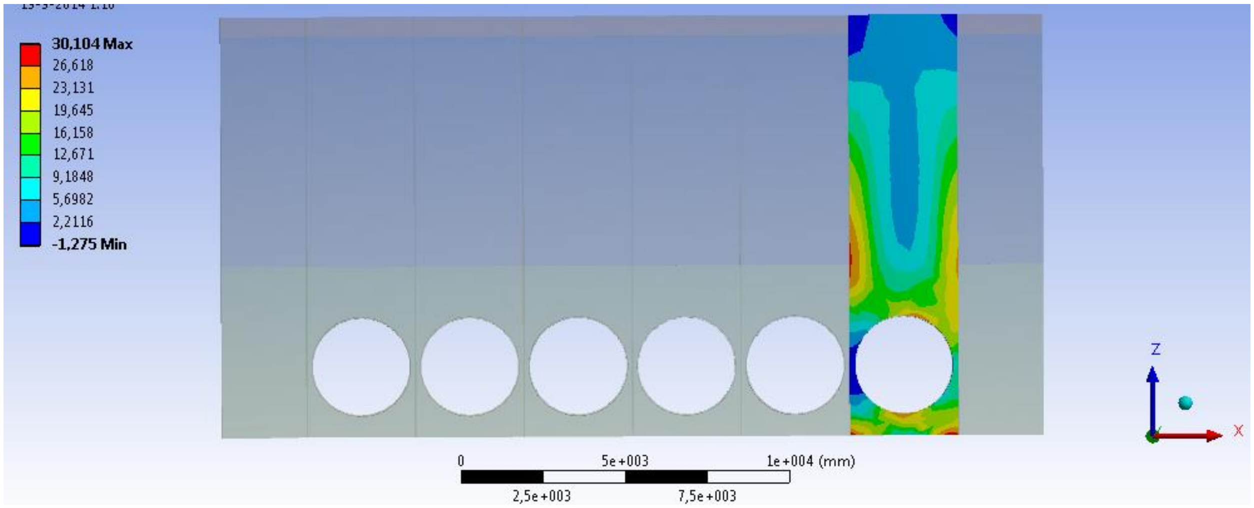

Figure 198: Model 6, local stresses at the bottom of the water retaining plate

Just as expected, the deformations at the bottom of the gate increase because of the load factor of 1,5 while the deformations at the top decrease due to a reduction of the local loads.The position of the highest stresses also got closer to the openings because the center of the forces has gotten closer to the bottom of the gate.

Model 7

Compared to model 6, model 7 consists of layered plates, of which the inner 50% of the plates consist of foam, of which the stiffness is neglicible to the skin stiffness.

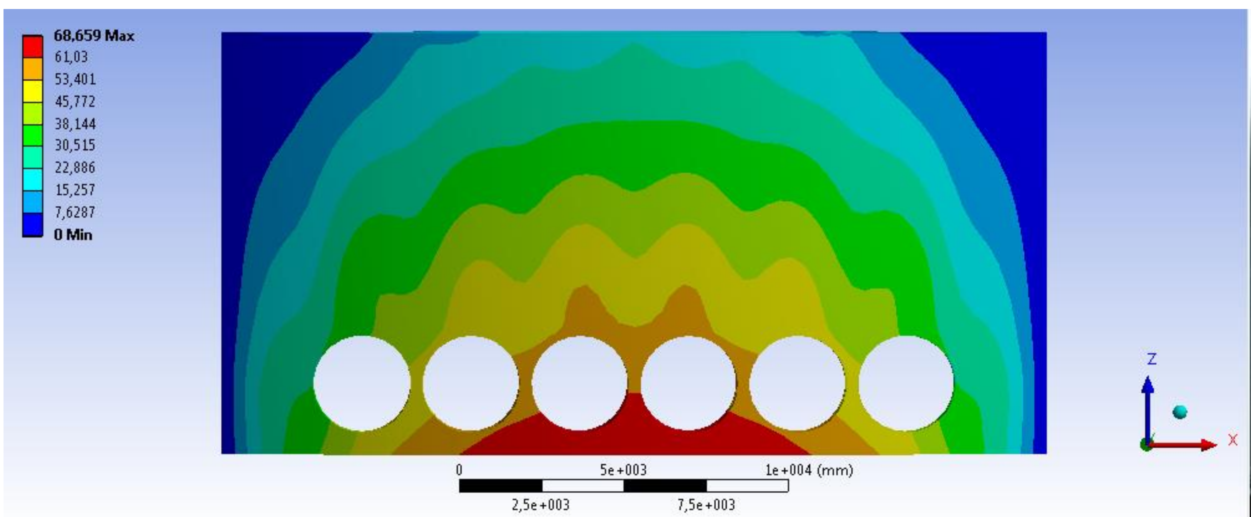

Figure 199: Model 7, deformations of the gate

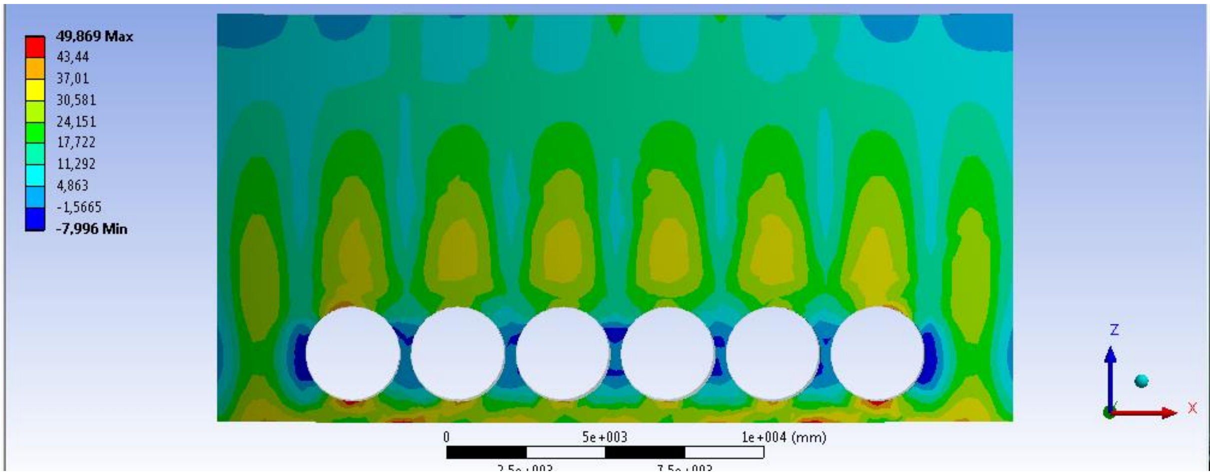

Figure 200: Model 7, global stresses at the top of the water retaining plate

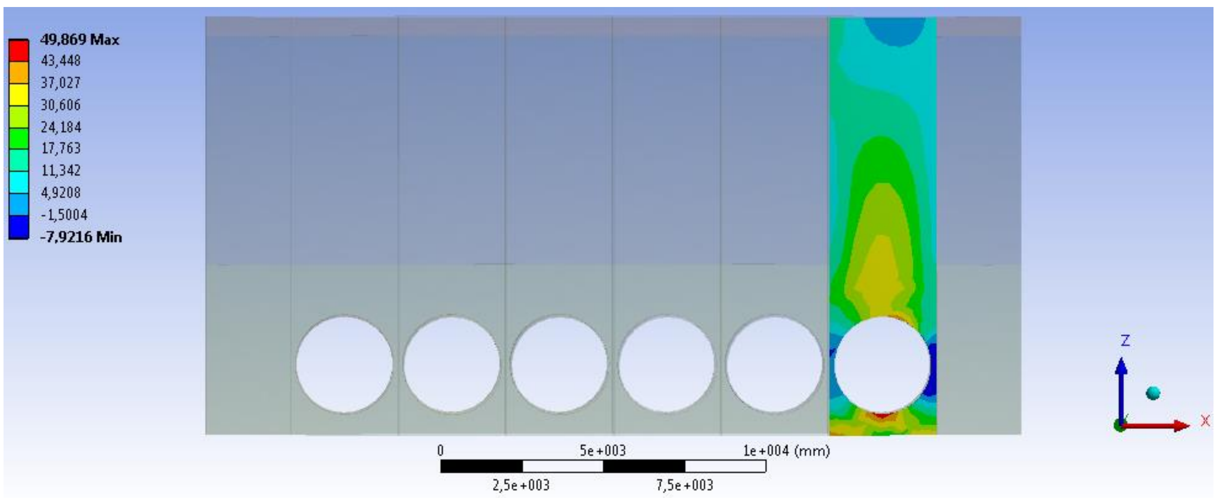

Figure 201: Model 7, local stresses at the top of the water retaining plate

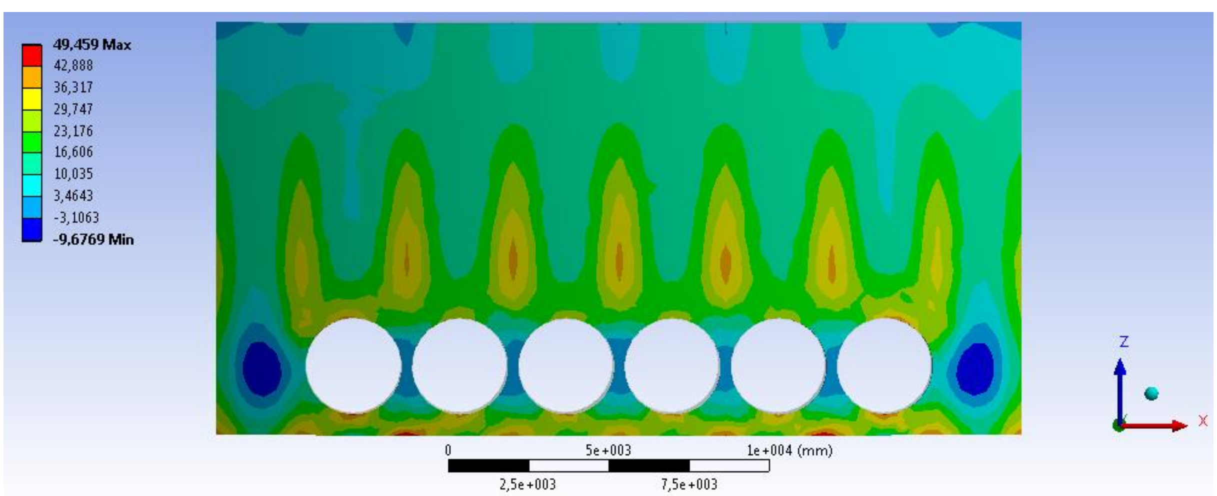

Figure 202: Model 7, global stresses at the bottom of the water retaining plate

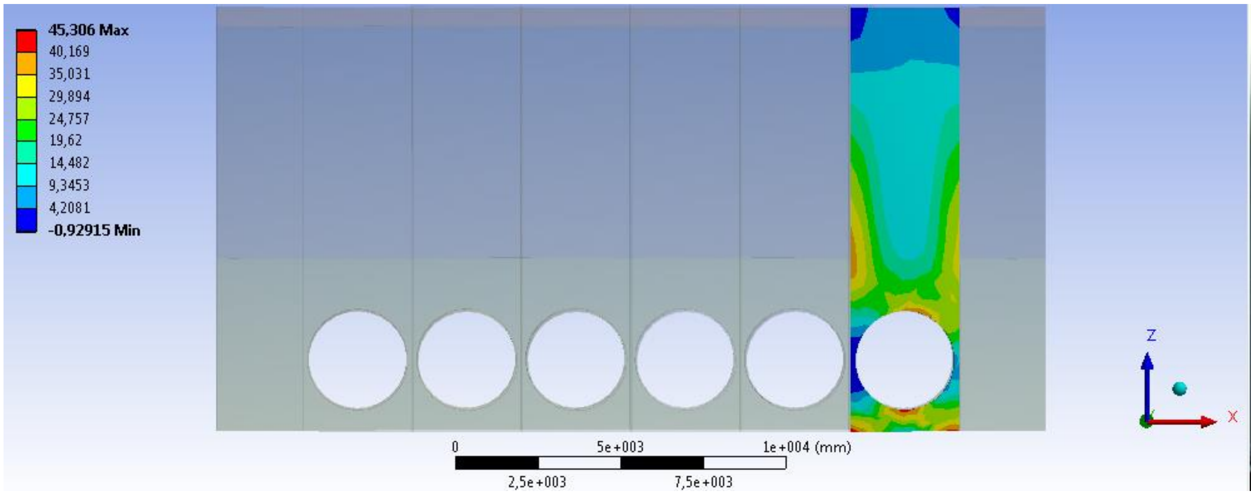

Figure 203: Model 7, local stresses at the bottom of the water retaining plate

Appendix J) Efffects of construction of a line support at the sill

The effects of construction of an additional horizontal line support has been investigated by the finite element model. The resulting deformations, normal strains and shear stresses are presented below.

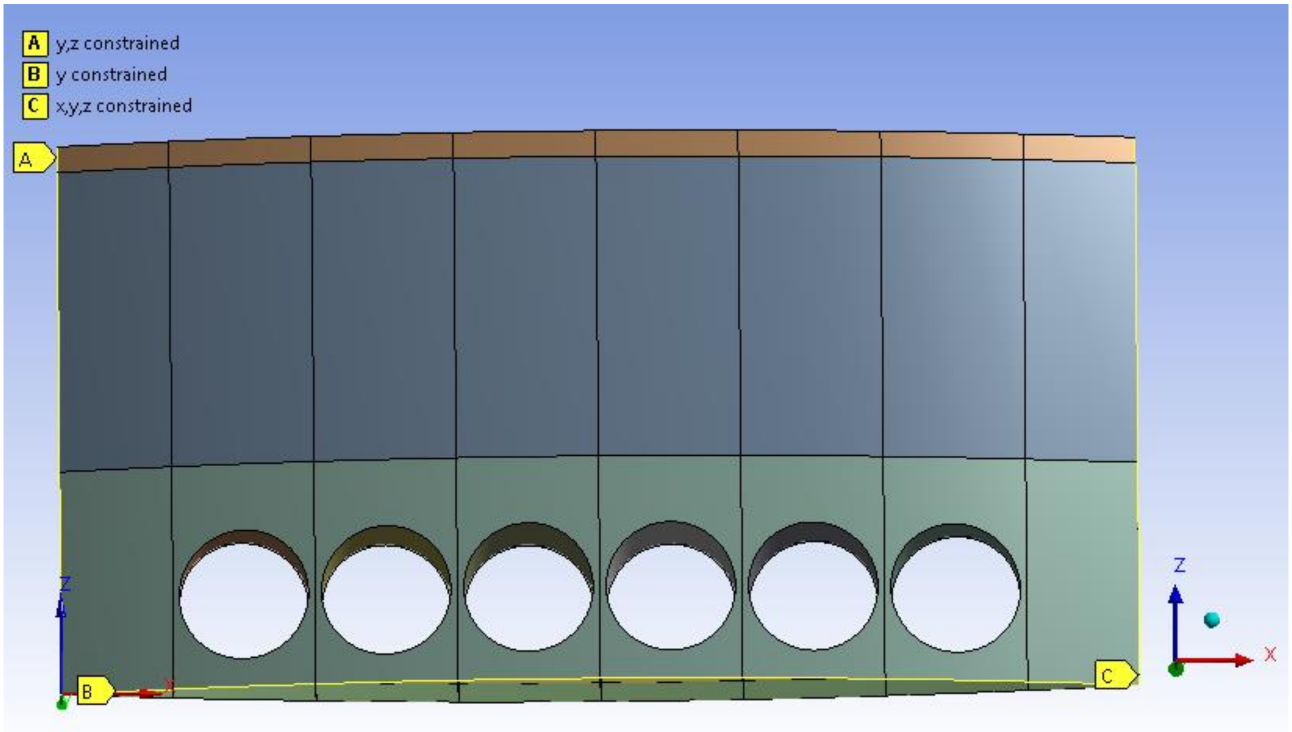

Figure 204: Overview of the supports after adjustments to the gate

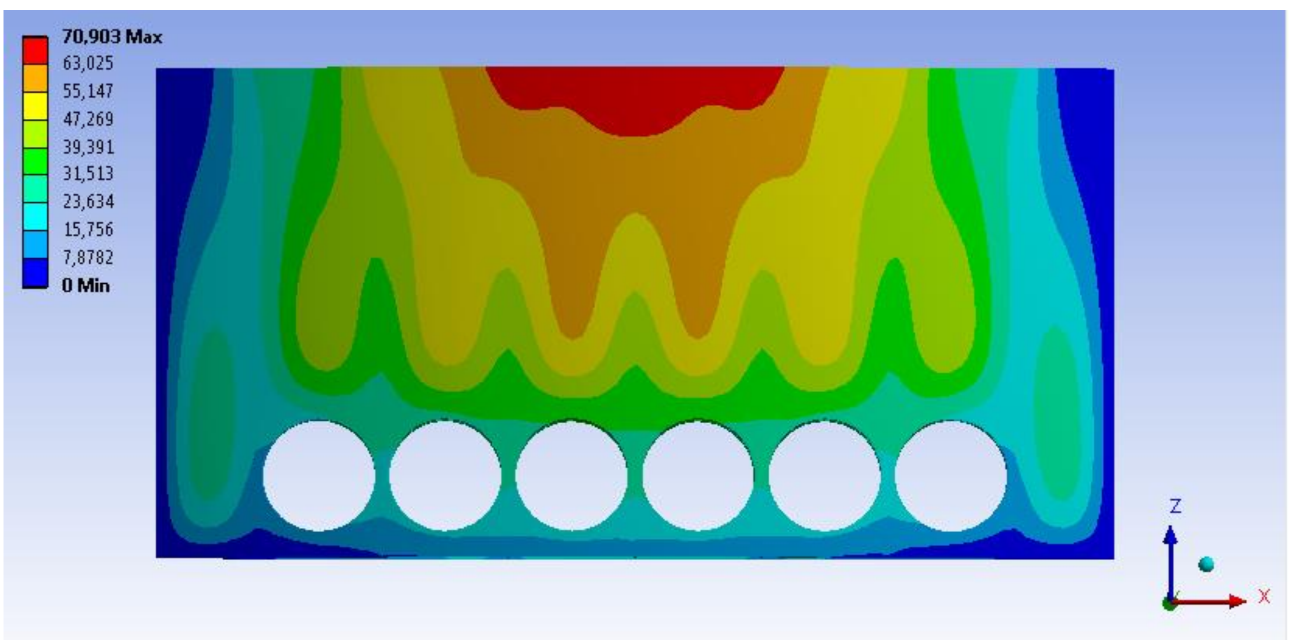

Figure 205: Deflections after the adjusments to the structure

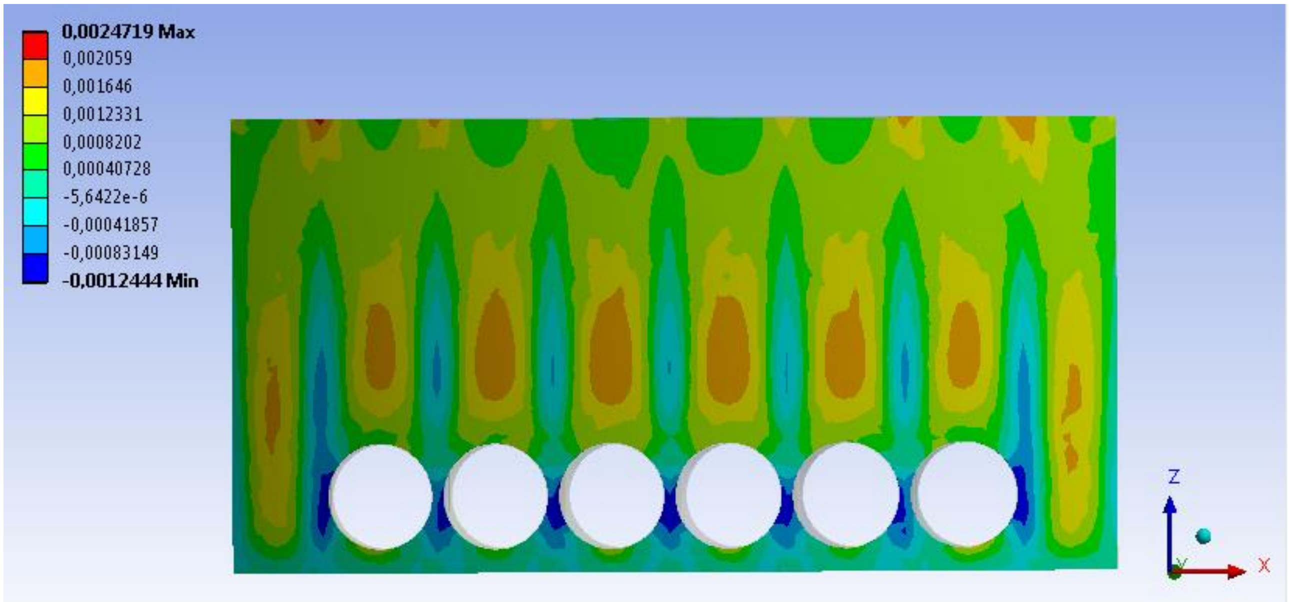

Figure 206: Normal elastic strains in the plate loaded by hydrostatic pressures after structural adjustments

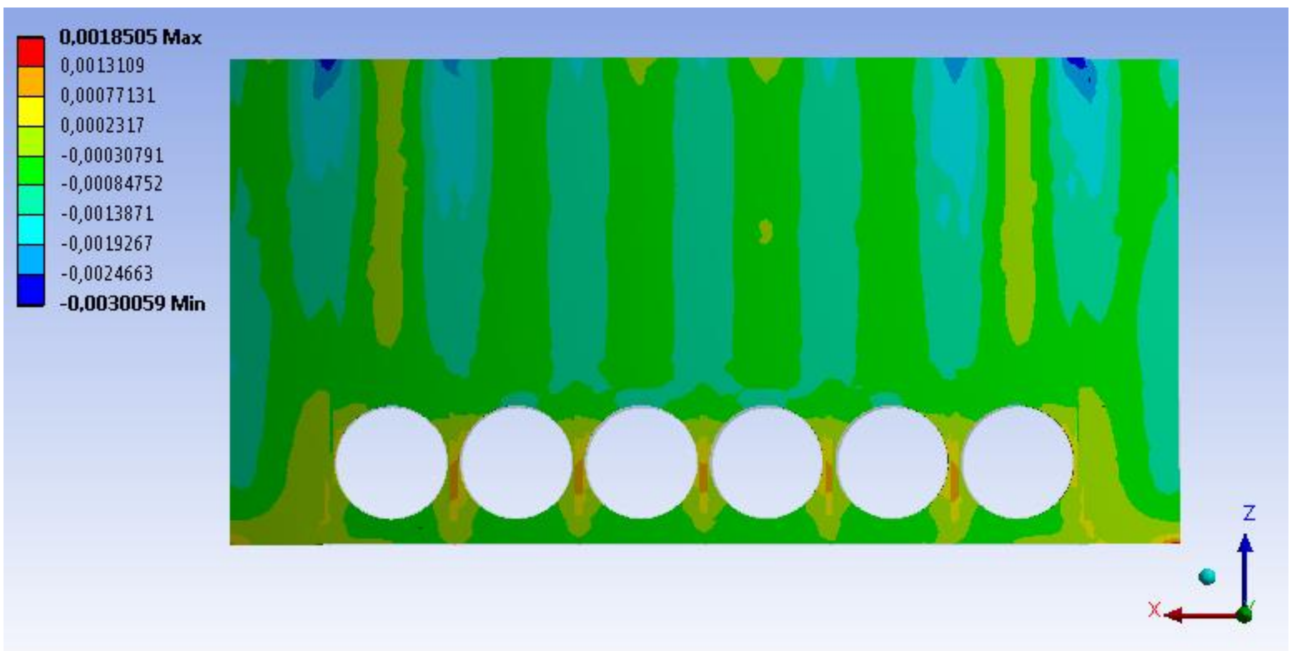

Figure 207: Normal elastic strains in the plate loaded by the valves after structural adjustments

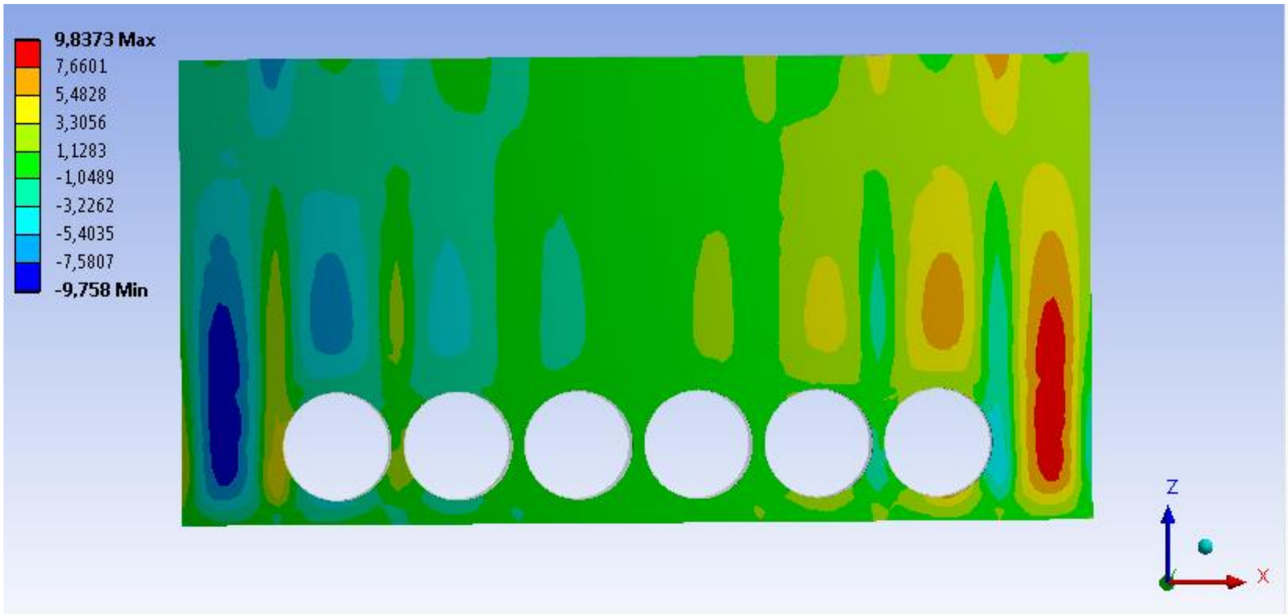

Figure 208: Shear stresses in the plate loaded by hydrostatic pressures after structural adjustments

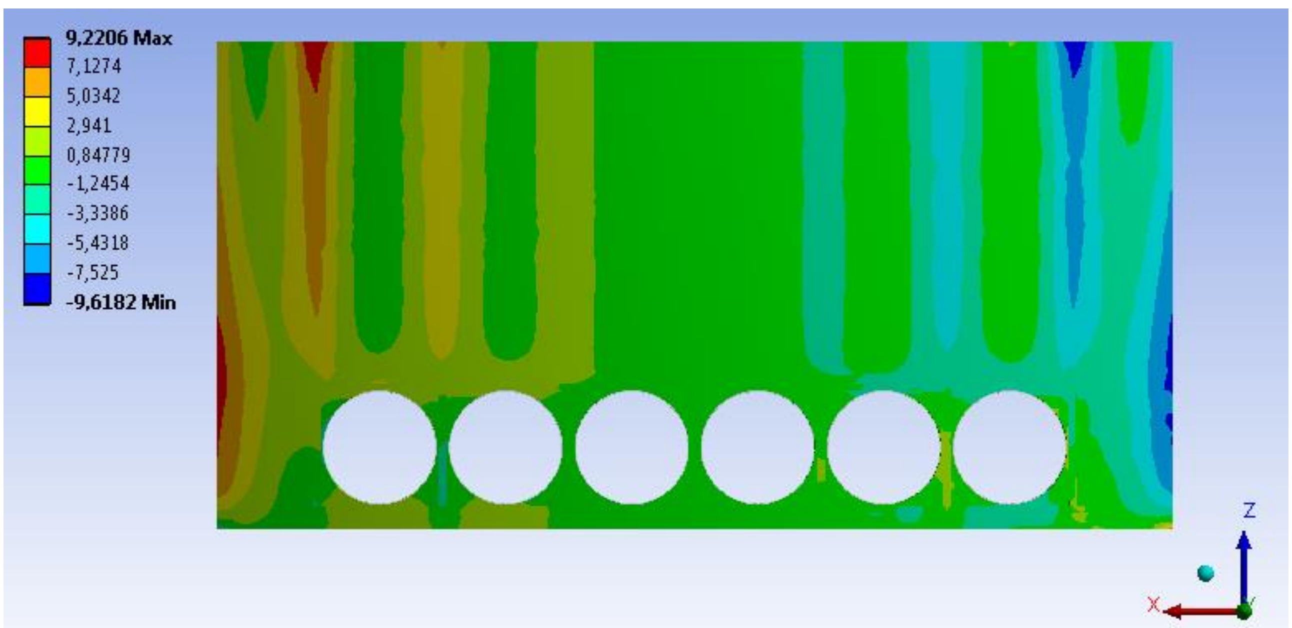

Figure 209: Shear stresses in the plate loaded by the valves after structural adjustments

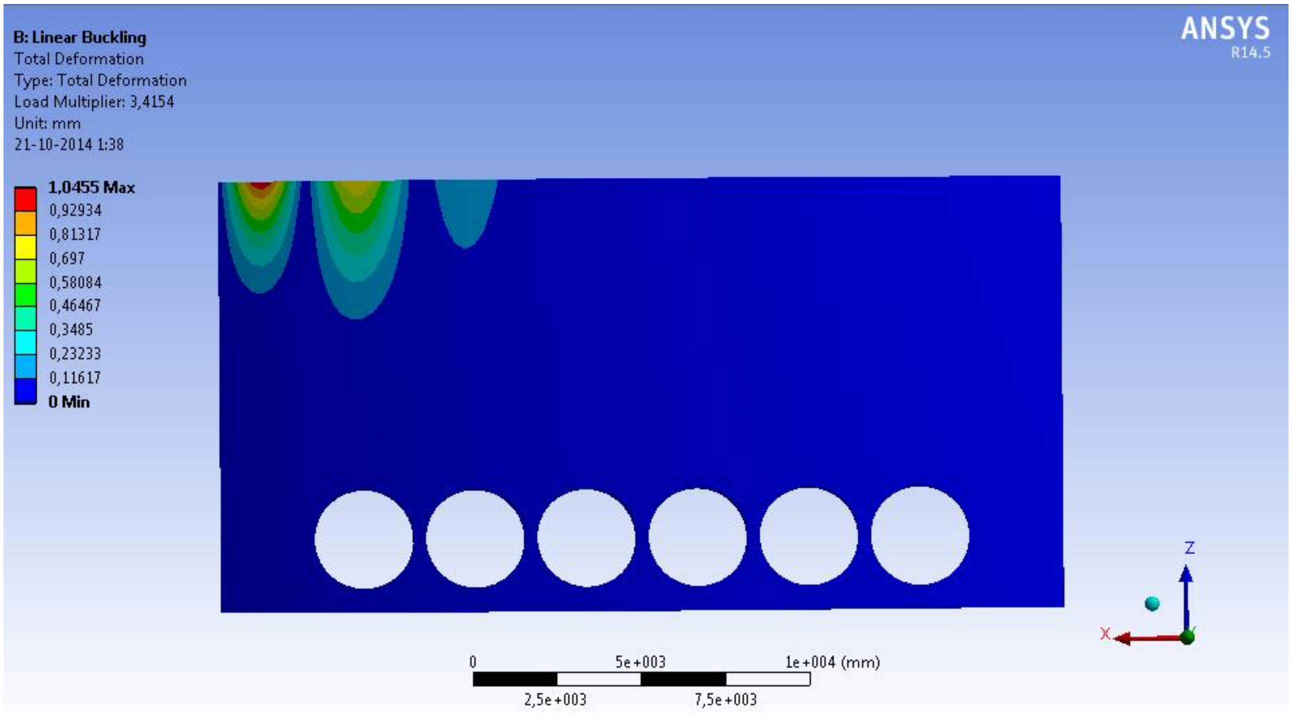

Figure 210: Stability check for the first modal shape

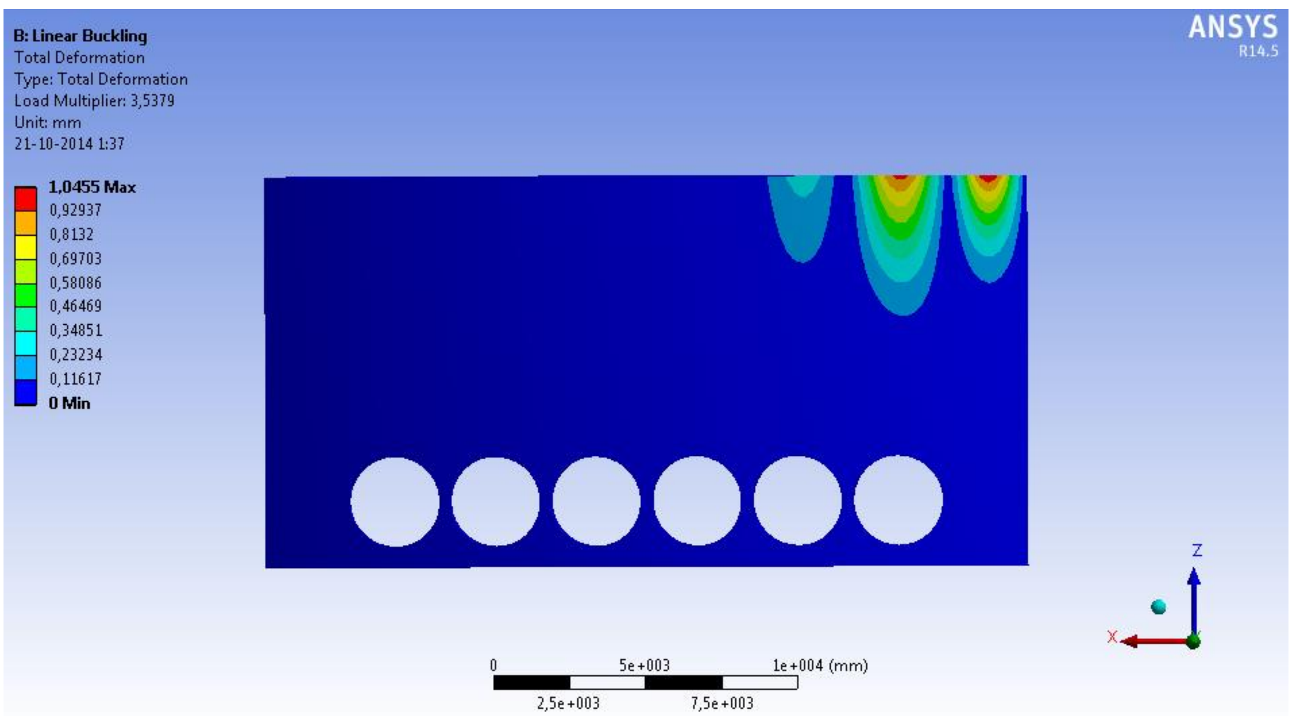

Figure 211: Stability check for the second modal shape

As expected, the first two modal shapes are nearly identical but mirrored due to the combination of a symmetrical structure and symmetrical load conditions. The small difference in safety on buckling is caused by numerical errors.

It appears that the construction of a horizontal line support at the lock sill is sufficient to fulfill the functional requirements for fiber strength, interlaminar shear strength and member stability. The following unity checks are now obtained:

$$UC1 = \frac{\varepsilon_d}{\varepsilon_{R;d}} = \frac{0{,}30\%}{0{,}33\%} = 0{,}91$$

$$UC2 = \frac{\tau_d}{\tau_{R;d}} = \frac{9{,}84}{12{,}35} = 0{,}80$$

$$UC3 = \frac{N}{N_{buckle}} = 3{,}42 > 2{,}5$$

Next to the strength after construction of a lock sill, also the watertightness of the connection between gate and sill has been investigated. In order to keep the leakage of the gate to a minimum, full contact between the bottom of the gate and the sill shall be present. This is checked by modelling the connection between bottom of the gate and the sill as a pressure-only support in SCIA Engineer. Although the design has changed a bit compared to the SCIA Engineer model (openings are now circular instead of rectangular), this does not have major implications for displacements at the position of the lock sill. The results of this analysis are presented in Figure 212.

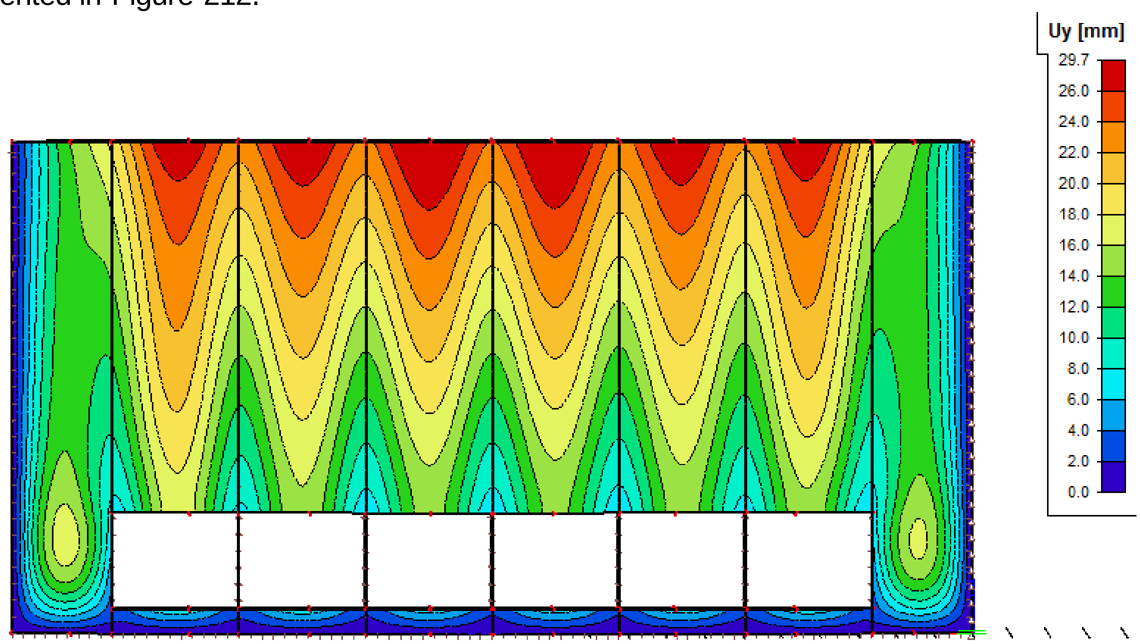

Figure 212: Deformed structure in the SLS if the support at the bottom is schematized as "pressure only"

It appears that the horizontal deflections at the bottom of the gate are still zero at the entire bottom as the gate is exposed to the hydrostatic pressures related to a head difference of 7 meters. This means that the watertightness is still guaranteed. If this would not have been the case, leakage between gate and sill would take place. A solution to these leakage gaps would have been placement of a flexible strip between gate and sill which is able to follow the deformations of the plate. Materials like hakorit (UHMPCE), balsa wood and rubber are frequently applied for this purpose.

Appendix K) Results of the fatigue analysis

This appendix shows the governing normal strains in the structure which are used during the fatigue analysis. The strains still need to be multiplied with the Young's modulus of the material to obtain the charasteristic stresses. Plots of the results for load cases 1 until 10 are presented in the table below.

	Governing strains
1	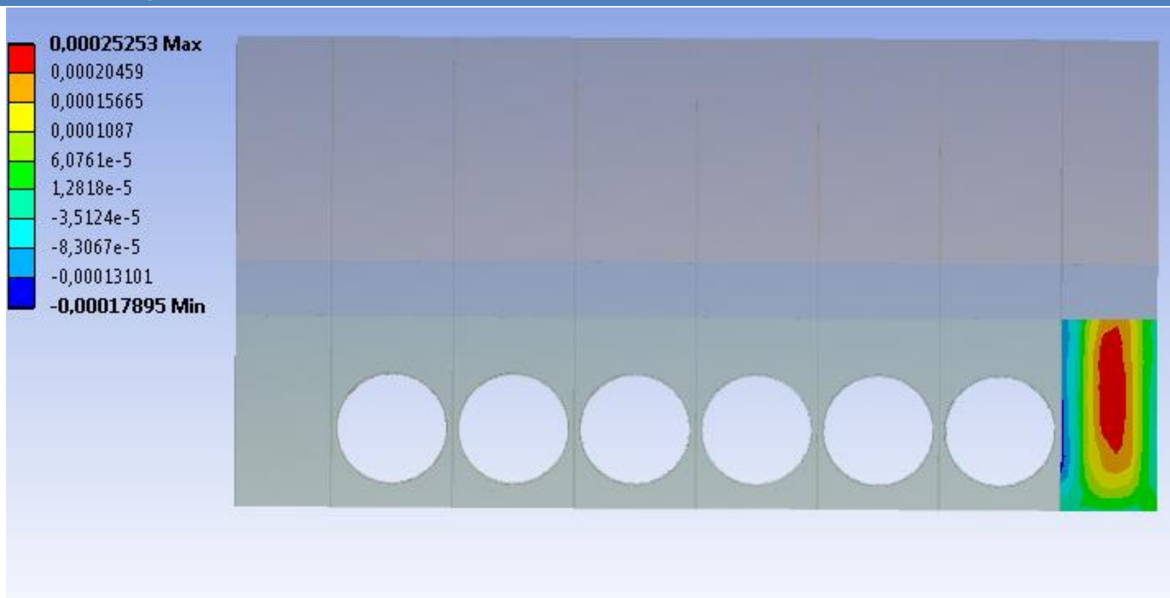
2	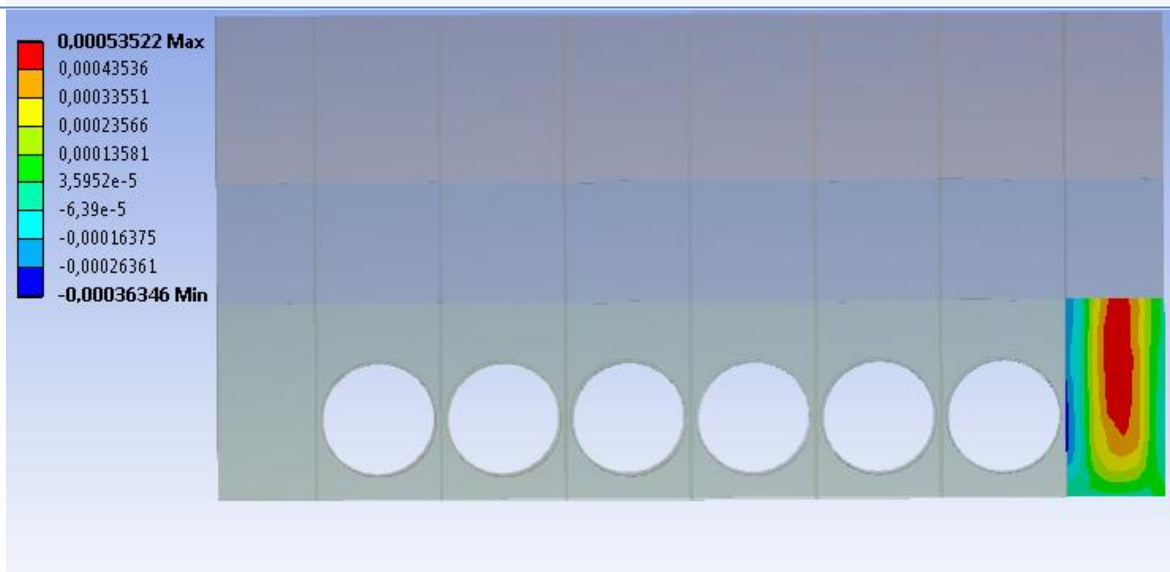

3

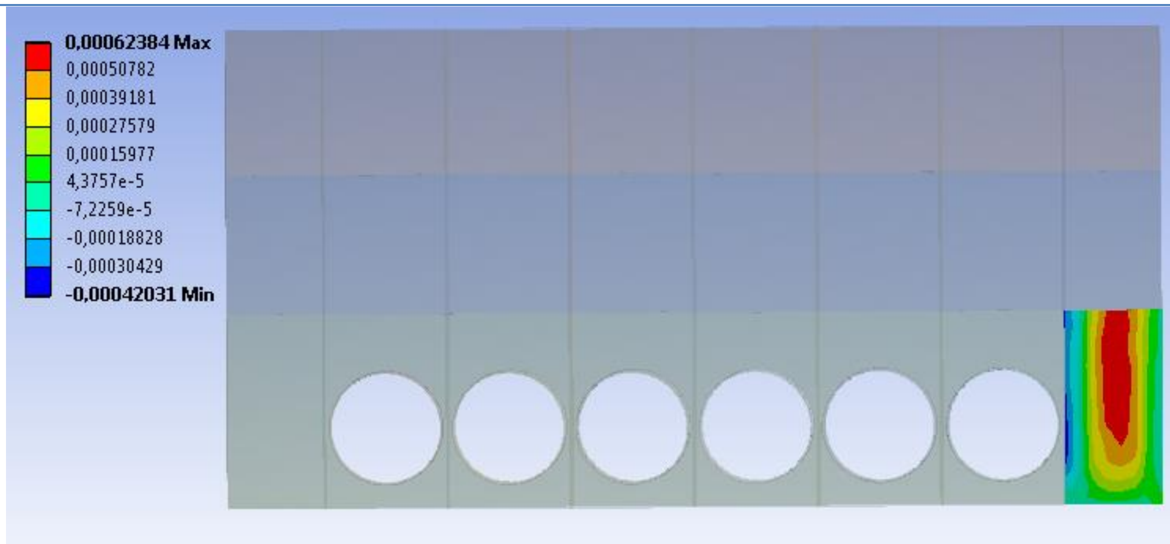

0,00062384 Max
0,00050782
0,00039181
0,00027579
0,00015977
4,3757e-5
-7,2259e-5
-0,00018828
-0,00030429
-0,00042031 Min

4

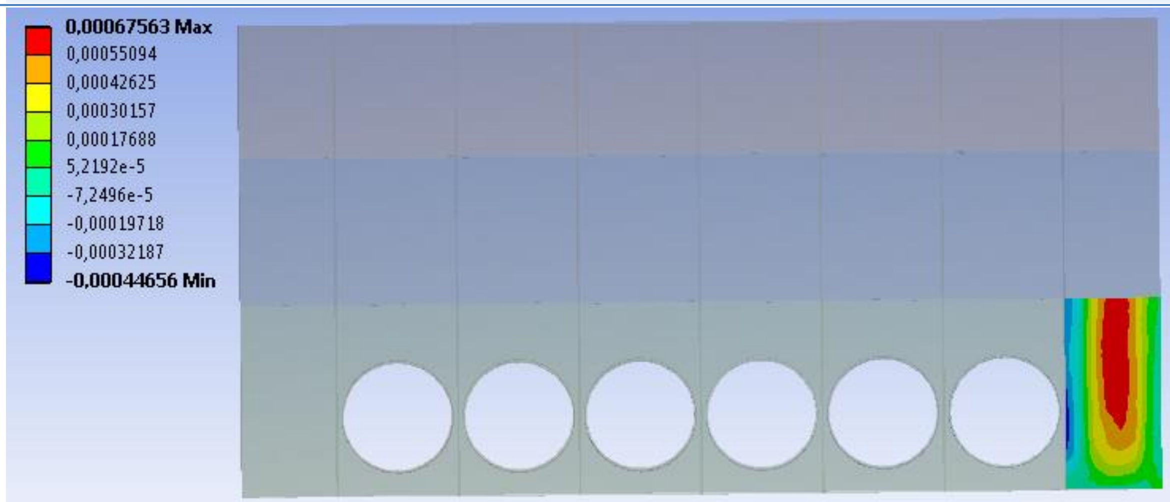

0,00067563 Max
0,00055094
0,00042625
0,00030157
0,00017688
5,2192e-5
-7,2496e-5
-0,00019718
-0,00032187
-0,00044656 Min

5

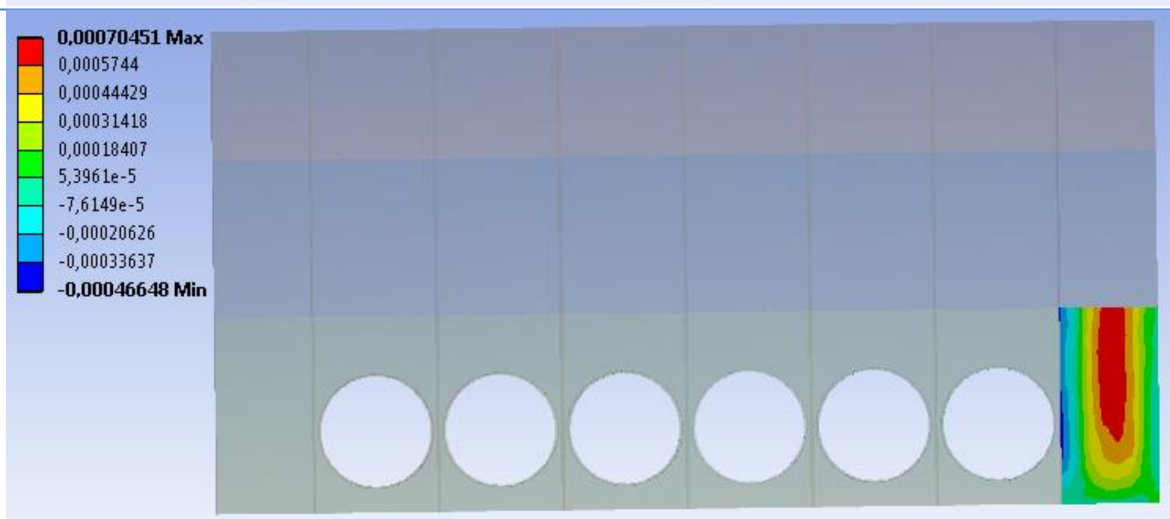

0,00070451 Max
0,0005744
0,00044429
0,00031418
0,00018407
5,3961e-5
-7,6149e-5
-0,00020626
-0,00033637
-0,00046648 Min

6


0,00073029 Max
0,00059601
0,00046172
0,00032744
0,00019316
5,8881e-5
-7,5401e-5
-0,00020968
-0,00034396
-0,00047824 Min

7

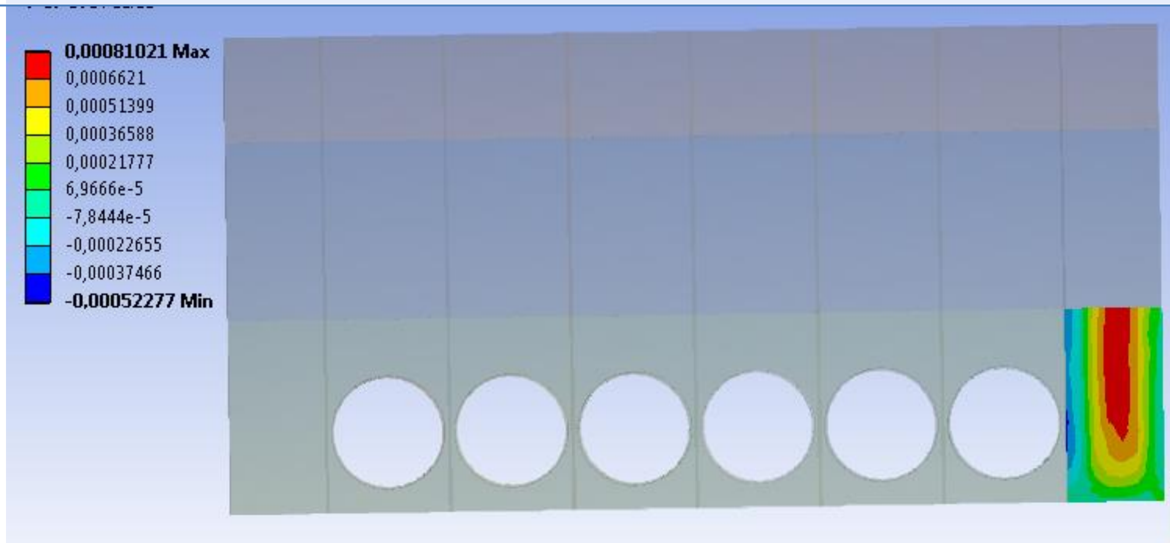
0,00081021 Max
0,0006621
0,00051399
0,00036588
0,00021777
6,9666e-5
-7,8444e-5
-0,00022655
-0,00037466
-0,00052277 Min

8

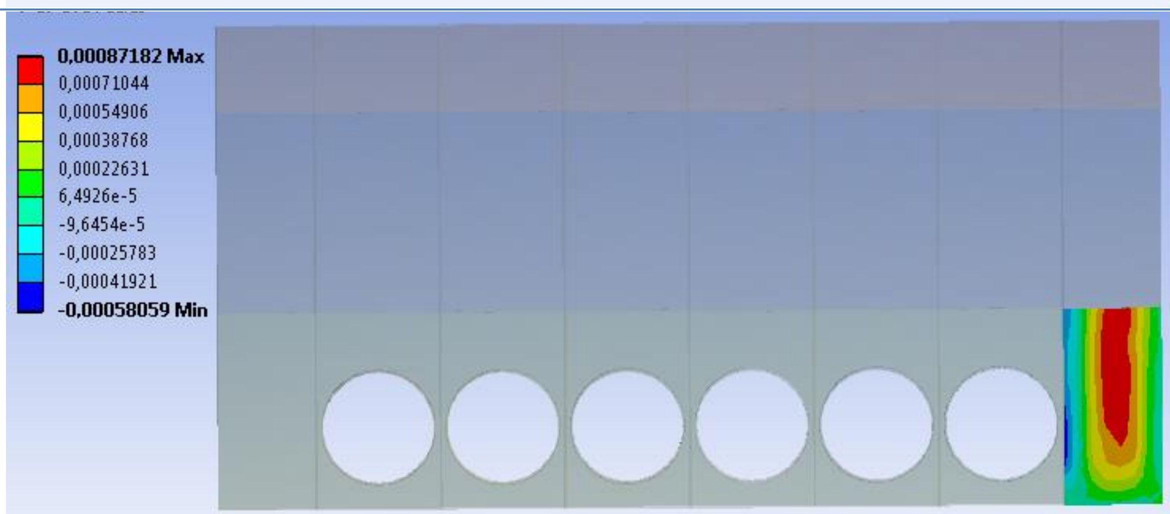
0,00087182 Max
0,00071044
0,00054906
0,00038768
0,00022631
6,4926e-5
-9,6454e-5
-0,00025783
-0,00041921
-0,00058059 Min

9	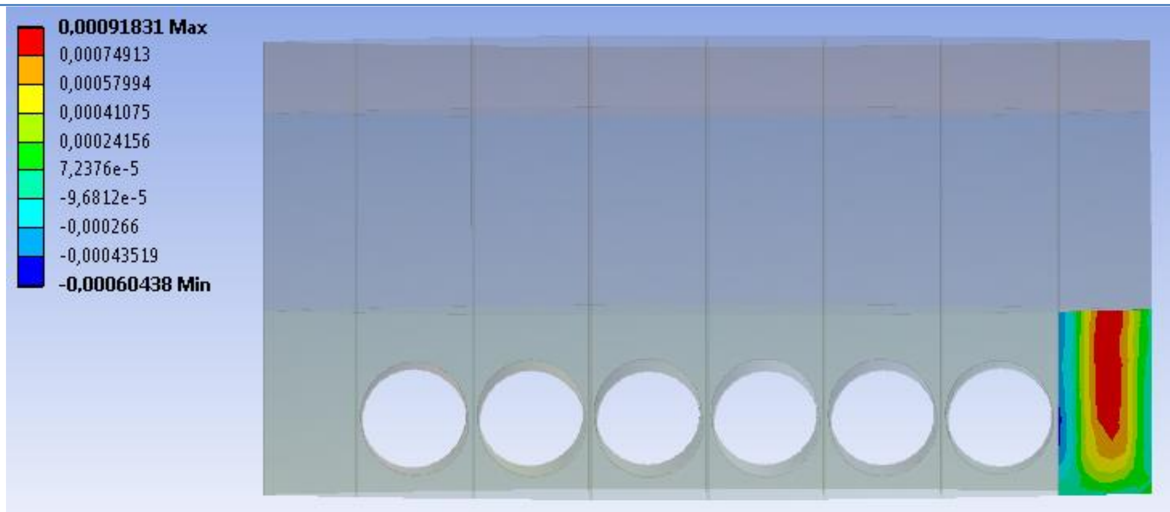 0,00091831 Max 0,00074913 0,00057994 0,00041075 0,00024156 7,2376e-5 -9,6812e-5 -0,000266 -0,00043519 -0,00060438 Min
10	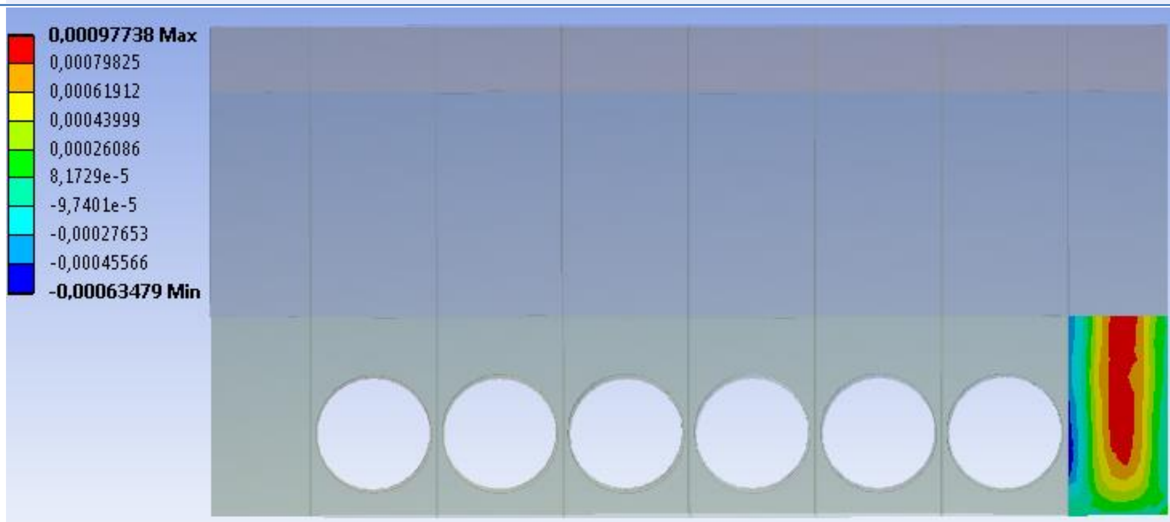 0,00097738 Max 0,00079825 0,00061912 0,00043999 0,00026086 8,1729e-5 -9,7401e-5 -0,00027653 -0,00045566 -0,00063479 Min

Appendix L) Overview of the considered fastening techniques

Option 1: Laminated T-joints

The first considered option to connect individual members is by laminated T-joints. Fiber-reinfored fabrics are placed at the corners and filled with a resin. The fabrics are placed with a certain overlap length so that the forces can be transfered through shear stresses.

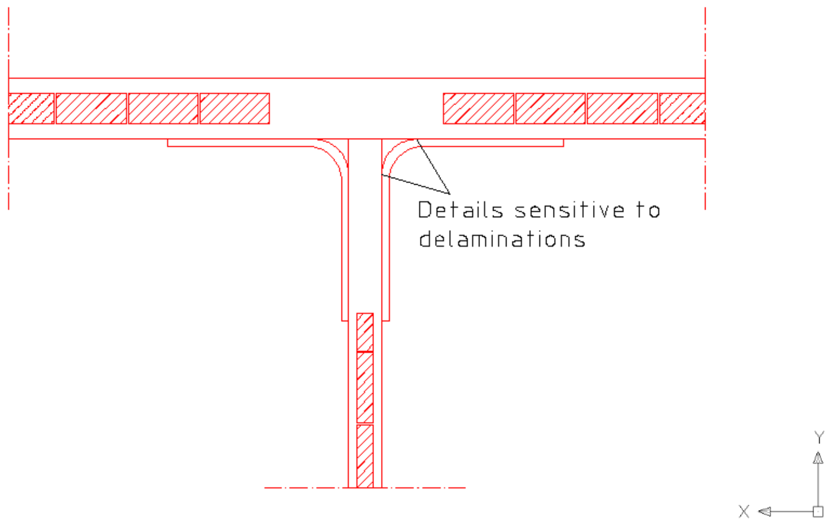

Figure 213: Weak spot of laminated T-joint connections

The problem with these types of connections is however that the radius of the fabric at the corner is limited. The risk of delaminations near the corners is present in case a (cyclic) bending moment is exterted to the connection, because the loads are solely resisted by the resin.

Option 2: Mechanically fastened joints

The second option is to produce corner profiles of fiber-reinforced polymers by pultrusion. These profiles are attached at the corners and prestressed bolts are penetrated through the profiles and plates. Transfer of forces takes place by friction between the different plates.

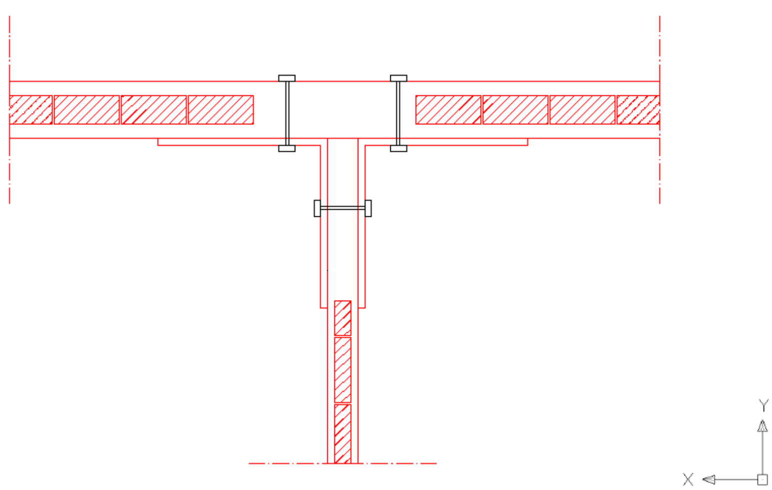

Figure 214: Mechanically fastened connection between web and water retaining plate

This option hoewever results in disruptions of both skins of the water retaining plates by the bolts, endangering the watertightness of the structure. Besides, high stress concetrations are expected to occur around the bolts due to disruptures of the skin plates.

Option 3: Peg-and-hole joints

The third considered option for the connection between elements is the peg-and-hole joint. A vertical hole iscreated over the entire height of the water retaining plate to accommodate the pin. The part to be connected is equiped with steel shoes and rings attached to it. Several savings over the height of the water retaining plate need to be constructed to accomodate these rings. Finally, a pin is placed inside the vertical hole in the water retaining plate through the rings to connect the members to each other. In the area around the connections, the core of the plates need to be replaced by FRP to resist the shear forces coming from the pin. The connection is fully hinged, meaning that the rotational stiffness is equal to zero. An impression of the connection is presented in Figure 215.

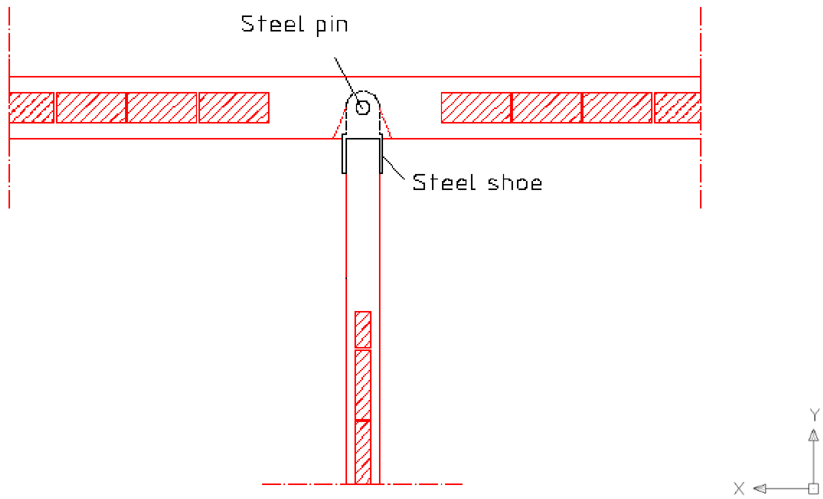

Figure 215: Peg-and-hole connection between webs and water retaining plate

An advantage of this type of connection is that the parts are dismountable for inspection and maintenance. The main disadvantage are the peak stresses which are expected to occur around the savings in the water retaining plate to accommodate the rings. Besides, local application of steel is at the expense of the maintenance-friendliness of the structure as a whole.

Appendix M) Calculations of the detailed design

Forces at the connection between webs to water retaining plate

The maximum tensile force in the connection between web and water retaining plate is equal to 1524 kN, as presented in Figure 216.

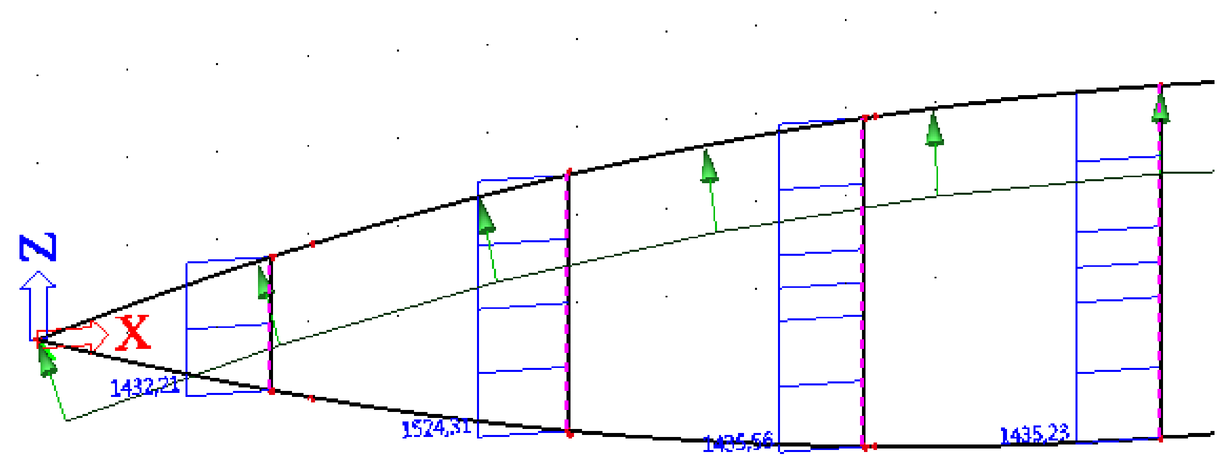

Figure 216: Tensile forces in the webs for the governing load case

Forces at the connection between the water retaining plate and support

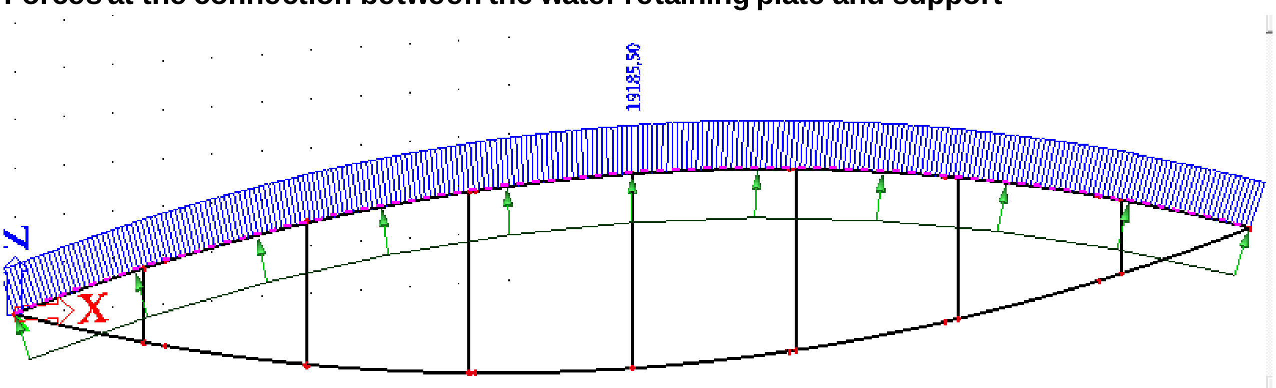

Figure 217: Normal forces in the water retaining plate

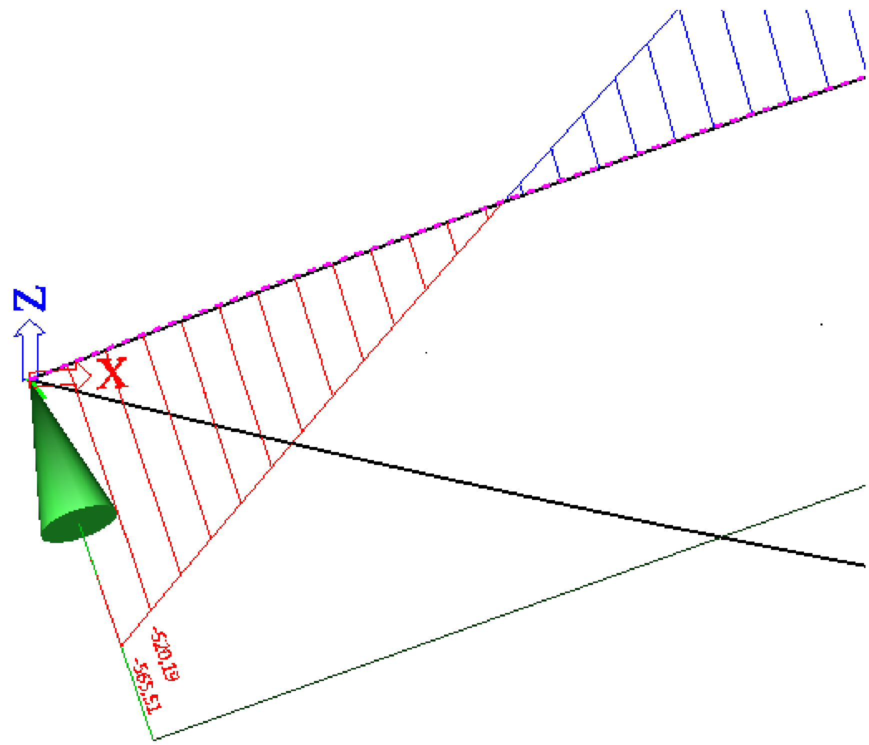

Figure 218: Shear forces at the connection between water retaining plate and support

Appendix N) Structural design of the valves in FRP

The functional requirements which have to be met by the valves are presented in Table 56.

Table 56: Functional requirements for the valves

	Requirement	Origin
1	The maximum strain in the material shall not exceed 0,33%	CUR 96 [25]
2	The deformations (both elastic and creep) shall not hinder the vertical movement of the gate;	Own decision
3	The valves shall be able to close by their self weight;	Own decision
4	The deformations of the valves need to be able to follow the gate deformations to prevent leakage gaps;	Own decision
5	The bottom of the valves should be sharp edged with minimum angles as presented in Figure 219, in order to prevent vibrations.	Ontwerp van Schutsluizen [37]

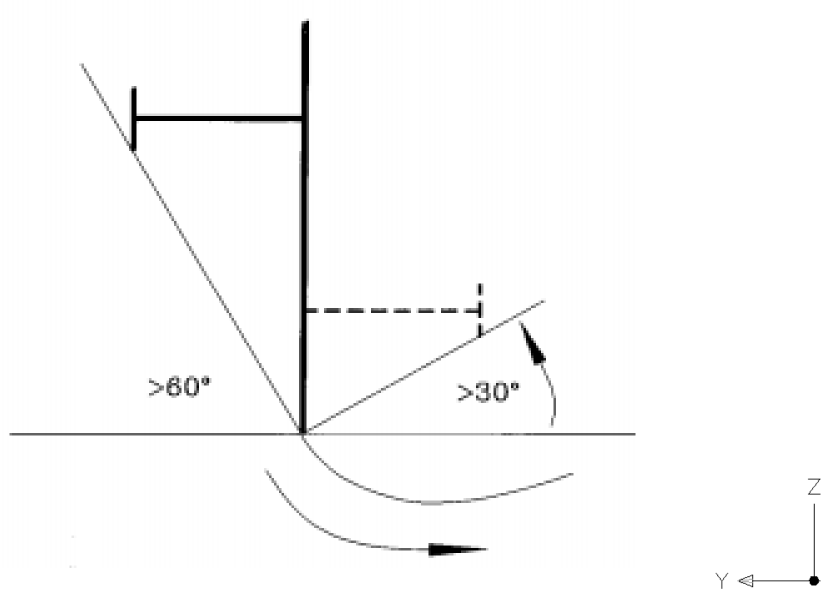

Figure 219: required angles of the bottom of the valves to prevent dangerous vibrations [37]

The valves have been modelled in SCIA Engineer as stiffened plates which are only supported in horizontal direction at the vertical edges. For the ULS calculation, a distributed load of $70\ kN/m^2$ related to the hydrostatic pressures has been multiplied by a safety factor of 1,5. The following points have been checked:

- Strength of the ribs
- Strength of the plate in x- and y-direction
- Deformations of the plate
- Deformations of the horizontal ribs with respect to the horizontal sealing attached to the gate

To ease the production, it has been decided to design the valves as solid plates, on four edges stiffened by ribs. This configuration has also been applied in the Spieringsluis [5]. The global geometry is presented in Figure 220.

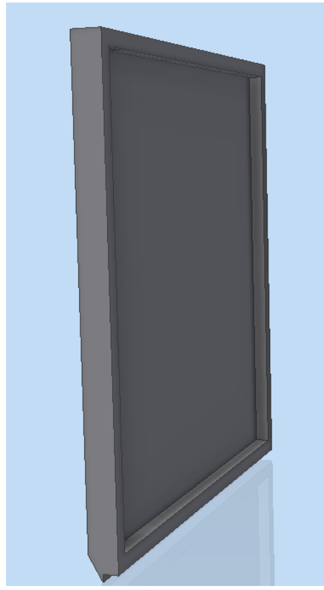

Figure 220: Global shape of the valve

Furthermore, the fiber orientations and volumes are chosen to be the same as for the the gate. This leads to a Young's modulus in the main (horizontal) direction E_1 of $25.800\ N/mm^2$, while the E_2 equals $15.900\ N/mm^2$. The maximum allowable stress in the valves equals $85\ N/mm^2$. The width of the stiffeners is determined by the horizontal distance between the openings in the gate and is equal to 100 millimeters. The width and height of the entire valve equal both 3,2 meters. The parameter which can be varied during the design is the ratio between plate thickness and rib thickness. Once this ratio has been determined, individual member thicknesses follow from strength- and stiffness requirements.

The following checks have been performed:

- The deformations of the valves in closed position need to be larger than the deformations of the gate to prevent leakage gaps (SLS);
- The chamfer applied to the ribs of the valve needs to be larger than the differential deformation between the valves during opening and the gate;
- The stresses in the ribs of the valve may not exceed $85\ N/mm^2$;
- The stresses in the plate of the valve may not exceed $85\ N/mm^2$.

The plate thickness and rib height have been varied until a valve configuration has been found which fulfills the functional requirements presented in Table 56. The calculations on the performance has been performed with help of finite element software SCIA Engineer.

The situation where the valve is only supported at the vertical edges turned out to be governing for the design on strength, even for the smaller head difference compared to the second considered load case. Figure 221 shows that stresses in the ribs do not exceed the design strength of the material of $85\ N/mm^2$.

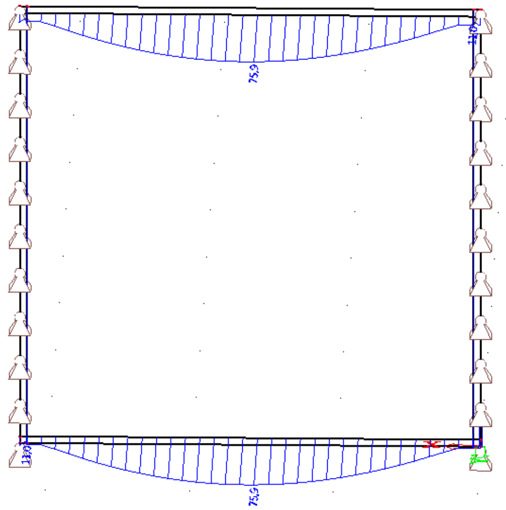

Figure 221: Member stress of the stiffening elements (ULS)

Furthermore, the design values of the stresses in the x- and y-direction of the plate have been investigated. Figure 222 and Figure 223 show that these values do not exceed the design values of the material strength.

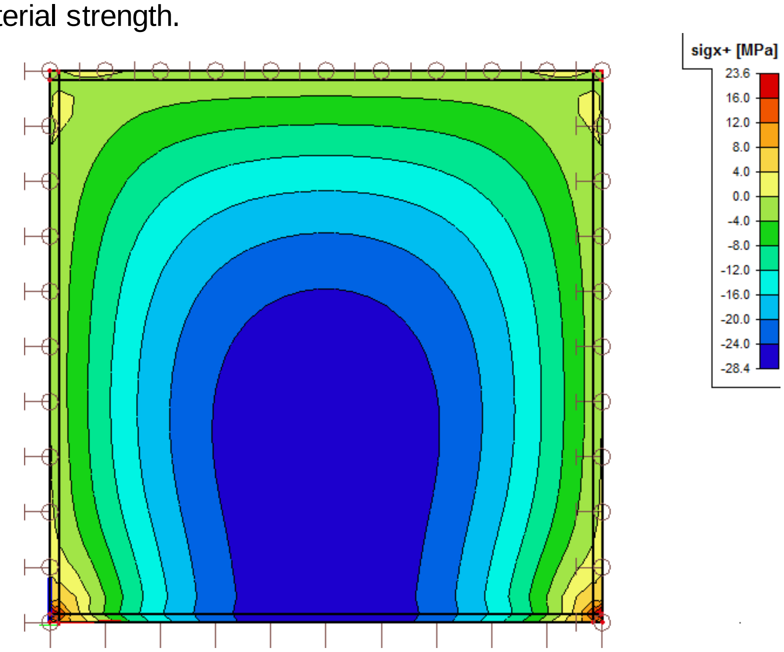

Figure 222: Stresses in x-direction in the plate (ULS) for the governing load situation

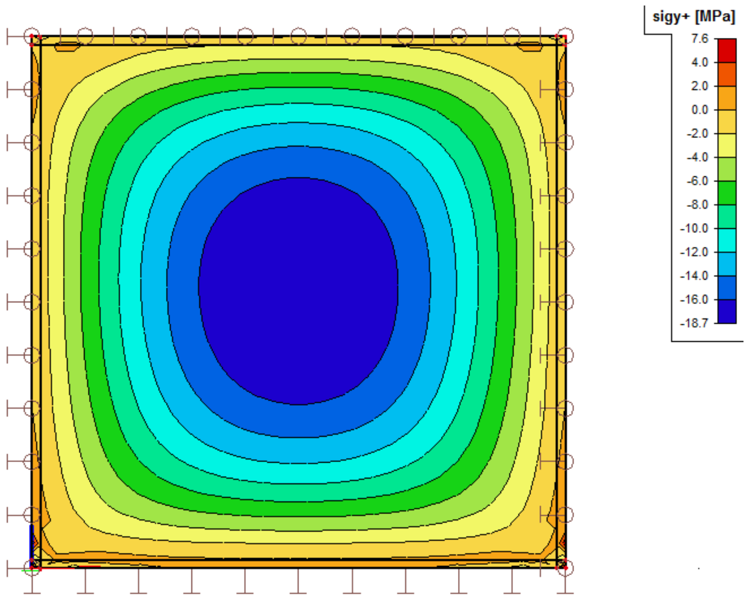

Figure 223: Stresses in the y-direction in the plate (ULS) for the governing load situation

Now that the strength of the structure is proven to be sufficient, the next step is to check if the deformations are small enough so that the valves are unhindered during opening- and closing. The valves can get jammed due to deformations as a result of creep induced by long term loading and elastic deformations of both the gate and the valves.

Creep deformation of the valves is investigated for the load situation where the valve is fully closed and the hydrostatic pressures related to the average head difference of 1,5 meters are acting on the valve. The elastic deformations for this load case are presented in Figure 224.

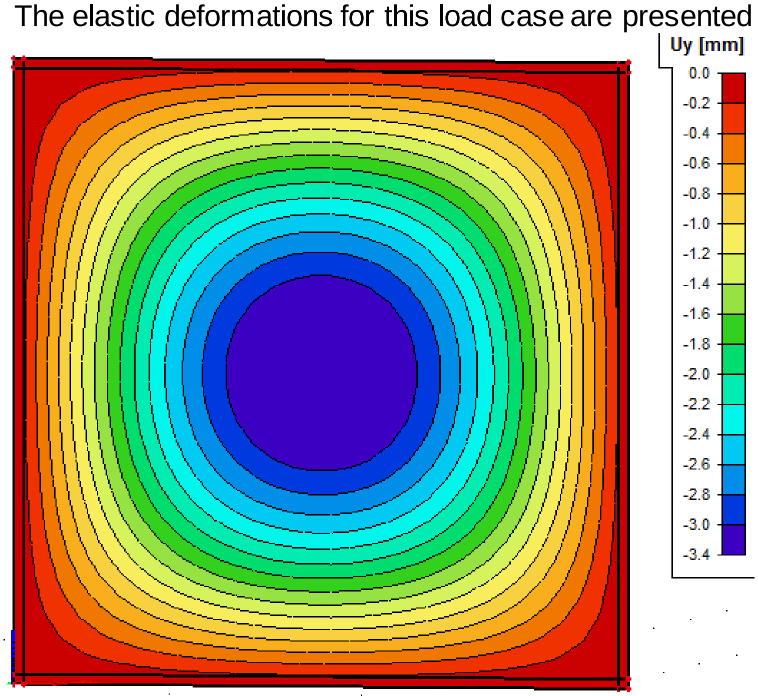

Figure 224: Elastic deformations of the valve under long-term loading conditions

Since the fiber lay-up is similar to the fiber lay-up of the gate, the same creep factor of 50% is valid. This means that the long term creep of the gate will be less than 2 millimeters.

To find the elastic deformations of the valve during opening, the absolute upperboundary is investigated where the valve is only supported at the vertical edges and the hydrastatic pressure related to a maximum head difference during locking of 6,4 meters is acting on the entire surface. This is an overestimation of the deformations for the following two reasons:

- When the valves are halfway opened, the head difference has already decreased;
- The hydrostatic pressures will only be present at the position of the openings in the gate and not at the entire valve.

The elastic deformations for the maximum head difference where locking is still allowed are presented in Figure 225.

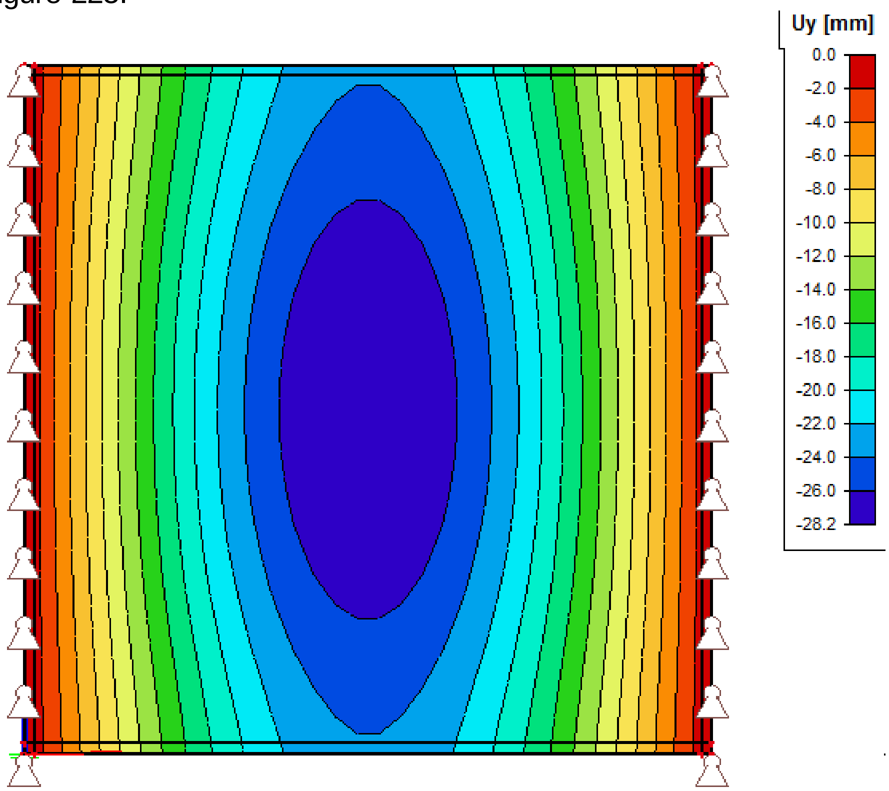

Figure 225: Elastic deformations for an opened gate during maximum head difference for which navigation is allowed

It appears that even for this upper boundary the sum of creep deformations and elastic deformations is still al lot less than the thickness of the ribs. This means that the valves can not get jammed because of the deformations of the plate itsself.

The last requirement which has to be met is that the horizontal ribs of the valves need to be able to pass along the horizontal sealing profile attached to the gate above the openings.This means that the sum of the elastic deformations of the horizontal rib at the bottom of the valve and a combination of creep deformations and elastic deformations of the gate should be less than the chamfer which is applied to the ribs.

For the elastic deformations of the valve, the same assumptions have been made as for the elastic deformations of the gate. The result is presented in Figure 225. The maximum elastic deformations of the horizontal rib at the bottom of the valve are approximately 24 millimeters.

The creep deformation of the gate at the position of the horizontal sealing profile above the governing opening has been investigated in section 6.7 and is equal to 2 millimeters.

The elastic deformations of the gate during opening are investigated for a head difference of 6,4 meters. It appears that the maximum elastic deformations are eual to 19 millimeters at the position where the deflections of the rib of the valves are the largest (see Figure 226).

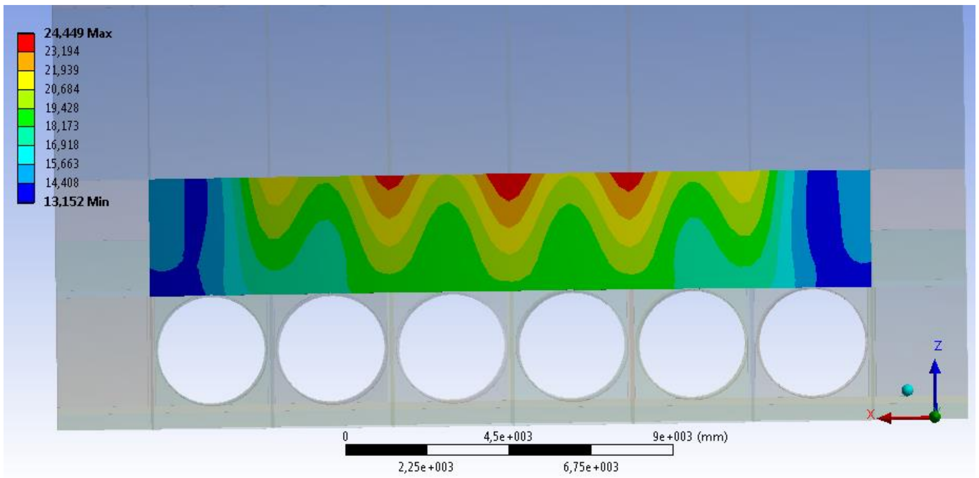

Figure 226: Elastic deformations for the maximum head difference where locking is allowed

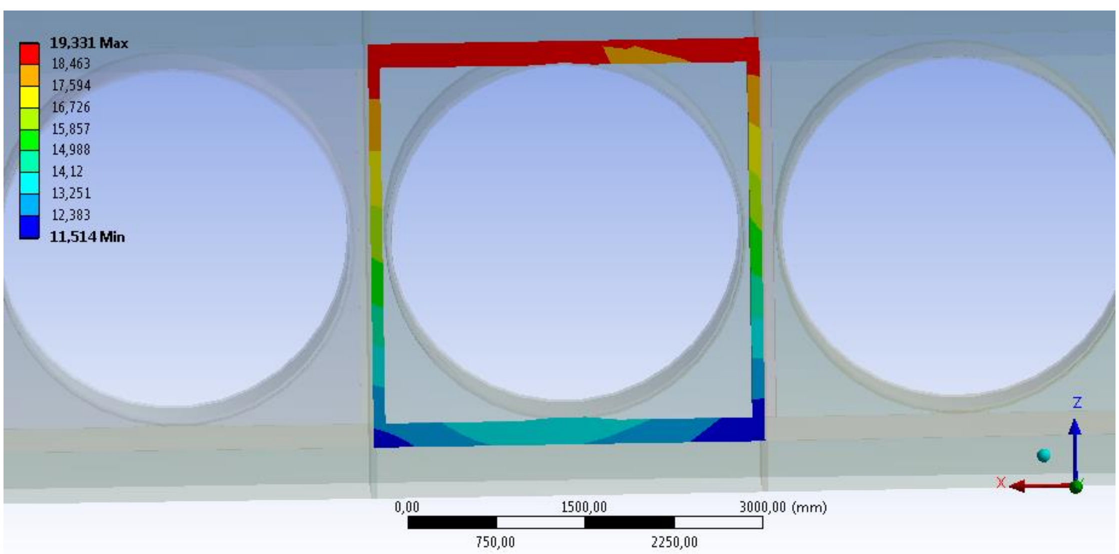

Figure 227: Deformations around the governing openin

The mass of a single valve is approximately 2 tons.The final design of the valve is presented in Figure 228, Figure 229 and Figure 230.

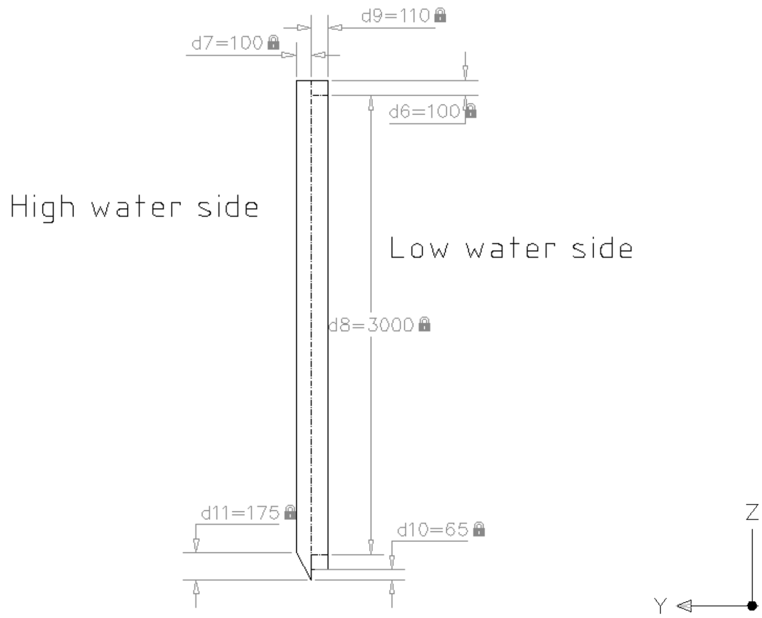

Figure 228: Dimensions of the valves

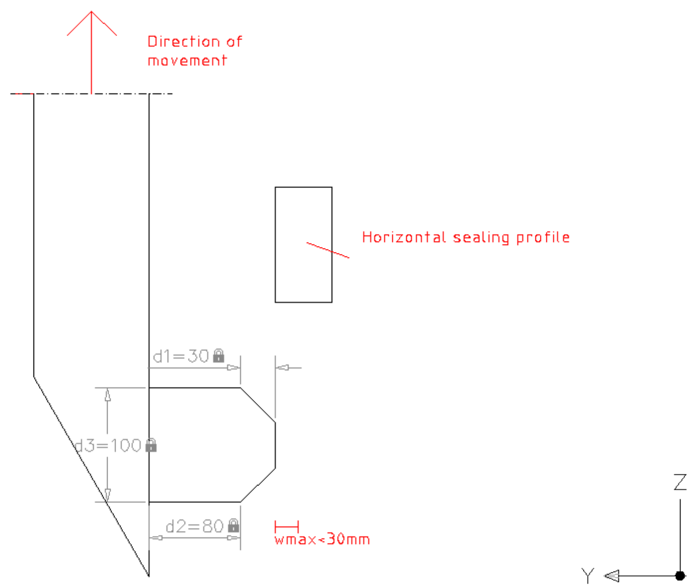

Figure 229: Detailed view on the bottom of the valve

The valves will be opened and closed by vertical translation. The valves are placed inside vertical C-profiles of FRP which are equiped with sliding strips of stainless steel. Figure 127 shows the top view of the valve.

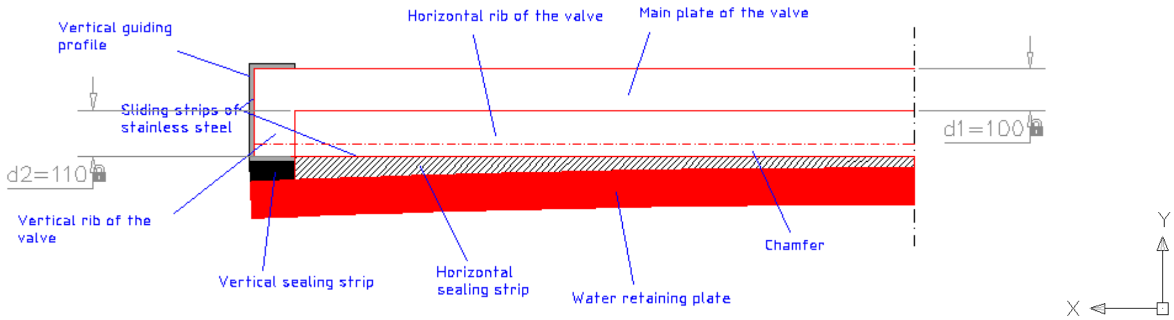

Figure 230: Top view of the valves including the vertical guiding profiles

Further optimization of the valves is possible by adjustment of the global lay-out and fiber orientation. This is however out of the scope of the research. Besides, vibrations of the valves due to the fluid-structure interaction are not included in this study. Reference is made to the (Dutch) book "Dynamisch gedrag van waterbouwkundige constructies deel A,B en C [61]" for further elaboration on this subject. The design of the moving equipment hasalso been left out of the scope of the project.

Appendix O) Energy approach to ship impact

To calculate the maximum stresses in the designed gate due to impact, a vessel with a mass of 8000 tons and a sailing velocity of 1 m/s is considered to be representative (CUR report 151 recommends a value between 0,5 and 2 m/s).

The contact area between vessel and gate has, in accordance with the eurocode, a width of 2 meters and a height of 0,5 meters. The location of impact is chosen to be in between the two webs in the middle of the gate, at a height of 1,5 meters above the average water level at the Lek.

The following coefficients are used to account for the added hydrodynamic mass (c_m), rigidity of the ship (c_s) and confined water between ship and gate (c_c) [60]:

$$c_m = 1{,}2$$

$$c_s = 1$$

$$c_c = 0{,}8$$

The kinetic energy which needs to be dissipated during impact is calculated as follows:

$$E_{kin} = c_m * c_s * c_c * \frac{mv^2}{2} = 3{,}84\ MJ$$

$E_{kin} =$	Kinetic energy of the colliding vessel [J]
$m =$	Total mass of the vessel [kg]
$v =$	Design velocity of the vessel [m/s]

The energy which is stored by deformations of the gate is equal to the integral of the force-displacement diagram:

$$E_{spring}(w) = \int_0^{w_{max}} F(w) * dw$$

Under the assumption that the displacement of the spring is linear to the force exerted on the spring, this relation can be simplified to the following:

$$E_{spring}(w) = \frac{kw^2}{2}$$

$E_{spring} =$	Energy stored in the spring [J]
$k =$	Spring stiffness [N/m]
$w =$	Deflection of the spring [m]

The spring stiffness is found by a application of a unity load of $100\ kN/m^2$ in the static model presented in chapter 6 at the position of the impact zone. The stiffness of the spring is found by the following formula:

$$k = \frac{F}{w} = \frac{\int_0^A q(x,y) * dA}{\overline{w}}$$

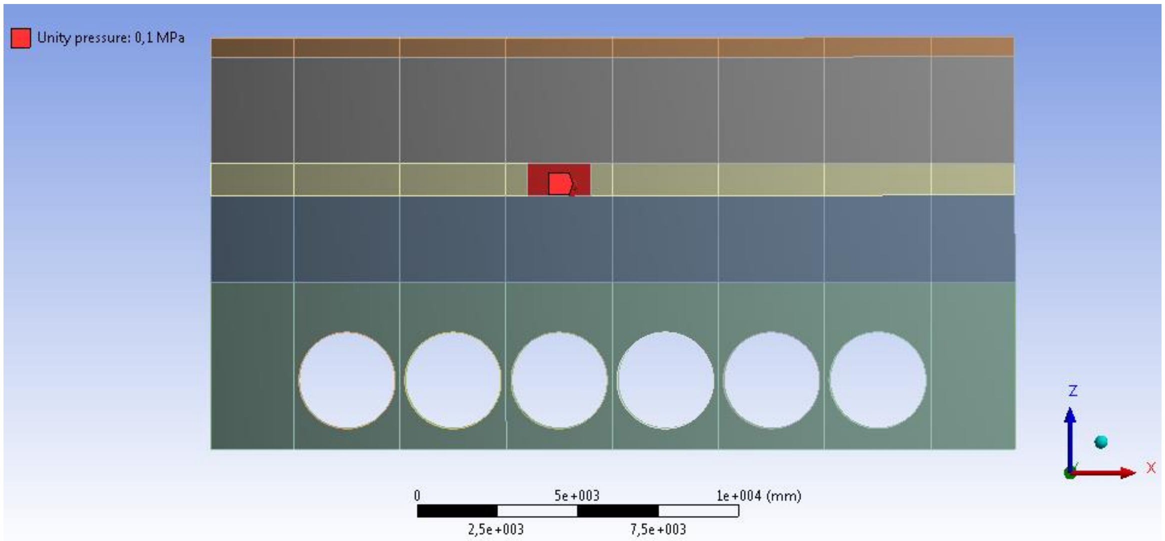

Figure 231: Position and value of the unity load which has been applied

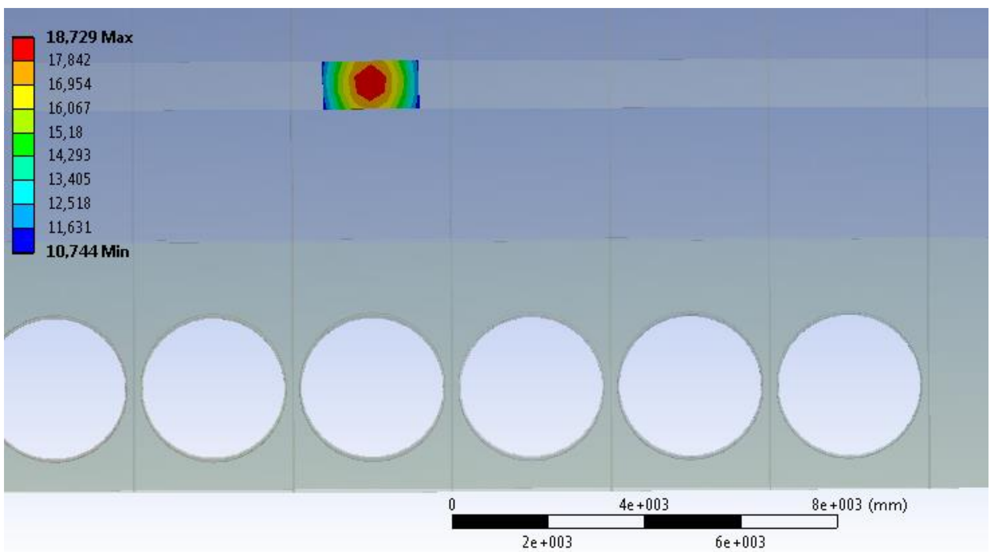

Figure 232: Deformations caused by the unit load

The average deflection of the gate over the full area of the unit pressure is approximately 14,7 millimeters, resulting in a spring stiffness of approximately $6800\ kN/m$. Under the assumption that the deflection is linearly dependent on the applied pressure (which is true for full linearly elastic behaviour without instabilities of members), an energy balance can be used in order to find the maximum displacements caused by ship impact:

$$w_{max} = \sqrt{\frac{2 * E_{kin}}{k}} = 1{,}06\ meters$$

The maximum static force is subsequently found by multiplication of the maximum deflection by the spring stiffness:

$$q(x,y) = w_{max} * k = 1{,}06 * 6800 * 10^3 = 7{,}2\ MN/m^2$$

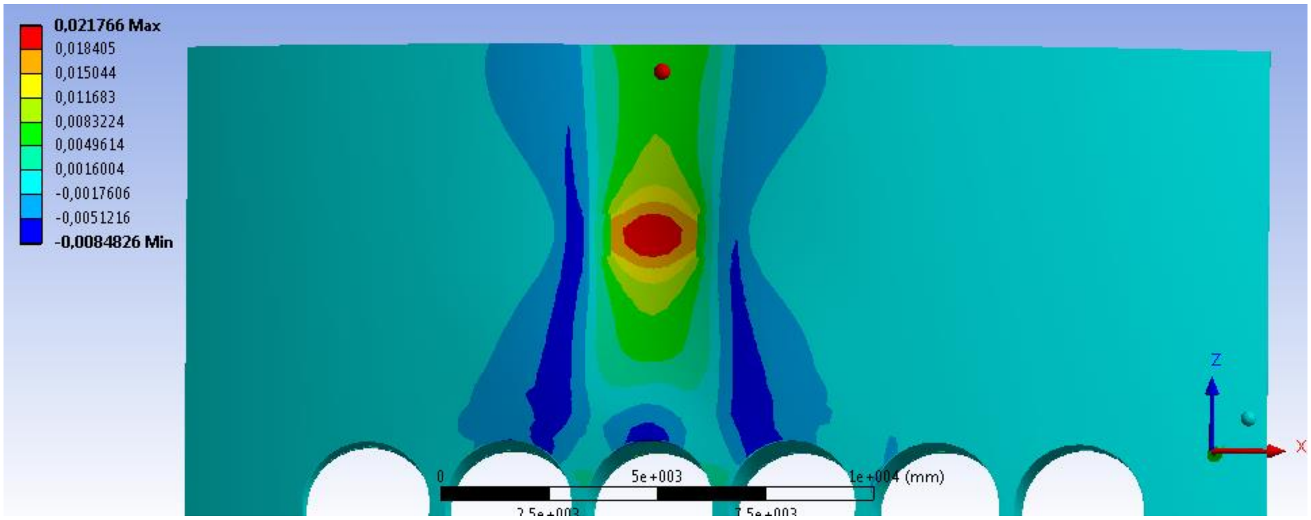

Figure 233: Normal elastic strain in the gate

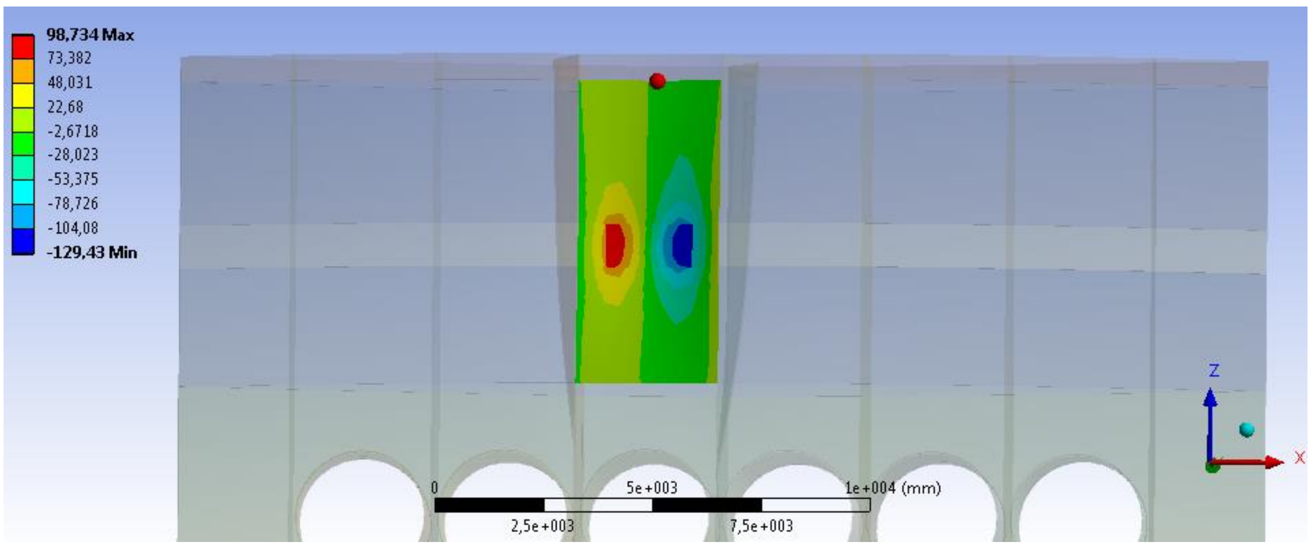

Figure 234: Shear stress in the gate

It is clear that both the ultimate strain limit of 1,2% and the maximum shear forces of 15 MPa are exceeded, even without application of partial safety factors. Without investigation of the energy dissipation caused by the material failure, it is impossible to say anything about the extents of the damage and whether this damage could be repaired or not. These subjects will be further elaborated with help of a a dynamic model in ANSYS in the next paragraph.